Swansea University
Prifysgol Abertawe

Cronfa
Setting Research Free

Swansea University E-Theses

Dynamic performance modelling of tidal stream turbines in ocean waves.

Orme, James A. C

How to cite:

Orme, James A. C (2006) *Dynamic performance modelling of tidal stream turbines in ocean waves..* thesis, Swansea University.
http://cronfa.swan.ac.uk/Record/cronfa42663

Use policy:

This item is brought to you by Swansea University. Any person downloading material is agreeing to abide by the terms of the repository licence: copies of full text items may be used or reproduced in any format or medium, without prior permission for personal research or study, educational or non-commercial purposes only. The copyright for any work remains with the original author unless otherwise specified. The full-text must not be sold in any format or medium without the formal permission of the copyright holder. Permission for multiple reproductions should be obtained from the original author.

Authors are personally responsible for adhering to copyright and publisher restrictions when uploading content to the repository.

Please link to the metadata record in the Swansea University repository, Cronfa (link given in the citation reference above.)

http://www.swansea.ac.uk/library/researchsupport/ris-support/

CIVIL & COMPUTATIONAL ENGINEERING CENTRE
UNIVERSITY OF WALES SWANSEA

DYNAMIC PERFORMANCE MODELLING OF TIDAL STREAM TURBINES IN OCEAN WAVES

JAMES A. C. ORME
BEng.(Hons)

THESIS SUBMITTED TO THE UNIVERSITY OF WALES IN CANDIDATURE
FOR THE DEGREE OF DOCTOR OF PHILOSOPHY

DECEMBER 2006

ProQuest Number: 10807432

All rights reserved

INFORMATION TO ALL USERS
The quality of this reproduction is dependent upon the quality of the copy submitted.

In the unlikely event that the author did not send a complete manuscript
and there are missing pages, these will be noted. Also, if material had to be removed,
a note will indicate the deletion.

ProQuest

ProQuest 10807432

Published by ProQuest LLC (2018). Copyright of the Dissertation is held by the Author.

All rights reserved.
This work is protected against unauthorized copying under Title 17, United States Code
Microform Edition © ProQuest LLC.

ProQuest LLC.
789 East Eisenhower Parkway
P.O. Box 1346
Ann Arbor, MI 48106 – 1346

SUMMARY

The primary aim of this work is to develop a tool to predict the lifetime performance of a tidal stream turbine. This involves the experimental validation of Blade Element Momentum Theory (BEMT) and implementation of an extended model to optimise blade design and predict performance over the operating range.

Time varying non-linear upstream flows, such as wave action and velocity gradients are considered and the model is extended into the time domain to obtain the dynamic response of the rotor. In addition, to rationalise the environmental conditions that a device will encounter in its lifetime, representative sea-states and occurrences must be defined.

A 1m diameter turbine is tow tested in the River Tawe. It is monitored and controlled such that the performance can be analysed over the operating range. An automated electrical control system is also tested. The results are compared to BEMT.

The BEMT is numerically implemented and examined to determine its limitations. Off-optimum performance is considered. The model is extended to incorporate a time dependent flow field with additional velocity and acceleration terms to allow the consideration of wave kinematics. Resultant forces are defined and calculated for particular environmental conditions. Finally the results are interpreted to allow the estimation of lifetime loadings including peak loads and fatigue.

The model is validated and a good correlation is found relative to standard BEMT. It is concluded that both a velocity gradient and a wave action may significantly reduce power output whilst increasing the loads on a system. It is also concluded that a 3 bladed rotor encounters far lower loadings than a 2 bladed equivalent over the device lifetime.

It is also the intention of this study to compare and contrast various tidal stream turbine support structure concepts in terms of the suitability of each to withstand the lifetime loadings at reasonable cost. A number of support structure concepts are investigated from an impartial perspective. In conclusion there is not one concept which clearly surpasses the others in all areas.

ACKNOWLEDGEMENTS

This work was funded jointly by the *Welsh Assembly Government Knowledge Exploitation Fund* and a Doctoral Training Grant from the *Engineering and Physical Sciences Research Council.*

The author wishes to thank;

Dr Ian Masters at the School of Engineering, Swansea University, for his support, guidance and unfailing optimism.

The staff of the School of Engineering workshop who's skills and experience proved pivotal in the manufacture of the experimental turbine.

Milford Haven Port Authority for their support and advice throughout the duration of the project.

The Swanturbines team for their support and encouragement, especially in the home stretch.

Mr Roger Griffiths for inspiration, support and of course, the underlying BEMT.

Professor Arthur Lees for his encouragement and experience. Also for his efforts in understanding the rotordynamic characteristics of the experiment.

Professor John Chaplin for the use and advice on his wave kinematics software.

Dr Steve Hardy for his support and insight in stress analysis and design.

Mr Keith Naylor for his expert skills at the helm of the Noctiluca and can do attitude.

Mr Peter Matthews for patient and unwavering support in instrumenting the prototype device.

M. Christian Hilario for his dedicated work in the area of electrical system construction.

Mr John Chapman as someone who knows the finer details of turbine modelling and for providing confidence through validation.

Mr Gareth Stockman for his technical input, design and practical assembly skills.

Ian Rees for his machining skills and unrivaled lifting ability.

Finally to my parents, for their unswerving support, years of direction, gentle pressure and pride. For all the skills imparted from communication to confidence, I thank you.

CONTENTS

NOMENCLATURE ..... **vi**

1.0 INTRODUCTION **1**
1.1 Achievements **3**
1.2 References **4**

2.0 LITERATURE REVIEW **5**
2.1 Introduction **5**
2.2 Technology Overview **6**
2.2.1 Historical Context 6
2.2.2 Design Factors 7
2.2.2.1 Resource 7
2.2.3 Rotor design 10
2.2.4 Support Structures 19
2.3 Technical Solutions **21**
2.3.1 Research 21
2.3.2 Proof of concept 24
2.3.3 Demonstrations 26
2.3.4 Proposed full scale system 28
2.4 Blade Element Momentum Theory **29**
2.4.1 Origins of BEMT 29
2.4.2 BEMT applied to wind turbines 29
2.4.3 Experimental validation of BEMT 30
2.4.4 Limitations of BEMT 31
2.4.5 Stall delay 32
2.5 Conclusions **34**
2.6 References 35

3.0 EXPERIMENTAL DESIGN AND INVESTIGATION **38**
3.1 Introduction **38**
3.2 Objective **38**
3.3 Design of the System **39**
3.3.1 Diameter 39
3.3.2 Generator 40
3.3.3 Blade Design 42
3.3.3.1 Design tip speed ratio (TSR) 42
3.3.3.2 Aerofoil selection 44

3.3.3.3 Aerofoil detailed specification 44
3.3.3.4 Aerofoil characteristics 46
3.3.3.5 Blade number 47
3.3.3.6 Chord and twist distribution 47
3.3.4 Blade construction 49
3.3.4.1 Computer Aided Design 49
3.3.4.2 Plug construction - Rapid prototyping 51
3.3.4.3 Mould construction 52
3.3.4.4 Stainless spar 52
3.3.4.5 Joining and finishing 53
3.3.5 Chassis and nacelle 54
3.3.5.1 System Layout 54
3.3.5.2 Shaft 54
3.3.5.3 Bearings 54
3.3.5.4 Coupling and torque monitoring 54
3.3.5.5 Braking System 55
3.3.5.6 Sealing system 55
3.3.5.7 Bilge system 56
3.3.6 Electrical system 58
3.3.6.1 Proven Controller 58
3.3.6.2 Power box 58
3.3.6.3 Data box 60
3.3.6.4 Data logger 60
3.3.6.5 Frequency voltage converter 60
3.3.6.6 Batteries 60
3.3.6.7 Inverter 61
3.3.6.8 Divert loads 61
3.4 Experimental procedure 63
3.4.1 Overview 63
3.4.2 Vessel and test conditions 63
3.4.2.1 RV Noctiluca 63
3.4.2.2 River Tawe 64
3.4.3 Installation 64
3.4.4 Dunk test 66
3.4.5 Flow measurement 66
3.4.6 Experimental runs 67
3.5 Experimental results 69
3.5.1 Analysis 69
3.5.2 Sampling Frequency 70
3.5.3 Statistical Analysis 70

3.5.4 Performance analysis 71
3.5.4.1 Electrical performance 71
3.5.4.2 Rotor power and torque coefficients Cp and Ct 72
3.5.4.3 Blade number 73
3.6 Conclusions 76
3.7 References 77

4.0 DETAILED BLADE MODELLING 78
4.1 Blade element momentum theory 78
4.1.1 Addition of flow rotation 79
4.1.2 Optimisation of blade design 82
4.1.3 Real fluid effects 83
4.1.4 Estimation of performance characteristics 84
4.1.5 Estimation of aerofoil characteristics 85
4.2 Optimisation of blade geometry 91
4.2.1 Implementation 91
4.2.2 Issues with the method 92
4.2.3 Results 93
4.2.4. Conclusions 98
4.3 Performance prediction 99
4.3.1 Implementation 99
4.4 Results 106
4.4.1 Torque 107
4.4.2 Power 108
4.4.3 Axial force 109
4.4.4 Interference factors a & b 110
4.4.5 Effective angle of attack 112
4.4.6. Torque and Axial force 113
4.5 Discussion 115
4.5.1 Assumption and limitations 115
4.5.2 Rotor performance 116
4.5.3 Irregularities 116
4.6 Conclusions 118
4.7 References 119

5.0 EXTENSION OF BLADE MODEL FOR DYNAMIC LOAD ESTIMATION 120
5.1 Introduction 120
5.2 Background 120
5.2.1 Wave kinematics 121
5.2.2 Stream function theory 123

5.2.3 Solution of the stream function 125
5.2.4 Morison's equation 126
5.3 Formulation of a dynamic model 129
5.3.1 Addition of time dependent vector flow field 129
5.3.2 Dynamic time step 129
5.3.2.1 Generator torque reaction 129
5.3.2.2 Rotor inertia 130
5.3.2.3 Rotor speed 132
5.3.3 Addition of depth characteristics 132
5.3.3.1 Location of blade element 132
5.3.3.2 Summary of assumptions 133
5.3.3.3 Velocity gradient 133
5.3.4 Addition of wave characteristics 135
5.3.4.1 Typical wave characteristics 135
5.3.4.2 Vector flow field applied to each element 138
5.3.4.3 Effect of wave flow effects 138
5.3.4.4 Axial velocity 139
5.3.4.5 Vertical velocity 140
5.3.4.6 Axial acceleration 140
5.3.4.7 Vertical acceleration 142
5.3.5 Outputs 144
5.3.5.1 Torque and Axial Force 144
5.3.5.2 Yaw, Teeter and Heave 145
5.4 Implementation 148
5.4.1 Input parameters 149
5.4.1.1 Tidal Velocity Regime 149
5.4.1.2 Wave Climate Analysis 152
5.4.1.3 Wave data lookup 156
5.4.2 Timestep & inertia 157
5.4.3 Inputs 158
5.4.4 Outputs 158
5.4.5 Process flow chart 159
5.5 Results 160
5.5.1 Uniform flow 160
5.5.2 Velocity gradient 161
5.5.3 Wave action 162
5.5.3.1 Torque coefficient 162
5.5.3.2 Axial force coefficient 164
5.5.3.3 Yaw coefficient 166
5.5.3.4 Teeter coefficient 170

5.5.3.5 Heave coefficient 173
5.5.4 Life time loadings 175
5.5.4.1 Maximum and minimum values 175
5.5.4.2 Fatigue loads 176
5.6 Conclusions 179
5.7 References 180

6.0 ANALYSIS AND COMPARISION OF SUPPORT STRUCTURE CONCEPTS 181
6.1 Introduction 181
6.2 Background 182
6.3 Methodology 183
6.3.1 Support Specification 183
6.3.2 Comparators 184
6.3.3 Cost estimations 185
6.4 Tidal turbine concepts 189
6.4.1 Sheath system 189
6.4.2 Anchored system 190
6.4.3 Guyed tower 190
6.4.4 Top mounted nacelle 191
6.4.5 Telescopic 192
6.4.6 Shroud concept 193
6.5 Results 194
6.6 Conclusions 198
6.7 References 199

7.0 Conclusions 200
7.1 Summary 200
7.2 Significance in an industrial context 202
7.3 Recommendations 203

NOMENCLATURE

$1/n$ Velocity gradient characteristic

a Axial interference factor

α Angle of attack (degrees)

A Swept area of the rotor (m^2)

b Rotational interference factor

β Chord inclination angle $\beta = \phi + \alpha$

c Chord variation with radius (m)

C Wave speed (ms^{-1})

C_{AA} Axial coefficient of added mass

C_D Aerofoil drag coefficient

C_E Rotor overall coefficient of power

C_F Rotor axial force coefficient

C_L Aerofoil lift coefficient

C_m Coefficient of inertia

C_{mA} Axial coefficient of inertia

C_{mV} Vertical coefficient of inertia

C_P Rotor power coefficient

C_T Rotor torque coefficient

C_{TS} Starting torque coefficient

D Depth of water (m)

dD Drag force on a blade element (N)

dF_A Axial force on a blade element (N)

dF_{Ain} Axial force for a blade element owing to inertial forces (N)

dF_T Torque force on a blade element (Nm)

D_H Depth of hub (m)

dL Lift force on a blade element (N)

dr Radial thickness of a blade element (m)

dT Torque on a blade element (Nm)

dT_{in} Torque generated by a blade element owing to inertial forces assuming vertical acceleration is normal to blade (Nm)

dT_{inS} Torque generated by a blade element owing to inertial forces including sine correction (Nm)

f Velocity gradient friction factor

ϕ Twist variation with radius (deg)

F_A Rotor axial force (N)

$F_{A3(i)}$ Axial force generated by blade (i) including the effects of wave action and velocity gradient (N)

F_{AR} Axial force generated by rotor including the effects of wave action and velocity gradient (N)

γ Rotor blade angular displacement for the vertical position (rad)

γ_o Rotor blade start angle (rad)

γ_s Anglestep (rad)

γ Flow inclination angle (in section 4.3.1.1)

h Hub radius (m)

$H_{3(i)}$ Heave force generated by blade (i) including the effects of wave action and velocity gradient (Nm)

H_R Heave force generated by rotor including the effects of wave action and velocity gradient (Nm)

I_R Rotor inertia (kgm2)

k Keulegan Carpenter number

L Wave interval (m)

L_A The frontal length of the aerofoil for use with axial acceleration (m)

L_V The frontal length of the aerofoil for use with vertical acceleration (m)

M_{aA} Axial added mass coefficient per unit length

N Number of blades

$v(a,b)$ Objective function

$P_{3(i)}$ Power generated by blade (i) including the effects of wave action and velocity gradient (W)

P_R Power generated by rotor including the effects of wave action and velocity gradient (W)

P_s Shaft power (W)

Q Total constant head for a particular wave (m)

θ Effective angle of attack $\theta = \beta - \gamma$ (degrees)

r Radial position (m)

R Radius (m)

S Cross sectional area of the aerofoil section (m^2)

T Rotor torque (Nm)

$T_{3(i)}$ Torque generated by blade (i) including the effects of wave action and velocity gradient (Nm)

$Te_{3(i)}$ Teeter force generated by blade (i) including the effects of wave action and velocity gradient (Nm)

Te_R Teeter force generated by rotor including the effects of wave action and velocity gradient (Nm)

T_{inS} Torque generated by a blade element owing to inertial forces including sine adjustment (Nm)

T_R Torque generated by rotor including the effects of wave action and velocity gradient (Nm)

t_s Timestep (s)

TSR_D Design tip speed ratio

T_W Wave period (s)

u Axial velcotiy in the plane of the rotor (m/s)

U_d Flow velocity at a particular depth d (m/s)

U_L Upstream velocity local to the blade element (m/s)

U_{RATED} Rated flow speed for a turbine

U_{sf} Surface velocity (m/s)

V Local flow velocity (m/s)

V_L Sine adjusted local velocity of the fluid in the vertical direction at the plane of the rotor disc due to wave action (m/s)

ω Rotational speed of the flow well downstream of the turbine rotor ($rads^{-1}$)

Ω Rotational speed of the rotor ($rads^{-1}$)

W Wave number

W_0 Start wave number

W_s Wave step

x Local speed ratio

x_L Local speed ratio including the effect of wave action.

x/X Wave position as a fraction of wavelength

x/X_0 Initial wave position

Ψ Stream function

y Surface elevation under wave action (m)

$Y_{3(i)}$ Yaw force generated by blade (i) including the effects of wave action and velocity gradient (Nm)

Y_R Yaw force generated by rotor including the effects of wave action and velocity gradient (Nm)

1.0 INTRODUCTION

The rapidly expanding tidal stream energy industry is receiving a great deal of attention from many sectors. There is interest around the world from governments, investment groups, engineering firms and academic institutions. The climate change issue is becoming ever more prominent and renewable energy is high on the global agenda. The most recent estimates predict that tidal stream energy is set to become a £4bn industry in the UK alone with world market estimates between £115bn and £444bn [1]. The rising price of fossil fuels and increasingly serious issues of national security mean that alternative energy sources are becoming attractive. Electricity prices rose by 9.4% in real terms over the past 12 months in 2004 [2], which, in combination with Renewables Obligation Certificates (ROCs) boosts the price of wholesale electricity to 6.5p/kWh. With fossil fuels declining and the national appetite for renewables steadily increasing, the price of energy appears set to rise for the foreseeable future.

Tidal stream energy has the potential to produce 3% of UK electricity in a predictable, invisible, economic manner [3]. The Carbon Trust estimates 3000MW of installed capacity in Europe by 2020 [3]. Worldwide, in parallel to the sustained demand for electricity, the population is increasingly concentrated on the coast, with the United Nations acknowledging that about 3.2 billion people in the world were living within 100km of the sea, of which nearly 2.1 billion live in Asia [1]. In the United States, the Department of State forecasts that 75% of the population will live on the coast by 2030 whilst about 60% of the Chinese will have concentrated on the shoreline as a result of internal migration. This represents a massive potential for further industry growth.

At present the industry is still in a fledgling form. In reality only two tidal stream turbines of a meaningful size have been deployed for any length of time. These have been installed by two independent companies, Marine Current Turbines Ltd in Lynmouth, North Devon, and Hammerfest Strom AS in Hammerfest, Norway. The testing has been successful and has led to many developers emerging into the industry. The Swanturbines device is one of these under development by a company exploiting the research done at Swansea University.

Research into turbines began at Swansea University in the late 1970s when Griffiths developed the basis for wind turbine rotor design and performance prediction theory [4]. Woollard continued this work with an experimental investigation of a wind turbine in 1980 [5]. Some work was carried out by Al-bier around the same time involving the testing of wind turbine rotors in a water test tank [6]. Building on this research, Orme, Masters and Griffiths undertook an investigation into biofouling and tidal stream turbines in 2000 [7]. This led to an

opportunity to build and test a small-scale tidal turbine funded by the Welsh Assembly Government Knowledge Exploitation Fund (KEF) in 2001.

Further funding has been obtained through KEF to undertake the design and costing of a medium scale commercial demonstrator. This is a 300kW direct drive device and is intended to be installed in 2008. Further fund raising is ongoing to provide resources to build, deploy and monitor the demonstration device. Swanturbines Ltd is a company that has been set up as the vehicle for this development.

The following chapters start with a brief review of the literature relevant to the development of a tidal stream turbine performance model. This includes a historical overview of the technology in the tidal stream industry and the factors affecting the design of the devices. Blade Element Momentum theory (BEMT) is also discussed as a method used to predict the performance of axial flow rotors.

In chapter 3 an experimental test rig is then designed and tested to verify the validity of BEMT as a rotor design and performance prediction technique. A 1 metre diameter prototype is towed behind a research vessel to obtain torque and power coefficients over the operating range. A brake is used to maintain constant tip speed ratio. It is found that BEMT predicts the performance well, although Reynolds number and other effects introduce complexities which are not thoroughly understood. An investigation into the effect of varying solidity through blade number is also undertaken. It is found that lowering the solidity reduces power capture but enables the turbine to operate at a higher tip speed ratio.

In chapter 4, the numerical model is adapted such that it will analyse the performance of the device at off design conditions. This is to enable power and load prediction at various tip speed ratios. The lift and drag coefficients for the aerofoil used along the blade are estimated over 180 degrees so that start up behaviour and overspeed conditions can be accurately predicted. The results are consistent with other blade element models over most of the operating range, but at very low and high tip speed ratios some anomalies are identified.

In chapter 5, the model is then extended to incorporate non-uniform flow effects, specifically a 2 dimensional velocity gradient and wave effects. This necessitates the introduction of a dynamic, time depended model which facilitates the prediction of loads over the lifetime of the device. The variation in flow field requires the definition of extra loads; these are defined as yaw and teeter moments and heave load. These are described in terms of dimensionless coefficients. Results are generated which quantify the effects of waves on device loadings and it is shown that wave action will cause a significant variation in loads over time. This is then extended to incorporate real wave climate data and lifetime loads and frequencies are

found. A lifetime comparison of the loads on 2 and 3 bladed rotors shows that a 3 bladed rotor encounters significantly lower loads and hence will perform better in terms of fatigue.

Finally, chapter 6 details an analysis of various supporting structure concepts and a commentary on the salient issues involved in design and deployment is given. It is found that there are various factors affecting the cost of support structures which may vary from site to site. These include depth, distance to port and frequency of minor maintenance. It is concluded that no single device concept will perform best in all situations and hence it is likely that more than one device will succeed in the tidal stream energy market.

1.1 Achievements

As a result of the work presented here, the author and the Swanturbines consortium have had a number of significant successes:

1.) A journal paper entitled '*Design and testing of a direct drive tidal stream generator*', is published in the Journal of Marine Design and Operations, Proceedings of the Institute of Marine Engineering, Science and Technology No. B9, 2005/6.

2.) A conference paper entitled '*Analysis and comparison of support structure concepts for TSTs*' is published in the Proceedings of the 4th International Conference on Marine Renewable Energy, 2006

3.) A conference paper entitled '*Design and testing of a direct drive tidal stream generator*' is published in the Proceedings of the 3rd International Conference on Marine Renewable Energy, 2004

4.) A conference paper entitled 'Aspects of the performance prediction of tidal stream turbines in yawed flow' is published in the Proceedings of the NAFEMS World Congress, Vancouver, 2007.

5.) Significant funding has been accessed by Swansea University and Swanturbines Ltd using this work as the basis for application. This consists of:

- Welsh Assembly Government, KEF funding for the development of a small scale prototype, 2001. (£50k)
- Welsh Assembly Government, KEF CIRP funding for the design and development of a medium scale technology demonstrator, 2004. (£360K)

- Welsh Energy Research Centre, WERC CIRP funding for the design and development of a medium scale technology demonstrator, 2006. (£300K)
- Department of Trade and Industry, Technology Programme funding for CYGNET Stage 1, technology demonstrator deployment, 2006. (£800k)

6.) The author gave evidence on tidal stream energy at the House of Commons Welsh Affairs Select Committee - 'Energy in Wales' consultation in March 2006.

7.) Three patents have been filed as a result of this work:

Two of these were filed recently in April 2006. One discloses an arrangement of the whole device and the other specifically protects details of a support and installation system. The first, filed in 2004, patent number W0 2005/057006, discloses the direct-drive arrangement in two separate configurations, telescopic and river bank mounted.

1.2 References

1. Douglas Westwood Ltd, *Tidal Stream Industry Market Research - A report to Swansea University.* 2006.
2. Royal Academy of Engineering, *The Costs of Generating Electricity.* ISBN 1-903496-11-X, 2004.
3. Callaghan J, R. Boud, *Future Marine Energy.* Carbon Trust, UK, Jan 2006.
4. Griffiths RT, Woollard MG, *Performance of the optimal wind turbine.* Applied Energy 4, Applied Science Publishers Ltd, 1978.
5. Woollard MG, *PhD Thesis: 'A design study for and experimental horizontal axis wind turbine'.* 1980.
6. Al-Bier MY, *Towing tank tests on model wind turbines.* University of Wales Swansea internal report, 1978.
7. Orme JAC, Masters I. Griffiths RT, *Investigation of the effect of biofouling on the efficiency of marine current turbines.* Proceedings of the 1st International Conference on Marine Renewable Energy, 2002.

2.0 LITERATURE REVIEW

2.1 Introduction

Tidal power has been used to power machinery for nearly a thousand years and some examples of original systems still exist [1]. But the relatively recent idea of using the motion of the water without restricting the flow with a barrage [2] is under development. Tidal stream energy uses the currents found around the coastline to generate electricity, much in the same way that a wind turbine uses wind [3].

The potential of tidal stream energy is the focus of extensive investigations[4-14]. World estimates of the total resource range from 22PWh/y to 29PWh/y, but it is only possible to extract a fraction of this and the recoverable world resource is estimated at between 620TWhpa and 1,775TWhpa [15]. Although more recent estimates are lower at 120TWhpa [6] and there is a large variation in resource estimations, the consistently high figures show that it is significant.

In 1996, the potential in the UK and Europe was estimated as 48TWhpa [12]. Owing to the recent interest in the UK, a report commissioned by the Carbon Trust has estimated the economically extractable resource as 18TWhpa which would provide 3% of UK electricity[9].

Owing to the great potential for a growth industry in the UK and the export market, political support for tidal stream energy is growing rapidly. The recent UK Energy Review [16] gives support to the industry, and the Scottish Executive [17] is very keen to encourage commercial deployment in terms of increased Renewables Obligation subsidy. Following the ROS consultation 2006, the Welsh Assembly Government has also issued a statement of strong support in the Welsh Affairs Select Committee Energy in Wales report [18].

This same excitement is being felt by the emerging industry with numerous tidal developers coming forward with technology. The World Wave and Tidal Database [19] contains records of 26 tidal developers, and at least another 10 which are not included have devices planned. In the UK the current market leaders are Swanturbines [20], Marine Current Turbines [21], Lunar Energy [22], and SMD Hydrovision [23]. The

concepts are quite diverse and the main variations are in the areas of support structure, deployment method and power conversion format.

It is thought that the technology in the tidal stream industry will converge to a particular design [9] and this will provide economic advantages in terms of rationalisation of components in a similar way to the wind industry. The present leading devices are all axial flow turbines and it might be suggested that this is an indicator of what form the converged design may take. Thus an accurate performance model for this type of turbine will be extremely valuable.

The review of literature will present an overview of the technology under development to date with a focus on design drivers and key components. The technical solutions that have been tested or are under testing are explained along with some of the proposals for future developments. Finally an introduction to blade element momentum theory is given with the origins and applications to date.

2.2 Technology Overview

2.2.1 Historical Context

Tidal stream and river current generation is designed to extract energy with minimum environmental impact and low initial investment. It was first considered on a commercial scale in the early 1970s at the 1974 MacArthur Workshop [24] where an initial feasibility is undertaken. In 1976 Wyman [25]concluded that the principle deserves consideration as an insurance technology. The first experiments appear to have been conducted between 1976 and 1984 by IT Power in Egypt [26] in which a turbine was placed in a river for 2 years, and it was realised that there was potential for large scale generation. And in the 1970s Ampair [27] released a small turbine to provide power for river craft. In the US Congress 1978 [28] a theoretical evaluation from MacArthur was presented focussing on larger schemes planned for the Florida current.

The main focus of the research to date has been to develop the technology in terms of deployment strategy and other practicalities such as survivability. Thus far, the literature available regarding detailed performance and load modelling is relatively sparse.

Substantial work is being undertaken in terms of array modelling and resource evaluation, but the theory used to predict individual turbine performance is limited.

2.2.2 Design Factors

2.2.2.1 Resource

In 1979 Musgrove and Fraenkel [29] undertook an evaluation of the UK potential. They conclude that tidal stream is a high density power source that could provide 6% of the UK's energy needs.

In Macnaughton et al [30], a number of locations to site a prototype system were investigated and ranked in order of preference. The site requirements are convenient access and a maximum flow rate of 2m/s in a depth of 12-20m. There also needs to be sufficient flow speed without interfering with shipping. If it is visible from the land is an advantage as telemetry can then be transmitted to shore. The site that was chosen is Corran Narrows which is a constriction in Loch Linnhe in Scotland. It is particularly suited and has a line of sight telemetry link to a lighthouse.

Around this time, a European Commission initiative called JOULE supported research and development into renewable energy projects. The section designated to Tidal and Marine Currents Energy Exploitation is CENEX [31]and is authored by Technomare SpA and IT Power Ltd. It examines the resource, economics and technology of extracting this energy and some detail with regard to the theory of turbine operation and the design of a conceptual 1MW unit is presented. Paish summarises the EU JOULE research programme [32]. It concludes that the European resource is 48TW/year at 106 locations and that the best way for the industry to proceed is to build a prototype at a meaningful scale.

The assessment of the potential of the European tidal resource has become a matter of much further work with two primary methods being used. These are the farm and flux methods and are described by Black and Veatch[6]. Essentially the difference between the methods arises from the lack of information concerning the effect of energy extraction on the flow. The farm approach assumes that the power output of a particular site is dependent on the device size, efficiency and packing density. Black and Veatch [6] find that this method is not accurate and has the tendency to over estimate the resource as it does not take account of the energy extracted from the flow. A new

approach is developed by Black and Veatch and Robert Gordon University (RGU) which incorporates a Significant Impact Factor (SIF). The SIF is factored in to the total energy to give the extractable resource as a proportion of the total. This development is based on modelling by Bryden [33] which suggests that the amount of energy extractable will depend on the type of site. Sites governed by a head difference that is not dependent on the flow through the site, such as the Orkney Channels will have a much lower SIF than those sites where the head is dependent on the flow of water such as the flow at the entry to a sea loch. In this study an initial estimate is made for a general SIF of 20% to be applied for all sites. Phase I and Phase II of these reports do vary slightly owing to a number of refinements in Phase II. In Phase I the technically extractable resource is estimated at 22TWhpa and in Phase II this is reduced to 18TWhpa.

The most recent report has been published by the Carbon Trust [9] and utilises a predictive model to estimate the rate or exploitation of the resource. It estimates that the installed capacity of tidal stream turbines will be between 1000MW and 2500MW by 2020. If a utilisation factor of 0.4 is applied to this, it represents an annual power output of 3.5TWh and 8.8TWh.

Work headed by Ian Bryden at Edinburgh University is the most advanced in terms of array modelling and the effect that energy extraction has on the flow itself. In partnership with Professor Peter Fraenkel of Marine Current Turbines Ltd, Robert Gordon University and Heriot-Watt University, Bryden has developed shallow water equations to incorporate energy extraction in terms of a retarding force. No attention is given to the local hydrodynamics as the intention is to investigate the physics of large scale energy extraction from tidal flows. The most relevant paper; Couch and Bryden [34], were briefly examined and conclude that only in the most extreme cases will blockage owing to the installation of a tidal array be as severe as to substantially reduce the power output of the array. Bryden's work assumes that the power extraction characteristics are simple in terms of power extracted from a particular cell of the model and no attempt is made to estimate detailed time-dependent loadings or power outputs with flow fluctuations.

2.2.2.1.1 Velocity profile

CENEX [31], considers the effect of the surface to seabed velocity profile on current flow. A standard $1/7^{th}$ power law is used to estimate the variation of velocity with depth.

It is concluded that the vertical velocity profile is critical to determining the size of a marine rotor and that over 75% of the energy is in the upper 50% of the flow.

It is stated that in tidal areas there is often a variation in water depth and the velocity profile is not constant. In some places, the variation is amplified by marine topography and in others is it cancelled out. This is considered to be another site specific variable and must be taken into account when determining rotor diameter. To avoid extreme forces and the risk of collision, the rotor must remain submerged during the lowest tides and beneath the draught of any shipping in the area.

2.2.2.1.2 Wave Action

Wave action is said to be important in CENEX [31] as surface and subsurface waves can generate extreme loadings on the structure. The guidelines supplied by the UK Department of Energy [35] on the design of offshore structures are implemented here. The change in depth caused by wave action is recommended to be considered when deciding upon the size of the rotor, so that it does not pierce the surface in the lowest wave troughs. Wave action is not considered in any more detail.

2.2.2.1.3 Other Factors

In CENEX [31] it is stated that the condition and strength properties of the seabed are very important when considering mooring methods. It is thought that owing to the rapid currents present in areas suitable for marine current extraction, the majority of softer materials such as silt and clay will be eroded away. This implies that the seabed in these places is likely to be rock and gravel.

Marine growth is discussed in a general form. Typical fouling species are listed and it is stated that the abundance of such species is dependent on the supply of oxygen and food. For this reason it is thought that the splash and intertidal zones are particularly vulnerable to fouling. It is thought that the fouling rate will be low owing to the velocity of the current. However, species such as barnacles and hydroids will increase the surface roughness of the structure and it is stated here that this will increase the drag force in the structure and the efficiency of the blades will be particularly affected. This is discussed further by Orme and Masters [36].

The final environmental consideration mentioned is hazard to shipping. This also includes similar activities such as leisure and fishing. It is important that these devices do not cause danger to other marine users. Either they should be deployed in an area where no hazards are present, or they should be designed to mitigate the risks to other such activities, or alternatively, an exclusion zone can be placed around the installation.

2.2.3 Rotor design

The design of a tidal turbine rotor can be considered in much the same way as a wind turbine. However there are a few important differences resulting from the environmental conditions. There is a significant amount of literature concerning the differences and similarities and a review of the issues is presented here.

Firstly rotor performance characteristics must be defined. They are assessed using dimensionless coefficients of torque, axial force and power. This enables different rotors to be compared under different conditions. The primary performance coefficients are defined therefore defined as:

$$C_T = \frac{T}{\frac{1}{2}\rho ARU^2}$$

$$C_F = \frac{F_A}{\frac{1}{2}\rho AU^2}$$

$$C_P = \frac{P_S}{\frac{1}{2}\rho AU^3}$$

Also , tip speed ratio (TSR) is a quantity that allows the assessment of a flow regime regardless of the flow speed and rotational velocity. This is defined as:

$$TSR = \frac{r\Omega}{U}$$

In Macnaughton et al [30], the design of the rotor is undertaken using the same approach as wind turbines. Some differences are noted including the magnitude of structural forces on the rotor. In wind turbines the primary forces are due to centripetal forces and gravity. In tidal stream turbines the rotor blades are smaller and the gravity is reduced by the effects of buoyancy. Hence the dominating forces are hydrodynamic forces caused by lift and drag on the rotor. To obtain the required 10kW, the diameter of the turbine is designed to be 3.5m. To avoid cavitation, the tip speed must be limited to 8m/s. This theoretically avoids the risk of cavitation and in a flow speed of 2m/s, limits the tip speed ratio to 4. A 2-bladed configuration was selected as this gives a low blade aspect ratio, i.e. short, fat blades. These are intended to be easier to handle and more robust than greater blade number configurations. They are constructed from 2 piece aluminium castings.

The reference rotor used in CENEX [31] is fixed pitch, coupled to a constant speed generator. This can then be either an axial or vertical axis machine, and allows a reasonable comparison of both. The fixed pitch of the blades results in a theoretical efficiency curve as shown in Figure 2.01. This shows how the Power Coefficient C_p varies with the flow speed relative to the design flow speed. With a constant speed device such as this, U/U_{RATED} is inversely proportional to relative tip speed ratio.

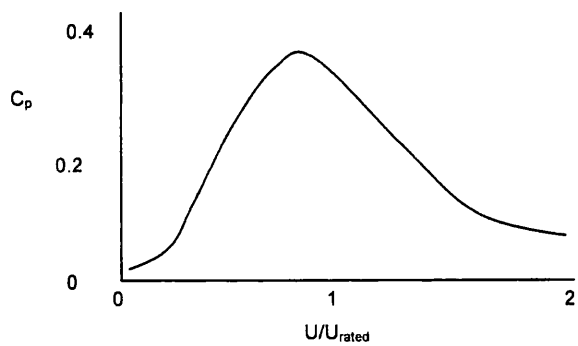

Figure 2.01 - Power coefficient for CENEX reference rotor

In this curve, there is a peak just before the design speed followed by a sharp decrease in performance. U_{rated} is defined here as the flow velocity at a particular site with an exceedence of 20%. This means that the velocity at the site exceeds this value for 20% of the time. A Load Factor is also defined here as being the ratio between the average annual power and the rated power. This value is greatly affected by the exceedence curve which is specific to the site.

The technical factors affecting the design of the turbine are considered, the first being the operating range of current velocities. The relationship between diameter, power and thrust is discussed. It is stated that for a specified power output, a higher velocity and hence a smaller diameter, results in lower thrust forces on the structure and hence is more economical. It is concluded here that a peak flow of between 2 and 3 m/s is a good design speed as locations with speeds like this are common, they have a high energy density and higher speeds make it difficult to avoid cavitation.

To qualify the previous discussions on depth of water and rotor size, two approaches are presented to determine the maximum allowable rotor size. The first is a pessimistic approach taken from the DTI Tidal Stream Energy Review [14] that assumes that shipping is allowed into the area containing the turbines. Because of this the uppermost tip of the rotor must be at least 9m below the LAT, (Lowest Astronomical Tide). A more optimistic approach suggests that if an exclusion zone is enforced around the turbines, an alternative rule can be implied in which the rotor diameter is half the depth, and the rotor centre is positioned at half depth.

Extreme loading conditions come from various environmental factors and they are discussed briefly here. It is recommended that the criteria developed for designing offshore structures be applied.

At the Sustainable Energy Research Group Marine Energy Project in Southampton, Bahaj [37] has undertaken substantial work in the area of tidal turbines, array studies and some work on performance experimentation.

An initial analysis on the issues which will affect the operation of TSTs is presented by Bahaj and Myers [38]. In addition to qualifying the potential of these devices for baseload supply, areas for future investigation are cited including the validation of practical rotor designs, loadings with yaw misalignment and the electrical performance of scale turbines.

An overview of the current state of research into turbine performance modelling, resource modelling and cavitation is given by Bahaj [4]. It is stated that Blade Element Momentum Theory BEMT and cavitation analysis can be used to predict the performance of blades for TSTs but current limitations include the effect of turbulence, fixings and moorings of the structure. The performance characteristics are predicted in more detail in Batten [39], where a clear account of the design and performance validation of a marine rotor is given. Various aerofoil sections are applied to a notional

blade shape and the performance of the rotor is then predicted over the operational range. Power characteristics are predicted for two angles of attack and over a velocity range. It is concluded that BEMT is suitable for modelling TSTs owing to the narrow blades and near 2D flow. However the acceptable level of cavitation and adjustment for non-linear flow such as wave action has not been specified.

2.2.3.1 Horizontal or vertical axis rotors

A theme in the early development of wind turbines was the debate concerning whether vertical or horizontal axis turbine rotors are more suitable for commercial use. It is clear that in the wind industry, horizontal axis wind turbines (HAWTs) dominate the market. However, it is possible that in tidal stream the advantages offered by a vertical axis device may favour its use.

Musgrove & Fraenkel [29] suggest that the Darrieus type rotor provides a simple and efficient means to collect that energy although no detailed performance evaluation is presented.

Paish [40] reports on the Scottish Nuclear project in a separate paper in which work to date on tidal flow energy extraction is summarised. Some of the reasons that an axial flow propeller turbine was chosen for the Scottish Nuclear experiment are stated. The first is that an axial flow turbine is fully self starting whereas Darrieus type turbines require assistance. Axial flow turbines are also efficient over a wide range of tip speed ratios enabling them to operate at fixed speed in different flow speeds. Additionally, they are already well understood from wind turbine applications. They are also less sensitive to lift drag ratio than the vertical axis type and hence are less sensitive to marine growth and surface finish. The final advantage mentioned is also very important; the cavitation encountered by aerofoils in underwater applications first occurs only at the tip in axial flow turbines implying that most of the blade remains unaffected. In Darrieus type cavitation occurs simultaneously along the blade meaning that there is a severe and instantaneous loss of efficiency.

The reference rotor in CENEX [31] is a fixed blade pitch constant speed generator type. Within this category are a number of different configurations. A section is devoted to system concepts to explore these configurations. The primary variable is rotor type as this affects the entire system. Axial and Darrieus rotors are the only two to have a high enough efficiency to be considered. Both types of rotor can be arranged to have fixed or

variable pitch blades and can be augmented to include a duct to increase the flow velocity through the rotor. It is assumed here that in the case of tidal flows the rotor is operating primarily in two directions at 180 degrees from one another. Consequently some method of enabling the rotor to operate in both directions must be employed. The Darrieus rotor generally rotates about a vertical axis and therefore can be utilised to generate from a flow from any direction. The axial rotor requires a mechanism to reorient it. Three possibilities are discussed here, in the form of yawing the rotor head about the vertical axis, pitching it about an axis perpendicular to the flow and pitching the blades around their centre of pressures to reverse the direction of operation.

The engineering study CENEX [31] includes information regarding rotor parameters and some theory is presented. The maximum practical coefficient of power for both axial and Darrieus is quoted as 0.4.

This figure is taken from the wind industry, and it is also stated that axial flow rotors may be slightly more efficient but no reasoning is included. An example Cp TSR curve is given although no details of the calculation are shown. It is also of note that this curve corresponds to the previously defined Cp and relative velocity curve. The two curves inversely represent the same thing and although neither is quantitative. They are clearly different shapes, the most obvious difference being that the maximum Cp is 0.34 on one curve and 0.4 on the other, implying that neither is presented as reliable.

It is stated that axial flow turbines can be designed to operate with an optimum TSR of 1-10. The cross flow rotors are much more limited with the TSR in the range of 3-5. Varying the pitch of the blades can move the point at which Cp is optimum. Variable pitch is mentioned here for both types of turbine as a means of increasing the operating range.

A presentation of the basic theoretical performance calculations is given, with a theoretical dimensional graph of rotor speed against shaft power output. This is of a similar form to that given in Paish [40]. It is stated that this graph applies to a vertical axis turbine with the same swept area and it is only intended to provide typical values rather than a specific characteristic.

A proposal for a vertical axis turbine is presented by Salter [41]. The general arrangement of the moored floating design is shown in Figure 2.02. The primary conceptual advantages of a vertical axis rotor are stated by Salter [42] and are that:

- A vertical axis rotor (VAR) allows a large diameter rotor in shallow water.
- VARs can generate energy from flows in any direction without a yawing mechanism.
- Generation plant can be above the surface and so is easily accessible.
- Blades can have a constant cross section which makes them inexpensive to manufacture.

The proposed idea has a toroidal floating ring on the diameter of the top of the rotor blades. This floats the device on the surface. The mooring is then taken from a central section which resists the torque loading. The power takeoff is proposed as a hydraulic ring cam system.

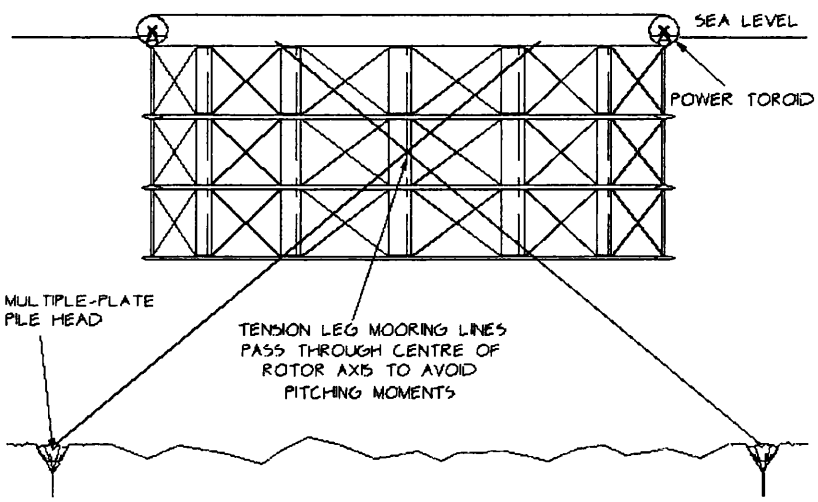

Figure 2.02 – Professor Salter's proposed tidal stream device [41]

Salter [42] states that pitch controlled blades will be needed to ensure the efficient operation of the system and a method is proposed. It is worth noting that the proposed device is shown as having 12 blades and that any pitching mechanism will have significant complexity.

It seems from the information available that vertical or horizontal axis machines could be used for the extraction of tidal stream energy. It is likely that the market will decide which format will become the most common form in use.

2.2.3.2 Yaw capability

Initial studies of tidal streams indicate that, unlike wind, the direction from which tidal streams originate is much more predictable. This offers a potential opportunity for cost saving with regard to the yawing system. This has not been validated by flow measurements at the time of writing.

A theoretical design of the 1MW unit is undertaken in CENEX [31] with regard to the environmental conditions. A qualitative study is undertaken with a comprehensive list of considerations. The first being the tidal ellipse and the effect on turbine design. In agreement with Paish [32], it is stated that the effect of the tidal velocity vector pattern is to determine the requirement for a yawing mechanism. It is stated that, in most cases, turbines can be designed to operate uni-directionally, with the flow directions 180 degrees apart.

However, Bahaj [43] has undertaken 2D modelling of the tidal currents around Portland Bill which clearly shows a 90 degree variation in the tidal velocity. In this situation a yawing mechanism would offer clear advantages.

Further work needs to be undertaken to ascertain how much of the available resource has an appreciable variation in inflow angle and under what circumstances will yaw devices be viable in a cost benefit analysis.

2.2.3.3 Cavitation

One of the major differences between wind and tidal turbine rotor design is the issue of cavitation. Cavitation is a factor in any hydraulic power application to prolong the lifetime of a device and it must be controlled and mitigated. It also may play a part in reducing the efficiency of the device and hence has further economic ramifications.

Cavitation is mentioned in CENEX [31], and it is suggested that the first generation systems will limit their tip speeds to 7m/s in an attempt to avoid cavitation. However, it is noted that this limitation creates slower rotational speeds and hence higher torque and drive train costs. Ships' propellers operate at speeds much higher than this, requiring special designs and advanced materials.

The issue of cavitation,has been studied in some detail by Molland, Bahaj, Chaplin and Batten [44]. An aerofoil section was tested in the cavitation tunnel to observe the pressure distribution and determine the cavitation inception point. The results of this test were used to validate results obtained from the predictive 2D aerofoil code XFoil [45] which uses the panel method to estimate the pressure distribution over the aerofoil surface. It was found that the experimental data matched the predicted data closely giving confidence in the code. Of some importance is the omission of 3D flow effects which greatly influence the behaviour of the fluid through an axial flow turbine.

So although further work is being undertaken to quantify the effects and energy lost in detail, it appears that cavitation will be able to be mitigated by limiting the tip speed of a device. Further work is required to ensure that rotor blades are not adversely affected by cavity impingement.

2.2.3.4 Power take-off options

As is found in the wind industry, there are various options for converting the energy of the fluid into electrical energy. At the time of writing there are even more varied options in tidal stream energy, presumably due to the earlier stage of industry development. Although there appears to be only one thorough account of an experimental system, many generation formats are described in outline.

The most unusual of these is the Engineering Business Stingray concept [46] with an oscillating hydrofoil and hydraulic power take-off. This uses the reciprocating action of a hydrofoil to drive a hydraulic pump. The power is transmitted hydraulically to a hydraulic motor which drives an electrical generator. This system is partially mirrored in the concept proposed by Tidal Hydraulic Generators Ltd [47] which uses rotary turbines to drive the hydraulic pumps. However, hydraulics aside, there are two primary issues concerning the generation format of tidal stream turbines, namely gears and electricity type. The challenge is to transfer the energy from the rotating shaft into electrical energy in the most cost effective manner. This involves efficiency, versatility of operating conditions and reliability.

The standard wind turbine format, which uses a constant speed system, a gearbox and a field coil type high speed generator, is used in MCT's Seaflow concept [21]. However in the wind industry, persistent problems with gearboxes suggest that downtime could

be reduced by 33% if a gearless solution is employed [48]. Enercon GMBH [49] have developed a gearless generator which now commands nearly half of the German market, the biggest in Europe. A gearless tidal system has been proposed by Swanturbines Ltd [20] and another by Open Hydro [50]. The Swanturbines device uses a permanent magnet, radial flux generator directly coupled to the shaft. The Open Hydro system uses a rim generator with the rotor blades in the centre. Cost benefit studies are currently being undertaken by the companies but no data on efficiency or cost is currently available. It is also known that power is generally transmitted from wind turbines at high voltage and alternating current, Grainger [51]. This may or may not be suitable for use in tidal stream systems. A high voltage DC link has been proposed for some systems which will reduce the need for offshore power electronics, Swanturbines Ltd [20].

Macnaughton et al [30] report on the Loch Linnhe project. The gearbox used is a 25:1 two stage epicyclic with an external thrust bearing to absorb the axial force from the rotor. The electricity produced is dumped into heaters and consequently the generator was easily controlled to enable the rotor to run under different load cases. Some of the power was diverted to power the telemetry and monitoring equipment.

A standard 10kW, 415V, asynchronous alternator is used via a coupling as the main generator and a secondary belt-driven 24V marine alternator is used to maintain battery charge. The electrical system is simple. There is no grid connection and the alternator is directly attached to heaters that are capable of dissipating 18kW. The alternator is also capable of running in overspeed, it is of standard type but has had its normal voltage regulator removed and the field coils are excited by the batteries via a bespoke control system. The control adjusts the field coils to achieve the required level of power dissipation in the heaters. The battery is maintained by the secondary alternator; this is essential to run instrumentation and navigation lights in the event of turbine malfunction.

2.2.4 Support Structures

In Macnaughton et al [30], various options for the technology are considered relating to all aspects of the system and a detailed description of the design solution is presented. The rotor is automatically orientated into the flow by trailing it downstream of the structure.

In CENEX [31] the authors also state that corrosion, installation methods and inspection maintenance and repair be considered early on in the design process. A similar analysis is undertaken by Orme and Masters [52]. The viability of the design is critically dependent upon the techniques used for installation and maintenance. A study is undertaken in CENEX [31] to analyse different techniques. Two basic categories are summarised; the seabed mounted and moored-buoyant configurations. Subcategories of the seabed mounted type are piled and gravity based structures. Piled versions require one or more piles to be drilled or sunk into the seabed to provide a firm anchor to resist bending and sliding forces. Gravity based systems are secured by means of self-weight only. Pile mounted structures are less massive than the gravity base type, but the single pile type are limited to about 30m depth if they are to be surface piercing. The depth can be increased if triangular combination pilings are used; however this incurs considerable extra expense. Gravity bases are constructed of steel or concrete and can be floated into position then sunk and filled with rock. The existing gravity structures fabricated for huge platforms in the North Sea are not considered suitable, although smaller units could be investigated.

Buoyant moored structures are said to have greater flexibility with respect to water depth. The main element that changes with depth is the length and size of the mooring line. In very shallow water there may be lack of height to give the catenary weight. Conversely, in deep water the weight of the line may become excessive. It may be necessary to provide redundant lines to act in the event of line failure.

It is concluded that a pile mounted, surface piercing device is preferable in shallow water and a moored buoy type for deeper locations. Either an axial flow or Darrieus type turbine could be used.

An engineering study then is undertaken to design the structure and turbine. A detailed analysis of each of the above concepts is undertaken. For a depth of 20-30m, a monopile concept is used. A pile of 2m diameter and 50mm wall thickness is chosen from standard sizes. It is intended to be surface piercing for maintenance operations. It

is likely that the seabed will be hard owing to the speed of the current and consequent erosion by scour. Because of this it is unlikely that a hammered pile will be possible, hence a drill and grout procedure would be necessary. Unlike a hammered pile which cannot be guaranteed to leave the seabed at a precisely vertical trajectory, a grouted pile can be levelled during installation. Because of this, the rotor can be affixed to the pile directly without any need for a levelling clamp or device.

For depths of 30-60m, a multiple pile system with a tripod tower can be used. It is not stated exactly why the tripod structure is required. However it does say that it is more suitable than the monopile for deeper waters with a hard seabed and it may be able to support a larger diameter rotor. However this concept requires much greater complexity of fabrication.

For deeper water, buoyant structures are recommended. This case study shows a moored barge with two rotors suspended on vertical columns at either end. The maximum trim displacement allowed is 10 degrees. The mooring could be either catenary or taught line and in either case 4 to 6 lines should be considered. Installation would occur in two stages. The moorings would be installed in advance, and then the barge, complete with turbines, can be towed out and the mooring can be picked up. The turbines would then be lowered into position.

2.3 Technical Solutions

2.3.1 Research

In 1979 Musgrove and Fraenkel [29] undertook an evaluation of the technology. A 1m diameter vertical axis turbine was tested experimentally. Drag plates were used to load the rotor. These were mounted outboard of the blades and consequently interacted with the flow through the turbine. For this reason the results of the testing were pessimistic. The power coefficient was measured at a maximum of 0.4 although the onset of cavitation at higher flow speeds (3.5kts) reduces this dramatically to 0.2.

Macnaughton et al [30]report on what they believe to be the first serious attempt to develop a tidal stream power generator in 1993. Scottish Nuclear Ltd, IT Power and NEL (National Engineering Laboratory) initiated the design and manufacture and testing of a basic 10kW device. The specification was to produce 10kW in a current of 2m/s for a limited test period of 2-3 months.

The general system configuration is shown in the diagram below,

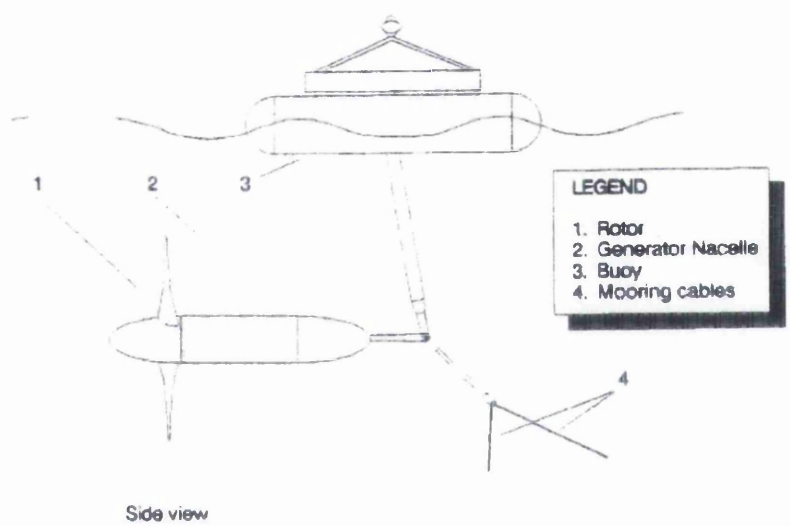

Figure 2.03 - System layout of IT Power's Loch Linnhe test [30]

The rotor is mounted 5m beneath the surface, suspended from the buoy which is anchored to the seabed. The system consists of a twin hulled 5m length, 1m diameter buoy with twin gravity anchors and a semi-catenary mooring. All of the instrumentation and electronics are onboard the buoy. The tubular member attaching the nacelle to the mooring carries both the torque and thrust from the rotor. The torque capacity is 3kNm.

The rotor and nacelle weigh 1.5 tonnes and are slightly positively buoyant to permit maintenance by floating the unit to the surface.

The nacelle consists of 3 parts; the upstream section is polystyrene filled, the mid section houses the generator and gearbox, which is then connected to the hub. A pair of PTFE radial lip seals on a stainless steel journal bearing are used as the primary rotating seal with grease packed between the seals. It is noted that alternative sealing methods maybe required for larger more permanent systems – a bilge system and positive pressure inert gas are suggested.

The results of the experiment are published in Paish [40] in a simple form and experimentally determined performance curves are included. The primary results are 10kW shaft power at the rated 2m/s and 17kW at 2.5m/s. This gives an average power coefficient at the rated speed of 0.26, decreasing to 0.23 at 2.5m/s. It can be inferred from their data that the efficiency of the electrical system is approximately 0.7.

Two institutions have published papers regarding testing of scale turbines, these are Swansea University and the University of Southampton. Orme and Masters at Swansea University have published a number of papers concerning the testing of a small scale turbine [53], and biofouling of marine rotors[36]. The results presented Orme [52] and Orme [53] are derived from the experiment described in this thesis.

An experimental investigation into marine rotors has been undertaken and is described by Myers and Bahaj at Southampton, [54] and [55]. A 0.4m diameter 1/30 scale turbine was tested in a recirculating water channel. The performance characteristics and wake effects were observed and although the effects may have been exaggerated by the effect of scale, it is concluded that similar observations will be made on full scale devices. The surface elevation was found to increase at a point just upstream of the rotor plane owing to blockage effect. It is concluded that further work needs to be undertaken to explore the effects and to determine if they are caused by the limitations of the laboratory test section. Myers and Bahaj infer that the rise in surface elevation could lead to a reduction in the required rotor / surface clearance, consequently allowing a larger rotor to be used for a particular depth of channel.

Myers [55] undertakes further testing on the 1/30 scale rotor is presented at differing yaw angles and flow speeds. The hydrodynamic performance is predicted using the commercial wind turbine code, 'Bladed' [56] using two dimensional aerofoil data from 'Visualfoil' [57]. Pre stall data is generated using panel method boundary layer analysis.

For post-stall data, three sets of equations are used to predict the lift and drag characteristics of the aerofoil in an attempt to compare different methods. The first is flat plate theory, where C_L and C_D, the lift and drag coefficients of the aerofoil respectively, are calculated in terms of a simple trigonometrical relationship with alpha. The second are Viterna-Corrigan [58] post stall equations which estimate C_L and C_D relative to alpha by combining C_D at stall, with C_D at α = 90 in a proportion relative to angle of attack. Thirdly, Tangler [59] determined a new value for C_D which is more dependent on the aspect and thickness to chord ratios.

The results of the experimental testing are only presented in parts, focussing on the effect of low speed operation and hence partial rotor stall conditions. It is observed that when the blade is operating in the un-stalled condition, the panel method and flat plate equations match the performance extremely well. However under stalled conditions it appears that a phenomenon that they have described as over-power occurs, where the measured power output exceeds all three predicted values by up to around 100%. This is attributed to the three dimensional nature of the flow and a delay in the onset of stall . This is owing to radial flows and hence a different effective aerofoil shape resulting in the delay of flow separation. The results of this are not presented fully, but it is clear that at higher angles of yaw misalignment, the Viterna-Corrigan and Tangler methods appear to be more accurate as prediction of power output. It is recommended that more research into the delay of stall be undertaken to investigate these effects.

Further experimental research on the nature of the flow around the blades is undertaken by Robinson et al. [60]. A 10.1m diameter rotor is instrumented with four pressure transducer stations to measure pressure distributions over the blade surface. A data sample rate of 521Hz was used to enable the capture of dynamic and transient pressure events. The inflow velocity was measured 12m upstream of the turbine with a variety of instrumentation and this enabled the results to be interpreted with regard to fluctuations in velocity.

2.3.2 Proof of concept

At the proof of concept stage the level of publicised information decreases as the level of commercial interest increases. For this reason, only generic information is available. There are a number of proofs of concept that have been tested but only the most advanced will be summarised here.

SMD Hydrovision Ltd are developing the TidEl concept, which is novel in that it is a submerged buoyant system which relies upon chains to affix it to the seabed, not unlike the Loch Linnhe device. A 10th scale system partly funded by the DTI has successfully completed a seven week trial programme at the New and Renewable Energy Centre (NaREC) in Blyth. The system was tested in the dry dock, which was partitioned by a central section. A bow thruster from a ship was used to accelerate the water around the dock hence simulating controlled tidal conditions. The tests have reputedly been successful, though limited clearance between the turbine rotor and the test section have raised some concerns about the validity of the results.

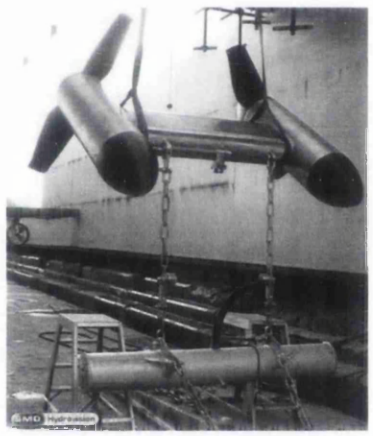

Figure 2.04 - The SMD TidEl 1/10th scale concept under test at NaREC

Lunar Energy have independently begun to develop a design for a shrouded rotor. This is reputed to have the advantage that it removes the need for a yawing mechanism and accepts misaligned flow with no loss in efficiency. A 0.8m diameter device was tested in a tow-tank as shown in Figure 2.05. The test results have been stated as a success but no data is available. Interestingly, it is claimed that the rotor obtains greater efficiency when the flow is misaligned.

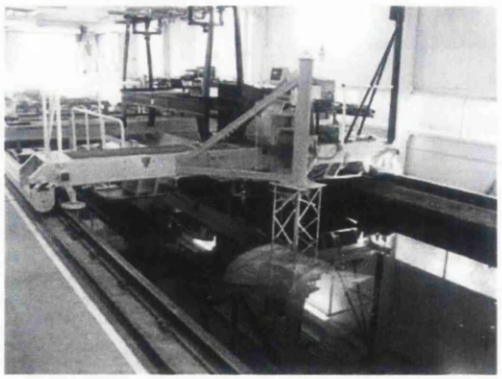

Figure 2.05 - The Lunar energy towing tank test with rotor under-slung

2.3.3 Demonstrations

More recently, with the successful deployment and testing of the Marine Current Turbines Ltd 'Seaflow' project many papers have been presented. In Fraenkel [61] the issues experienced in deploying and operating a prototype tidal stream turbine are discussed. Three key areas are identified; structural and fixing, access and installation. The monopile approach is discussed and the advantages stated. The commercial focus appears to have taken hold in this document and very little useful information can be gleaned. A graph is presented illustrating that the actual power output is 27% greater than predicted. Unfortunately no flow speeds are included. Costings and the commercial development plan are discussed.

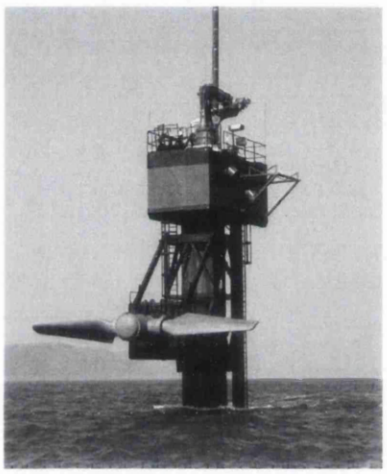

Figure 2.06 - Marine Current Turbines 'Seaflow' demonstrator raised for maintenance

Hammerfest Strom AS are based in Hammerfest, Norway and they installed the first grid-connected system in 2002. The system is a 3 bladed, bottom mounted system and has been running successfully since installation. It is shown during installation in Figure 2.07. It reverses flow direction by pitch control of the blades in the same way as the MCT device. The status of the company's development plan is unclear and there is no information available regarding the performance of the device.

Figure 2.07 - Hammerfest Strom device being transported to the installation site.

2.3.4 Proposed full scale system

The Seagen concept is a development of the Seaflow as pictured in Figure 2.08. The technology consists of twin axial flow rotors of 15m to 20m in diameter, each driving a generator via a gearbox. The twin power units of each system are mounted on wing-like extensions either side of a tubular steel monopile some 3m in diameter which is set into a hole drilled into the seabed as shown in Figure 2.08. The power units are able to be raised up the pile for maintenance.

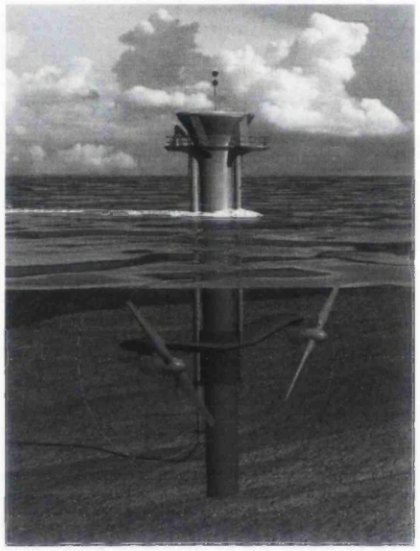

Figure 2.08 - An artists impression of MCT's 1MW 'Seagen' concept.

It is anticipated that Seagen will be installed in 2007 in Strangford Loch in Northern Ireland.

2.4 Blade Element Momentum Theory

Investigations into using tidal stream energy for electricity generation have only been undertaken for a period of approximately 20 years. During this period the main focus has been to develop the technology in terms of deployment strategy and other practicalities such as survivability. Thus far, the literature available regarding detailed performance and load modelling is relatively sparse. Substantial work is being undertaken on array modelling and resource evaluation, but the theory used to predict individual turbine performance is limited and Blade Element Momentum Theory (BEMT) remains the most practical method. However very little is published on BEMT applied to tidal turbines.

2.4.1 Origins of BEMT

Blade Element Theory was originally developed to increase the understanding of ship and aircraft propellers. Its conception can be attributed to William Froude in the 1870s, although it was not fully explored until the early 1900s. It involves discretising the blade radially and analysing each element in turn with regard to the aerodynamic forces it will experience. When combined with Momentum Theory, BET becomes BEMT which has become the leading computational analysis theory of light-loaded free-stream rotors. Momentum theory was developed by Rankine and Froude and then Betz who introduced rotation of the slipstream in 1920. Momentum theory is also known as Actuator Disk Theory and cannot be used as a stand alone tool to analyse rotors, but in combination with BET brings useful results. Momentum theory concludes that for propellers, the down wash is twice as fast as the inflow, the ideal power is a simple function of the thrust, and if the down wash is uniform, the ideal efficiency is maximized. These results are combined with BET and become BEMT which has the capability to analyse the design and performance of wind turbines and tidal stream turbines, with adequate accuracy.

2.4.2 BEMT applied to wind turbines

Griffiths [62] developed a method to design an optimised wind turbine using BEMT. The paper describes the development of the method from Actuator Disc Theory in three

stages. The initial approach models the turbine as a disc that extracts energy from the fluid. It assumes that fluid is inviscid, incompressible and that there is no rotation of the flow downstream of the disc. It is shown that the effect of the energy extraction is to reduce the flow velocity and hence expand the streamtube. This approach gives an exact solution, but the effect of the assumptions made is to decrease the accuracy, hence the theory is developed further by Griffiths. Firstly, the rotor is modelled as a real rotor in a perfect fluid. As described by Betz [63], the fluid is assumed to acquire a downstream rotational velocity in the opposite direction to that of the rotor. The magnitude of this rotational velocity in the plane of the rotor disc is assumed to be half that of the magnitude well downstream of the device. On this basis, the relative axial and rotational velocities at the plane of the rotor can be described in terms of the interference factors that are introduced. These interference factors vary along the blade length and hence are calculated individually for each radial element. The performance of the rotor can be expressed in terms of torque and power from the interference factors. Finally, the analysis is developed to incorporate real fluid properties by describing the performance in terms of the lift and drag forces on each blade element. This combination of the momentum equations and energy equations results in a method to optimise the design and assess the performance of rotor blades. This takes into account the complex nature of the flow and the fluid dynamic drag experienced by the rotor.

In a subsequent paper, Griffiths and Woollard [64], present an arrangement of the above method which allows the performance of the rotor to be estimated using iteration of the interference factors. The approach also adds a tip loss correction factor as used by Prandtl [65]. This shows that given the geometry and characteristics of a rotor, the method can be used to assess the performance over the operating range.

2.4.3 Experimental validation of BEMT

Kishinami et al [66] compare a BEMT approach similar to that of Griffiths with experimental data from a small wind turbine. The fundamental theory is identical and although the way in which the equations are derived uses a thrust / energy method rather than a thrust / torque method, the result is identical. The main difference in employing the thrust /energy method is that it enables the wake effect to be examined more easily. A term is introduced which describes the energy dissipated by the blade and this is interesting when considering wake effects. The other difference to the BEMT used by Griffiths is the method of tip loss correction. It is stated that the effective radius

of the rotor, for any r greater than $0.97R_0$ the rotor, is taken as R_0 (the radius at the tip). This should only reduce the lift coefficient and not affect the drag coefficient. This is presumably because the effective angle of attack is reduced, but no explanation of this is given. Some comparisons of different aerofoils and blade pitch are given and the experimental data is found to have some good correlation with predicted performance. There is some discussion of the lift and drag coefficients used and how this will affect the output dramatically.

2.4.4 Limitations of BEMT

Badreddine [67], comments on the limitations of BEMT, specifically that in the standard form, no account is made of the complex nature of the flow through the disc. All 3D effects such as radial flow between the concentric stream tubes, wake effects and tip losses are ignored in the basic assumptions. However the BEMT used for comparison in this paper does not take the energy equations and hence viscous drag effects into account, unlike the BEMT used by Griffiths. Badrreddine goes on to develop a vortex wake model using lifting line theory as described in the paper. It is said to model the wake more realistically than BEMT, although it does limit the angle of attack that can be analysed. Lifting line theory is presented as being superior to BEMT although a direct comparison is not made. It is stated that the Navier-Stokes approach is more accurate than either as it fully captures the viscous and compressible flow effects, but the high computational demand limits its application at the present time.

Mikkelsen also undertakes an investigation into the lifting line approach in [68]. A wind turbine system was modelled using this theory and Navier-Stokes to analyse the assumptions made in BEMT. The assumptions considered are that;

Each annular streamtube can be considered independently and there is no interaction between them,

- The pressure in the wake well downstream is equal to the pressure well upstream
- The induced velocity in the rotor plane is half that of the induced velocity in the far wake
- Axial momentum theory can be applied in the differential form neglecting the resulting axial force of pressure acting on lateral boundaries of the stream tube

- Conservation of circulation may be ignored

Although it is found that these assumptions do cause an inherent inaccuracy in BEMT, the results indicate that the maximum error caused by this is 3%. This error is said to be negligible under most operating conditions.

Mikkelson also describes tip correction factors for real rotors. The approach developed by Prandtl [69] and used by Griffiths [64] corrects the aerodynamic force components. The correction is applied to the momentum equations as implemented by Glauert [70] which gives revised interference factors. It is stated that although this method is widely used, it does suffer from some limitations. For example, as the radius is approaching the tip, the axial interference factor approaches unity, implying that the axial velocity becomes zero and hence the axial force becomes zero. Both Wilson and Lissaman [71] and De Vries [72] have made refinements, but both are said to lack rigorous consistency at the tip. Shen, Mikkelsen et al [73] have introduced a mathematically rigorous system which considers the balance of momentum for a real rotor with finite blade number and real aerodynamic forces. Although this appears to be an improvement, it does not model the real tip effects exactly and must be calibrated using model testing.

Maalawi and Badawy [74] also implement Prandtl's tip loss factor in combination with BEMT equations to predict the performance of a turbine system. They conclude that they are able to solve the equation system directly and hence lower the computational demand compared to standard iterative techniques.

Robinson et al. [60] state that BEMT is not able to capture the three dimensional effects of the flow in their entirety, but the low computational demand associated with BEMT still makes it a very useful tool for both the design and analysis of axial flow rotors. especially in the unstalled flow region of operation. It is stated that most wind turbine structural design codes using BEMT are unable to capture the full flow regime, even with the use of empirically derived stall models. It also states that there is a lack of empirical information regarding the flow owing to the difficulties associated with making localised flow measurements around the rotor.

2.4.5 Stall delay

The most interesting aspect of Robinson et al. [60] is the focus on stalled conditions, where transient flow and 3d effects are greatly dependent on variations in the inflow

velocity in the form of turbulence and other fluctuations. It may be possible that the levels of turbulence experienced by tidal stream turbines are less than the corresponding levels in wind devices; nevertheless in the area of wave rotor interactions they may be of great interest. The paper focuses on stall delay which is a phenomenon where forces experienced on the blade at high angles of attack are far higher than predicted. It seems that the stall point is somehow delayed until a higher angle of attack, and it is postulated that this is the result of a radial flow along the blade owing to the rotation of the system. Fine thread tufts are used to visualise the initiation of flow separation. In the regions of flow separation, the flow is immediately seen to acquire velocity from the hub to the tip, and once established seems to be stable. However, the most important point is that loads may be increased by the phenomenon of stall delay.

Danmei Hu et al [75] have also studied the issue of stall delay in wind turbine rotors. Over-power production at low speed ratios has been observed in turbines, propellers and helicopter rotors and this condition is referred to as stall delay. BEMT is cited as being incapable of predicting forces and power under these conditions because of the lack of information regarding the inception and characteristics of stall delay. A basic attempt has been made by Viterna and Corrigan [76], which involves introducing a correction factor based on the aspect ratio. Myers [55], has examined and compared other methods and other theories in which the phenomenon is said to be caused by the effect of solidity and the influence of one blade on another. However, this paper uses Fluent which is a full Navier Stokes equation solver with viscous, incompressible, steady flow. Flow separation inception was analysed in both 2D and 3D, and the 3D case showed delayed separation under rotating conditions. It was also found that as Reynolds number increases toward the blade tips, this increasingly drives the degree of separation as opposed to the radial velocity effects meaning that there is greater correlation between 2D and 3D predictions near the tip.

This paper also outlines a scale wind turbine test that was used to validate the theoretical predictions. It was found that the 2D predictions underestimated the forces on the turbine in the stalled region whereas the 3D model increased the accuracy significantly. This again illustrates the limitations of BEMT when predicting loads and performance, and shows the advantages of the Navier-Stokes 3D method for verification work. It also shows that corrections can be made to BEMT to improve accuracy and take advantage of the lower computational demand.

2.5 Conclusions

There are many demonstrations and tests of tidal stream devices anticipated in 2007/8 with the fledgling industry beginning to expand. This may result in fewer details being published concerning the technical details of different concepts. Patents and DTI dissemination are likely to become the primary source of information.

The primary areas of interest appear to be rotor performance and structural considerations. There is currently limited discussion of the detailed power characteristics of prototypes. The results that are available are discussed in the next section.

It is apparent that BEMT is an extremely useful tool for estimating the loading and performance of horizontal axis rotors and is used in the industry because of the low computational resource required. However, owing to the assumptions made and the limitations imposed by two dimensional analysis, empirically derived factors of correction may be required to improve the accuracy. It also seems clear that Navier-Stokes analysis is a suitable tool for verification of BEMT and specific research applications such as stall delay. Stall delay is a condition that appears prevalent in horizontal rotors both in air and water and may become relevant in the introduction of fluctuations in inflow velocity owing to wave action.

It can be seen from the papers reviewed that the modelling of performance and loading characteristics of TSTs is an important area of research that will greatly influence the development of the marine renewables industry. Some initial work has been undertaken which explores some of the operational conditions which a device will experience over its lifetime. However, there is a great deal of work still to be done to fully understand the nature of the hydrodynamic flows and application of BEMT to modelling TST performance and loadings, especially under conditions away from the laminar flow in which BEMT was first developed.

2.6 References

1. Eling Tide Mill, *The history of* [online 2006 http://www.elingtidemill.wanadoo.co.uk/hist.html] (accessed 03/07/06).
2. Strathclyde University, Tidal Power Case Studies, [online 2006 http://www.esru.strath.ac.uk/EandE/Web_sites/01-02/RE_info/tidal1.htm] (accessed 19/07/06),
3. BWEA, Introduction to Marine Energy, [online 2006 <http://www.bwea.com/marine/intro.html>] (accessed 04/07/06),
4. Bahaj AS, *The Potential of Harnessing Electrical Energy from Marine Currents* Proceedings of World Renewable Energy Congress (Elsevier): p. 257-264, 2005.
5. Binnie Black & Veatch, *The Commercial Prospects of Tidal Stream Power.* DTI UK, 2001.
6. Black & Veatch Ltd., *UK, Europe and Global Tidal Stream Energy Resource Assessment.* Carbon Trust, UK, 2004.
7. Black & Veatch Ltd., *Tidal Stream Energy Resource and Technology Summary Report.* Carbon Trust UK, 2005.
8. Bryden IG, *Tidal Current Power.* Next Steps for Wave & Tidal Power in Scotland (26/11/2003).
9. Callaghan J, R. Boud, *Future Marine Energy.* Carbon Trust, UK, Jan 2006.
10. Carbon Trust, *Low Carbon Technology Assessment 2002.* Carbon Trust UK, 2002.
11. Carbon Trust, Guide to Marine Energy, [online 2006 http://www.thecarbontrust.co.uk/ctmarine3/Page2.htm] (accessed 12/07/06),
12. CENEX Project, *Tidal and marine currents energy exploitation.* ref. JOU2-CT-93-0355.Report EUR16683EN, 1996.
13. Entec, *Marine Energy Challenge, Marine Energy Glossary.* Carbon Trust UK, 2005.
14. UK Department of Trade and Industry, *Tidal stream energy review.* (ETSU T/05/00155/REP), 1993.
15. Douglas Westwood Ltd, *Tidal Stream Industry Market Research - A report to Swansea University.* 2006.
16. UK Department of Trade and Industry, *The Energy Challenge Energy Review Report.* 2006.
17. Future Energy Solutions, *Opportunities for Marine Energy in Scotland.* Scottish Executive UK, 2002.
18. House of Commons Welsh Affairs Committee, *Energy in Wales.* Third Report of Session 2005–06 I.
19. Douglas Westwood Ltd, World Wave and Tidal Database, [online 2006 www.dw-1.com] (accessed 12/7/06),
20. Swanturbines Ltd, *Power from flowing water.* [online 2006 www.swanturbines.co.uk] (accessed 12/07/06).
21. MCT Ltd, *Marine Current Turbines.* [online 2006 www.marineturbines.com] (accessed 12/07/06).
22. Lunar Energy Ltd, *Harnessing tidal power.* [online 2006 www.lunarenergy.co.uk] (accessed 12/07/06).
23. SMD Hydrovision Limited, *TidEl Tidal Stream Demonstrator.* [online 2006 www.smdhydrovision.com] (accessed 12/07/06).
24. Stewart HB, Palm Beach Shores, Feb 27 to March 1 1974, Edited by *Proc. of the MacArthur Workshop on the feasibility of extracting useable energy from the Florida current.* 1974.
25. Wyman PR, Peachey CJ, *Tidal Current Energy Conversion.* GEC Hirst Research Lab. Proc. Future Energy Concepts, IEE London, 1979.
26. Cave PR, Evans EM, *Tidal energy systems for isolated communities.* West E, editor. Alternative energy systems. New York: Pergamon: p. 9–14, 1984.
27. Ampair, Towed Turbine Generator, [online 2006 www.ampair.com] (accessed 12/07/06),
28. Morrison RE, *Energy from ocean currents.* Energy from the ocean, (Library of Congress, Science Policy Research Division-Congress. Res. Serv. 95th Congress Washington: US: p. 149–73, 1978.

29. Musgrove P, *Tidal and river current energy systems.* Proc. Conf. "Future Energy Concepts". London: Inst Elec Eng: p. 114–7, 1979.
30. MacNaughton D, et al., *Tidal Stream Turbine Development.* IEE Conference No. 385 (London), 1993.
31. "CENEX"Project, *Tidal and marine currents energy exploitation.* ref. JOU2-CT-93-0355.Report EUR16683EN, 1996.
32. O.Paish, P.Fraenkel, *TIDAL STREAM ENERGY: ZERO-HEAD HYDROPOWER.* International Conference on Hydropower into The Next Century, Barcelona, 5-8 June, 1995.
33. Bryden IG, Naik S. Fraenkel P. Bullen CR., *Matching Tidal Current Plants To Local Flow Conditions.* Energy 23(No.9 Pergamon UK): p. 699–709, 1998.
34. Couch J, Bryden IG, *Numerical Modelling of Energy Extraction in Tidal Flows.* Proceedings of World Renewable Energy Congress: p. 550-555., 2005.
35. Offshore installations guidance on design construction and certification 1990, HMSO, City
36. Orme JAC, Masters I. Griffiths RT, *Investigation of the effect of biofouling on the efficiency of marine current turbines.* Proceedings of the 1st International Conference on Marine Renewable Energy, 2002.
37. University of Southampton, Welcome to the Marine Energy website [online http://www.marineenergy.soton.ac.uk/] 2006 (Accessed 12/07/06),
38. Bahaj AS, *Fundamentals applicable to the utilisation of marine current turbines for energy production.* Renewable Energy 28: p. 2205–2211 2003.
39. Batten WMJ, Bahaj AF. Molland JR. Chaplin JR, *Hydrodynamics of marine current turbines.* Renewable Energy 31 (Elsevier): p. 249-256, 2006.
40. Paish O, Fraenkel P, *TIDAL STREAM ENERGY: ZERO-HEAD HYDROPOWER.* International Conference on Hydropower into The Next Century, Barcelona, 5-8 June, 1995.
41. Salter S, *Proposal for a Large, Vertical-Axis Tidal-Stream Generator with Ring-Cam Hydraulics.* Third European Wave Energy Conference, Patras, 1998.
42. Salter S, *Pitch–Control for Vertical-Axis, Marine-Current Generators.* World Renewable Energy Congress (WREC) 2005.
43. SERG, *Modelling of Tidal Currents.* [online 2006 http://www.marineenergy.soton.ac.uk/] (accessed 01/08/06).
44. Molland F, Bahaj AS. Chaplin JR. Batten WMJ, *Measurements and predictions of forces, pressures and cavitation on 2-D sections suitable for marine current turbines.* Proceedings of the Institute Mechanical Engineers 218(Part M: J. Engineering for the Maritime Environment), 2004.
45. Drela M at MIT, XFoil Subsonic Airfoil Development System [online http://web.mit.edu/drela/Public/web/xfoil/] 2006 (Accessed 03/07/06),
46. UK Department of Trade and Industry, Engineering Business, *Research and development of a 150kW tidal stream generator.* 2002.
47. THGL & BMPG, *Tidal hydraulic turbines.* [online 2006 http://www.bmpg.co.uk/download/pembroke%20tidal.pdf] (accessed 01/08/06).
48. WindStats 17, *ISSN 0903-5648.* No. 2 Spring 2004,.
49. Enercon, Energy for the world, [online 2006 http://www.enercon.de/en/_home.htm] (accessed 01/08/06),
50. Open Hydro, *Silent, invisible, predictable, renewable energy.* [online 2006 www.openhydro.com] (accessed 10/10/06).
51. Grainger W, Jenkins N, *Offshore Wind Farm Electrical Connection Options.* BWEA 20, 1998.
52. Orme JAC, Masters I, *Analysis and comparison of support structure concepts for TSTs.* Proceedings of the 4th International Conference on Marine Renewable Energy, 2006.
53. Orme JAC, Masters I, *Design and testing of a direct drive tidal stream generator.* Proceedings of the 3rd International Conference on Marine Renewable Energy, 2004.
54. Myers L, Bahaj AS, *Wake Studies of a 1/30th Scale Horizontal Axis Marine Current Turbine.* Proceedings of World Renewable Energy Congress (Elsevier): p. 1205-1210, 2005.
55. Myers L A.S. Bahaj, Bahaj AS, *Power output performance characteristics of a horizontal axis marine current turbine.* Renewable Energy 31(Elsevier): p. 197-208, 2006.
56. Garrad Hassan & Partners Ltd, GH Bladed: Wind Turbine Design Software [online www.garradhassan.com/products/ghbladed] 2006 (accessed 04/01/2005),

57. Hanley Innovations "", I , accessed: 05/05/2006., *VisualFoil Plus: Accurate Lift, Drag & Moments for all Airfoil Shapes.* [online http://www.hanleyinnovations.com/air_16.htm] 2006 (accessed 12/07/06).
58. Viterna LA, Corrigan RD, *Fixed pitch rotor performance of large horizontal axis wind turbines.* DOE/NASA workshop on large wind turbines (Ohio), 1981.
59. Tangler JL, *Horizontal axis wind turbine post stall airfoil characteristics synthesization.* Report contract no. DEAC04-76DP03533 rocky flats test site, 1984.
60. M.C. Robinson "", Proceedings of the 3rd ASME/JSME Joint Fluids Engineering Conference, San Francisco, California, National Renewable Energy Laboratory, 1999., Hand MM. Simms DA. Schreck SJ, *Horizontal Axis Wind Turbine Aerodynamics: Three-Dimensional, Unsteady, and Separated Flow Influences.* Proceedings of the 3rd ASME/JSME Joint Fluids Engineering Conference. National Renewable Energy Laboratory, San Francisco(California), 1999.
61. Fraenkel P, *THE "SEAFLOW"PROJECT:PIONEERING THE DEVELOPMENT OF TIDAL STREAM TURBINES,.* SUT-ICE London, 2003.
62. Griffiths RT, *Energy From the Wind.* University of Wales Swansea internal report, 1974.
63. Betz A, *Die Naturwissenshaften.* Volume 9(No. 46), November 1927.
64. Griffiths RT, Woollard MG, *Performance of the optimal wind turbine.* Applied Energy 4, Applied Science Publishers Ltd, 1978.
65. Prandtl L, *Appendix to 'Schraubenpropeller mit geringstem Energieverlust' by Betz,.* Gottinger Nachr: p. 193-217, 1919.
66. K. Kishinami et al. . *Theoretical and experimental study on the aerodynamic Characteristics of a horizontal axis wind turbine.* Energy 30, Elsevier: p. 2089–2100, 2005.
67. Badreddine K, Ali H. David A., *Optimum project for horizontal axis wind turbines 'OPHWT'* Renewable Energy 30, Elsevier: p. 2019–2043, 2005.
68. Mikkelsen R, *Actuator Disc Methods Applied to Wind Turbines.* Dissertation for Technical University of Denmark, Jun 2003.
69. Shen WZ, Mikkelsen R. Sørensen JN, *Tip Loss Corrections for Wind Turbine Computations.* Wind Energy 8, Wiley Interscience,: p. 457-475, 2005.
70. Glauert H, *Airplane propellers.* Aerodynamic Theory 4, Dover & New York,: p. 169-269, 1963.
71. Wilson RE, Lissaman PBS, *Applied aerodynamics of wind powered machines.* Report NSF/RA/N-74113. Oregon State University, , 1974.
72. De Vries O, *Fluid dynamic aspects of wind energy conversion.* AGARD-AG-243, , 1979.
73. Shen WZ, Mikkelsen R. Sørensen JN. Bak C, *Evaluation of the Prandtl Tip Correction for Wind Turbine Computations.* Proceedings of Global Windpower Conf. Paris France, , 2002.
74. Maalawi KY, Badawy MTS, *A direct method for evaluating performance of horizontal axis wind turbines.* Renewable and Sustainable Energy Reviews 5 Pergamon(175-190), 2001.
75. Hu D, Hua O. Du Z, *A study on stall-delay for horizontal axis wind turbine.* Renewable Energy Elsevier, 2005.
76. Viterna LA, Corrigan RD, *Fixed pitch rotor performance of large horizontal axis wind turbines.* DOE/NASA workshop on large horizontal axis wind turbines Cleveland, (OH), 1981.

3.0 EXPERIMENTAL DESIGN AND INVESTIGATION

3.1 Introduction

This section describes the experimental validation of an existing BEMT model. A direct drive, permanent magnet generator (PMG) system with a 1m diameter rotor is built and tested. This provides an opportunity to undertake a study on the design of such a system and some of the challenges and issues are described. Particular attention is given to the design and optimization of the rotor blades for a particular generator. The practicalities of deployment and installation are also described. The system is tested under controlled conditions to obtain performance characteristics over the potential operating range. The results of the testing are presented and compared to existing BEMT.

3.2 Objective

The method of analysis described in Griffiths[1] applies to an axial flow rotor. This analysis is specifically intended for use in air for a wind turbine, however it is proposed that this analysis is also valid in water provided that cavitation does not occur, i.e. no region of the flow experiences a dynamic pressure lower than the cavitation pressure. The experiment is intended to verify this theory in a practical instance to provide confidence that it can be used in the design of axial flow turbines on a large scale.

The most important things to observe are the relationships between the operating tip speed ratio and the coefficients of power and torque. These will provide information regarding the performance of the rotor under varying operating conditions. The torque experienced by the rotor whilst stationary is also very important when compared to the torque required to start the system spinning. This will determine the flow speed at which generation will start to occur, ultimately affecting the utilisation factor achieved by the device.

A series of experiments is also undertaken to examine the effect of varying the number of blades on the performance and compare this with theory. There is a cost advantage offered by a lower number of blades, and the dynamic characteristics of the system will also vary.

Additionally, the experiment is an investigation into the use of a direct drive alternator and the behavioural characteristics and efficiency of this combined with the marine rotor. An electrical control system based on a system of divert loads is employed to allow the system to run in automation. This method of control is adapted from a wind turbine application and is investigated in this experiment.

The system is monitored in some detail and the design and evaluation of the monitoring system is an investigation into methods that can be applied to an underwater electricity generating device.

3.3 Design of the System

This experiment, is the second phase of the KEF sponsored project 'Development of a prototype River Current Turbine'. The first phase involved the design, fabrication and testing of a prototype. Although the results were qualitative, and it became clear that the technology was feasible, problems were encountered with alternator compatibility, support vibration and consequent rotational dynamic loads. This resulted in low electrical power generation, overspeed and buckling of parts of the structure.

The second phase and prototype aims to have rectified these problems. It incorporates an entirely new alternator with power storage and conversion system and a greatly strengthened structure. It also includes an improved monitoring system to provide more information about the rotor performance.

The primary design parameters and methods are discussed here.

3.3.1 Diameter

The primary design specification for a marine turbine rotor is the diameter [2]. The diameter is constrained by the location and the structure available to support the device. The limit of the diameter that can be safely installed at a site is discussed in detail in many papers. The most pessimistic approach is presented in [3] which suggests that the blade tip should be at a minimum of 9m beneath the surface. This accounts for wave action, storm surges and shipping. However if an exclusion zone were placed around

the device then the proximity of the blades to the surface is less critical and it is suggested in [4] that a diameter of half the depth would be permitted. However the effect of the seabed boundary layer must also be taken into account as the water is slower here. In the case of this experimental device, the factors influencing the maximum allowable diameter do not involve clearances of this type. It is intended that the device be able to be installed in a small river. The depth available is approximately 1.5m. A diameter of 1m is used to allow for movement of sediment beneath the device and to ensure that the blade tips do not pierce the surface.

3.3.2 Generator

The diameter of the device and the flow velocity range at the intended site of installation are used to predict the approximate power characteristics of the turbine. A simple power coefficient is used to estimate the rotor power and speed. This power curve is then used to assess the suitability of generators for use in the system.

A number of generators were considered based on 'off the shelf' designs which could be used or modified slightly for this purpose. Three estimated power curves are shown in Figure 3.01. The alternator power curves are theoretical and are based on developing maximum power at 300rpm. The rated value is the electrical power out and a conversion efficiency of 0.5 has been added to calculate the required mechanical power input P_s.

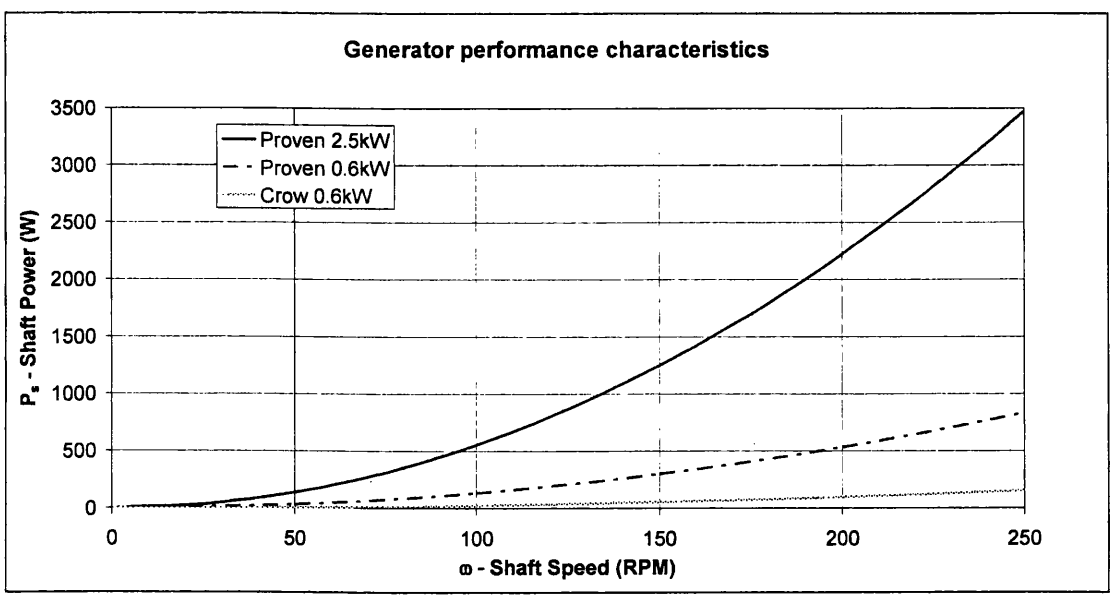

Figure 3.01 - A comparison of generator power / speed characteristics

The Proven Ltd 2.5kW permanent magnet generator is adapted from a wind turbine for this particular application. It is designed to output 1kW, at 48V at 180rpm. It is a standard 120V winding from a 2.5kW wind turbine but run at a lower speed. It produces a 3-phase A.C. output that is rectified to D.C. for battery charging. The Crow Electric data on Figure 3.01 is based upon measured data from the first turbine test. It is clear that the Crow alternator was not operating at the correct magnitude. The 600W line indicates the predicted performance, and a comparison shows the degree to which it underperformed.

The performance of the modified 2.5kW Proven generator is tested in the laboratory and the graph shown in Figure 3.02 is produced. The generator power and conversion efficiency characteristics can be clearly seen.

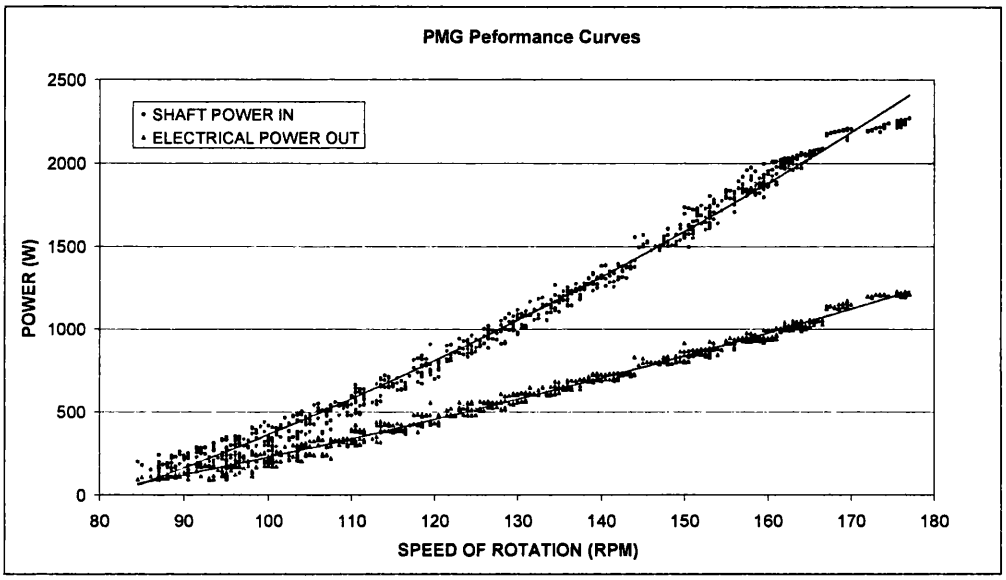

Figure 3.02 - Experimentally determined Proven 2.5kW generator performance

Figure 3.03. shows the comparison of the power curves for the rotor and various alternators to illustrate the different shapes of optimum rotor power and speed against generator optimum. The theoretical power output of the rotor is calculated using BEMT from [1] with a power coefficient, C_p, of 0.5. This is shown over a range of TSR from 2 to 7.

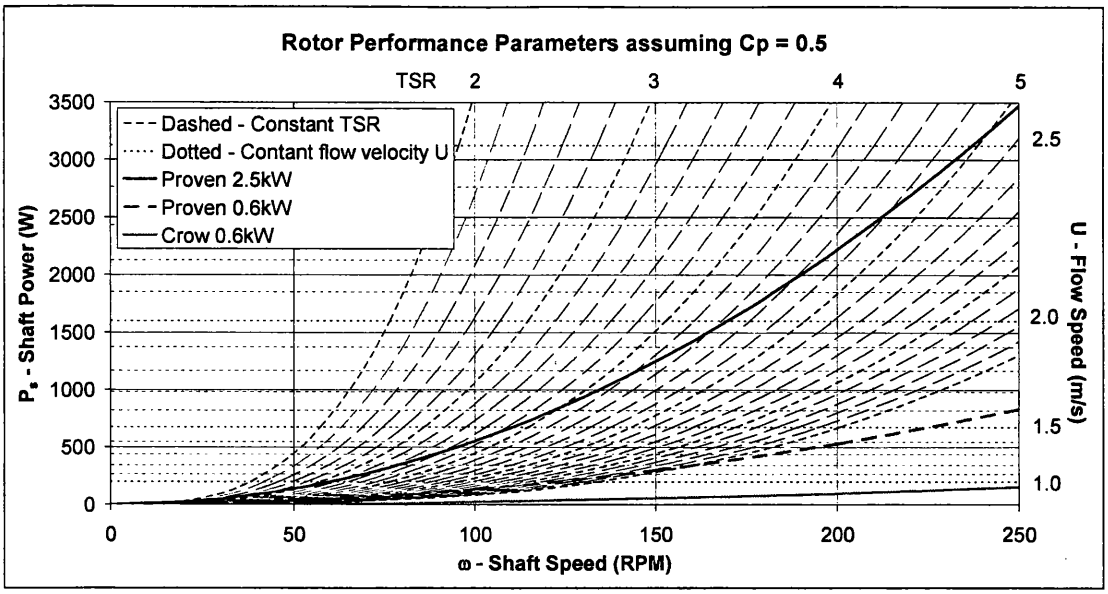

Figure 3.03- Rotor performance parameters

It is clearly seen that at constant TSR the rotor power increases with the cube of the speed, whereas the generator power increases with the square of the speed.

The theoretical 2.5kW curve shows that with an efficiency of 0.5, the power will be matched to the turbine whilst operating at a TSR of just under 5. This is the basis of the prediction that the turbine will run at TSR 4.5 under automated electrical load.

3.3.3 Blade Design

The blades have been designed using the theory described by Griffiths [1]. However the equations have been rearranged to enable them to be solved using the solver included in the Microsoft Excel package.

3.3.3.1 Design tip speed ratio (TSR)

Modern wind turbines generally use a blade pitching system to adjust the angle of attack of each individual blade and optimize performance at different speeds. This is especially important when the turbine is stationary, as the blades are pitched to increase the torque and enable the turbine to start. The turbine designed in this study uses a fixed pitch rotor to reduce complexity and cost. It is thought that rotors of this type will be most cost

effective when installed in-situ owing to the reduced capital cost and maintenance requirement and similar peak performance. However the disadvantage is that the turbine will not overcome its own friction and start until a higher flow speed. The result is that power at low flow speed is lost.

To mitigate this effect, the blades are designed to be most efficient at a lower TSR. This has the effect that the blades are larger and have greater solidity. The greater chord length and lower angle of attack means that a greater proportion of the blade is stalled to a lesser degree when stationary. The effect is a higher starting torque and a lower starting velocity.

The disadvantages of this technique are reduced maximum power output owing to the slightly less efficient blade profile, and a tendency for the blades to run in overspeed owing to the power characteristics of the generator. The BEMT model described in Chapter 4 is used to analyse this situation and the relationship between maximum power coefficient C_p, Starting torque coefficient C_{ts} and Design TSR (TSR_D) is shown in Figure 3.04.

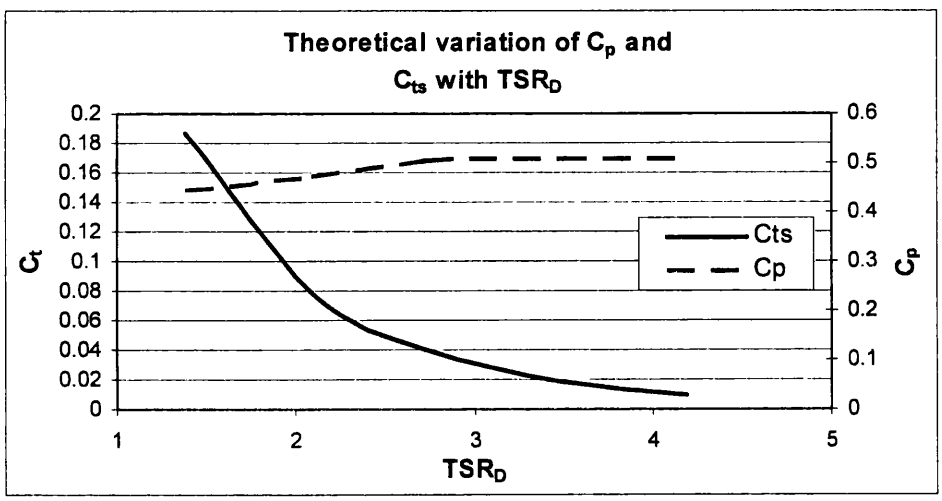

Figure 3.04 - Variation of start up torque and efficiency with design TSR

Examination of the interaction between the Proven generator and the blades in Figure 3.03 shows that in the useful power range of 1000-3000W shaft power (corresponding to 500-1500W electrical power) the predicted TSR of the rotor will be between 4.1 and 4.9. It can therefore be concluded that the machine has a notional operational state of TSR 4.5.

3.3.3.2 Aerofoil selection

The second stage in the design process is the selection of a suitable aerofoil section. Extracting power from the flow of water as opposed to air has a number of implications as far as aerofoil selection is concerned. Firstly the power density is increased. This is a measure of the rate of kinetic energy flowing through a particular area as defined by Betz [5]. Power density is dependent upon the velocity of the fluid and density and is given by:

$$\text{power density per unit area } \Psi = \frac{1}{2}\rho U^3 \qquad (3.1)$$

To compare the power density available to wind and water turbines, values for the density of air and water of 1.23kgm^{-3} and 1014kgm^{-3} respectively and typical values for the velocity of wind and water current of 12ms^{-1} and 2.5ms^{-1} are inserted into equation (3.1). This shows that the typical power density available to a water turbine is approximately 7.5 times higher than is available to the rotor of a wind turbine.

This increased power density has an effect on the design of the blades. There is more power available to blades of a smaller radius. Consequently the blades of a certain diameter will encounter much higher loadings in water than in air. The result is that shorter stronger blades are required. The effect of this is that an aerofoil section with a high thickness to chord ratio is preferred for structural reasons as this gives a high second moment of area and space to incorporate an adequate load bearing structure inside the blade. This is opposed to the hydrodynamic ideal which would use a thinner aerofoil to maximise the lift/drag ratio and hence the performance of the turbine[6]

However with regard to the design of a marine blade, stall characteristics and pressure gradient to avoid cavitation will play an important role in determining the optimum aerofoil profile.

3.3.3.3 Aerofoil detailed specification

The operation of a fixed pitch axial flow turbine requires the blade aerofoil to operate at variable angle of attack. When stationary, the angle of incidence is very high and hence the majority of the blade is stalled. To enable the turbine to start effectively the blade must create a torque when in the stationary and hence stalled position. The stall

behaviour of an aerofoil is dependent upon its shape and particularly its thickness to chord ratio.

The smaller the thickness to chord ratio, among other factors, the sharper the stall tends to be. This implies that the lift coefficient drops very rapidly after the stall angle of attack is reached. Conversely, aerofoils with larger thickness to chord ratios stall less sharply and the lift coefficient is maintained to a greater degree after stall occurs. This is advantageous as the lift produced creates torque about the axis to start the turbine.

The NACA 4 digit aerofoils have gentle and predictable stall characteristics [7] and there is much information regarding their performance available. They also are tolerant to variation in surface roughness making them more resilient to marine growth than other aerofoil sections. The primary disadvantage is the low maximum lift coefficient.

The thickness to chord ratio of this series varies from between 6% to 24%. For structural strength and stall behaviour the thickest possible section should be used. Conversely the maximum available lift coefficient occurs with the thinner sections and the onset of cavitation occurs at higher speeds with thinner sections.

It is intended that the device will be designed for a low tip speed ratio for ease of starting, and to aid the efficiency of the generator it will operate in overspeed in normal operation. Overspeed is the condition in which the turbine is operating at a TSR higher than its design TSR. Operation in overspeed reduces effective angle of attack across the blade. The pressure differential across the blade is reduced and the pressure minima increase. This implies that the blades can withstand higher speeds before the onset of cavitation occurs.

The lift coefficient of a thick section can be increased by increasing the camber of the mean chord line. In the NACA 4 digit series, the first number concerns the maximum camber as a percentage of chord. The maximum in this series is 4.

As structural integrity and starting performance are of great value to a marine turbine, a thicker section will be used, but to maximise the lift, the section of greatest camber is also selected. For this reason the NACA4424 has been selected for use on the experimental device. This has a maximum camber of 4% of the chord which is located at a distance of 40% chord from the leading edge with a thickness to chord ratio of 24%.

3.3.3.4 Aerofoil characteristics

The basic lift and drag curves for the NACA4424 section are presented in Figure 3.07 [8]

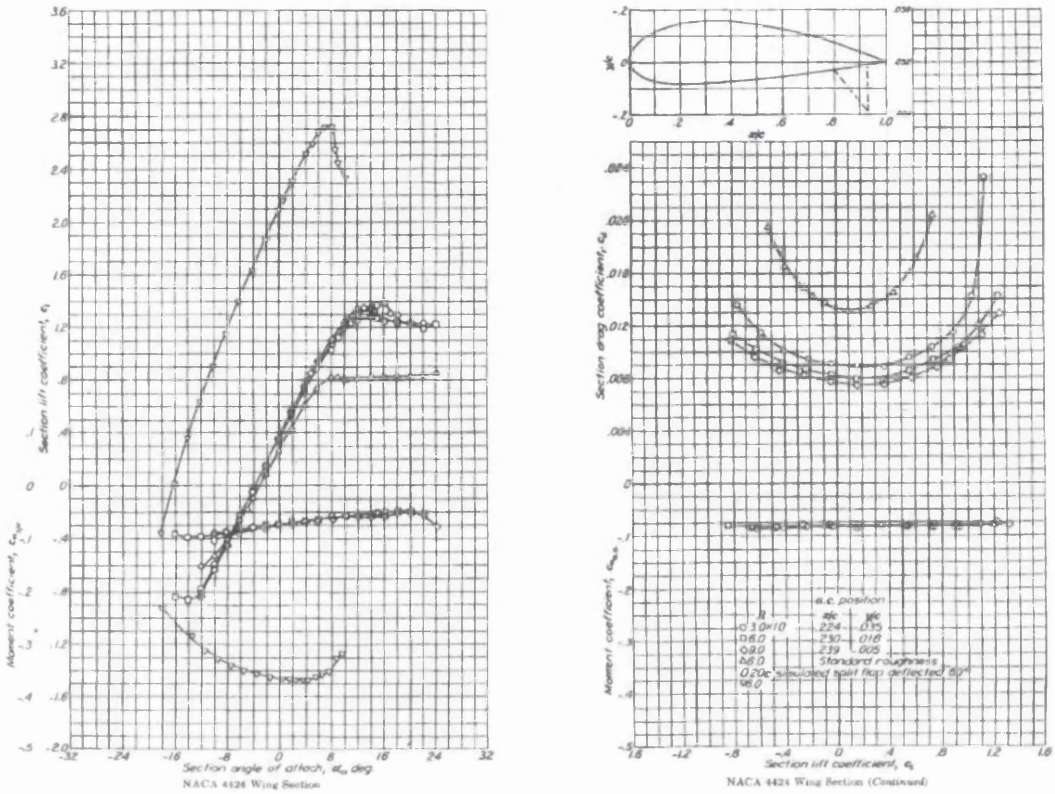

Figure 3.07 - NACA4424 aerofoil properties [8]

Assuming a chord of 0.2m the Reynolds number across the blade will vary from approximately 4E5 to 2E6. These are quite low and the data here only covers Re 3E6 to 9E6.

In Figure 3.07, it can be seen that the maximum lift/drag ratio is around 76 at Re=3E6. It is known that the drag coefficient increases dramatically as Reynolds number falls. The 'Profili' aerofoil analysis software [9] indicates that the drag coefficient increases negligibly as Re falls from 3E6 to 2E6, but increases by approximately 45% as Re decreases from 3E6 to 4E5. The lift coefficient also falls but only by ~2%. This illustrated in Figure 3.08 where the C_L/C_D ratio falls by ~40%.

For this reason a max lift/drag ratio of 50 is used in the design of the blades. This is a simplification which assumes uniform maximum lift/drag ratio over the blade radius.

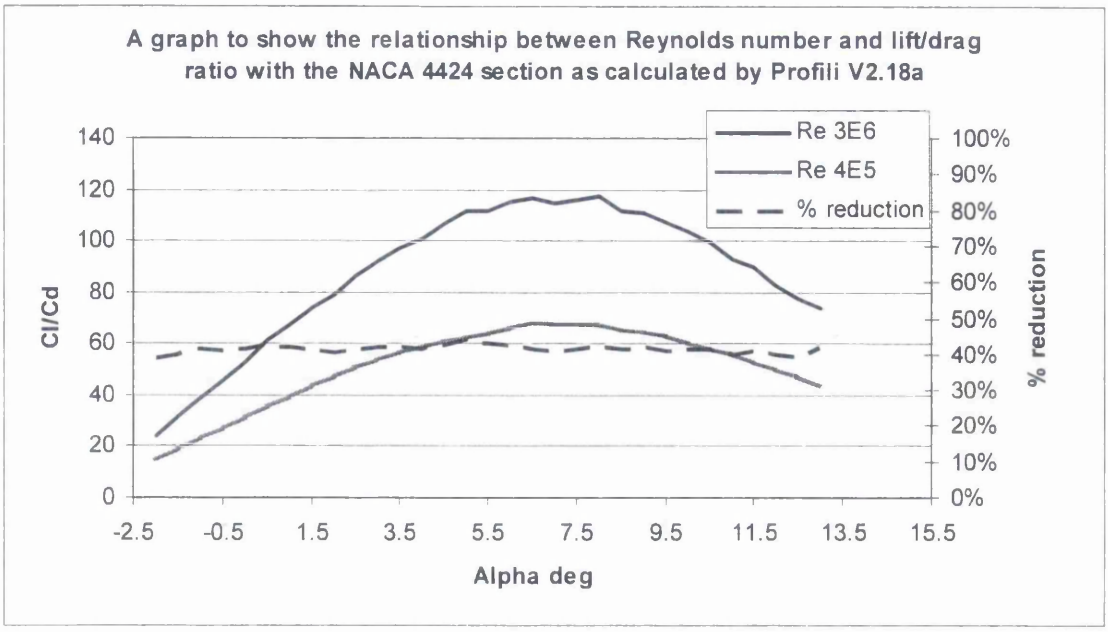

Figure 3.08 - The influence of Reynolds Number on aerofoil performance

3.3.3.5 Blade number

The number of blades used for wind turbines has been the subject of much debate throughout the industry's history. It is generally considered that odd numbers provide better dynamic stability in bigger machines and lower numbers of blades are more economic, DWEA [10]. The 3 bladed configuration is often used for these reasons. However in the case of the experiment, the TSR is very low and consequently the solidity is very high. This results in particularly large blades which would be very heavy and consequently present a disadvantage.

As the experimental device is small scale and the dynamic forces are expected to be low, it is considered that the requirement for an odd number of blades is reduced. At blade number 4 the chord size and hence blade mass is reduced and the manufacturing cost is still low, hence the 4 bladed configuration is used. Blade numbers of 2,3 and 4 will be tested on different hubs as part of this experiment.

3.3.3.6 Chord and twist distribution

Of critical importance to the operational characteristics of the rotor is the radial distribution of the aerofoil chord and twist. This determines the load distribution across

the blade and the performance in terms of lift and drag. The following methodology used is taken directly from Griffiths [1] and is adapted to be calculated in Microsoft Excel. The implementation of the theory is presented in detail in Chapter 4.

A BEMT is developed based on propeller theory for the design of wind turbine blades. It takes some account of the complex nature of the flow and the aerodynamic drag on the blades. The forces are described in terms of torque and axial force and these equations can be solved to determine the optimum blade profile in terms of chord length and twist relative to the plane of rotation. Interference factors are defined as follows:

$$a = \frac{u}{U} \quad b = \frac{\omega}{2\Omega}$$

Where Ω is the angular velocity of the rotor, ω is the angular velocity of the fluid well down stream, u is the axial velocity in the plane of the rotor and U is the velocity upstream.

The system is solved by determining values for the interference factors a *and* b. The resulting solidity and inflow velocity is used to calculate chord length and blade angle. The optimum values for a and b are those that allow the aerofoil to operate at maximum efficiency over the blade radius, that is when torque is a maximum for each value of r. This is described in more detail in section 4.1.2.

The input variables are diameter, design TSR, and aerofoil maximum lift/drag ratio. The blade is discretised along the radius and the profile is described for each section in terms of chord length and twist. The resulting profile is described in Figure 3.09.

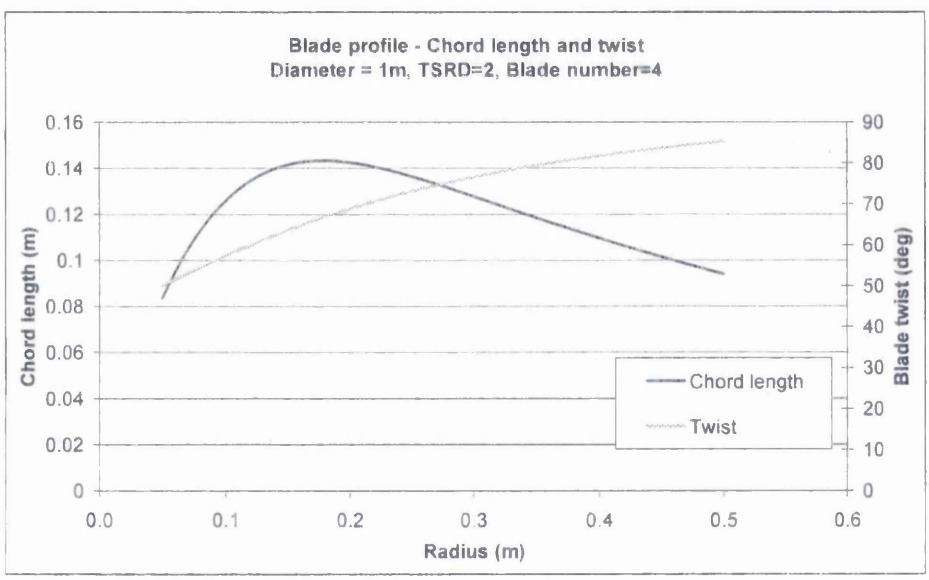

Figure 3.09 - Blade geometry used in the experiment

3.3.4 Blade construction

The method of transferring these parameters from data to a physical blade is essentially taken from Woollard [11]. A plug is made in the profile of the blade, from which female moulds are taken. Blade halves are created in these and joined together over a central spar.

The outputs of the design stage are a series of chord lengths and twists. The transfer to physical form involves dividing the blade into sections along the radius and making each section individually. To make the plug, the sections are then combined, in effect 'stacked' and rotated to the correct position. Woollard [11] undertakes this using plywood sections and a lathe to rotate and combine them. In this experiment, computer aided design and rapid prototyping techniques are employed.

3.3.4.1 Computer Aided Design

A three dimensional model of an individual blade is generated on a computer from the outputs of the design stage. The CAD package 'Autocad' was used for this operation. To enable an accurate profile to be created, the blade is discretised into 5000 radial elements of 0.1mm thickness. Each element is defined by radial position, chord length, angular displacement and the NACA4424 aerofoil profile.

A script file was created to undertake the generation of each element automatically. This was created using the design data in Microsoft Excel and processed with Fortran to ensure the correct formatting.

The operation undertaken by the script file is described in Figure 3.10.

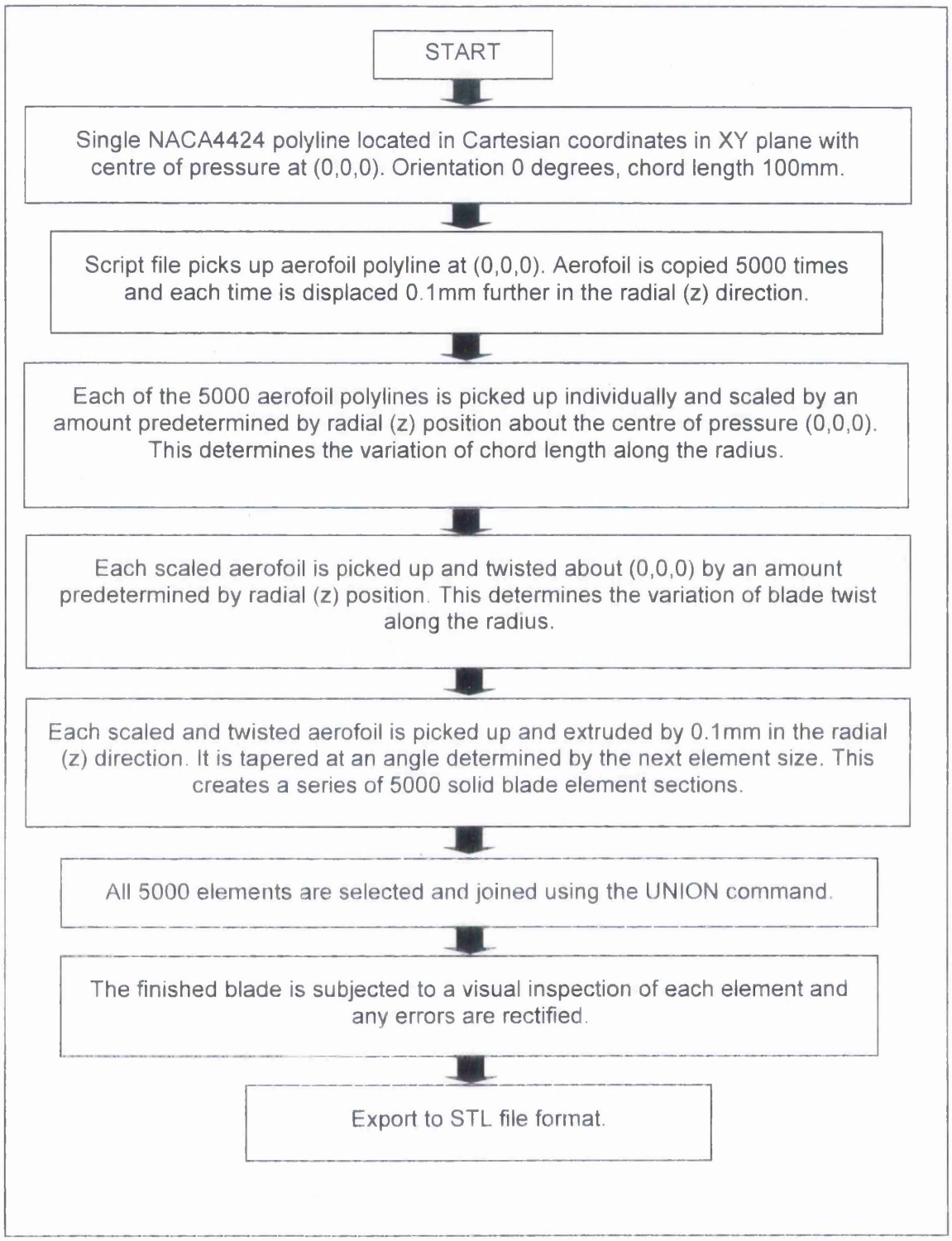

Figure 3.10 - Script file operation flow chart

The resultant blade profile model is shown in Figure 3.11.

Figure 3.11 - Computer generated blade profile

3.3.4.2 Plug construction - Rapid prototyping

The Engineering Department at Swansea University has a rapid prototyping machine which operates like a 3D printer, differing in the way that it applies a polyester based plastic to the substrate rather than ink. Objects are built up layer upon layer, each layer having a thickness of approximately 0.3mm. The object geometry is defined by the STL format, which is a triangular surface mesh.

The workspace available for use inside the printer is of dimensions 200 x 400 x 200mm. It is therefore clear that a 0.5m radius blade cannot be created in one piece. After extensive investigations into the method which the printer uses to create objects, it is concluded that the most effective orientation for the object is to have the radius in the Z plane. This is because the layers are applied sequentially in the XY plane. As the first layer is applied, the perimeter of the aerofoil shape is printed. The central section is then filled in using a tight zig-zag. To obtain a continuous external surface it is necessary to orientate the blade in this manner.

The blade plug is made in 5 sections. Section 2 can be seen under construction in Figure 3.12. Once complete, the sections are joined using polyester resin. The surface is then smoothed to eliminate surface imperfections, and a tip piece is added and smoothed. The resultant plug is complete and ready to cast the female moulds.

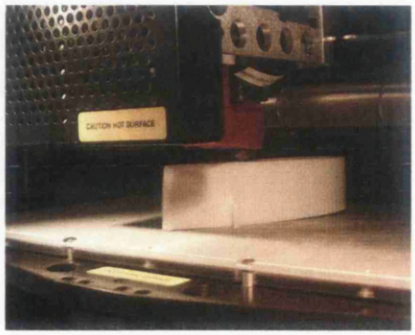

Figure 3.12 - Rapid prototyping of the blade mould plug

3.3.4.3 Mould construction

The female mould is created in two halves and therefore the point at which the halves meet is defined by the centre of the leading edge and the trailing edge. To create the first mould, the blade is embedded in modeling clay up to the mid point. Layers of GRP are placed over the blade plug and the clay. Release agent is used to stop the GRP adhering to the blade plug. 1 layer of fine mat is used followed by 4 layers of chopped strand for rigidity.

The plug is released from the mould and then reinserted. Release agent is again used and the second half is laid up across blade plug and mould as shown in Figure 3.13.

Figure 3.13 - The blade plug in one half of the mould

3.3.4.4 Stainless spar

To maintain the structural integrity of the blades under full load operation, it is determined that a steel spar is necessary. The dimensions and connections associated

with this are designed using the applied loads calculated by the theory from [1]. This is inserted between the blade halves and aligned with the trailing edge. At the blade root, the spar is 20mm diameter. The spar is shown in Figure 3.14 being inserted into a blade half.

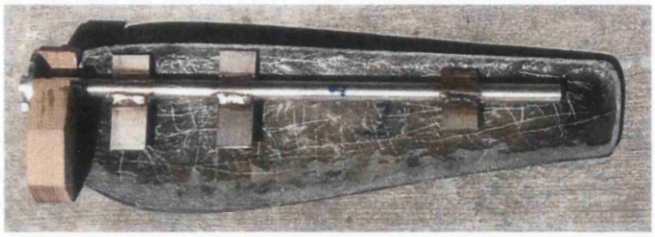

Figure 3.14 - Stainless spar inserted and aligned in finished blade half

3.3.4.5 Joining and finishing

To enable the blade halves to be joined securely, some glass fibres from each of the halves are left proud of the internal GRP surface. Additional chopped strand mat and polyester resin are pushed between the two halves before joining. The blade halves are joined within the two mould halves which are bolted together to ensure a correct and tight fit. Any irregularities in the blade surface or joins are then removed by hand to ensure a waterproof seal. The finished blades are smoothed and polished.

Figure 3.15 - Finished rotor blades on 3 bladed hub.

3.3.5 Chassis and nacelle

The structure of the experimental device is designed using loads predicted by the methodology in [1]. However owing to dynamic effects including turbulence and imbalance, additional software was used to predict the rotordynamic characteristics of the system [12]. The fundamental theory behind this can be found in [13].

3.3.5.1 System Layout

The system layout is shown in Figure 3.16.

3.3.5.2 Shaft

The required shaft diameter is calculated using [12]. This takes into account the effects of imbalance and ensures that the frequencies of operation are well below the critical speeds of the device. The primary shaft diameter is 55mm. The material is stainless steel AISI Type 502.

3.3.5.3 Bearings

The bearings used in the front housing are both taper roller bearings. The thrust load is resisted by the front bearing. The bearings in the generator section are simple roller bearings as supplied by Proven Engineering.

3.3.5.4 Coupling and torque monitoring

A torque meter strain ring is mounted in a flexible coupling which serves as the main coupling from the shaft to the generator.

The torque meter is fitted between the rotor and the load to measure the torque transmitted to the load either braked or electrical. It is rated from 0-125Nm to cope with 1500W at 120rpm. It maintains accuracy between 12.5Nm and 125Nm but is unreliable below this range.

The shaft mounted strain ring includes a transmitter that sends a signal to a close mounted E60RX reciever. This is mounted on one of the pipes of the mid section structure. This signal is fed to the monitor screen and converted into a 0-10V output to be recorded by the data logger.

3.3.5.5 Braking System

The braking system serves two functions, to stop the turbine and to control the speed during testing. A hydraulic car brake from a mk3 Ford Fiesta is used. This is over powerful so to desensitise it the pad area has been reduced by 2/3.

The brake is fitted inside the generator frame to save space, however this presents he difficulty that the shaft cannot be easily removed. For this reason the brake disc is made in two halves that are bolted together onto the shaft.

The caliper is supported by a mounting frame on the front plate of the alternator. The brake pipe is fed through the plate, protected by plastic sheath, through the midsection and out of a cable gland in the front housing plate.

The master cylinder actuator is designed to be hand operated. A simple screw thread is used to transform the rotation of the handle into a linear motion to force the master cylinder. A table top frame supports this mechanism. Return of the brake to the open position relies solely upon a slight misalignment of the disc to force the pads open and hence the master cylinder back.

3.3.5.6 Sealing system

- The shaft seal is a ceramic carbon bellows type face seal. This is located within the sealcap.
- The front plate seal is an O-ring type seal held between the mid section flange and the front plate.
- The rear plate seal is a circumferential O-ring type seal which is held between the generator housing and the rear plate.
- All cables are sealed using cable glands rated at 5 bar.

3.3.5.7 Bilge system

In the event of water ingress a bilge pump is fitted. It is located below the generator which is the lowest point of the device. In the event that water needs to be pumped out of the system, atmospheric air must be allowed to replace it so that a vacuum is not formed. If a vacuum occurs, this would increase the pressure differential across the seals. For this reason an atmospheric air intake is provided.

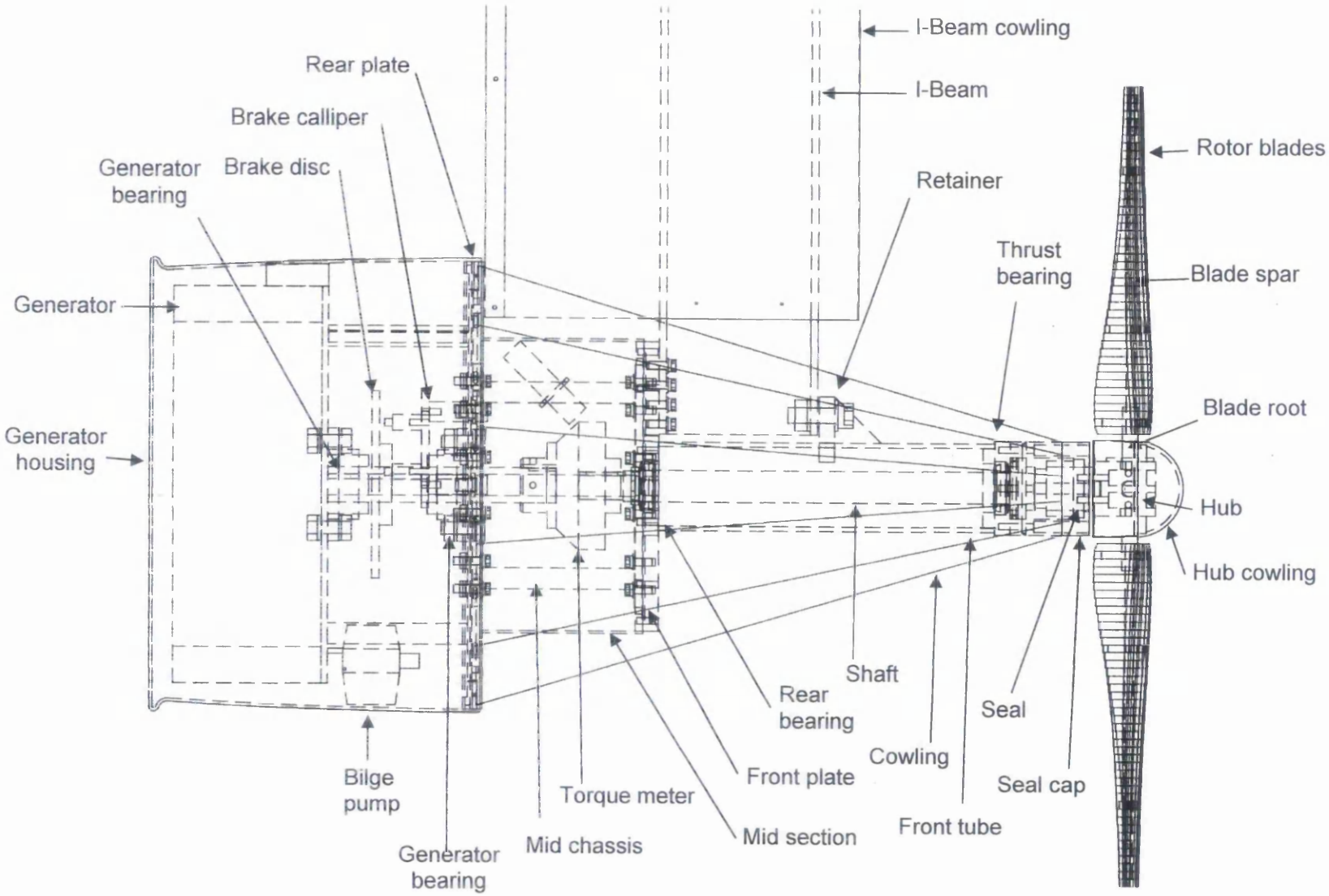

Figure 3.16 - Turbine system layout

3.3.6 Electrical system

3.3.6.1 Proven Controller

The power utilisation system is sourced from Proven Engineering Products Ltd. It is matched to the alternator as a 2.5kW system. It is a voltage controlled divert system which will adjust the load on the system in accordance with the power being generated.

The first stage of the system is the controller box. This incorporates the system of divert loads which are switched in at increasing voltages. The 3 phase supply is rectified to produce DC. The DC voltage is measured by a circuit that controls the divert relays.

When the voltage exceeds the battery voltage the batteries begin to be charged. At specified additional voltages two DC divert relays are switched in, enabling the power to be dissipated in the load of the users choice. Three AC divert loads are switched in the same way.. These are loads that draw current through the inverter. The inverter automatically switches on when these are switched in.

Another feature is battery charging. If the controller senses that the battery voltage is below a certain threshold it switches a relay that supplies mains power to the inverter. This automatically switches the inverter on in battery charging mode. This is to protect the battery from being damaged by too deep a charging / powering cycling. All of the switched relays incorporate hysteresis to stop them switching in and out repeatedly.

On the front of the controller box there are voltage and current meters taken from the battery and a shunt respectively. These are crude indicators and although useful are intended for observation only.

3.3.6.2 Power box

Two separate boxes are used for the data acquisition system. The power box contains power supplies and larger currents and voltages. It was designed and built with the help of Mr Christian Hilario of the University of Reims. See Figure 3.17. Included features are:

1. Mains supply in – a plug to connect the entire system to a mains power supply; protected by a emergency stop switch.

2. Mains supply for the inverter charging function

3. Power supply transformer for the data logger – a standard 13A plug socket to supply the 9V data logger adaptor.

4. Power supply transformer for the LEM current meter – an integrated transformer providing –15 +15 V.

5. Power supply transformer for the pump – a 15V 6.7A capacity transformer

6. Power supply transformer for the Frequency Voltage converter – a 24V transformer.

7. Frequency voltage converter signal transformer – 10:1 ratio transformer designed to bring the signal voltage down to an acceptable level.

8. Potential dividers for battery and rectifier voltage measurement – 2 potential dividers : The battery circuit is in the ratio 1/8.62 and the rectifier in the ratio 1/16.

9. Pump and battery charging relays – two 24V actuated relays

10. Auxiliary mains power socket

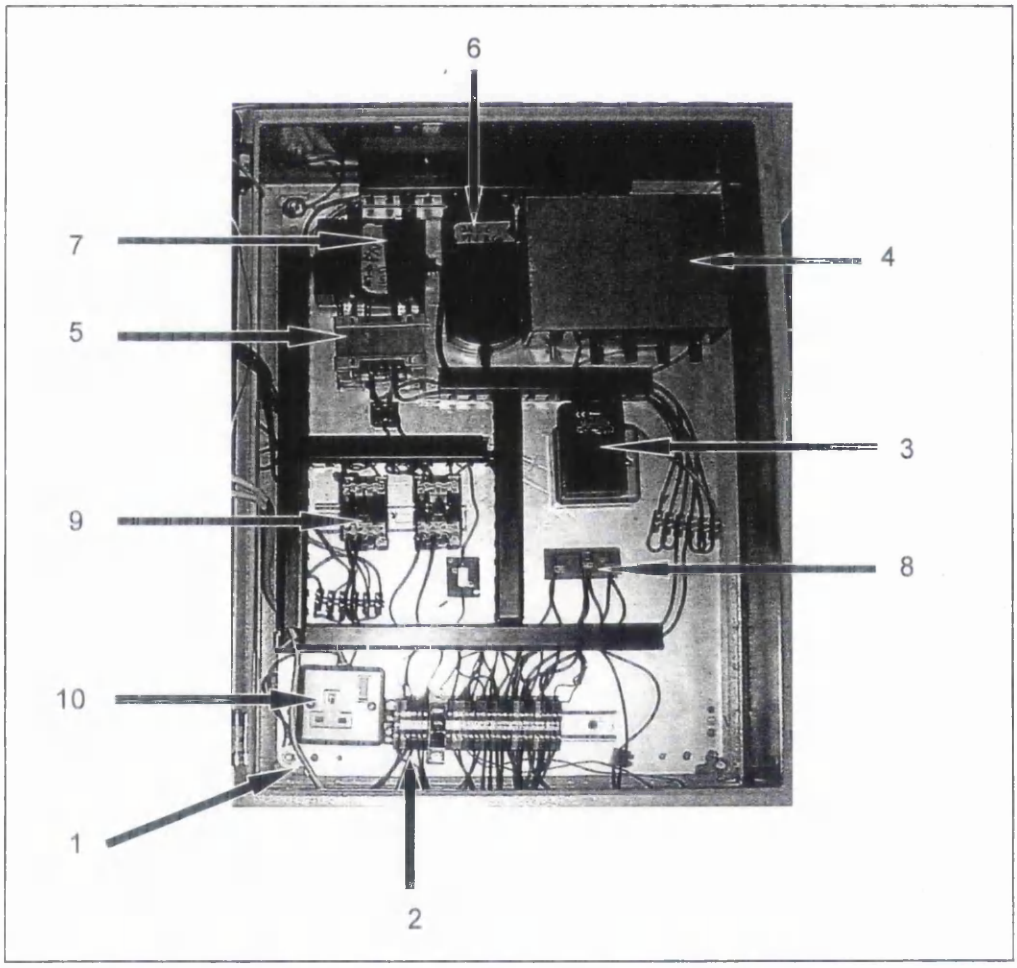

Figure 3.17 - The power box layout

3.3.6.3 Data box

The data box includes the data logger, the frequency voltage converter circuit and a visual display for rotor speed. The frequency voltage converter is separated form the power box as it is very sensitive to external signals i.e. mains frequency interference.

3.3.6.4 Data logger

- 8 Channel recording + 1 pulse count channel.
- Direct connection of thermocouples, voltage, 4 to 20mA current, and thermistors.
- Direct connection to laptop or PC for direct monitoring
- External triggers can start and stop the logger.
- Environmental operation: -30 to +65°C, 0 to 95%RH.
- External power supply: 9 to 14Vdc (9V internal battery included).
- Communications via RS232C with auto-baud detect.
- Rapid memory download at 19.2 kbit/s.
- Optional alarm features.

3.3.6.5 Frequency voltage converter

The F/V converter circuit is a method of determining the speed of the rotor. It measures the frequency of the AC signal across 2 phases of the generator output. This frequency is converted into an output voltage of between 0 and 5V volts. This is displayed on a voltmeter on the front of the data box and recorded by the data logger.

3.3.6.6 Batteries

The battery is an extremely important part of the system as this allows the user flexibility to use the power at the time and in the quantity required. However, it is also a major cost consideration. A compromise is selected from Proven Engineering Ltd who supply Hawker batteries. A 48V 460 Ah long life tubular plate battery has been acquired. However the size and weight of these cells is restrictive in using them for experimental testing. Hence 4

standard 12V car batteries were used to simulate the battery for the experiment, this is 48V, 30Ah.

3.3.6.7 Inverter

Supplied by Proven Engineering Ltd, the inverter is a standard Studer Solartechnik Sinewave Inverter and Battery charger, capacity 3.5kW. The primary functions of the device are:

1. Converting the 48V DC from the batteries into a useable 240V 50Hz AC power source.
2. Charging the batteries from mains power to protect them from low charge damage.
3. To supply any loads using the inverter with power from the mains in the event of low battery condition.

The inverter input is connected directly to the batteries. The 240V output is sent back to the proven controller where there it is outputted to the AC load and AC divert loads by the control circuit. The low battery detector in the controller switches on the mains power in to the inverter and this automatically starts mains battery charging.

3.3.6.8 Divert loads

The controller sets the rate at which generated power is fed into the batteries. It does this by controlling the voltage differential between the batteries rated voltage and the input voltage from the generator. If this difference is too great then the controller switches in divert loads in parallel with the battery to increase the load and hence slow the turbine and reduce the voltage.

There are two types of divert loads, two D.C and three A.C. These can be set to cut in at particular voltages using variable resistors on the control circuit. The DC divert loads are connected in parallel with the battery charging DC from the generator. DC1 is used in the experiment, it is a 50 Ohm heating element. The A.C. loads are connected to the battery via the inverter. They are designed so that any power that has to be dissipated is dissipated in a useful and not wasteful manner, for example as heat to heat a building. In the experiment, two 500W flood lights are used to absorb power. The trigger voltages for these loads are shown in table 3.1 below.

Divert load	Dissipation capacity (W)	On Voltage	Off Voltage
DC1	50	56	51.7
DC2	100	56.2	52.6
AC1	300	56.6	53.0
AC2	500	57	53.4
AC3	500	57.4	54.0
DI	Disconnect	58.2	50.0

Table 3.1 – Details of divert loads used in the experiment

3.4 Experimental procedure

3.4.1 Overview

The object of the experiment is to evaluate the performance of the rotor blades, the generator and the control system. It is the intention that the theory used to design the rotor and predict the performance of the system will be evaluated against experimentally derived data. A secondary objective is to evaluate the design and functionality of the system components such as the generator, shaft, seals and structure.

To test the performance of the device over the operating range a controlled set of experiments is undertaken. The primary variables are flow speed, TSR and blade number. The turbine unit is towed behind the University Research Vessel 'Noctiluca', a twin hulled, twin propeller craft as shown in Figure 3.18. The testing is undertaken in the River Tawe in Swansea, UK.

3.4.2 Vessel and test conditions

3.4.2.1 RV Noctiluca

The RV Noctiluca is a 12.5m catamaran with a hull length of 12.5m and a distance of 1.1m between the hulls at the surface. It is equipped with an A-Frame with a winch capable of lifting 1.5 Tonnes. The structure and superstructure are constructed of aluminium and has an unloaded draught of 0.5m. It has twin 140kW diesel engines in each hull and a maximum cruising speed of 15knots.

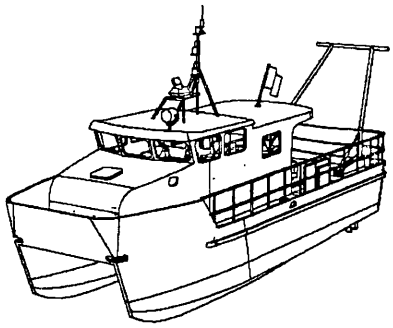

Figure 3.18 - The RV Nociluca

The RV Noctiluca is based at Swansea Marina and is ideally suited to the turbine test programme owing to the versatility of the vessel and the crew.

3.4.2.2 River Tawe

At the time of the experiment, the River Tawe at Swansea, grid reference 51° 36'.43N, 03° 55'.67W, has an uninterrupted stretch of water approximately 600m in length and 3m depth. Although the depth varies according to the state of the tide and river flow, it is consistently around 3m with a variation of 0.5m owing to local bathymetry.

The summer months see a significantly reduced rainfall and the weir at the barrage maintains the depth of water. The flow rate is considered to be negligible for two reasons, the first is that there is very little current, in the region of 0.05 knots and secondly the velocity is measured between the vessel and the water meaning that any river flow speed is negated.

3.4.3 Installation

The total weight of the turbine system is approximately 250kg and it is therefore necessary to use the marina hoist to install the system into place. The bulk of the structure is set up on the vessel so that when the turbine and frame are lowered it can be connected simply. The lowering procedure can be seen in Figure 3.19.

Figure 3.19 - Turbine being installed by marina crane

The turbine is arranged in such a manner that it can be raised and lowered by the A-frame and winch. Its lowest position is the operational position and the highest position brings it totally out of the water.

The diagram in Figure 3.20 illustrates the relative positions of the system.

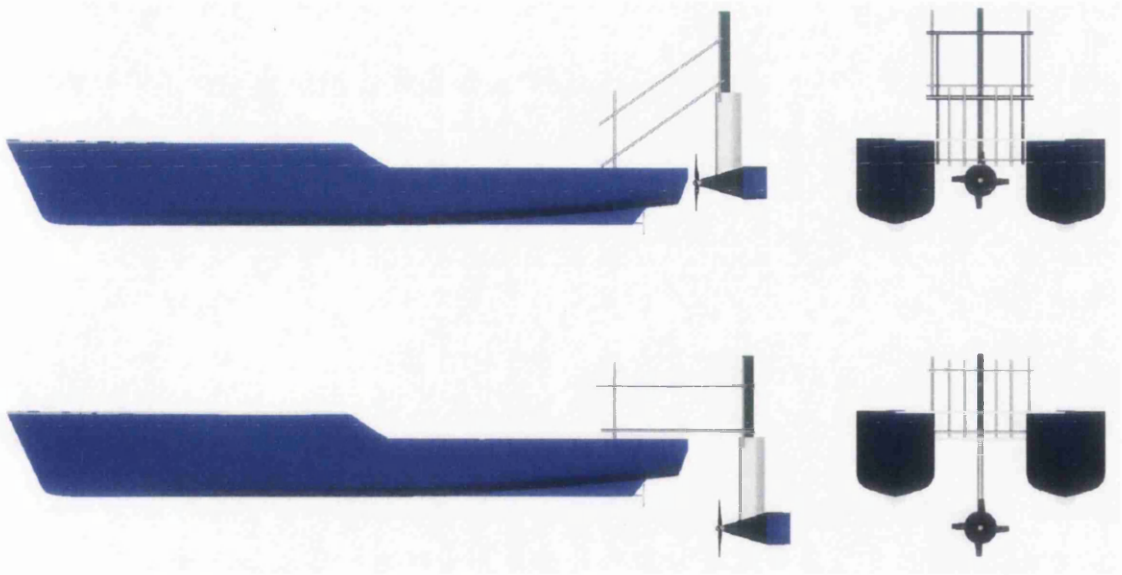

Figure 3.20 - Turbine in position at the stern of the RV Noctiluca, raised (top) and lowered

3.4.4 Dunk test

A dunk test is undertaken to evaluate the integrity of the primary seals and to ensure that the sub-systems function effectively underwater. This involves submerging the device momentarily in order to test the seals without a severe risk to the equipment. The turbine is removed from the water after a period of 15mins to ascertain the level of water ingress. All electronic systems are checked for functionality and to ensure there are no earth problems associated with submersion.

3.4.5 Flow measurement

The measurement of the flow speed is of critical importance to the results of the testing as the power output is proportional to the cube of the velocity. This implies that even small errors in flow measurement will result in significant error magnitude. For this reason a system was developed which adapted an Ott meter for electronic measurement. The Ott meter is an impeller flow meter designed to undertake flow velocity measurements in rivers and streams. For use in this experiment it is placed in front of the rotor blades at a distance of about 0.5m upstream. Each revolution of the impeller is recorded by the data logger and the flow speed is calculated from this using a calibrated scale.

3.4.6 Experimental runs

The experiments undertaken were controlled by flow speed and rotational speed. The vessel started from stationary and was accelerated to speed before beginning the test. The turbine begins to rotate at the cut-in speed and continues to accelerate. At this point, the boat may slow down in reaction to the increased axial force on the turbine and hence extra throttle is provided to maintain the hull speed. The brake is used to control the rotational speed of the turbine and this is adjusted until it is running at the desired tip speed ratio. By this method, the performance at different constant TSRs is investigated. By releasing the brake altogether, the overspeed characteristics can be observed.

Alternatively, to examine the characteristics of the electrical control system, the brake is released and the turbine is controlled automatically by the divert loads. In addition, blade numbers are varied to investigate off-design conditions. The full range of experiments is included in table 3.2 below. A run classified with RPM – 'free' is a run where no additional torque loading is applied to the shaft. The only load applied is the friction in the bearings and seal. This effectively allows the turbine to operate close to the propeller brake state. A run classified with RPM – 'auto' is a run under automated electrical control.

Table 3.2- Experimental runs

Run no.	Blade no.	Boat speed kts	Rpm	Elec status	Run no.	Blade no.	Boat speed kts	Rpm	Elec status
1	4	4	0	None	24	4	4	125	None
2	4	4	75	None	25	2	4	0	None
3	4	4	100	None	26	2	4	free	None
4	4	4	150	None	27	2	4	200	None
5	4	4	200	None	28	2	4	150	None
6	4	3.5	0	None	29	2	4	100	None
7	4	3.5	75	None	30	2	3	free	None
8	4	3.5	100	None	31	2	4	150	None
9	4	3.5	150	None	32	2	3.5	150	None
10	4	3.5	200	None	33	3	4	-	Auto
11	4	3--4	-	Auto	34	3	4	200	None
12	4	3	-	Auto	35	3	4	150	None
13	4	3.5	-	Auto	36	3	4	100	None
14	4	4	-	Auto	37	3	3.5	200	None
15	4	4.5	-	Auto	38	3	3.5	150	None
16	4	3	free	None	39	3	3.5	100	None
17	4	4.5	-	Auto	40	3	3.5	0	None
18	4	4.5	-	Auto	41	3	4	free	None
19	4	5	-	Auto	42	3	3	free	None
20	4	2.5	150	None	43	3	4	125	None
21	4	2.5	125	None	44	3	3.5	125	None
22	4	3	125	None	45	3	3	125	None
23	4	3.5	125	None					

3.5 Experimental results

3.5.1 Analysis

The Squirrelview 800 data logger exports to an Excel spreadsheet in the form of engineering units or voltages. These values are processed using conversion equations to output the required units. The measured parameters are listed in table 3.3.

Symbol	Parameter	Method	Issues
U	Upstream flow velocity (m/s)	Ott meter	Interference from environmental AC signals causes problems unless insulation and shielding is undertaken thoroughly.
T	Shaft Torque (Nm)	Strain ring	Strain ring mounted in shaft coupling very effective however limited minimum range left 2 runs with incomplete data. Straight line approximation to voltage scale extrapolated to acquire values.
ω	Shaft angular velocity (rad/s)	Frequency Voltage converter	F/V calibrated in lab. Incurred lag of 2-3 seconds resulting in smoothed signal, No problem at ~constant speed.
V_r	Rectifier Voltage (V)	Resistor bridge	None
V_b	Battery Voltage (V)	Resistor bridge	None
I	Charging current (A)	Current transducer	Solid core CT worked correctly
T	Temperature (C)	Thermocouple on generator coils	Interference from generator AC meant that temperature could only be measured when turbine was stationary
wa	Water ingress	Resistance monitoring	System worked well with alarm fuctioning on ingress.

Table 3.3 - Measured parameters

3.5.2 Sampling Frequency

The sampling frequency of 1Hz was adequate for measuring average values and general performance characteristics. This system was originally selected for its ability to measure the performance of the turbine in long-term deployment. However to allow investigation of the dynamic characteristics of the system a frequency of about 10Hz would be required.

3.5.3 Statistical Analysis

Owing to the limited sampling frequency, it is not possible to investigate the dynamic performance of the system. The results from each experimental run were averaged to obtain a meaningful comparison. Figure 3.21 shows a typical example of the averaging of a power data signal over a 2 minute run. The average is marked as the solid straight line.

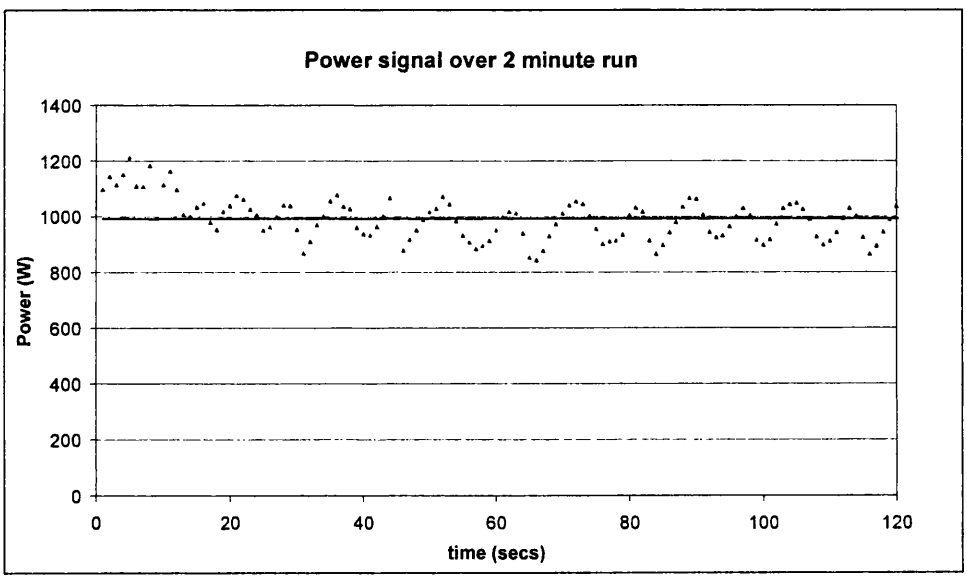

Figure 3.21 - Typical averaging of power values

3.5.4 Performance analysis

3.5.4.1 Electrical performance

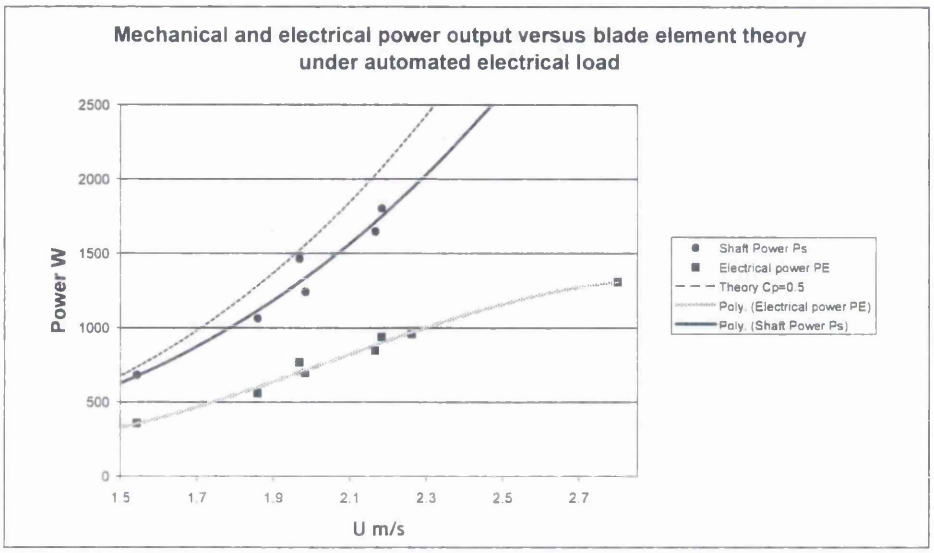

Figure 3.22 - Power output with respect to flow velocity

Figure 3.22 shows the relationship between the flow velocity and the power output of the rotor and the generator. The predicted rotor power output is shown as the line of C_p = 0.5. It can be seen that the experimentally determined rotor power is fractionally lower than the predicted output and this is reflected in Figure 3.23 where the power coefficients are slightly lower than 0.5. The trend is very similar to the theory in [1] and it is thought that the difference is mostly owing to mechanical losses in the drive train.

The scatter is thought to be owing to the automatic control of the way in which divert loads are switched in to the system. Hysteresis in the control system has the effect that there is more than one operating state for a given flow and this introduces scatter. This is most clearly seen in the two readings close to a flow speed of 2m/s in Figure 3.22.

The electrical power points show a similar scatter but to a lesser extent and a very clear trend is discerned with regard to the flow velocity. The higher values appear to be somewhat reduced and this is thought to be owing to the reduction in PMG efficiency at higher speeds. At higher speeds the PMG encounters an electrical current slightly above its design rating. This increases resistive losses owing to the build up of excess heat in the winding. The efficiency may be improved by increased cooling.

3.5.4.2 Rotor power and torque coefficients C_p and C_t

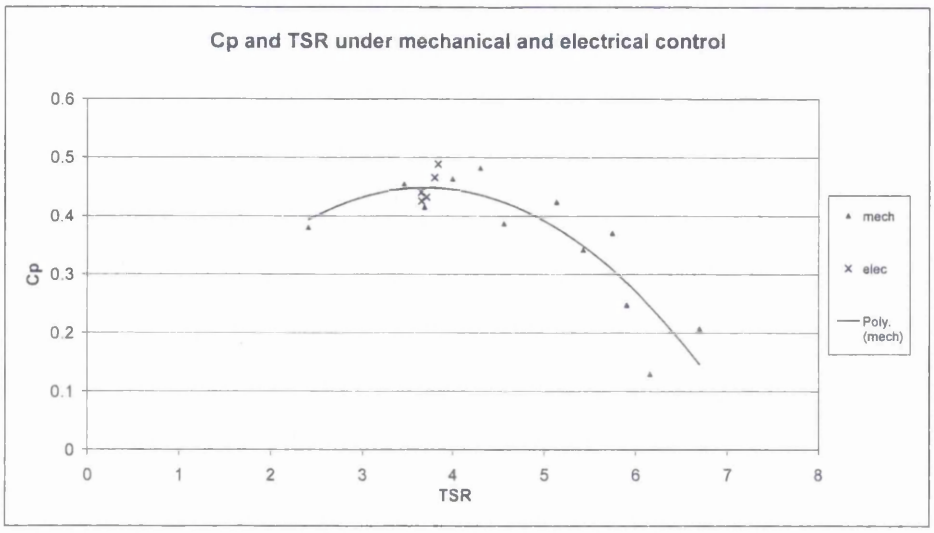

Figure 3.23 Experimental variation of power coefficient with TSR

Figure 3.23 shows the variation of C_p with TSR on mechanically loaded and electrically automated runs. Although the level of scatter is quite high, a clear pattern is discernable and this is indicated by the trend line. As predicted by blade element theory [1], there is a distinctive peak in the efficiency and then it drops off steadily into higher degrees of overspeed. A main point of interest is that the peak efficiency occurs at a TSR of just over 4. Note this is the power peak, while the blades are designed to the torque peak. The electrically controlled system also uses a TSR of around 4. Both are operating above the design speed of the blades but achieving good efficiencies of 0.4 to 0.5.

It is clearly seen and stated in Paish [14] that the rotor operates faster than the design point. This is desirable because if the design point is close to the stall point of the aerofoil, then any small reduction in speed results in a collapse of the efficiency as the rotor stalls. However, in this experiment, there is considerable scope for improvement by slowing the rotor by extracting more power. The generator would have been capable of this as a large generator was used to provide robustness, however the dump load did not have the capacity to load the generator further.

Figure 3.24 shows the variation of C_t with TSR on mechanically loaded and electrically automated runs. It can be seen that although the level of scatter is again significant, the general trend is distinctive and almost a linear decrease with TSR. It is also clear that no runs were undertaken in the stalled region of operation at very low TSR as the rotor is very

unstable in this region of operation and is prone to complete stoppage as stall occurs across the blade.

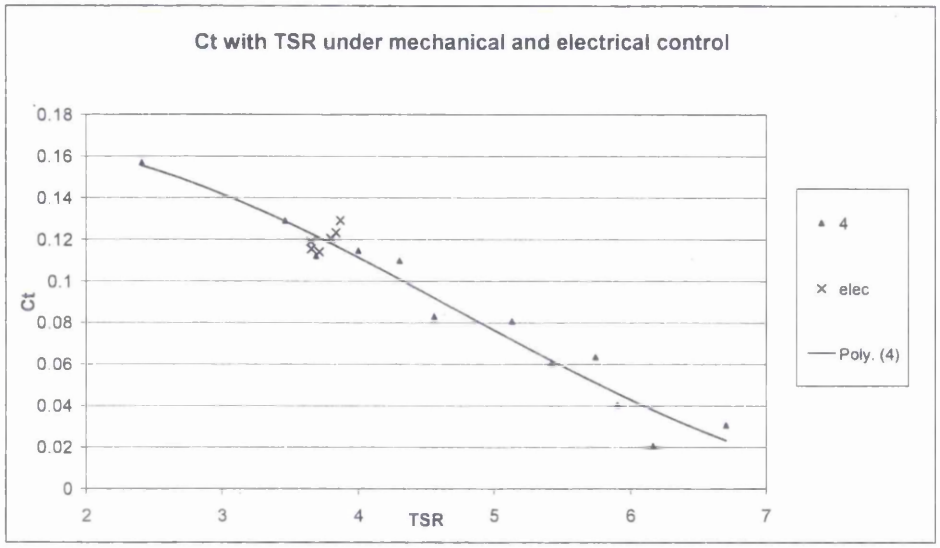

Figure 3.24 Experimental variation of torque coefficient with TSR

3.5.4.3 Blade number

Figures 3.25 and 3.26 show the effect of changing the blade number on the power and torque performance. Firstly it is important to state that it is not only blade number that is varied, but also solidity. This is because the same blades are used in different numbers and if the blades were designed for 2 or 3 bladed operation the chords would be larger to obtain the same solidity and operating TSR.

It is clear that the 4 blade configuration operates with the greatest efficiency over the greatest range of TSR. This is the result as expected. At a TSR of 4.25 the number of blades appears to make the least difference although there is still scatter at this point. For example at TSR 4.4 the three bladed configuration has a C_P that varies from 0.44 to 0.31. Here the velocity U varies from 1.95 to 1.58, the RPM from 161 to 134 and the C_T from 0.095 to 0.07. When C_p = 0.31 the rotor is operating at a less powerful level at the same TSR and there is proportionally less power output to the shaft. This is the result of the variation in Reynolds number at different operating conditions as shown in figure 3.25b. The lift and drag characteristics of the aerofoil vary with Reynolds number as shown in section 3.3.3.4. This will certainly result in various power coefficients at the same TSR which goes some way to describing the lack of consistency in figure 3.25.

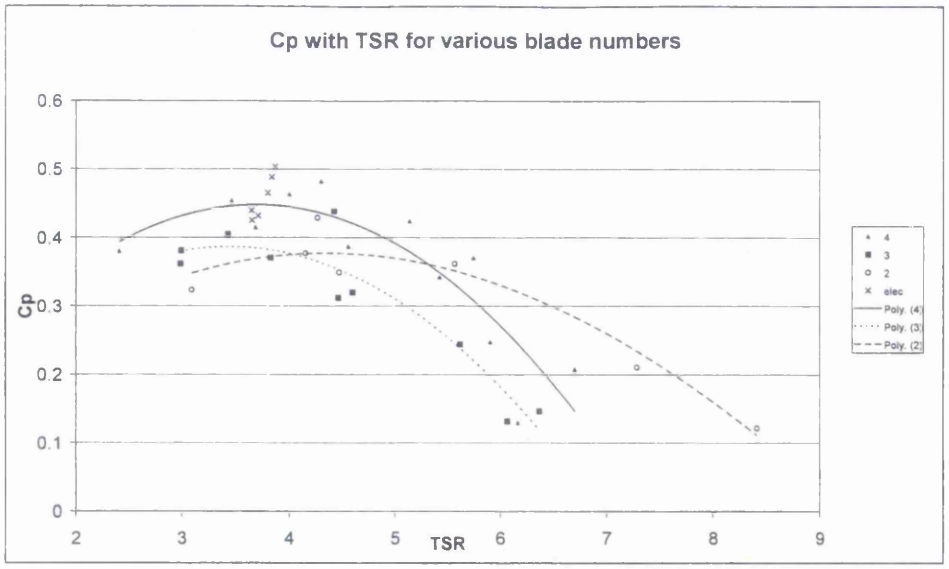

Figure 3.25 C_p with respect to TSR for various blade numbers

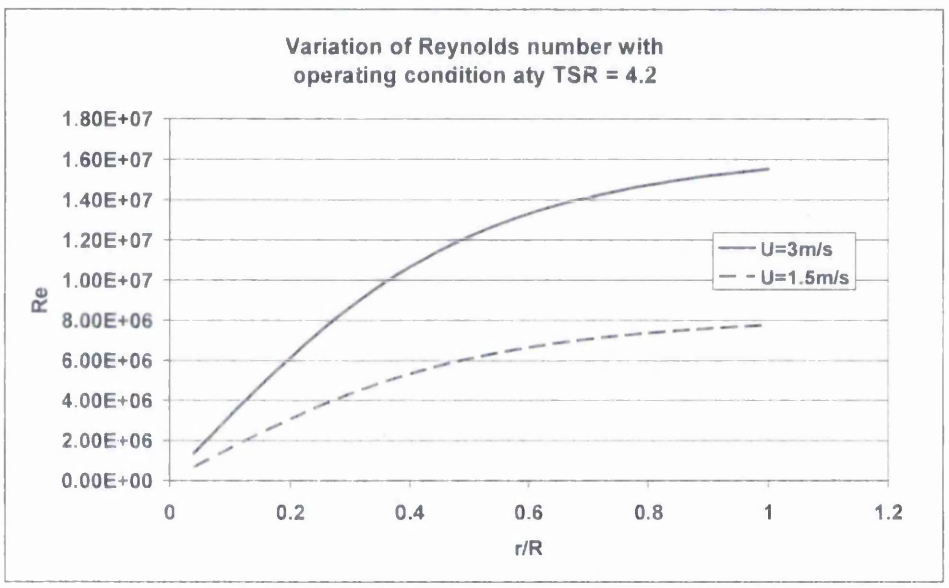

Figure 3.25b Variation of Reynolds number with operating condition

Figure 3.25 shows that 2 blades operate more effectively at higher TSR. This is owing to the lower solidity of this configuration. The fewer blades interacting with the flow, the less the axial interference factor. This means that the rotor can operate at higher TSRs before the overspeed condition is reached and the flow is diverted around the rotor. It is worth noting here that the runs on which no load was applied have still not reached propeller brake state i.e. C_p = 0. This is owing to the residual friction load in the bearings and seal, and to a small degree the air resistance on the generator flywheel.

Figure 3.26 shows the variation in torque coefficient owing to differing blade number. For the designed operating TSR of between 2 and 5 the 4 bladed configuration is clearly the most effective design. However it appears that 2 blades begin to supply more torque above TSR 5.5. This coincides with variation in C_P shown in Figure 3.25 and is again likely owing to the reduced solidity. It is not clear why this effect is not observed so clearly with the 3 bladed rotor and further more detailed experimentation is recommended.

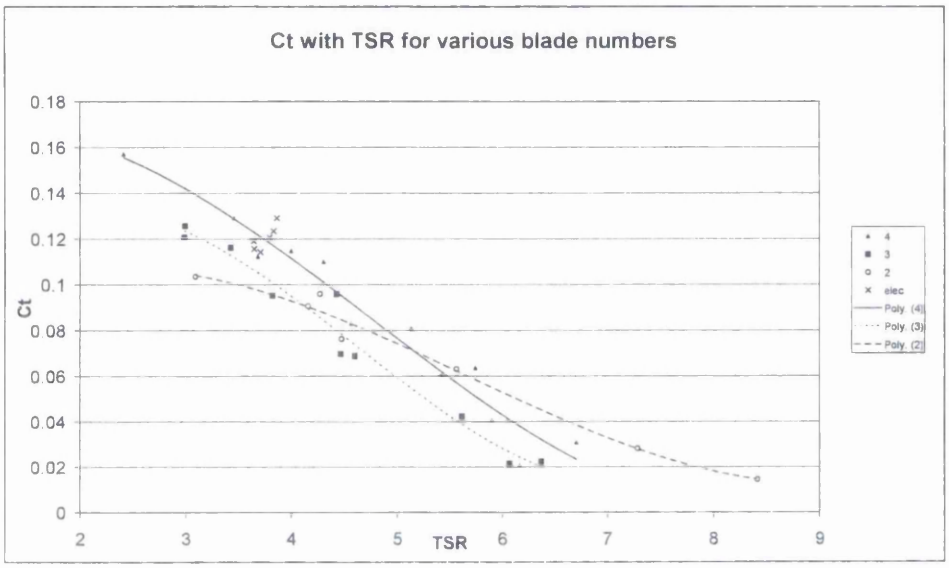

Figure 3.26 C_t with respect to TSR for various blade numbers

3.6 Conclusions

A 1m diameter, direct drive device has been designed, built and tested. The testing has concluded that competitive efficiencies can be achieved with a direct drive fixed pitch device.

The average rotor power coefficient under electrical operation is 0.46. This compares well to blade element theory.

- If an overall power coefficient C_E is defined as:

$$C_E = \frac{P_E}{\frac{1}{2}\rho U^3 A} \tag{3.2}$$

  Where P_E = electrical power output,

  the average C_E for this turbine is 0.24. This incorporates the blade efficiency, PMG efficiency, rectifier efficiency and mechanical and electrical losses up to the controller.

- In effect this means that the average electrical power that can be expected from a similar turbine for a particular flow rate is given by:

$$P_E = 0.24\frac{\rho\pi r^2}{2}U^3 \tag{3.3}$$

- There is a complex relationship between power and efficiency in overspeed conditions. However, intentional operation at overspeed appears to be an effective design strategy to allow a compromise between starting torque and PMG efficiency.

- At a particular TSR, the rotor can operate with different power characteristics. This is due to the effect of variations Reynolds number.

- A reduction in solidity by reducing the number of blades allows the rotor to operate at higher TSR before reaching propeller brake state.

- Rotors designed for a low TSR can be operated in overspeed and achieve this efficiency. This also allows the turbine to start at flow speeds down to 1.53m/s.

- A PMG is a suitable generator for a tidal stream or river turbine as it allows generation at varying rotational and flow speeds.

- The electrical divert-based control system is very effective, allowing the turbine to achieve high efficiencies under different conditions.

- The data capture and monitoring system worked well and can be transferred to other renewable systems for analysis of operating parameters.

3.7 References

1. Griffiths RT, *Energy From the Wind.* University of Wales Swansea internal report, 1974.
2. Cave PR, Evans EM, *Tidal energy systems for isolated communities.* West E, editor. Alternative energy systems. New York: Pergamon: p. 9–14, 1984.
3. UK Department of Trade and Industry, *Tidal stream energy review.* (ETSU T/05/00155/REP), 1993.
4. CENEX Project, *Tidal and marine currents energy exploitation.* ref. JOU2-CT-93-0355.Report EUR16683EN, 1996.
5. Betz A, *Die Naturwissenshaften.* Volume 9(No. 46), November 1927.
6. Griffiths RT, Woollard MG, *Performance of the optimal wind turbine.* Applied Energy 4, Applied Science Publishers Ltd, 1978.
7. Aerospace Web, NACA 4 Series, [online http://www.aerospaceweb.org/question/airfoils/q0041.shtml] 2006 (accessed 12/08/06),
8. Abbott I H, Von Doenhoff A E, *Theory of Airfoil Sections.* Dover, 1959.
9. Profili Airfoil Analysis Software, [online http://www.profili2.com/ 2006] (accessed 12/07/06).
10. Danish Wind Energy Association, *Wind turbines - how many blades?*, [online http://www.windpower.org/en/tour/design/concepts.htm 2006](accessed 12/07/06).
11. Woollard MG, *PhD Thesis: 'A design study for and experimental horizontal axis wind turbine'.* 1980.
12. Lees AW, *Rotordynamic Analysis Software.* 2001.
13. Friswell MI. Penny JE. Garvy SD. Lees AW, *Fundamentals of Rotor Dynamics.* Cambridge University Press, 2007 (To be published).
14. Paish O, Fraenkel P, *TIDAL STREAM ENERGY: ZERO-HEAD HYDROPOWER.* International Conference on Hydropower into The Next Century, Barcelona, 5-8 June, 1995.

4.0 DETAILED BLADE MODELLING

4.1 Blade element momentum theory

As described in Chapter 3, the turbine is initially modeled with a large number of blades so that it is effectively a circular disc where energy is extracted from the fluid. This approach was first used by Rankine and Froude and is commonly referred to as Actuator Disc Theory. The fluid is assumed to be perfect in that it is incompressible and inviscid. It is also assumed that there is no rotation of the flow downstream of the disc.

This analysis is taken directly from Griffiths [1]. For completeness the derivation is given here:

It can be shown [2] that the velocity in the plane of the disc is the mean of the velocities well upstream and well downstream of the device. As energy is absorbed from the flow by the rotor, the fluid slows and hence the streamtube bounded by the disc expands as shown in Figure 4.01:

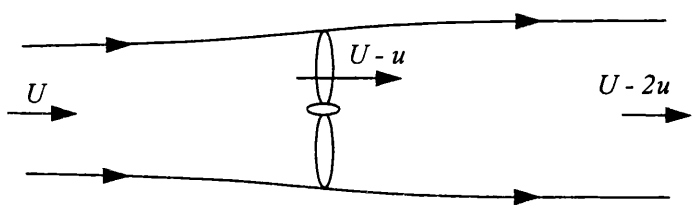

Figure 4.01 - Illustration of the assumptions made by Rankine and Froude

For an ideal rotor the power output on the shaft can then be described as the rate of loss of kinetic energy of the fluid. Assuming there is no rotational velocity well down stream of the rotor, this can be expressed as:

$$P = \frac{1}{2}\rho Q\left[U^2 - (U - 2u)^2\right]$$

where ρ is the fluid density, Q is the volume flow rate though the disc, U is the velocity well upstream of the rotor and u is the reduction in axial flow velocity at the plane of the disc. This can be expressed as

$$P = \frac{1}{2}\rho A(U-u)\left[U^2 - (U-2u)^2\right]$$

where A is the area of the disc. This is a maximum when

$$u = \frac{1}{3}U$$

and hence:

$$P_{\max} = \frac{8}{27}\rho A U^3$$

To define the efficiency of the energy conversion a power coefficient C_p is defined as:

$$C_P = \frac{P}{\frac{1}{2}\rho A U^3}$$

And therefore the maximum power coefficient is:

$$C_{P\max} = \frac{P_{\max}}{\frac{1}{2}\rho A U^3} = \frac{16}{27} = 0.593$$

This demonstrates that under artificially perfect conditions the theoretical maximum efficiency of the turbine is 59.3%. This is known as the Betz limit.

4.1.1 Addition of flow rotation

According to Newton's 3rd law of motion, for the fluid to cause a rotation of the turbine blades an opposite rotation will be imparted on the fluid. It is shown by Houghton [3] that the angular velocity of the fluid in the plane of the disc is half that of the angular velocity well downstream. Hence axial and rotational interference factors can be defined as follows:

$$a = \frac{u}{U} \quad b = \frac{\omega}{2\Omega}$$

Where Ω is the angular velocity of the rotor blades and ω is the angular velocity of the fluid well downstream.

The axial and rotational speeds of the water as it passes through the turbine are therefore $U(1-a)$ and $b\Omega$ respectively and hence the rotational speed relative to the blade is $\Omega(1+b)$. However owing to difference in tangential velocity and local speed ratio it is not necessary that the interference factors be equal over the blade radius. For this reason the blade is discretised across the radius R and a blade element of radius r, width dr and chord c is considered as shown in Figure 4.02.

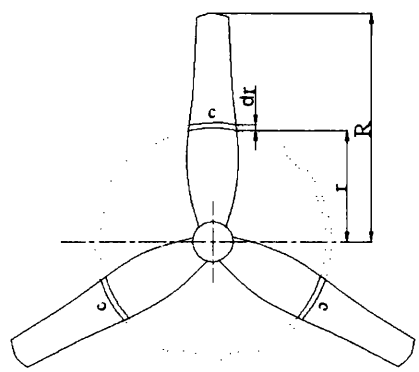

Figure 4.02 - Discretisation of the rotor

Each element experiences forces owing to the fluid and these can be broken down into to axial and tangential components as shown in Figure 4.03. The axial force components from each element combine to become the thrust or axial force experienced by the rotor. The tangential components combine to form the torque. For each radial annulus, the combined axial force and torque from all the blades are expressed as dF_A and dT respectively. The lift and drag for each element, dL and dD are defined by the angle of attack α of the blade element aerofoil section and the local velocity V. The blade twist angle ϕ is given by the direction of V relative to the axis of rotation when operating at the design point.

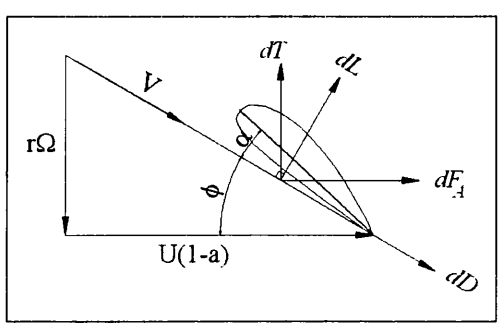

Figure 4.03 - Resolution of lift and drag forces

To obtain expressions for the annular axial force and torque, the momentum equation is applied between stations well upstream and downstream of the device where the pressures are assumed atmospheric and equal. The changes in angular velocity and axial velocity are ω and 2u respectively and the resultant expressions are:

$$dF_A = \rho.2\pi r.dr.(U-u)2u$$

$$dT = \rho.2\pi r.dr.(U-u)\omega r^2$$

which may be written:

$$\frac{dF_A}{dr} = 4\pi\rho r U^2(1-a)a \tag{4.1}$$

$$\frac{dT}{dr} = 4\pi\rho r^3 U\Omega(1-a)b \tag{4.2}$$

The fluid is assumed to be inviscid and the rotational flow of the fluid is in the opposite direction to that of the rotor and hence the energy equation for the annular element is:

$$(\Omega+\omega)dT = (U-u)dF_A$$

$$\text{or } \Omega(1+b)\frac{dT}{dr} = U(1-a)\frac{dF_A}{dr}$$

Substituting from equations (4.1) and (4.2) and calling $\frac{r\Omega}{U}$ the speed ratio x gives:

$$x^2 b(1+b) = a(1-a) \tag{4.3}$$

Also, the power generated by the rotor is given by:

$$P = \int_0^R \Omega dT$$

Substituting dT from equation (4.2) gives,

$$P = 4\pi\rho U\Omega^2 \int_0^R (1-a)br^3.dr$$

Therefore:

$$C_P = \frac{8}{X^2}\int_0^X (1-a)bx^3.dx \tag{4.4}$$

where $X = \frac{R\Omega}{U}$ the Tip Speed Ratio

4.1.2 Optimisation of blade design

C_P will be a maximum when *(1-a)b* is a maximum for each value of x. That is to say when:

$$\frac{db}{da} = \frac{b}{(1-a)} \tag{4.5}$$

Differentiating equation (4.3) and combining this with equation (4.5) to eliminate $\frac{db}{da}$ gives:

$$b = \frac{(1-3a)}{(4a-1)} \tag{4.6}$$

An inviscid analysis of the forces on a blade element gives only one force perpendicular to the local flow velocity, the lift force dL:

$$dF_A = dL \sin\phi$$

$$dF_T = \frac{dT}{r} = dL \cos\phi$$

where dF_T is the tangential component of the lift force for the blade element and;

$$\phi = \tan^{-1}\left[\frac{r\Omega(1+b)}{U(1-a)}\right] \tag{4.7}$$

ie.

$$\phi = \tan^{-1}\left[\frac{x(1+b)}{(1-a)}\right] \tag{4.8}$$

Comparing (4.8) with (4.1) and calling $\frac{Nc}{2\pi r}$ the local solidity σ;

$$\sigma C_L = \frac{4a\cos^2\phi}{(1-a)\sin\phi} \tag{4.9}$$

Where N is the number of blades and C_L is the lift coefficient for the aerofoil at optimum angle of attack.

This, with equation (4.7) gives the blade geometry for each blade element as the chord length and twist can be determined once the interference factors are known.

4.1.3 Real fluid effects

A real fluid has viscosity which means that tangential or shear forces are present. To accurately describe the effect of these forces, experimentally derived relationships are used. For a real fluid, the momentum equations (4.1) and (4.2) will still hold, but the energy equation (4.3) will not. A loss of energy will occur and a drag force dD will be experienced by the aerofoil. The axial and tangential components of the forces on the blade element are now:

$$dF_A = dL\sin\phi + dD\cos\phi$$

$$dF_T = \frac{dT}{r} = dL\cos\phi - dD\sin\phi$$

For the rotor, these are written in terms of the lift and drag coefficients as:

$$\frac{dF_A}{dr} = N\tfrac{1}{2}\rho V^2 c\left(C_L\sin\phi + C_D\cos\phi\right) \tag{4.10}$$

$$\frac{dT}{dr} = N\tfrac{1}{2}\rho V^2 cr\left(C_L\cos\phi - C_D\sin\phi\right) \tag{4.11}$$

Where:

$$dD = C_D\tfrac{1}{2}\rho V^2 c.dr$$

$$dL = C_L\tfrac{1}{2}\rho V^2 c.dr$$

and where C_D and C_L are experimentally derived functions of α.

Comparing (4.10) with (4.1) and noting that

$$\phi = \tan^{-1}\left[\frac{x(1+b)}{(1-a)}\right] \quad \text{and} \quad V = U\left[(1-a)^2 + x^2(1+b)^2\right]^{1/2}$$

there is an expression for local solidity:

$$\sigma = \frac{4a(1-a)}{\left[(1-a)^2 + x^2(1+b)^2\right]^{\frac{1}{2}}\left[C_L x(1+b) + C_D(1-a)\right]} \tag{4.12}$$

Similarly a comparison of (4.11) and (4.2) yields:

$$\sigma = \frac{4x(1-a)b}{\left[(1-a)^2 + x^2(1+b)^2\right]^{\frac{1}{2}}\left[C_L(1-a) - C_D x(1+b)\right]} \tag{4.13}$$

Eliminating σ between (4.12) and (4.13) gives and expression for the lift/drag ratio of the aerofoil:

$$\frac{C_L}{C_D} = \frac{x(a+b)}{\left[a(1-a) - x^2 b(1+b)\right]} \tag{4.14}$$

Calling R the maximum value of the lift/drag ratio for the aerofoil chosen, and differentiating equation 4.14;

$$\left[Rx^2(2b+1) + x\right]\frac{db}{da} = R(1-2a) + x \tag{4.15}$$

Substituting the requirement for maximum efficiency into equation (4.15) gives;

$$\left[Rx^2(2b+1) + x\right]b = (1-a)\left[R(1-2a) + x\right] \tag{4.16}$$

Combining (4.15) and (4.16) gives an expression for b:

$$b = \left\{\frac{R(4a-1)(1-a) + x(1-3a)}{x(Rx+1)}\right\} \tag{4.17}$$

For given values of the speed ratio x and the lift/drag ratio R, a and b can be determined from equations (4.14) and (4.17). The values of the interference factors can then be substituted into equation (4.4) to give the efficiency or into (4.7) and (4.8) to determine the optimum blade geometry.

4.1.4 Estimation of performance characteristics

To predict the power and loads on a rotor of a given geometry over the operating range, equations (4.1), (4.2), (4.10) and (4.11) are rearranged and given subscripts 1 and 2 to give equations (4.18) – (4.21). To solve this set, values of a and b are found which minimise ν, the residual difference between the torque and axial force terms as in

equation (4.22). (4.23) is used to find the value of V required in (4.19) and (4.21) and C_L and C_D are found from a lookup table from ϕ which is given by (4.24)

$$dF_{A1} = 4\pi\rho r U^2 (1-a) a.dr \tag{4.18}$$

$$dF_{A2} = N\tfrac{1}{2}\rho V^2 c(C_L \sin\phi + C_D \cos\phi).dr \tag{4.19}$$

$$dT_1 = 4\pi\rho r^3 U\Omega(1-a) b.dr \tag{4.20}$$

$$dT_2 = N\tfrac{1}{2}\rho V^2 cr(C_L \cos\phi - C_D \sin\phi).dr \tag{4.21}$$

$$v = (dF_{A1} - dF_{A2})^2 + (dT_1 - dT_2)^2 \tag{4.22}$$

$$V = U\left[(1-a)^2 + x^2(1+b)^2\right]^{1/2} \tag{4.23}$$

$$\phi = \tan^{-1}\left[\frac{x(1+b)}{(1-a)}\right] \tag{4.24}$$

By this method it is possible to estimate the performance of the blade at various tip speed ratios over the operating range.

4.1.5 Estimation of aerofoil characteristics

To enable the performance of the rotor to be estimated in conditions that are far away from optimum, aerofoil performance must be understood at a wide range of angles of attack. In it simplest form this is obvious at turbine start up, where the majority, if not the entire blade, is stalled at an angle of attack of 40 degrees and above.

Data concerning angles of attack of this magnitude is not readily accessible owing to the vast majority of data being acquired for aeronautic use. Readily available data is normally limited to about 20 degrees either side of zero and consequently a different approach is required to estimate CL and CD outside this range. It is likely that an axial flow rotor will experience no angles of attack outside the range of -20° to 90°, but it is estimated over 360° for completeness.

4.1.5.1 Lift coefficient

The variation of lift coefficient with angle of attack for the NACA4424 aerofoil section can be found in Abbott [4]. Many aerofoils are tested in a wind tunnel and experimentally determined data is presented. The experimentally determined lift coefficient for the NACA4424 is shown in Figure 4.04:

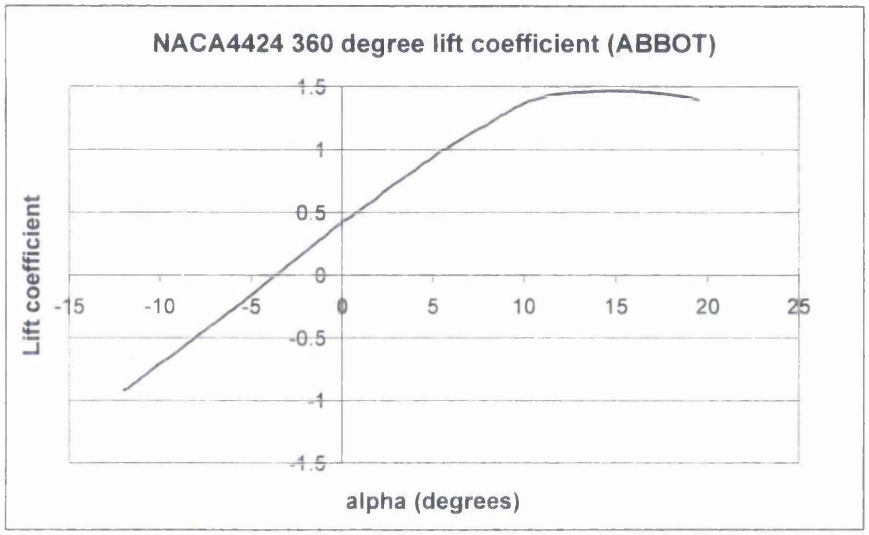

Figure 4.04 - Experimentally determined lift drag characteristics of the NACA4424 aerofoil

Where possible, experimental data is used to estimate C_L for a particular angle of attack and this is supplemented by a combination of approximated and theoretically determined data from Profili aerofoil performance prediction software [5] and inclined plate theory, Massey [6]. This is used for angles of incidence outside those shown in Figure 4.04.

To explain the method used to estimate the lift characteristics, it is beneficial to explain how a typical aerofoil lift coefficient varies with angle of attack α. In Figure 4.05, Sheldahl [7], the experimentally determined lift curve for the NACA0015 aerofoil is shown. At α=0°, C_L increases sharply and linearly until the onset of stall at α=12.5°.

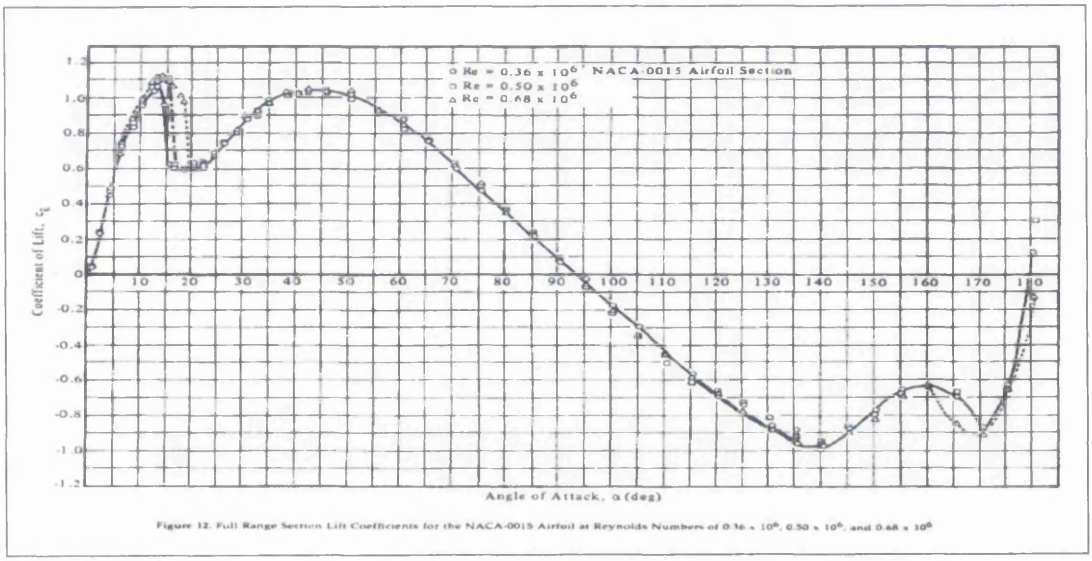

Figure 4.05 - Example of a full range aerofoil lift coefficient of a NACA-0015 aerofoil

At this point, the lift falls away sharply at the fluid separates from the top surface and becomes highly turbulent. This continues to occur until α=20° where the aerofoil begins to behave like a flat plate [8]. The flow becomes entirely separated and the boundary layer is so thick that the profile of the aerofoil has very little effect on the behaviour in this region. Flat plate theory predicts that C_L reaches a maximum of 1.2 at 45° before decreasing to 0.0 at 90°. This is mirrored quite closely by the experimentally determined data in Figure 4.05. It can also be seen that as the aerofoil inverts, a negative lift is experienced with sharper stall properties owing to the now very acute leading edge. A double negative peak is seen where the flat plate peak is of equal magnitude and the stalled region peak is approximately 0.85 of the positive value.

No data detailing the performance of the NACA4424 has been found to cover the complete 180° angle of attack range. Therefore, in this study, is estimated by combining the experimental data from Abbott [4] with a flat plat theory model and then is verified by using the Profili software.

In Figure 4.06, the results can be seen. The experimental data runs between -12° and 19.5°. This is then supplemented with the flat plate data, peaking at about C_L=1.1 as in Figure 4.05 above. The flate plate theory approximation bring C_L down to zero at 90° and then is mirrored in the negative angles of attack. The stall peak in the negative is calculated as 0.85 of the positive peak, again as in Figure 4.05. The two sections are then joined up using curves of best fit from the end of the experimental data to the flat

plat theory, ensuring that the curves are smooth so as to aid solving computationally. This covers the angles 19.5° to 27° and -12° to -27°.

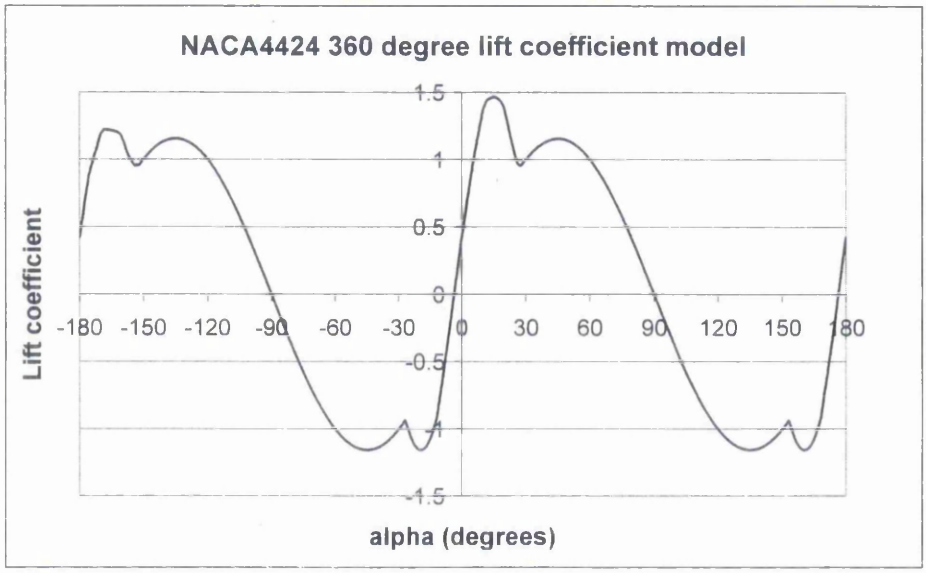

Figure 4.06 - The NACA4424 lift coefficient model

A comparison of the prediction made by the Profili software at Re = 700,000 gives the graph shown in Figure 4.07. This is a typical Reynolds Number found over the blade over the range of operation. It can be clearly seen that the experimental data yields lift values that are substantially higher in the critical region of operation. It is also clear that the oscillations present in the Profili prediction are absent. However, there is a high level of correlation between the two methods and it is considered that the experimentally determined data is more accurate in the critical region. Hence the lift curve shown in Figure 4.06 above is used.

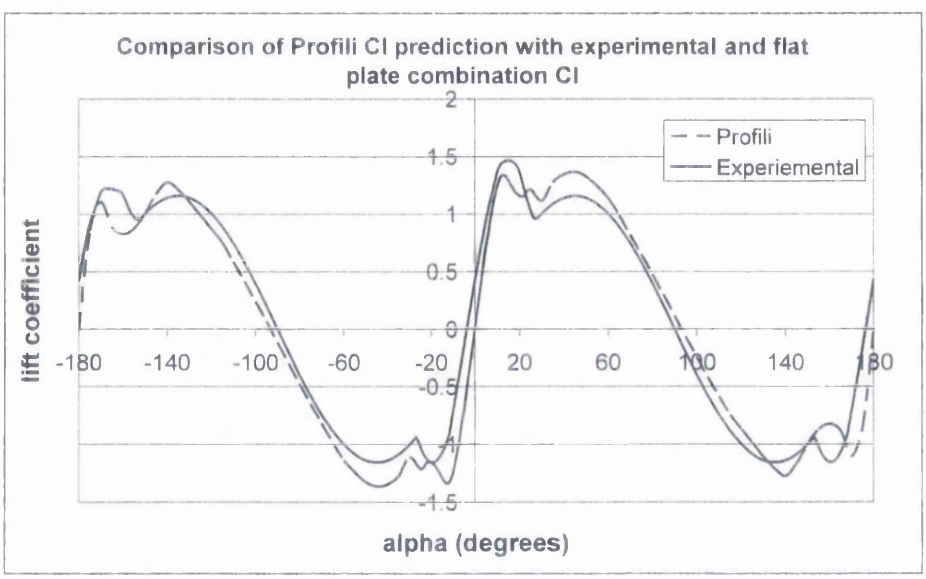

Figure 4.07 - Comparison of lift coefficient with Profili software data

4.1.5.2 Drag coefficient

The variation of drag coefficient with angle of attack for the NACA4424 aerofoil section can be determined by interpretation of Abbott [4]. The data presented links drag coefficient to lift coefficient and then the second set links lift coefficient to angle of attack. From this, the relationship between drag and angle of attack can be determined. It is presented in Figure 4.08 between the angles of -12° and 19.5°.

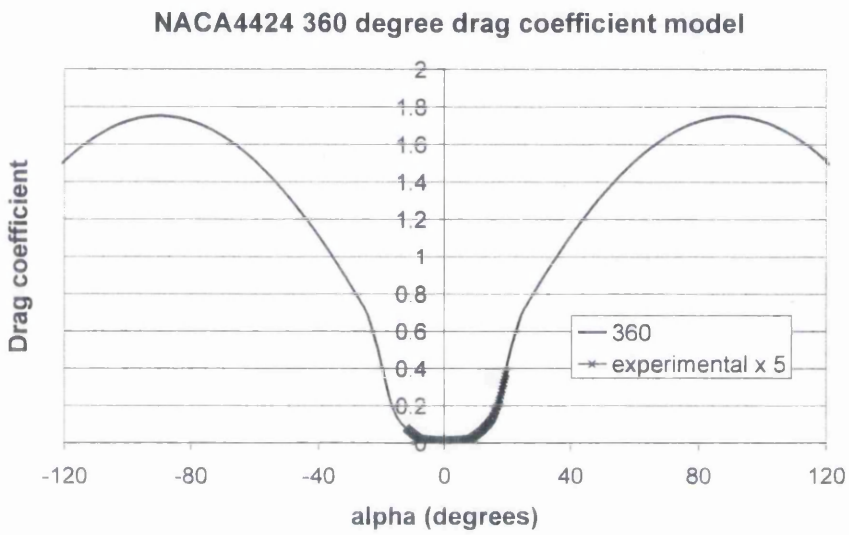

Figure 4.08 - The NACA4424 drag coefficient model

Outside the angles covered by the experimental data a flat plate model is used to approximate the behaviour. In the same manner as the lift coefficient this peaks at the flat plate value of nearly 1.8 at 90°. This sinusoidal relationship is validated using the Profili software as shown below in Figure 4.09.

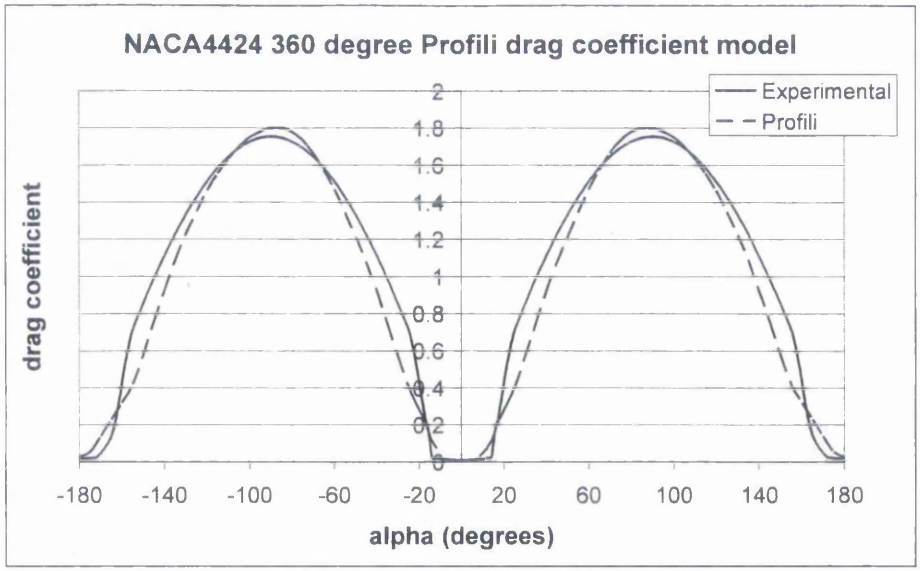

Figure 4.09 - Comparison of drag coefficient with Profili software data

The correlation is very strong and although there are slight differences in the rate of change in the stall region the experimental data is much smoother in the critical region around 0°. For this reason the experimental data is considered most suitable for use with the blade element model.

4.2 Optimisation of blade geometry

As described in section 4.1.2, equations (4.7) and (4.9) can be used together to determine the optimum blade geometry in terms of chord and twist. However this is only possible once the interference factors are known. To obtain values for a and b equations, (4.14) and (4.17) are solved for each blade element. The chord and the twist of each element can then be found. The optimisation process describes the blade geometry which offers the most efficient operation for each blade element. When combined, this offers the most efficient blade performance for the rotor as a whole at a specific TSR.

4.2.1 Implementation

Microsoft Excel is used to solve the equations for each station of the blade. The blade is split into a number of discrete radial segments, the number of which is limited only by computational time. For the purpose of this investigation the blade is split into 25 sections.

The expression for b (4.17) is substituted into (4.14) giving equation (4.25).

$$\frac{C_L}{C_D} = \frac{x\left(a + \left(\frac{R(4a-1)(1-a) + x(1-3a)}{x(Rx+1)}\right)\right)}{\left[a(1-a) - x^2\left(\frac{R(4a-1)(1-a) + x(1-3a)}{x(Rx+1)}\right)\left(1 + \left(\frac{R(4a-1)(1-a) + x(1-3a)}{x(Rx+1)}\right)\right)\right]}$$

(4.25)

The maximum lift / drag ratio, R is known for the aerofoil used, the rotational speed, radius and hence speed ratio are also known for each blade element. The goalseek function in Microsoft Excel is then used to set the value of C_L / C_D equal to R by changing a. Once this value of a is determined it can be substituted into (4.17) to give a value for b. At this stage both the interference factors are known and the chord and twist can be found from equations (4.8) and (4.9).

4.2.2 Issues with the method

The goalseek function in Excel is a simple solver which will set the product of an equation to a specified answer by changing one variable in the equation. The primary limitation is the fact that only one cell can be varied at a time, but also that it has no method for constraining the results. The solver function in Excel is more advanced but is unnecessary at this stage to undertake this task successfully and in a reasonable time frame.

One of the difficulties with this set of equations is that they have multiple solutions. Some of these can be very close together and others are extreme. Using the goalseek function works well if the input variable is close to the solution. Otherwise it can tend to zero or infinity which results in an erroneous or no solution. To avoid this problem approximate values of a are taken from [1]. A starting value of a = 0.25 is used for the element with the smallest radius. After the solution has been found it is substituted and used for the successive radius starting value. By this method the output results are reliable and consistent.

The other issue is that if a and b are linked directly to products other than (4.25), all values are changed during each iteration step. This causes a significant reduction in calculation speed which is rectified by calculating the values before inserting them in the dependent equations. This splitting up of the two stages results in a vastly decreased calculation time.

4.2.3 Results

The method provides a reliable system to create the optimum geometry for a particular design TSR. The variation of chord and twist angle are shown in Figures 4.10 and 4.11. This defines the shape of the blades.

4.2.3.1 Blade twist

The basis of the twist is that the further toward the blade tip an element is located, the more twist it has. This clearly reflects the fluid vector that is anticipated from the combination of rotation of the blades and the oncoming fluid. Figure 4.10 shows the variation of blade twist with design tip speed ratio, TSR_D.

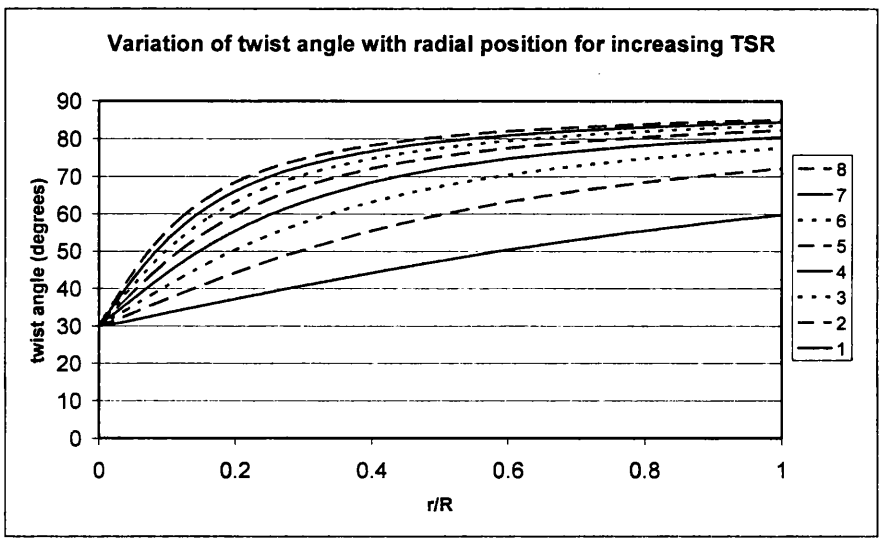

Figure 4.10 - Blade twist with radius and design TSR

It can be seen in Figure 4.10 that at any design TSR, the blade twist at zero radius converges to 29.6°. In addition, the twist at the blade tip tends toward 90° as the design TSR increases. This implies that as design TSR increases, the total twist over the radius increases. Finally, it is clear that as design TSR increases, more of the twist occurs at the hub end, for example at TSR 8, the blade elements are at over 80° for over 50% of the blade towards the tip.

4.2.3.2 Blade chord

In Figure 4.11 the blade chord distribution is shown for a 1m diameter blade.

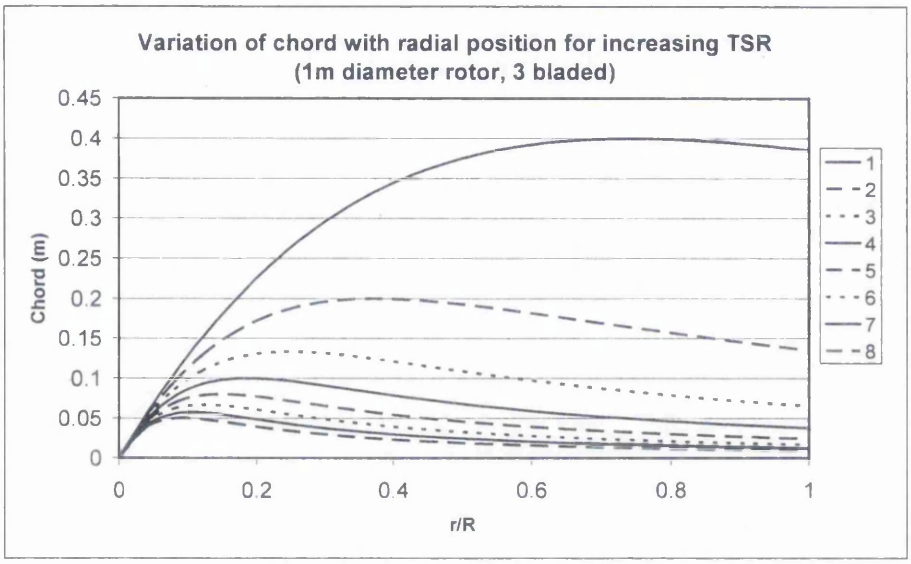

Figure 4.11 - Blade chord with radius and TSR

The general trend is that the chord increases from zero at the centre up to a maximum fairly quickly and then tapers off towards the blade tip. At the tip end, the chord tends towards zero as speed ratio increases. At very low TSR, the chord maximum is much nearer the blade tip and it does not converge before reaching the tip. It can be clearly seen that for higher TSR the chord decreases to an impracticall size which would create manufacturing difficulties.

4.2.3.3 Solidity

Figure 4.12 below shows the variation of solidity with radius. This is closely linked to Figure 4.11 (chord) as $\sigma = \frac{Nc}{2\pi r}$ and this gives the equations in a dimensionless form.

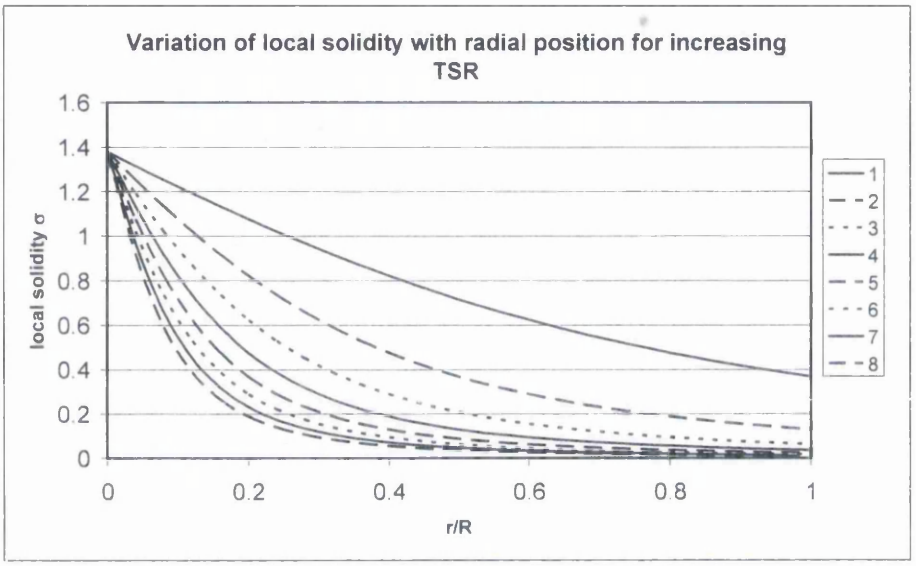

Figure 4.12 - Solidity with radius and TSR

4.2.3.4 Interference factors a & b

Figure 4.13 shows the variation of axial interference factor with radius and tip speed ratio. It is clearly seen from the scale of the y-axis that the variation is small in magnitude. However, it is significant in that at low design TSR, it can be inferred that the fluid is losing more axial velocity towards the tip of the blades and hence a greater proportion of the power is being developed by the rotor in this region. This is true because the design sets dF_T constant for all blade elements and because $T = F_T r$ more power is developed closer to the tip. Also of interest is the way that this distribution changes with design TSR. As this increases the peak of axial interference moves towards the hub and towards the tip it decreases significantly. It may be inferred from this that hub effects are of more importance to rotors designed for higher tip speed ratios.

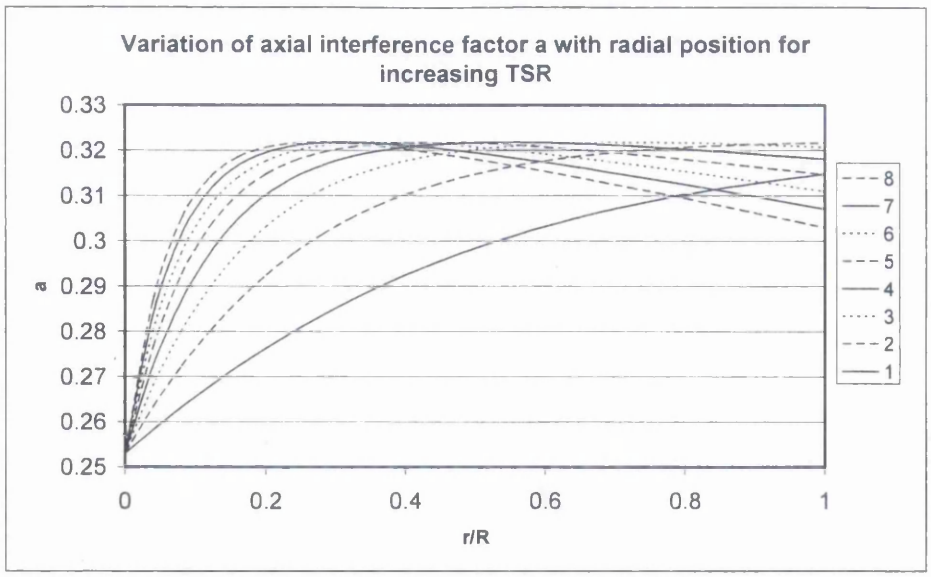

Figure 4.13 - Axial interference factor with radius and TSR

Figure 4.14 shows the variations of the rotational interference factor b. It is clear that b tends towards very high values at the hub. As design TSR increases this tendency to high value moves towards the tip. It can be inferred from this that lower TSR give rise to a much greater rotation of the wake and are hence likely to offer more torque. It is also inferred that a reduction in efficiency will occur owing to the rotation imparted on the fluid. The rotation of the fluid represents energy that is not being harnessed by the rotor. As the TSR increases the rotation imparted on the flow decreases and tends toward zero at the blade tip. It also appears that at high design TSR the curve tends to zero along the blade length.

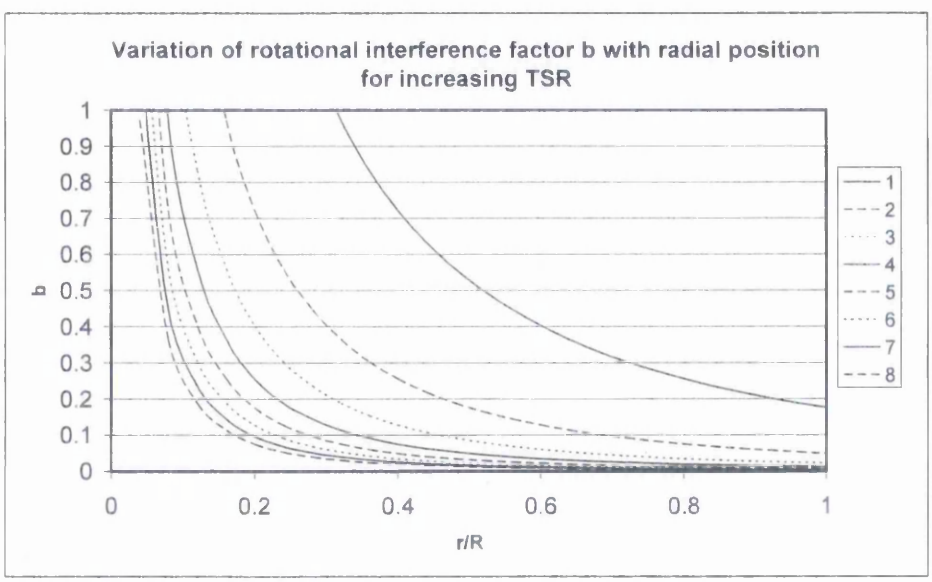

Figure 4.14 - Rotational interference factor with radius and TSR

4.2.3.5 Design operation performance

Equation (4.4) can be used to estimate the performance of the rotor at its design conditions using the calculated values $of\ a$ and b.

$$C_P = \frac{8}{X^2}\int_0^X (1-a)bx^3.dx \tag{4.4}$$

Figure 4.15 shows the variation in theoretical maximum efficiency of rotors designed for increasing TSR whilst operating at their design conditions. It is clear that the achievable efficiency of the rotor increases dramatically from design TSR=1 to a maximum at design TSR = 4 before it starts to decline. Of note here is that a maximum lift /drag ratio of 50 is used.

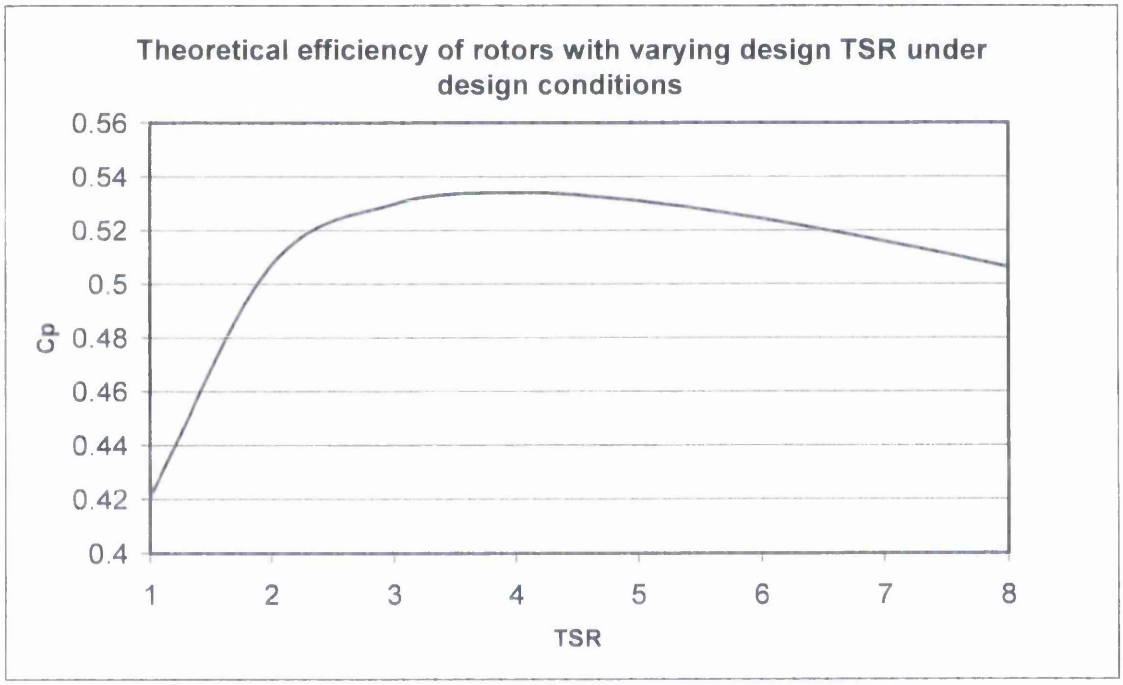

Figure 4.15 - Theoretical rotor efficiency variation with TSR_D

4.2.4. Conclusions

This system offers a simple and computationally efficient method of optimising a set of turbine blades for performance at various tip speed ratios. Microsoft Excel is a suitable software vehicle for this method, although it would also work well and would possibly be more efficient with a more advanced package such as Matlab.

The results generated by this method enabled the design and development of the blades for the prototype in Chapter 3. Much can also be learned about the geometry of rotors designed for different tip speed ratios and it can be clearly seen that the design TSR has great influence on the method of construction.

The distribution of the interference factors can be used to infer the behaviour of the fluid and hence some performance characteristics of rotors designed for different tip speeds. This includes hub effects and high torque applications.

Finally the design tip speed ratio has an effect on the maximum achievable efficiency of the rotor and a design TSR of 4 appears to yield the best performance. Practically the design TSR will be a function of the starting torque required, the generator power curve and gearing used. The optimum design TSR will be specific to the system.

4.3 Performance prediction

To predict the performance of rotors over the operating range, an additional level of analysis is required. The method described in section 4.2 only applies to a rotor which is operating on its design point. To calculate values of a and b over various operational tip speed ratios the method outlined in section 4.14 is required.

4.3.1 Implementation

The method is inputted to an Excel spreadsheet. The blade is again split into a number of discrete radial segments. For the purpose of this investigation the number of discrete elements is 25. The built in Excel solver package is used to output the performance of each blade element and these are summed over the blade to determine the total outputs in terms of power and torque.

4.3.1.1 Method description

The chord inclination angle β is the angle between the chord and the axis of rotation as shown in Figure 4.16. It is defined by:

$$\beta = \phi + \alpha$$

The flow inclination angle γ is also shown in Figure 4.16. It is defined from equation (4.24) in terms of local speed ratio and values of a and b for each blade element:

$$\gamma = \tan^{-1}\left[\frac{x(1+b)}{(1-a)}\right]$$

The difference between the chord and flow inclination angles is the effective angle of attack:

$$\theta = \beta - \gamma$$

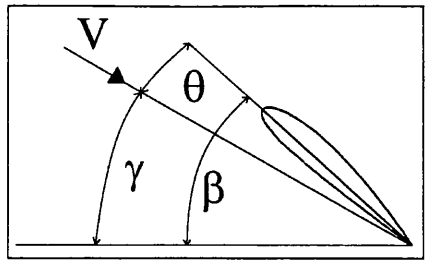

Figure 4.16 Chord inclination angle, flow inclination angle and effective angle of attack

Depending on the operating conditions, θ can be positive or negative. This value is inserted in look up tables as described in section 4.3.1.5 and the C_L and C_D for the aerofoil under the particular operating condition is found.

Equations (4.18) to (4.21) are calculated and the Microsoft Excel solver is employed to find values of a and b which minimises ν in (4.22).

4.3.1.2 Hub Effects

The equations break down at r = 0. However, this is unimportant as there is usually a rotor hub or centre body to consider. Although the effects of the flow pattern around the hub have been considered in various studies [9], it is common that the hub area is considered dead space [10]. This is because the torque at low radii is considered negligible.

It is possible to consider the effect of the hub in terms of acceleration of flow around it and hence more flow directed through the rotor. However, for simplicity this analysis is not undertaken in the method used. For blade elements with values of r below the hub radius h, the torque and axial force are set to zero. This effectively reduces the swept area of the rotor and the power output.

In practice this is implemented by using an IF THEN statement:

$$\text{IF}(r<h),\ \text{THEN}\ T_r = 0 \text{ and } F_{Ar} = 0$$

4.3.1.3 Tip Effects

BEMT assumes that the rotor has an infinite number of blades. In practice, there is a circulation of flow around each individual blade which gives rise to the lift forces. There is also a radial velocity which is especially pronounced around the tip. The radial velocity disrupts the circulation and for this reason a circulation reduction factor is sometimes introduced, which can also be called a tip loss correction. A detailed comparison of circulation reduction factors developed by Prandtl, Goldstein and Theodorsen is shown by Woollard [9]. However, it is also shown that for the most sophisticated correction, which is presented as the Theodorsen corrected Goldstein, the reductions in power, torque and axial force coefficients are less than 5%. Hence for the purposes of this investigation, tip loss correction has been neglected at this stage.

4.3.1.4 Overspeed

The rotor is analysed over the operating range, from stationary to overspeed and 'propeller brake state'. In the stopped condition the rotor can be considered as a series of stationary aerofoils in a linear flow. Whereas at 'propeller brake state' or the 'runaway condition' the rotor has accelerated to such an extent that towards the tip, the rotor is acting like a propeller such that the overall power of the rotor is reduced to zero.

As the rotor goes into an overspeed condition, i.e. at TSRs greater than its design TSR, it experiences a greater proportion of flow from the tangential direction and hence the flow inclination angle γ tends towards 90°. This is true along the radius but is particularly significant at the blade tips as these are most affected by the increase in tangential velocity. As this occurs, the effective angle of attack θ for each blade element decreases and may even become negative leading to a significant decrease in the lift generated by the section and in extreme cases a propeller effect.

The problem in terms of computation is that the functions for interference factors are complex in the region of propeller brake state.

When propeller brake state occurs, the rotor torque theoretically equals zero and hence there is no resultant rotation of the flow well downstream. If the rotor speed was to be increased further, it would start to act as a propeller and the rotation of the flow would now be in the same direction as the blades. In terms of the rotational interference factor

UNIVERSITY OF WALES SWANSEA LIBRARY

b, this implies that during turbine operation $b > 0$. As the turbine increases TSR b tends to zero as it reaches brake state and as the rotor accelerates into propeller condition b will become negative.

In terms of the axial interference factor a, during normal operation it fulfills $0 < a < 0.5$ as stated by Griffiths [11]. Additionally, by definition if $a = 0.5$ all the flow is diverted around the rotor as the velocity downstream of the device would be zero. However as the rotor approaches propeller brake state the axial interference factor tends towards zero. Again, if the rotor operates as a propeller, the axial interference factor will become negative.

4.3.1.5 Look up of lift and drag data

As the effective angle of attack for each blade element changes, the values of lift and drag coefficients also change. The values used for the lift and drag curves are presented in section 4.15.

In the absence of a mathematical expression which would give C_L and C_D as a function of θ, an automated lookup method is required. The values are stored in a table with 3 columns; θ, C_L and C_D with 1140 rows. It runs between -180° and 180° in steps of 0.25 of a degree. Values of C_L and C_D for all angles of attack are obtained from this table by linear interpolation.

4.3.1.6 Optimisation of the objective function

It is observed that with different starting values a multitude of near optimum solutions can be found for a particular operating condition. As the system is solved numerically, the problem lies in finding a consistent and accurate solution.

An example of a multiple solution is shown in Figure 4.17. This shows the results of a parametric study to investigate the relationship between interference factors a and b and the objective function $v(a,b)$ [12]. The rotor is operating at design TSR = 2 and Figure 4.17 shows $v(a,b)$ of the blade element at r/R =0.32.

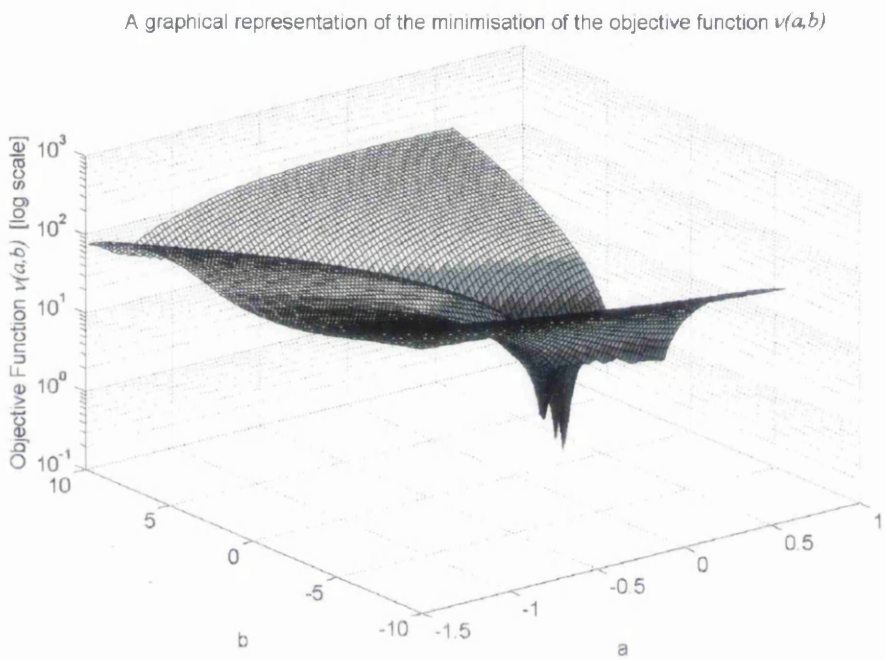

Figure 4.17 - Minimisation of the objective function [12]

Although one solution is noticeably closer to zero than the other two, it is likely that a standard solver package, such as the Microsoft Excel solver will encounter difficulties in differentiating between these points as feasible solutions.

In effect, a difference of this magnitude will not drastically alter the outputs. However without management it may result in an irregular set of results. To ensure that consistent results are obtained as far as possible, a system is used to obtain starting values for a and b. For the first element from the hub a value of 0.25 is used for a, and a value of 10 for b. This element is then solved and the resulting values of a and b are transferred as

the starting values for the second element. This method stabilises the system in the majority of cases.

4.3.1.7 Outputs

The solver is used to find values of a and b for each blade element and minimise $v(a,b)$ in (4.22). The corresponding products of equations (4.18) – (4.22) are then summed over the radius and then averaged to give values for axial force, torque and power as given by:

$$F_A = \frac{1}{2}\sum_{0}^{R}\left(dF_{A1} + dF_{A2}\right) \tag{4.23}$$

$$T = \frac{1}{2}\sum_{0}^{R}\left(dT_1 + dT_2\right) \tag{4.24}$$

$$P = \frac{1}{2}\Omega\sum_{0}^{R}\left(dT_1 + dT_2\right) \tag{4.25}$$

To enable the comparison of different rotors, these quantities are non-dimensionalised by Griffiths [11] and given by the force, torque and power coefficients:

$$C_F = \frac{F_A}{\frac{1}{2}\rho U^2 A}$$

$$C_T = \frac{T}{\frac{1}{2}\rho U^2 AR}$$

$$C_P = \frac{P}{\frac{1}{2}\rho U^3 A}$$

4.3.1.8 Generation of results

To solve each of the blade elements independently in Excel would require a prohibitive amount of user interaction. The VBA macro feature is employed to automate the generation of results. The primary macro entitled 'Solverzero' automatically sets the

starting values for a and b and then executes the series of optimisations to find a and b across the blade radius. Various other macros are used to generate different forms of results. Essentially these set the operating conditions, either blade number, flow speed or tip speed ratio and then initiate Solverzero. When Solverzero has completed, the desired selection of the results is stored in a particular location and the next set of operating conditions are inputted until the results set is complete.

4.4 Results

To illustrate the function of the model, a 3-bladed test rotor with design tip speed ratio $TSR_D = 2$ is used. This has a significant effect on the values of performance coefficients but does not effect the overall model characteristics. The test rotor has a diameter of 1m and is tested at a flow speed of 3m/s.

The model is run over the operating range using the test rotor. The operational TSR is varied from 0 to 8 in steps of 0.05. Additionally, this demonstrates the capability of the model in the start-up and overspeed range.

4.4.1 Torque

Figure 4.18 shows the variation of torque coefficient C_T with operational TSR. The starting torque coefficient is around 0.05 and this quickly increases as the rotor starts to spin. It decreases rapidly until TSR ≈ 1.3 where there is a sharp change of direction and it increases dramatically as the rotor becomes unstalled. C_T reaches a maximum of 0.227 at the design TSR of 2. Angle of attack is discussed below and shown in Figure 4.23. At the point of peak torque the entire blade is at optimum angle of attack.

As the TSR increases and the rotor begins to operate in overspeed, C_T begins to decline steadily in a near straight line. This continues though vortex ring flow until the rotor reaches propeller brake state at TSR ≈ 6. The model continues to operate into an unnatural operation condition which would involve inputting energy and the rotor operating as a propeller.

It is clearly demonstrated that the model is less robust in the start up region with a visible reduction in smoothness below TSR=1.

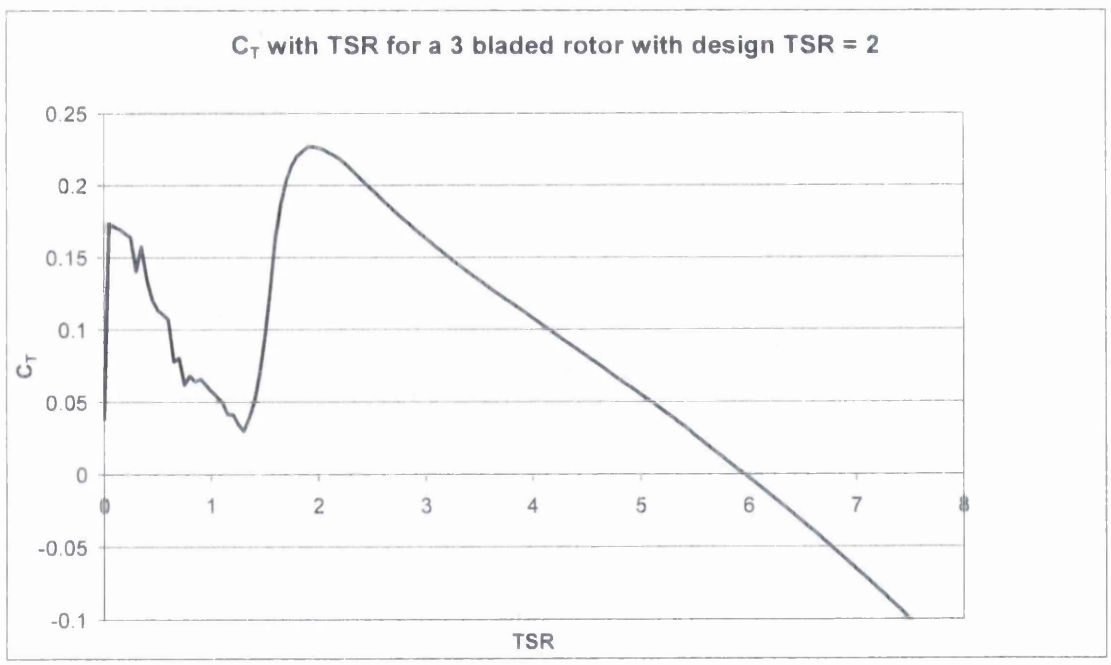

Figure 4.18 - Torque coefficient over the operating range

4.4.2 Power

The relationship between power coefficient and TSR is shown in Figure 4.19. Unlike the C_T curve, C_P begins from zero as the rotational speed is zero. The section between start-up and TSR=1.3 does not mirror the torque curve as the speed is steadily increasing. It remains level at approximately C_P = 0.05 until the sharp increase in power as the blades become unstalled. The power then starts to level off before reaching a maximum 0.493 at TSR=2.70. This is noticeably later than the peak in the torque curve. C_P then decreases gradually with increasing gradient until reaching the C_P =0 at TSR = 6.

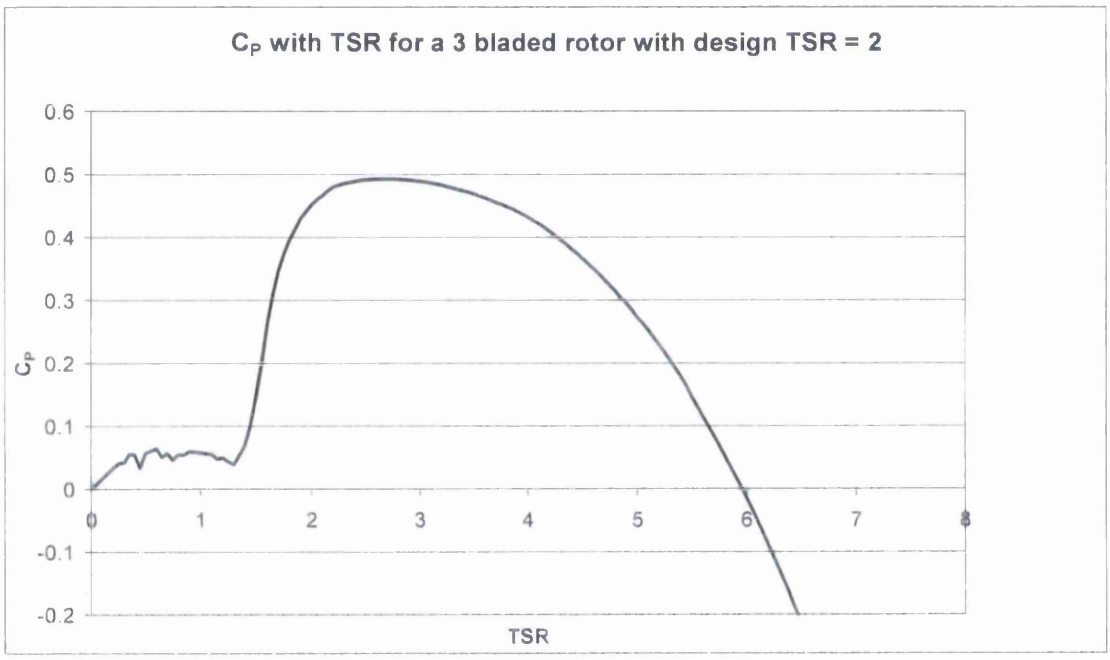

Figure 4.19 - Power coefficient over the operating range

4.4.3 Axial force

It is clear in Figure 4.20 that the axial force coefficient C_F varies in much the same way at the power coefficient. When the rotor is stationary there is an axial force on the rotor which equates to approximately half of the operational maximum. It continues at approximately 0.4 until TSR=1.3, when it increases steadily and peaks at 0.79 earlier than the power curve at TSR = 2.55. Interestingly it then decreases steadily but does not cross the zero line at the same time as power and torque. The propeller brake state condition has been reached, but an axial force remains until TSR = 7. At propeller brake state:

$$F_A \approx 0.375 F_{Apeak}$$

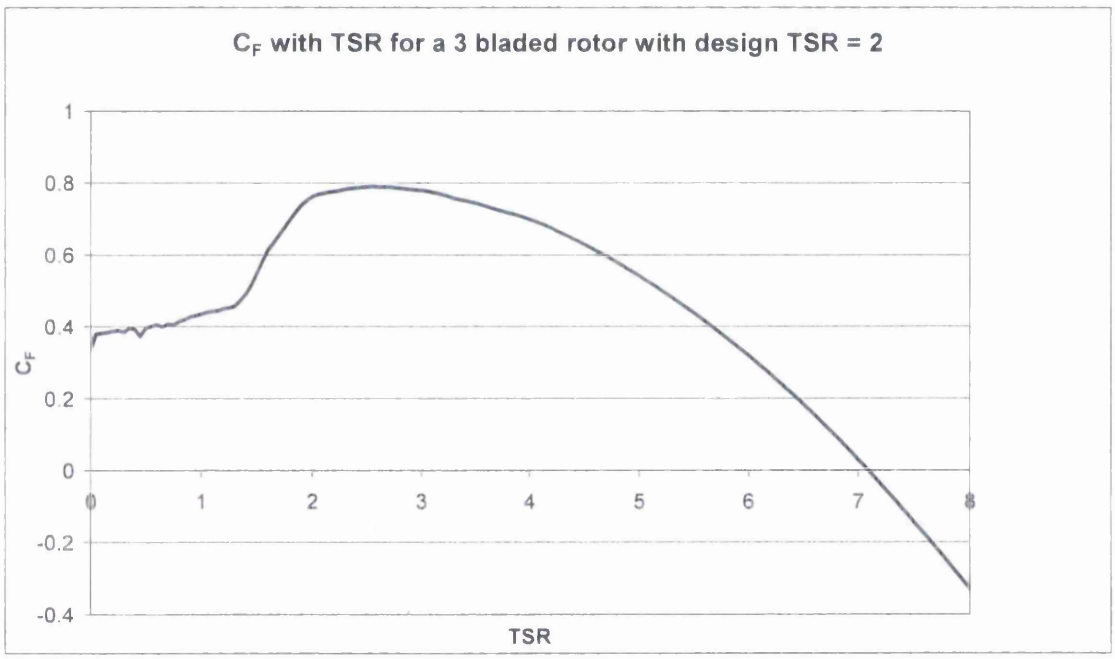

Figure 4.20 - Axial force coefficient over the operating range

4.4.4 Interference factors a & b

More can be learned about the nature of the flow across the blade from the interference factors. Figures 4.21 and 4.22 show the radial distribution of a and b over a range of tip speed ratios. Firstly, considering the design case, TSR = 2, it is clear that the axial interference factor remains relatively constant across the blade at around 0.25, but with a slight increase in the mid-range. Differently, the variation of b at the design condition is very distinctive. The rotation imparted on the flow near the hub is much greater than that at the tip. In higher tip speeds ratios as the blades go into overspeed, the axial interference factor falls dramatically in the mid section. As propeller brake state is reached at TSR = 6, a reaches zero, and beyond this becomes negative in the mid blade. It is also clear that b follows a similar pattern in reducing considerably as TSR is increases, again becoming negative after propeller brake state is reached.

In the startup region, at TSR=0, b appears constant across the whole blade. In contrast, a gradually decreases across the radius toward the tip owing to the chord distribution. At TSR=1, the line in a appears to reflect the static condition at the tip and the design operating condition at the hub. These values do not meet smoothly and there is a step at r/R =0.35. This is mirrored in the b values which also step at this point. However it is clear that the values of both a and b are lower than those at the design TSR over most of the blade.

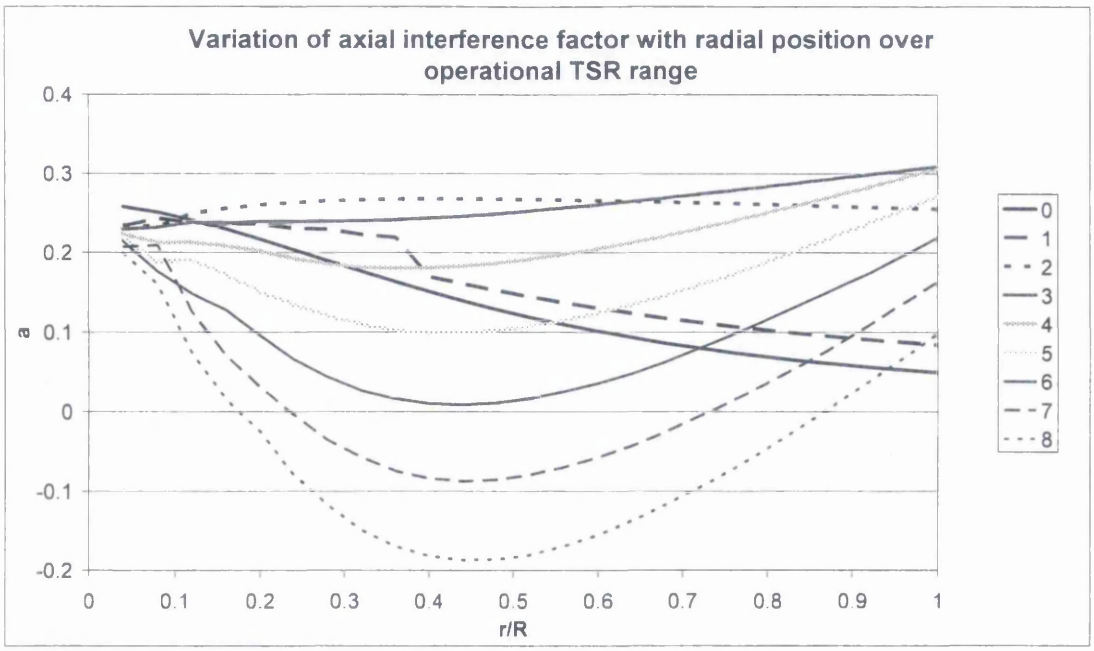

Figure 4.21 - Variation of axial interference factor over the operating range

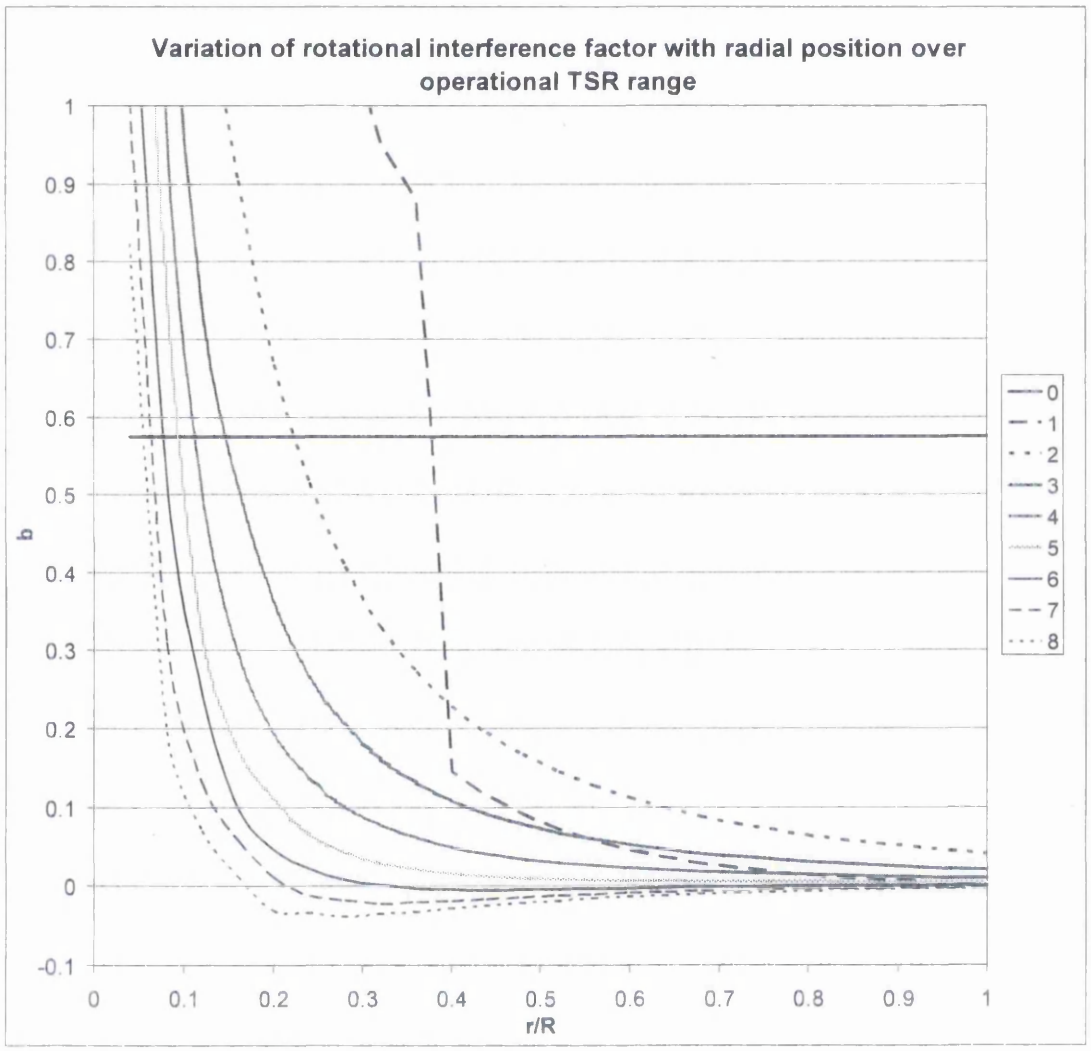

Figure 4.22 - Variation of rotational interference factor over the operating range

4.4.5 Effective angle of attack

The angle of attack at which the flow approaches the blade during operation is shown in Figure 4.23. The stationary position represents the geometry of the blade in that the flow approaches it from the axial direction. It is then shown at TSR = 1 that there are steps in the angle of attack where the model appears to breakdown, these mirror the steps as observed in a and b in Figures 4.21 and 4.22. The model may be switching between local minima on the objective function.

At TSR = 2, the angle of attack is at optimum across the entire blade with no significant variation, this is the designed operating condition and maximum ratio of lift to drag. As the TSR increases the effective angle of attack reduces from the tip inward owing to the relative effect of the tangential velocity. This becomes more pronounced as the rotor approaches propeller brake state with the first negative angle of attack seen at TSR = 4 in the mid-section. After propeller brake state, the entire radius of the blade has a negative angle of attack, with the area at the hub more severely affected owing to the tip being oriented in a more tangential direction.

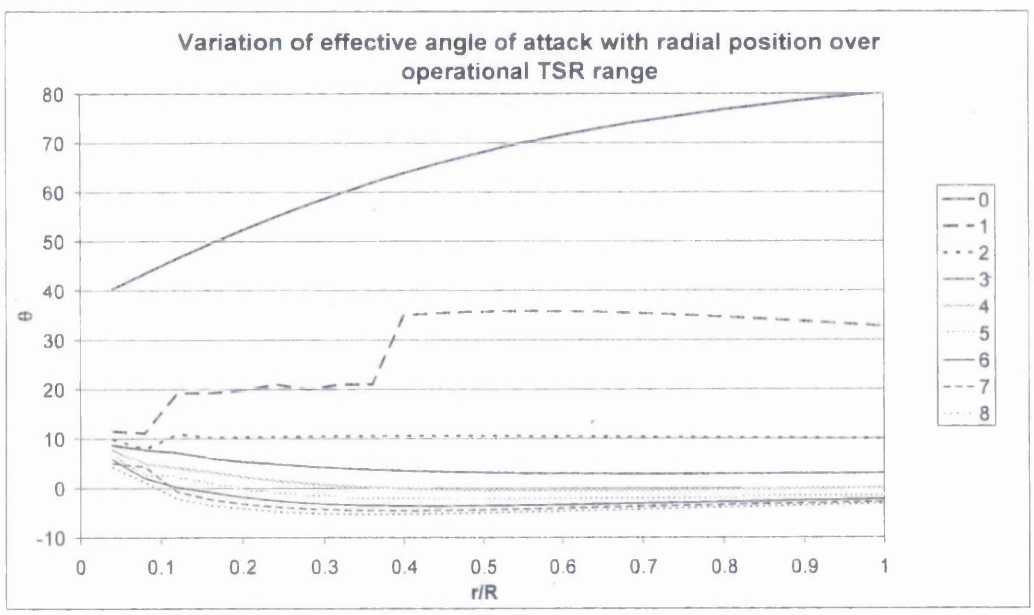

Figure 4.23 - Variation of rotational interference over the operating range

4.4.6. Torque and Axial force

The effect of the characteristics observed in a, b and θ manifests as a distribution of forces along the blade. These are presented in Figures 4.24 and 4.25.

At TSR = 0, the rotor behaves as a set of aerofoils with both the axial force and the torque following a similar pattern related to the geometry of the blade. At TSR = 1, the step as found in Figures 4.21 - 4.23 is clearly seen in the torque and axial force graphs. At the design condition, TSR = 2, the torque and axial force are linear and this clearly indicates that the blade tips are providing more power than the hub. This is an intentional result of the design methodology. The torque distribution remains close to linear across the blade until TSR = 5 where the mid-section torque begins to decrease. This pattern continues into the higher overspeed conditions, where eventually the entire blade experiences negative torque. Interestingly, at propeller brake state, the middle half of the blade is experiencing negative torque and the other parts are positive. This is not mirrored in the axial force graph where the entire blade remains in a positive force condition until after TSR = 6.

However, it is clear that axial force first begins to become negative in the mid section of the blade and the tips of the rotor retain a positive force into the highest tip speed ratios.

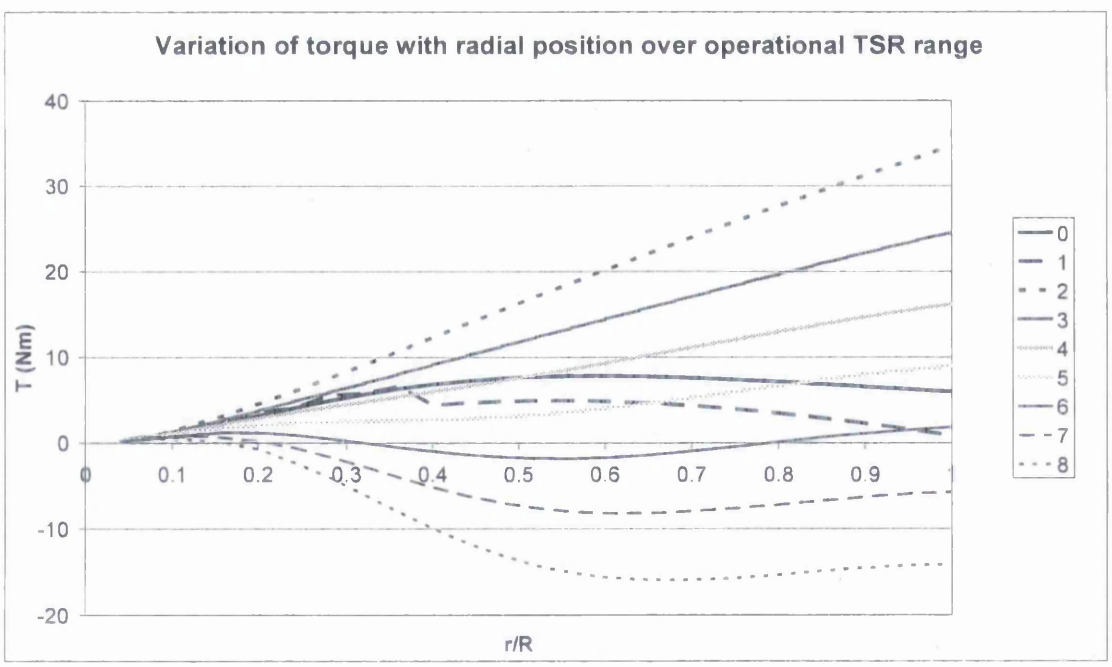

Figure 4.24 - Variation of torque with radius over the operating range

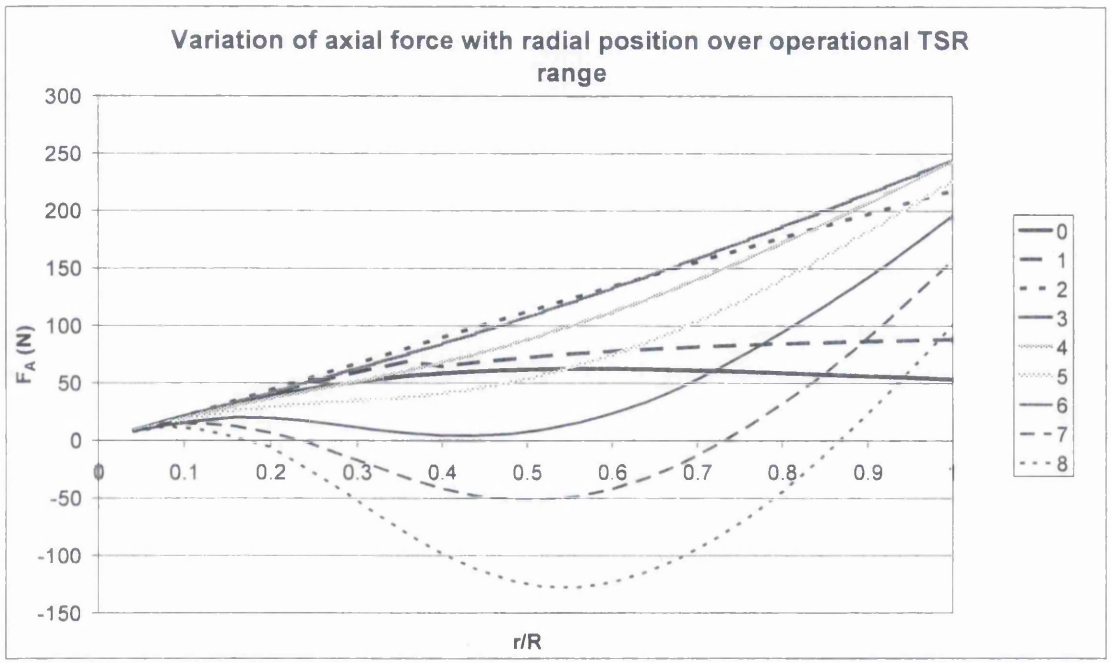

Figure 4.25 - Variation of axial force with radius over the operating range

4.5 Discussion

The model has produced a set of outputs that enable the performance characteristics of an axial flow turbine to be predicted and analysed. This illustrates the operational maximums in terms of torque and force which allow the structural design of the blade to be undertaken. The model also predicts the start-up and runaway characteristics of the rotor.

4.5.1 Assumption and limitations

The primary limitation of blade element momentum theory is that it does not include secondary effects such as 3 dimensional flow effects. The significant flow regimes that are neglected are tip loss effects and radial flow along the blade. It is also known [13] that the flow assumptions break down when the blade is in deep stall and high overspeed.

Tip loss effects have been investigated by Glauert and Prandtl and a comparison of the two methods is given by Woollard [9]. The theory concerning circulation of the flow owing to the finite number of blades is developed and a tip loss correction factor is introduced. This has been neglected in the analysis presented here because it is considered to be a superfluous addition for the purpose of developing a system to investigate wave loadings. This is a suitable subject for further research.

The lift drag curve used in this investigation neglects the influence of Reynolds number on the characteristics of the aerofoil. In practice, the Reynolds number will change with each blade element and operational condition. A more complex lookup function would be required to make this addition.

The other factor to be neglected is the recent work concerning the effect of a free surface on the performance of a marine rotor. In a wind turbine, the rotor is located in a fluid with a theoretically infinite depth. In a marine rotor this is possibly not the case, depending on the depth of the water relative to the diameter of the device. The work of Ian Bryden [14] focuses primarily on the effect of tidal devices on the tidal flow. However, the central theme is that a tidal flow will experience a change in head as it passes a turbine and consequently the flow velocity must increase to compensate for this. No account of this phenomenon has been built into the analysis presented here.

4.5.2 Rotor performance

The rotor torque, power and axial force have been successfully predicted across the operating range. In comparison to other studies [11] and [9], the values of predicted power output appear quite high. This is likely owing to the absence of a circulation reduction factor as the model appears robust in these areas.

Interestingly, the propeller brake state condition occurs at TSR = 6, where C_T and C_P cross the zero line. However, the axial force does not reduce to zero at the same point and C_F crosses zero at TSR = 7.1. This is to be expected as the rotor is not designed as a propeller and consequently once a negative torque is applied there is a delay until a thrust is produced.

Figures 4.24 and 4.25 show the distribution of torque and force across the blade. These values can be used to design the structure of the blades and ensure that they are capable of withstanding the required operational loads. This is particularly important in the runaway condition in which large negative forces are applied to parts of the blade. The addition of a geometrical dynamic response to these loads in terms of blade geometry would be a suitable area for extension of this investigation.

4.5.3 Irregularities

The model and implementation have limitations and these have manifested in a number of the results.

The first is that in Figure 4.22, the value of b is shown as constant across the radius at TSR = 0. When the rotor is stationary, b is zero as there is no rotation of the flow. This anomaly occurs because to run the model at TSR = 0 encounters calculations requiring a divide by zero. In these situations a value of 1E-10 is substituted to allow the model to operate.

Secondly, the irregularities that occur in the region between TSR = 0 and TSR = 1.3 are owing to the phenomenon of multiple solutions as discussed in section 4.3.1.6. In this region, the blade is heavily stalled and the lift and drag coefficients are changing rapidly. The double peak in the lift coefficient increases the relative variation in the multiple

solutions in the stalled region. Additionally, the values of torque and axial force are low in comparison to the variation in lift and drag. This reduces the accuracy of the solver in these regions and although convergence is still obtained, it is comparatively less precise.

Finally, the most significant error in the model is the step observed across the radius at low TSR. This is apparent in Figures 4.21 - 4.25 and is owing to a lack of convergence in torque values at some blade elements. This implies that the residual function in equation (4.22) cannot be reduced to zero. The non-converged values of T_1 and T_2 from equations (4.20) and (4.21) are shown in Figure 4.26.

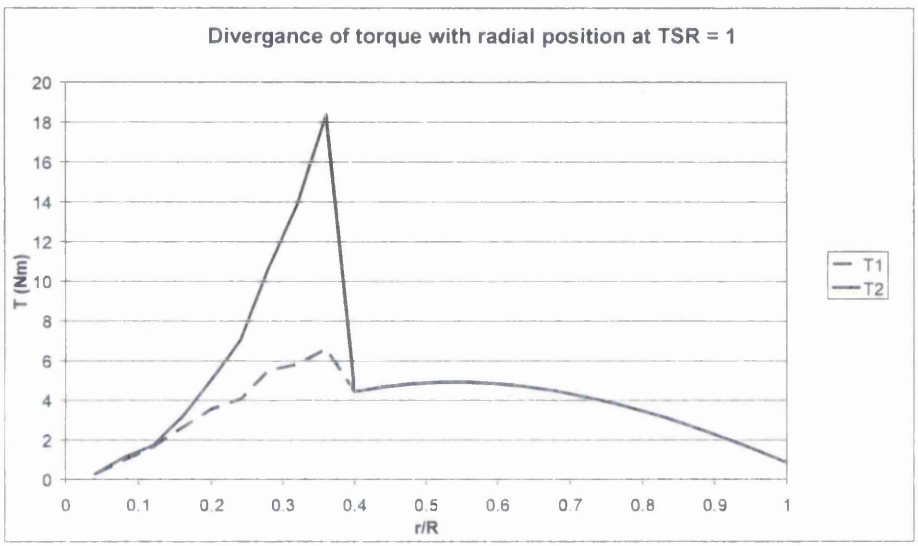

Figure 4.26 - Divergence of torque solutions at TSR = 1

A thorough investigation is undertaken of this characteristic and it is observed that using the objective function defined by equation (4.22), at TSR = 1 the torque values are small compared to the force values. For this reason the optimisation tends to optimise for force as a priority over torque. It is for this reason that a less significant step appears in the TSR = 1 curve shown in Figure 4.25.

A modification is made to the objective function as follows:

$$\left(dF_{A1} - dF_{A2}\right)^2 + \left(Z(dT_1 - dT_2)\right)^2 = f(m)$$

Where Z is the modification factor. If an analysis is undertaken using this modified form with Z=100, it is found that the torque is now optimised as a priority and the step occurs

in the force values and not in the torque values. It is therefore concluded that this is an error in the underlying model and no exact solutions exist for this region of operation.

4.6 Conclusions

- A computational analysis has been undertaken of the hydrodynamic performance of a marine rotor.

- Blade element theory has been implemented in a Microsoft Excel spreadsheet, making use of the goal seek, solver and VBA macro features.

- The limitations of the model and implementation method have been identified and considered. The model appears to work very well in the normal region of operation when TSR = 1.5 to 5. In the stalled region at TSR =1 there is some instability which causes a step in values across the radius. At lower TSR there is significant noise in the results owing to the solver not being able to distinguish between the various local minima in the objective function. At TSR = 0, the model brakes down and a numerical value of 1E-10 must be substituted to avoid errors caused by dividing by zero.

- The performance characteristics for a rotor designed for peak torque at TSR = 2 have been determined and presented. It is concluded that a rotor of this design will obtain a maximum power coefficient of 0.49 at TSR = 2.7. The maximum axial force coefficient is predicted to be 0.79 and this occurs slightly before maximum power at TSR = 2.55. The maximum torque coefficient is 0.23 at TSR_D = 2.0.

  The rotor continues to develop torque until TSR = 6 at which point the propeller brake state is reached and the rotor is in full overspeed. At this point the axial force coefficient is 0.32

- The model is effective over the operating range with only 25 blade elements. It is therefore shown that a model of this type is suitable for use in the development of a system to estimate loads on a marine rotor with dynamic environmental conditions. It is effective and demands a relatively low computational effort.

4.7 References

1. Griffiths RT, *Energy From the Wind.* University of Wales Swansea internal report, 1974.
2. Glauert H, *The Elements of Aerofoil and Airscrew Theory.* Cambridge University Press, : p. 201-207, 1947.
3. Houghton EL. Brock AE, *Aerodynamics for Engineering Students.* Vol. 1 P119,. 1960: EDWARD ARNOLD.
4. Abbott I H, Von Doenhoff A E, *Theory of Airfoil Sections.* Dover, 1959.
5. Profili Airfoil Analysis Software, [online http://www.profili2.com/ 2006] (accessed 12/07/06).
6. Massey B, *Mechanics of Fluids.* 7th ed, ed. Ward-Smith J. 1998: Stanley Thornes Ltd.
7. Sheldahl RE, Klimas PC, *Aerodynamic Characteristics of Seven Symmetrical Aerofoils Through 180-Degree Angle of Attack for Use in Aerodynamic Analysis of Vertical Wind Turbines* Sandia National Laboratories Energy Report, 1981.
8. Airfoils at high angles of attack,[online 2006 http://www.aerospaceweb.org/question/airfoils/q0150b.shtml] (accessed 27/10/06), City
9. Woollard MG, *PhD Thesis: 'A design study for and experimental horizontal axis wind turbine'.* 1980.
10. Windsave, Power for a given wind speed, [online 2006 http://windsave.staging.atwwwuk.com/page.asp?partid=67] (accessed 1/11/06),
11. Griffiths RT, Woollard MG, *Performance of the optimal wind turbine.* Applied Energy 4, Applied Science Publishers Ltd, 1978.
12. Chapman J, Masters I. Orme J, *Rotor Performance Prediction for Tidal Current Turbines.* Joint conference of The association for Computational mechanics in engineering (UK) and The Irish Society for Scientific and Engineering Computation 19th- 20th April 2006, Queen's University Belfast., 2006.
13. University of Sydney, Aerodynamics for students, [online 2006 http://www.aeromech.usyd.edu.au/aero/propeller/prop1.html] (accessed 12/10/06),
14. Couch SJ. Bryden IG, *Numerical Modelling of Energy Extraction from Tidal Flows.* World Renewable Energy Congress (WREC 2005) Editors M. S. Imbabi and C. P. Mitchell Elsevier Ltd, 2005.

5.0 EXTENSION OF BLADE MODEL FOR DYNAMIC LOAD ESTIMATION

5.1 Introduction

The blade element theory and stream tube analysis used here is presented in Chapter 4. This is the basis on which the dynamic load estimation model is built. In its fundamental form the hydrodynamic loads on each blade can be calculated as a combination of the velocity of the fluid, the blade geometry, the operational tip speed ratio and the properties of the aerofoil used in the construction of the blade.

If the flow through the turbine is uniform, the velocity of the oncoming fluid is constant at any point in a stream tube. This implies that the force on a blade operating at constant TSR is the same regardless of where in the rotation the blade is. A model using a uniform flow can therefore calculate the force generated on one blade of the rotor and multiply this by the number of blades to obtain total force on the rotor.

In reality, phenomena occur that drastically alter the velocity profile from its uniform state [1]. The effect of the seabed and free surface, waves, convection, salinity and turbulence contribute to the irregularity, some of which can be accurately predicted [2]. The effect of this non-uniform flow is that parts of the rotor will see a different flow condition to others at the same time. This has the effect that the forces on the blade vary greatly within each revolution and give rise to oscillatory forces about the hub.

With the addition of a depth and time varying velocity, the flow conditions are different for each blade. Each blade must be analysed separately with respect to its angular displacement and then the loads from each are resolved about the hub to determine the total rotor load. This requires a dynamic model which considers the rotor in quasi-static states throughout each revolution.

5.2 Background

There are essentially three steps involved in the application of wave action to a submerged body. The first is determination of the wave characteristics which involves the wave period, height and water depth. The second is the generation of the wave kinematics which describes the fluid motion throughout the wave in terms of velocities and accelerations. Finally, the forces on the structure are calculated locally before summing to obtain global structural forces. In the case of a concurrent velocity profile,

this is added to the wave kinematics before the forces are calculated. The procedure for the calculation of wave plus current forces is described by the American Petroleum Institute [2]. The flow chart in Figure 5.01 summarises this process:

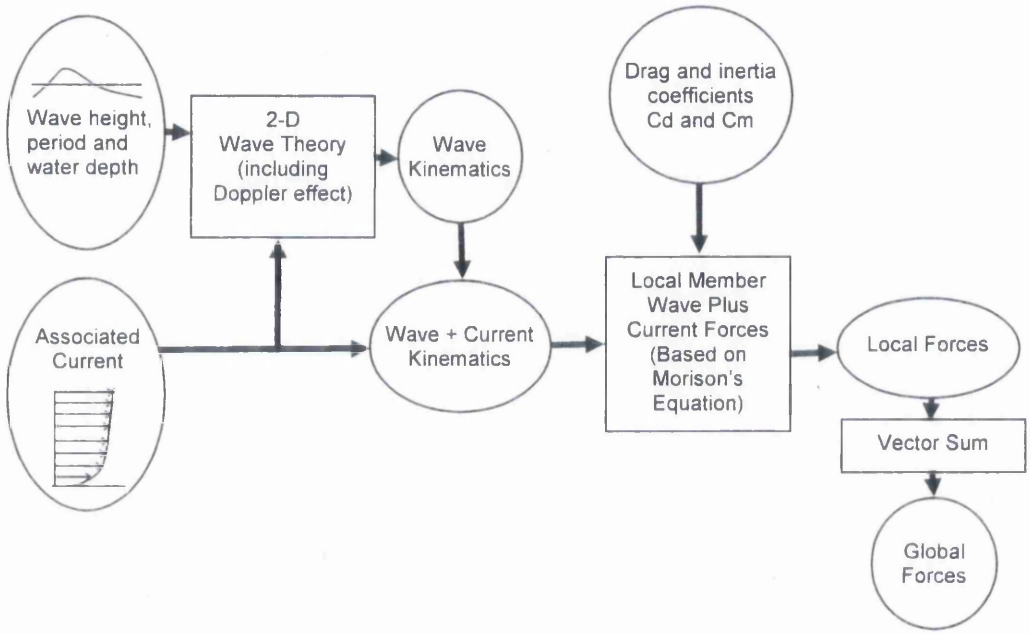

Figure 5.01 – Calculation of forces owing to velocity and wave effects [2]

Of note is the Doppler effect in which a current combined with a wave direction tends to increase the apparent wave period whereas a current opposing the wave direction tends to shorten the period as seen by a stationary object. In the case of calculating the loads on a structure at a particular site, it is likely that the wave period measured by the wave buoy or similar, will not take the current velocity into account and consequently the measured values are in fact apparent values and it is assumed that this step can be neglected. If the waves are generated from an estimated extreme wave, such as a 50 year return wave, this may not be the case.

5.2.1 Wave kinematics

To determine the two dimensional characteristics of a wave over its length a wave theory must be employed. A comprehensive comparison of different approaches with varying complexity is presented by Sarpkaya [3]. A similar comparison is beyond the scope of this study as only the results of such an analysis are used here.

The API make a comparison of different theories and the suitability of each to different wave conditions [2]. The graph is reproduced below in Figure 5.02. It is clearly seen that different theories are better suited to waves depending on the values of $\frac{d}{gT_{app}^2}$ and $\frac{H_w}{gT_{app}^2}$. The wave types considered for a typical tidal stream turbine application in section 5.4.1.2 have values as shown in table 5.1. These values are plotted as far as possible on Figure 5. 02.

Wave Type	1	2	3	4	5	6	7	8	9	10
H/gT_{app}^2	0.0110	0.0060	0.0045	0.0038	0.0032	0.0026	0.0017	0.0013	0.0020	0.0052
d/gT_{app}^2	0.6371	0.2832	0.1593	0.1019	0.0708	0.0520	0.0398	0.0315	0.0255	0.0211

Table 5.1 – Comparison of the typical wave types

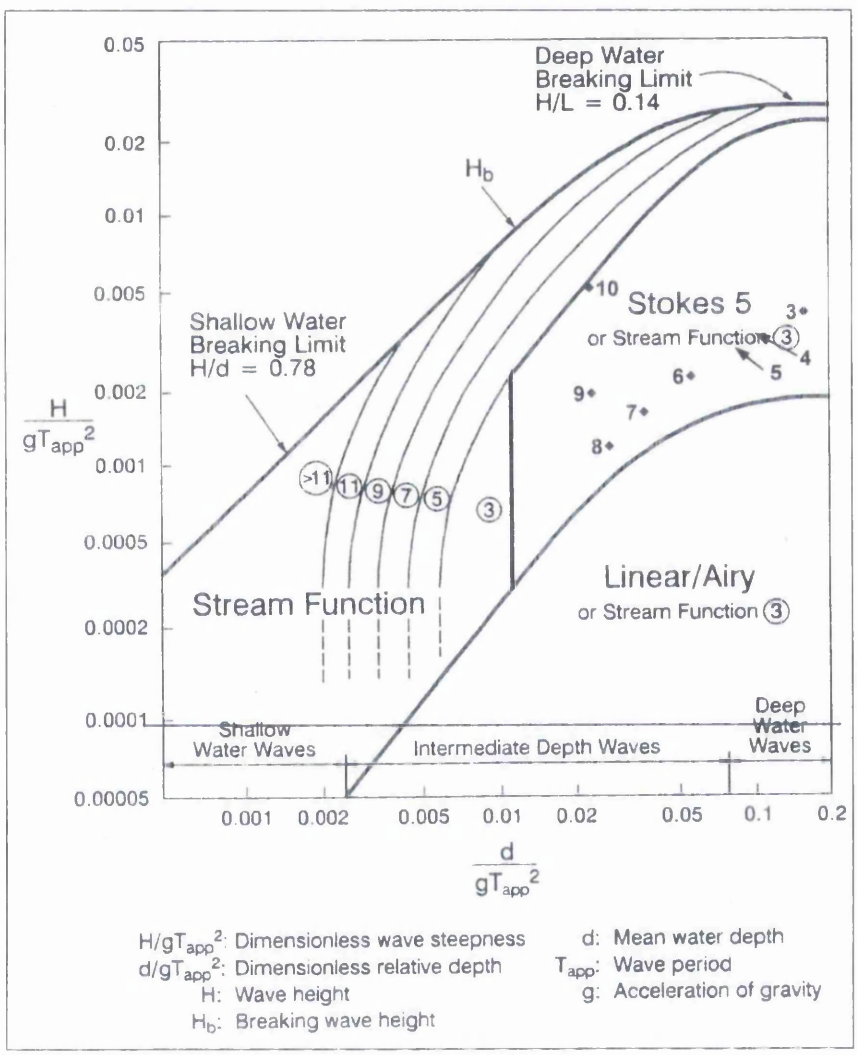

Figure 5.02 - Regions of applicability of various wave theories. Source - [2]

It is clear that the Stream Function is suited to all operating conditions and a 3rd order approximation would most likely prove adequate. However with computing facilities available, the order is able to be varied automatically to find the optimal solution for steeper waves. This gives the capability to solve steeper waves or waves in shallower water.

5.2.2 Stream function theory

The application of the stream function to wave kinematics is discussed in detail by Chaplin [4]. It is stated that the problem under consideration is one of two dimensional, irrotational periodic wave of permanent form. The wave can be defined in terms of mean water depth D, wave height H_w and wave period T. The aim of wave theory is to relate the wave kinematics to these parameters. The basis for the application of stream function theory is presented here for completeness and is taken from Chaplin [4].

The problem can be reduced to one of steady flow by observing a frame of reference moving at the same speed as the wave. The system is defined in Figure 5.03.

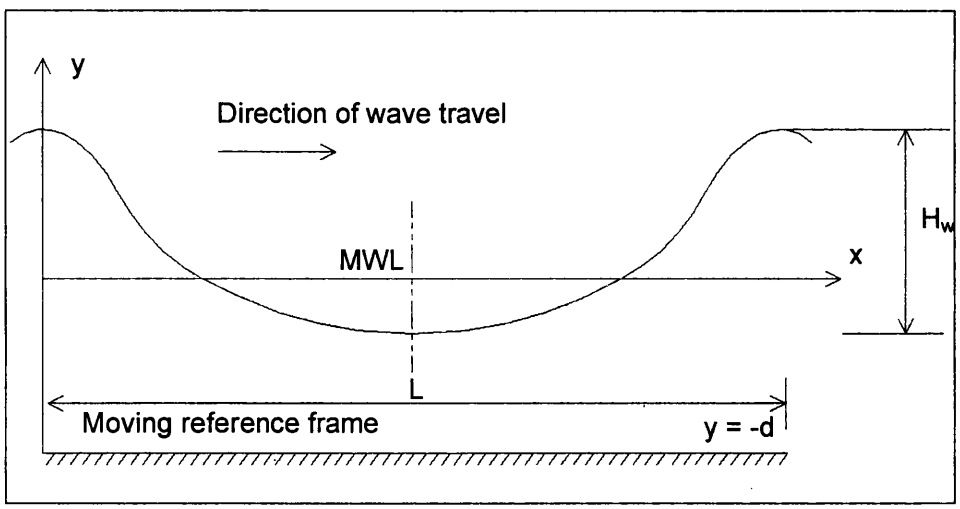

Figure 5.03 - Definition of wave parameters

The Stream Function $\psi(x,y)$ is constant along any streamline. Consequently the partial derivative of $\psi(x,y)$ with respect to any direction gives the component of velocity perpendicular to that direction [5]. At the frame of reference, the velocity components of the stream function are defined by:

$$U_w - C = \frac{\partial \psi}{\partial y}, \; V_W = \frac{\partial \psi}{\partial x}$$

Where U_w and V_w are horizontal and vertical components velocities in the x and y axes respectively and C is the wave speed.

The following conditions must be satisfied by the stream function [4] :

i) For the condition of irrotationality $\nabla^2 \psi = 0$

ii) The vertical velocity component at the seabed is zero $\frac{\partial \psi}{\partial x} = 0$ when $y = -d$

iii) The free surface is defined by $y = \eta(x)$ and is a flow boundary. The local velocity vector must be tangential to it $\therefore \frac{\partial \eta}{\partial x} = \frac{V_w}{(U_w - C)}$

iv) Since the pressure is zero on the surface: $\frac{\left[(U_w - C)^2 + V_w^{\,2}\right]}{2g} + \eta = Q$ where Q is the total head, a constant for a given wave.

v) The wave is periodic in x with interval L and is symmetrical about a vertical plane through the crest or trough.

Except for (iii) and (iv), all of these conditions can be satisfied by choosing a stream function such that:

$$\psi = -\frac{L}{T} y + \sum_n^N m_n \sinh \frac{2\pi n(d+y)}{L} \cos \frac{2\pi n x}{L} \tag{5.1}$$

Where N is the solution order.

The moving reference frame is accounted for by the first term and the wave induced effects are represented in the second term.

It is also possible to satisfy requirement (iii) by considering the free surface as a streamline on which ψ(x,y) is constant. It follows from the above equation (5.1) that the stream function equals $-dL/T$ along the seabed. However on the surface the value of the

stream function ψ_η is unknown and it differs by an amount that is proportional to the overall mass transport of fluid caused by the wave.

The solution of the wave theory is therefore numerical and requires finding values $of\, m_1$, m_2, m_N, L and ψ_η so that condition (iv), the dynamic free surface boundary condition, is satisfied as accurately as possible.

5.2.3 Solution of the stream function

Open source code to automatically optimise stream function theory has been developed by The Department of Civil and Environmental Engineering Hydraulics Group at Southampton University. This is available online [6].

The code selected as most suitable for this application is 'CW623'. This can be compiled in Fortran to generate an executable file. The main advantage of this code is that it automatically increases the order of the stream function expansion for steep waves. It also will incorporate a uniform current flow if required. Non-uniform currents are not included in the capabilities. The results can be post processed using a separate code 'CW61' which will output wave kinematics at any point in the wave or depth including the free surface.

A modification is made which enables the output to be generated as a matrix in the horizontal and vertical planes over the wave length. Discretised velocities U_w and V_w and accelerations $\frac{\partial U_w}{\partial t}$ and $\frac{\partial V_w}{\partial t}$ can be therefore be stored as a matrix as shown in Figure 5.04.

	Wavelength fraction x/X →									
Depth d ↓										

Figure 5.04 – The matrix used to store wave kinematics data

5.2.4 Morison's equation

In [7], Moe states that Morison's equation would be better expressed as Morison's formula as it is effectively an experimentally calibrated approximation rather than a rigorously derived mathematical expression. However the use of the equation is widespread in offshore engineering [2] and the experimentally determined parameters are analysed and presented by Sarpkaya [3].

Morison's equation considers the forces on a submerged cylinder in terms of form drag and inertial force. When the ratio of the wave length to the submerged member diameter is large (>5), this is expressed as:

$$F = F_D + F_I$$

Where:

F = hydrodynamic force vector per unit length acting normal to the axis of the member.

F_D = Drag force vector per unit length acting normal to the axis of the member in the plane of the member axis and U.

F_I = Inertial force vector per unit length acting normal to the axis of the member in the plane of the member axis and $\partial U / \partial t$.

When the fluid motion is large in comparison with the diameter of the cylinder, drag forces dominate and the flow can be considered as steady. In this case the standard form drag equation can be used with the necessary drag coefficient for the cylinder concerned. Hence:

$$F_D = \tfrac{1}{2} C_D \rho D |U| U$$

Where:

D = Cylinder diameter

C_D = Drag coefficient for the cylinder

U = Fluid velocity normal to the cylinder axis

$|U|$ = Absolute value of U

When the motion of the fluid is small in comparison to the cylinder, inertial forces dominate which gives a force equal to twice the displaced mass times the fluid acceleration in the absence of the cylinder [3]. Hence:

$$F_I = C_m \rho S \frac{\partial U}{\partial t}$$

Where:

S = Displaced volume of cylinder per unit length

C_m = Inertia coefficient for the cylinder

U = Fluid velocity normal to the cylinder axis

$|U|$ = Absolute value of U

Morison's equation in this form neglects any convective acceleration in the inertia calculation. It also ignores lift forces, slam forces and axial forces.

The values C_D and C_m must be determined experimentally and can vary over the wavelength. General approximations can be used for better accuracy and the coefficients can be expressed in terms of surface roughness, Reynolds number, Keulegan Carpenter number, current/wave velocity ratio and member orientation.

Values of C_D are available for many engineering applications but values for C_m are less common. Sarpkaya [3] presents the added mass of various bodies. From this, the added mass coefficient and hence C_m can be calculated for different bodies.

It is given by:

$$C_m = 1 + C_A$$

and:

$$C_A = \frac{M_A}{\rho S}$$

Where:

C_A = Added mass coefficient

M_A = Added mass per unit length

By this method forces on submerged structures subject to wave action can be estimated from wave kinematics data.

5.3 Formulation of a dynamic model

5.3.1 Addition of time dependent vector flow field

Using a non-uniform flow requires a method to describe the flow characteristics at any point in the swept area of the blade, at a particular time. The velocity of the oncoming fluid is now expressed as a function of depth. The depth is taken as the depth of the centre of pressure of the element aerofoil section. Although the diameter of the stream tube increases as the flow passes the plane of the rotor, it is assumed that the flow experienced by a section of the rotor at a certain depth corresponds to the fluid at the same depth in the flow well upstream of the rotor. This assumption is reasonable for a first iteration as the variation in streamtube diameter is small.

5.3.2 Dynamic time step

One significant effect of using a non-uniform flow is that there is now an acceleration of the rotor depending upon its angular displacement. This is caused by the variation in torque as each blade undertakes a revolution. The acceleration is counteracted by the inertia of the rotating components of the system and the added mass of the rotor. However, the acceleration adds to the complexity of the dynamic model as the rotor experiences changes in rotational velocity. This is added to the model so that with each step the rotor speed is updated due to the net torque on the system. The most significant contribution is due to the reaction of the generator against the rotor.

5.3.2.1 Generator torque reaction

In a tidal stream turbine, the majority of the torque applied to the rotor is transformed into electrical energy by the generator. The torque which the generator absorbs, T_G is a function of the rotor speed. Shown in Figure 5.05, is the assumed relationship between speed and torque for a typical low-speed generator, which is also the generator model used in this investigation.

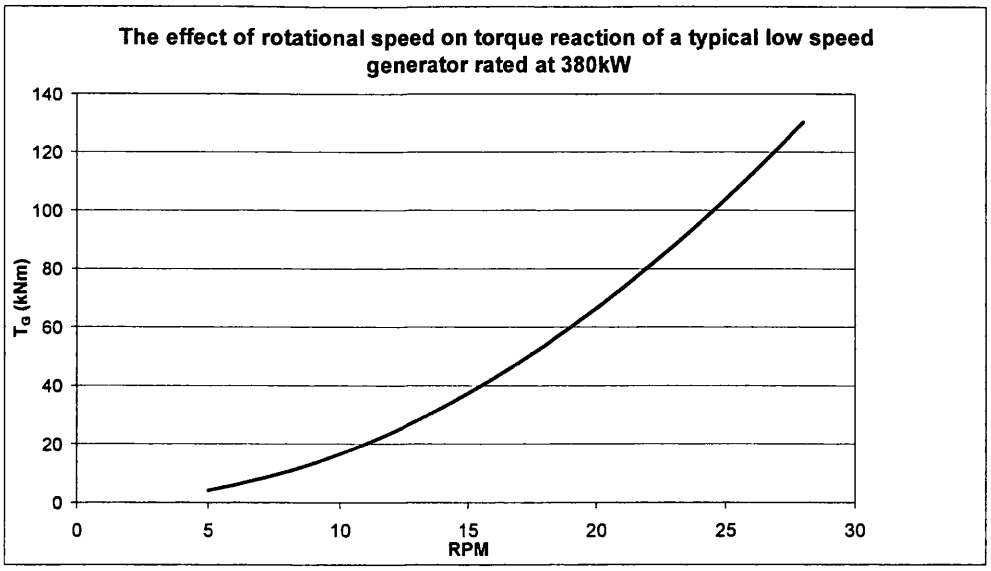

Figure 5.05: The relationship between torque and speed for a 380kW PMG

A particular generator will have specific torque characteristics. As an approximation to enable the generator performance to be estimated for any sized rotor, the relationship is given by:

$$T_G = \frac{C_{P(\max)} \rho \pi A \left(\frac{\Omega R}{TSR_D} \right)^3}{2\Omega}$$

5.3.2.2 Rotor inertia

The inertia of the rotor system is a summation of the various components. This varies with the power and design TSR of the rotor and also with the number of blades. The various components and their inertias for the test rotor are shown in Figure 5.06 and table 5.2. The main contributors are the rotor blades and it is found that owing to the relative volumes of different blade numbers, the inertia of the system also varies with blade number.

A model of the blades is generated in a computer aided design package which can then be used to determine the moment of inertia though the 'Enquiry' function. The dimensions and values required to estimate the remaining components are taken from a design report [8].

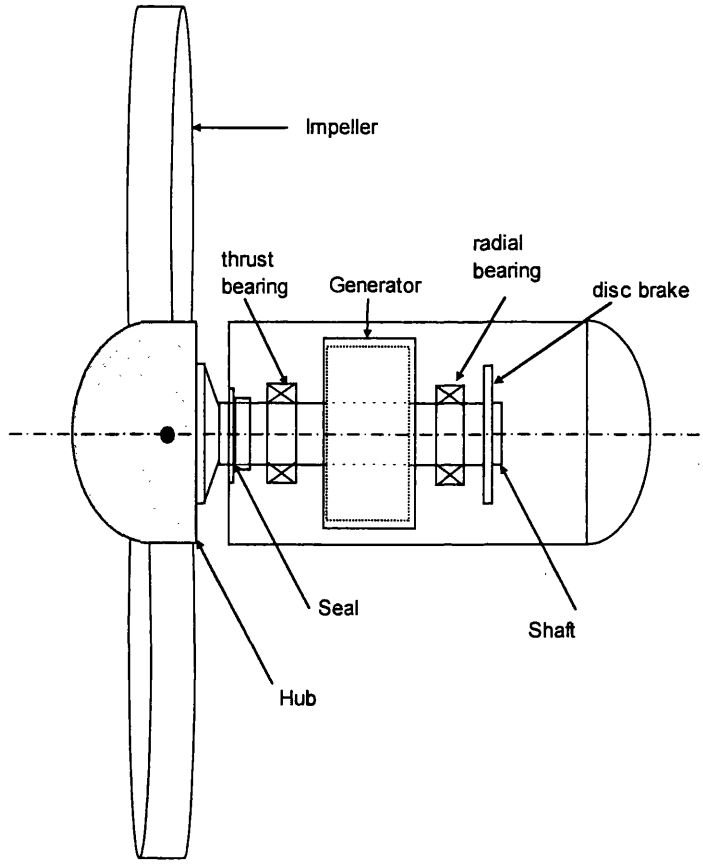

Figure 5.06 – The components comprising rotor inertia [8]

Moment of Inertia by Component	Value (kgm^2)
2 bladed impeller	93528
3 bladed impeller	62352
4 bladed impeller	46764
Hub	611
Generator rotor	1721
Shaft	194
Seal	7
Brake disc	45
Total (2 bladed)	**96106**
Total (3 bladed)	**64930**
Total (4 bladed)	**49342**

Table 5.2 – Values of inertia for the various system components

5.3.2.3 Rotor speed

The acceleration of the rotor is governed by:

$$I\dot{\Omega} = T_n - T_{Gn}$$

Where n is the timestep number, the timestep is considered to be so small that the relationships between torque and acceleration can be approximated to linear within it. Therefore taking a linear discretisation of $\dot{\Omega}$ in time, the rotor speed for step $n+1$ is therefore given by:

$$\Omega_{n+1} = \Omega_n + \frac{(T_n - T_{Gn})(t_{n+1} - t_n)}{I_R}$$

Where:

Ω = Rotational speed of the rotor (Rad/s)

n = number of time step

T = Rotor torque (Nm)

T_G = Absorbed generator torque (Nm)

I_R = Rotor inertia (kgm^2) (comprises rotor, generator, shaft and associated components)

t = time (s)

5.3.3 Addition of depth characteristics

5.3.3.1 Location of blade element

The conditions experienced by a particular blade element must be able to be found relative to the depth of the aerofoil centre of pressure. This is achieved using the angular displacement of the rotor relative to the vertical position. The depth of the axis of rotation

is known as the hub depth and this is used in conjunction with the radial position of the blade element to calculate the depth.

The depth of the blade element is given by:

$$D_{BE} = D_H - r\cos(\gamma)$$

Where:

D_{BE} = Depth of blade element centre of pressure (m)
D_H = Depth of rotor axis (hub depth) (m)
γ = Angular displacement of rotor from vertical (rads)

The horizontal location is immaterial as there is no variation in flow conditions parallel to the primary flow axis.

5.3.3.2 Summary of assumptions

It is assumed that:

- There is no variation in flow velocity or acceleration in the direction perpendicular to the flow.
- There is no rotation of the flow in the upstream vector flow field.
- The depth of the water remains constant at all times and there is no variation caused by tidal effect.
- The variation in diameter of stream tube has no effect on the relationship between the depth of the blade element and the velocities corresponding to that depth.

5.3.3.3 Velocity gradient

A theoretical analysis of a boundary layer makes the assumption that the velocity at the seabed is zero. Using a power law approximation as described in [5], the velocity profile over the depth is given by:

$$U_d = U_{\max}\left(1 - D_{BE} / D\right)^{1/n}$$

where; $1/n = \sqrt{f}$, for f < 0.1.

In turbulent pipes, the friction factor f is generally such that n = 7 and this is called the 7th power law. However for tidal stream currents it is assumed that the 1/10th power law can be used [9]. This can be seen graphically in Figure 5.07.

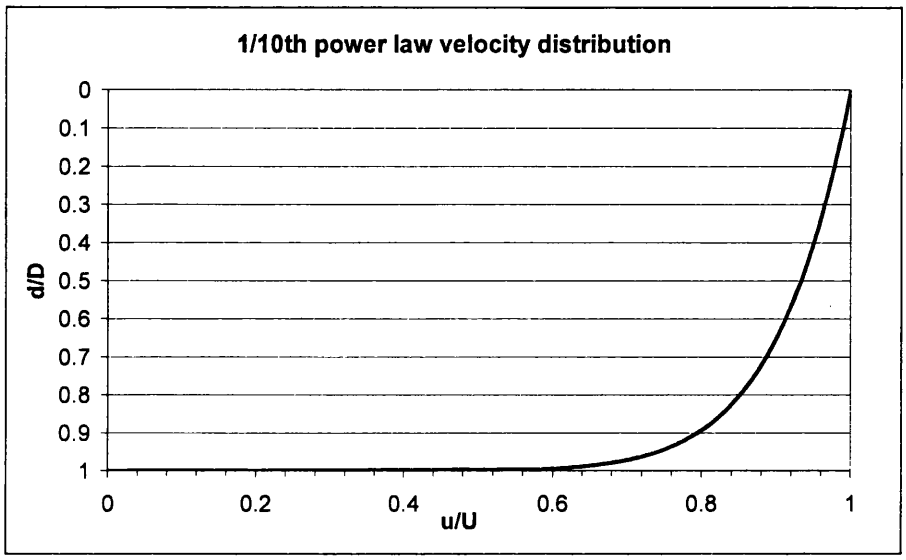

Figure 5.07 - A graphical representation of variation of velocity with depth

If a 2 bladed rotor is considered, it is apparent that whilst the one blade is nearest the surface and hence the faster fluid, the other blade is directly opposite in the slowest flow. Both the blades are rotating together and hence the TSR is effectively different on each blade.

The uniform flow of a real fluid will cause the rotation of the turbine blade at a constant TSR depending upon the load placed on the shaft. If the load is such that the turbine is operating at its design condition, the flow though the blades will be uniform in that at every position along the radius the aerofoil at that position will see the oncoming fluid at its optimum angle of attack as seen in section 4.25. If at this same flow speed the TSR increases, the angle of attack will move off optimum and a loss in efficiency will occur as the blade element moves into overspeed. The performance of the blade can be assessed in this manner at any combination of flow speed and TSR. In the case of the

seabed induced velocity gradient the local TSR varies across the radius, and some parts will experience optimum angle of attack whereas others will be off optimum. Because of the variations in velocity and hence local TSR and efficiency, the forces experienced by the blades differ and resultant forces are experienced by the hub and shaft.

5.3.4 Addition of wave characteristics

Including velocity gradient in the flow field results in a fluctuation in the loads generated on the rotor throughout each rotation. However, the fluid velocity remains constant over time. The addition of wave effects introduces a flow variation which is characterised by changes in velocity and acceleration in the axial and vertical directions over time. As described in section 5.2.4, Morison's equation describes the force of wave action on submerged structures as consisting of two parts; drag and inertia forces. The wave velocity generates the drag forces, whereas the accelerations develop the inertia forces.

5.3.4.1 Typical wave characteristics

Wave kinematics software developed at the University of Southampton by John Chaplin [6] uses stream function theory as described in section 5.2.2 to obtain velocities and accelerations over the wavelength and depth of a wave. These outputs are defined by the depth of water, wave height, wave period and current flow in the axial and vertical planes at discrete points in the wave.

A wave modeled in two dimensions moves the fluid through which it is passing in a circular motion. There are therefore velocities and accelerations in the axial and vertical directions as follows:

U_W – Velocity of the fluid in the axial direction at the plane of the rotor disc due to wave action.

V_W – Velocity of the fluid in the vertical direction at the plane of the rotor disc due to wave action.

$\frac{\partial U_w}{\partial t}$ - Acceleration of the fluid in the axial direction at the plane of the rotor disc due to wave action.

$\frac{\partial V_w}{\partial t}$ - Acceleration of the fluid in the vertical direction at the plane of the rotor disc due to wave action.

Illustrations of the typical variation in the parameters over the wavelength and depth are shown in Figures 5.08 to 5.11.

It can be seen that the variation in flow speed and acceleration decreases with depth throughout the graphs and that the effect of the waves is generally more pronounced at the surface. The circular motion of the wave action is also clear when comparing the velocities and accelerations in both planes.

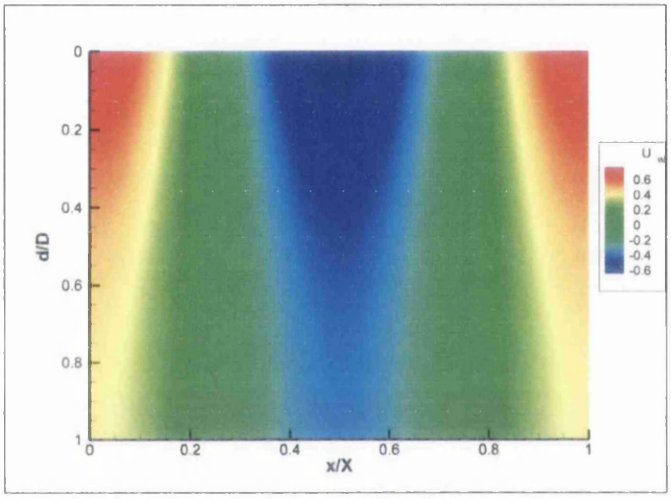

Figure 5.08 - Variation of axial wave velocity in m/s with depth and wavelength

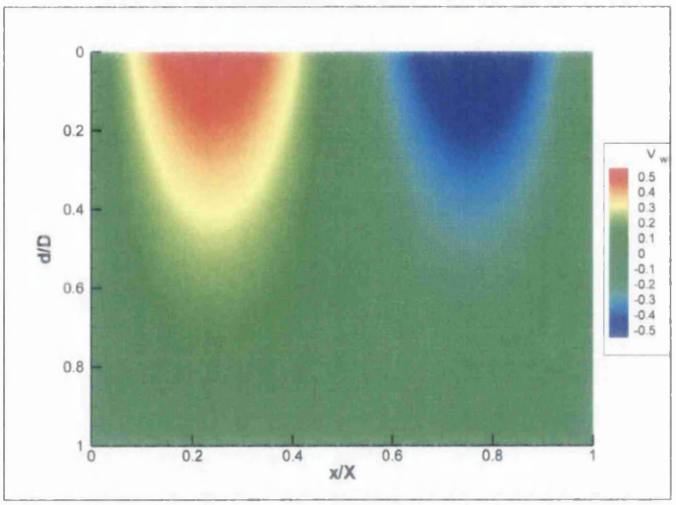

Figure 5.09 - Variation of vertical wave velocity in m/s with depth and wavelength

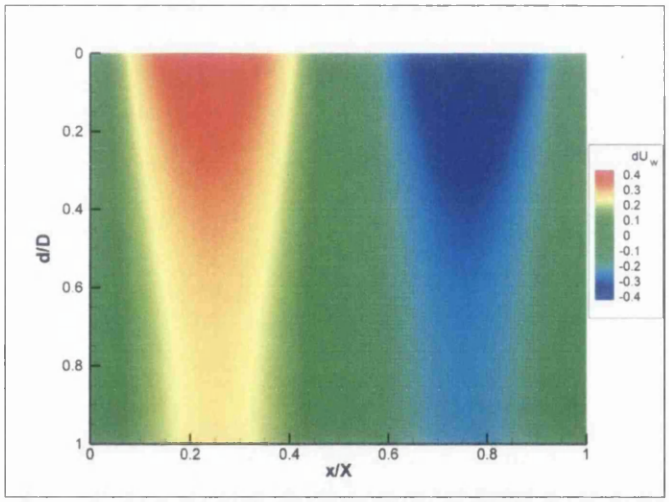

Figure 5.10 - Variation of axial particle acceleration in m/s with depth and wavelength

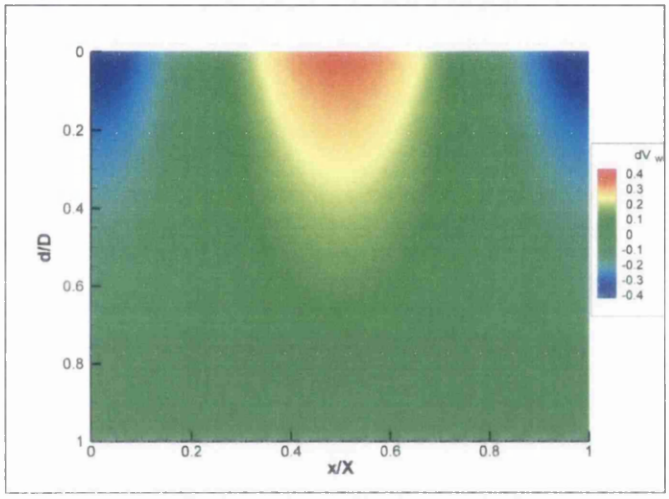

Figure 5.11 - Variation of vertical particle acceleration in m/s with depth and wavelength

5.3.4.2 Vector flow field applied to each element

The vector flow field in the plane of the rotor disc is given in a 2D sense as shown in Figure 5.12. Both velocities and accelerations in the axial and vertical plane are included.

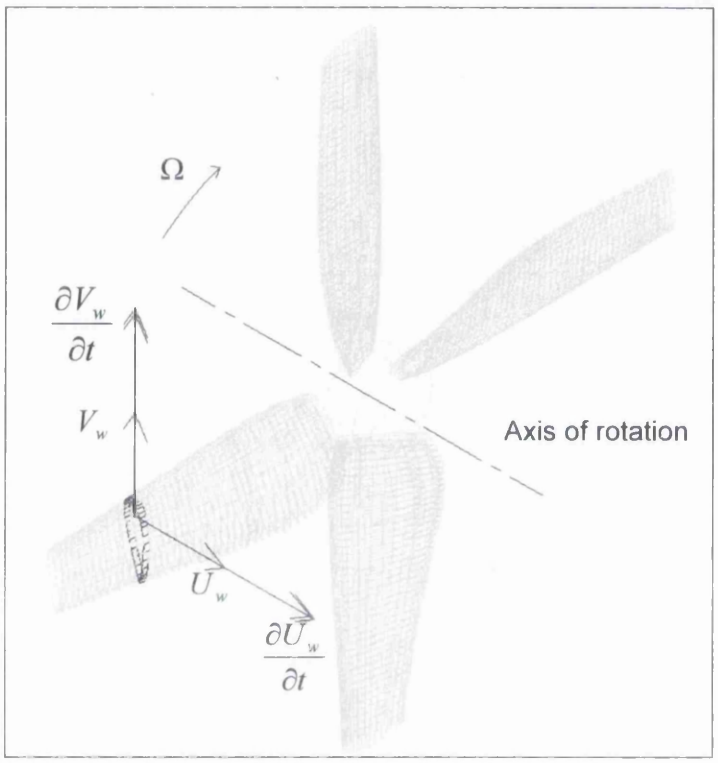

Figure 5.12 - The vector flow field as applied to each blade element

The quantities, U_w, $\frac{\partial U_w}{\partial t}$, V_w and $\frac{\partial V_w}{\partial t}$ are found with respect to the depth of the centre of pressure for the blade element.

5.3.4.3 Effect of wave flow effects

The wave velocity fluctuations and accelerations are input to the rotor model in different ways. All are a function of depth and the position of the blade element in the wavelength x/X as shown in Figures 5.08 to 5.11. In addition to changing the inflow velocity, the variation in velocity changes the flow regime differently depending on the angular

displacement of the rotor blade. The accelerations also expose the rotor to inertia forces, the effect of which again depends on the position of the blade. These inertial forces result from the displacement of the fluid by the blade. This is commonly modelled in offshore structures and is an integral part of Morison's equation which indicates that forces on submerged structures are composed of drag forces and inertial forces. Drag forces result from wave induced velocity whereas inertia forces are the result of induced accelerations. The predominance of these forces is governed by the Keulegan-Carpenter number. This gives a measure of the magnitude of the fluid motions relative to the structure [3] and in this case is expressed as:

$$k = U_w T_w / D$$

Where T_w is the wave period and D is the effective diameter of the submerged member.

When k > 40 drag forces are dominant, and when k < 10 inertia forces dominate. The range of operation for a typical tidal stream turbine rotor varies from 0 when stationary in calm conditions up to approximately 200 at full current and wave state operation. This implies that wave induced drag forces are dominant over most of the operational range. This means U_w and V_w have more effect than the corresponding accelerations $\frac{\partial U_w}{\partial t}$ and $\frac{\partial V_w}{\partial t}$. However, the inertial effects will still be significant and consequently are factored in.

5.3.4.4 Axial velocity

The axial wave velocity U_w is added to the velocity of the oncoming fluid for each blade element. The equation for the local upstream velocity U_L becomes:

$$U_L = U_d + U_w$$

There are two primary effects, the first being a change in local speed ratio, and secondly a change in axial force and torque. The relationship is complicated by the local speed ratio, as this affects the local angle of attack. It is possible that with a very sharp rise in the velocity of the oncoming fluid the blade will stall. Conversely, with a negative U_w, the

blade is likely to overspeed and hence may begin to act as a propeller over some of the radius as described in section 4.3.1.4.

5.3.4.5 Vertical velocity

The vertical wave velocity V_w is added to the tangential velocity of the blade element when the blade is moving in the vertical plane. For one half of a rotation this velocity is positive and for the other it is negative depending on whether the motion of the fluid is with or against the tangential velocity of the rotor. When a rotor blade is at the top or bottom of its cycle, V_w has no effect on the relative tangential velocity of the blade element and the fluid. Conversely when the rotor blade is horizontal the effect is maximized. For this reason a sine function is used to factor in the effect of V_w throughout the rotation. The expression for the local vertical velocity V_L is therefore given by:

$$V_L = V_w \sin(\gamma)$$

The local speed ratio is therefore now given by:

$$x_L = \frac{r\Omega - V_L}{U_L}$$

5.3.4.6 Axial acceleration

The acceleration of the fluid is a quantity that is not considered in BEMT and consequently is not easily added to the system of equations. However, it is clear from Morison's equation that the drag and inertia effects can be added to obtain the total value for wave force and the same approach is used here. For the axial acceleration $\frac{\partial U_w}{\partial t}$, the inertia effects are made as an addition to the solved BEMT system, such that equation (4.23) for axial force becomes:

$$F_{A3} = \sum_{0}^{R}\left[\frac{1}{2N}\left(dF_{A1} + dF_{A2}\right) + dF_{Ain}\right]$$

Where dF_{Ain} is the axial inertia force for the blade element which is defined by:

$$dF_{Ain} = C_{mA}\rho S\frac{\partial U_w}{\partial t}.dr$$

Where:

C_{mA} = Axial coefficient of inertia
S = cross sectional area of the aerofoil section

The aerofoil cross sectional area for the NACA4424 section is given in terms of chord by:

$$S = 01658c^2$$

The axial coefficient of inertia for the aerofoil section of the blade C_{mA} can be estimated using the Inertia coefficient of an ellipse with the same diameter as the aerofoil frontal length. This coefficient is calculated in the same way for an ellipse with the same significant diameter [3]. It is given by:

$$C_{mA} = 1 + C_{AA}$$

and:

$$C_{AA} = \frac{M_{aA}}{\rho S}$$

Where:

C_{AA} = Added mass coefficient
M_{aA} = Added mass per unit length

The added mass per unit length is calculated in the same way as an ellipse and is given by Figure 5.13 and:

$$M_{aA(ellipse)} = \rho\pi b^2 = \rho\pi L_A^{\ 2}$$

Where L_A is the effective radius of the aerofoil as shown in Figure 5.13 and is given as a function of blade inclination angle β:

$$L_A = f(\beta)$$

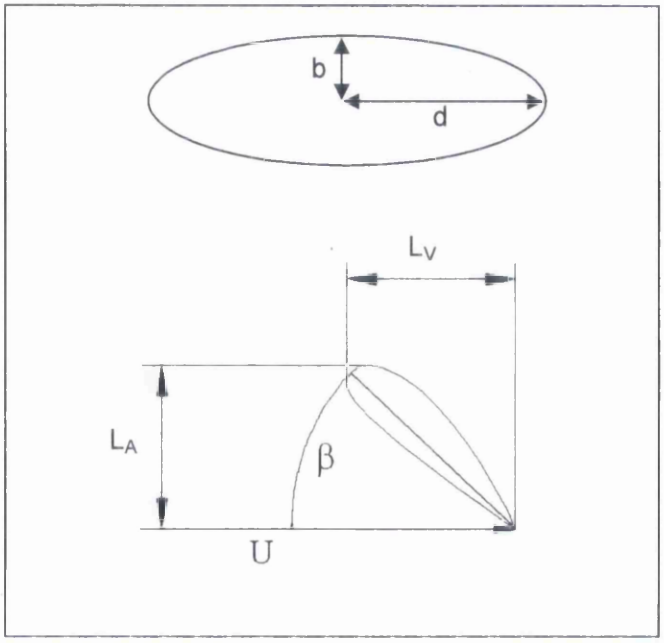

Figure 5.13 - The elliptical approximation for added mass

The assumption made here is that the inertial impact of the wave on the blade element is in the direction of the wave, and the frontal length of the aerofoil is given by L_A for the axial acceleration and L_V for the vertical accelerations. This assumes the acceleration impacts the blade as if the blade is stationary and no rotational acceleration of the rotor occurs within the timestep.

5.3.4.7 Vertical acceleration

The acceleration in a vertical direction is considered in much the same way as the axial acceleration. However, the effect is different as the vertical acceleration $\frac{\partial V_w}{\partial t}$ impacts upon the torque rather than the axial force. An upward acceleration will increase the torque on a blade travelling upward and a negative torque on a blade travelling downward. The torque equation therefore becomes:

$$T_3 = \sum_0^R \left[\frac{1}{2N} (dT_1 + dT_2) + dT_{inS} \right]$$

Where an acceleration in the same direction as blade travel is positive.

Consequently the expression for power becomes:

$$P_3 = \Omega \sum_0^R \left[\frac{1}{2N} (dT_1 + dT_2) + dT_{inS} \right]$$

The vertical inertia force for a horizontal blade element is defined by:

$$dT_{in} = C_{mV} \rho S \frac{\partial V_w}{\partial t} r.dr$$

However, the effect of the inertia force on the torque is dependent on the blade angular displacement. When the blade is directly vertical there is no effect on the torque. In Seigerstetter [10], wave forces are considered to be acting on vertical cylinders and only the horizontal components are considered to be of importance when considering vertical constructions. The same approach is taken here. As the blade rotates about the rotor axis, the vertical positions occur once at the revolution top and one at the bottom. To incorporate this effect into the torque, a sine function is used. The effect of this is two fold, firstly at the revolution top and bottom, the effect of the vertical acceleration on the torque is zero, whereas when the blade is horizontal it has maximum effect. Secondly during the first half of the revolution the effect is positive and as the blade passes the 180° position the effect becomes negative. The sine adjusted torque effect is therefore expressed by:

$$dT_{inS} = C_{mV} \rho S \frac{\partial V_w}{\partial t} \sin(\gamma) r.dr$$

Where C_{mV} is the vertical coefficient of inertia and is calculated in much the same way as the axial equivalent but using the corresponding frontal length L_V as shown in Figure 5.13:

$$C_{mV} = 1 + \frac{\pi L_V^{\ 2}}{S}$$

This assumes the acceleration impacts the blade as if the blade is stationary.

5.3.5 Outputs

The addition of a non-uniform flow field creates a variation in blade forces over the rotation. For this reason it is no longer possible to consider a single blade and multiply the forces by the blade number to obtain the forces on the hub. Each blade must be considered separately and the forces resolved about the hub centre to determine the total loads. The rotor model considered in Chapter 4 considers one blade as if it is a part of a rotor with uniform conditions. The case considered here is a 3-bladed rotor where each blade is given a subscript *i*, *ii*, or *iii*.

5.3.5.1 Torque and Axial Force

The torque of the rotor is given by summing the torque from each blade. The expression for rotor torque is therefore:

$$T_R = \sum_{i=0}^{N} T_{3i}$$

Similarly the axial force is given by:

$$F_{AR} = \sum_{i=0}^{N} F_{A3i}$$

This gives rise to the performance coefficients C_T and C_F :

$$C_T = \frac{T_R}{\frac{1}{2}\rho ARU^2}$$

$$C_F = \frac{F_{AR}}{\frac{1}{2}\rho AU^2}$$

And similarly the power coefficient C_P is given by:

$$C_P = \frac{T_R \Omega}{\frac{1}{2}\rho A U^3}$$

5.3.5.2 Yaw, Teeter and Heave

As the forces on the blades are no longer constant, moments and vertical forces are exerted on the hub. The directions of these forces are shown in Figure 5.14. They are resolved about the centre of the rotor at the point where the lines of blade centre of pressure meet.

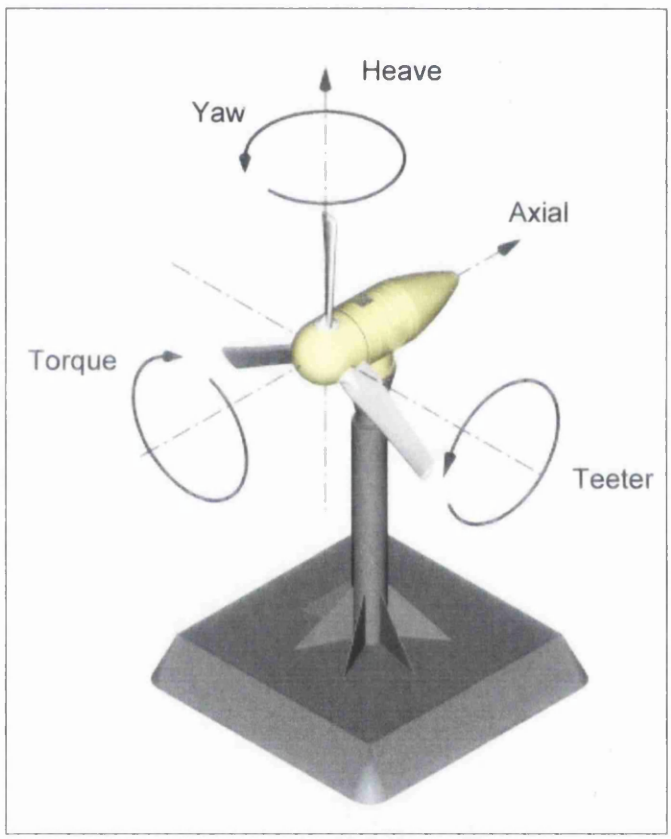

Figure 5.14 – The direction of the resolved forces and moments

Yaw and teeter are moments that are derived from the resolved axial force of the blade.

Yaw and Teeter are given by:

$$Y_R = \sum_{i=0}^{N} Y_{3i}$$

$$Te_R = \sum_{i=0}^{N} Te_{3i}$$

Where for each blade i;

$$Y_{3i} = \sum_{0}^{R} \left[\frac{r\sin(\gamma)}{N} \left(\frac{1}{2}(dF_{A1} + dF_{A2}) + dF_{Ain} \right) \right]$$

$$Te_{3i} = \sum_{0}^{R} \left[\frac{r\cos(\gamma)}{N} \left(\frac{1}{2}(dF_{A1} + dF_{A2}) + dF_{Ain} \right) \right]$$

Heave is a force that is derived from the vertical wave accelerations. It is generally smaller in magnitude than yaw and teeter but can be equally as important depending on the type of support structure used. Heave for the rotor is given by:

$$H_R = \sum_{i=0}^{N} H_{3i}$$

Where for each blade;

$$H_{3i} = \sum_{0}^{R} \left[\frac{1}{r} \left(\frac{\sin(\gamma)}{2N} (dT_1 + dT_2) + dT_{inS} \right) \right]$$

Note that the sine adjusted vertical inertia force dT_{inS} is used. The assumption is that when the blade is vertical the heave force is zero and it increases only as it moves toward the horizontal.

This gives rise to performance coefficients which are expressed as C_Y, C_{Te} and C_H respectively:

$$C_Y = \frac{Y_R}{\frac{1}{2}\rho ARU^2}$$

$$C_{Te} = \frac{Te_R}{\frac{1}{2}\rho ARU^2}$$

$$C_H = \frac{H_R}{\frac{1}{2}\rho AU^2}$$

5.4 Implementation

The basis of the dynamic loading model is the performance prediction model as described in Chapter 4. The model is extended to include time steps, individual blade calculations, velocity gradient, wave forces and post processing. The overall aim of the model is to predict the performance and loading of the device under any operating conditions which may be experienced over the device lifetime. This requires the definition of environmental conditions including the tidal current and wave regime. These are defined in section 5.4.1.

The basis for the model operation is represented by Figure 5.15:

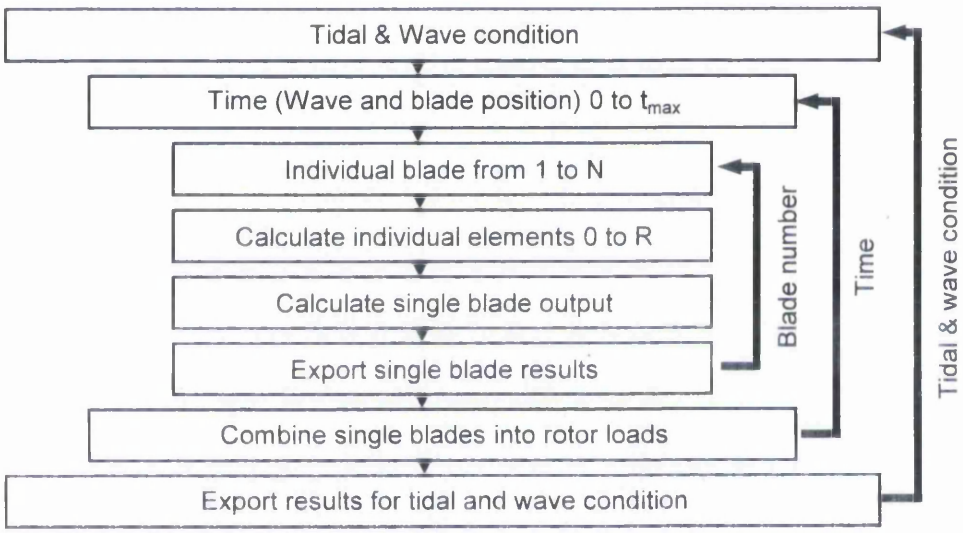

Figure 5.15 – A conceptual representation of the dynamic model with loops

For a particular operating condition, the outputs are generated over a finite time period. Each blade of the rotor is considered individually and the blade elements are solved over the radius. The results are summed to give single blade values and these are exported to file. The next blade values are calculated in the same way until all blade values are complete. The blade values are then combined to give rotor torque output and the other loads. The next time step occurs in which the wave position and rotor angular displacement are adjusted. The rotor speed may also be adjusted depending on the torque. Rotor loads are found in this way until the time limit is reached and the results are post processed to give all rotor values over the time period. A new operating condition can then be selected and the process is repeated.

5.4.1 Input parameters

The loadings on a submerged tidal stream energy converter over its lifetime are a function of the environmental conditions that it encounters. These conditions are dominated by two factors; the tidal regime and the wave climate. These factors are particular to a specific location.

5.4.1.1 Tidal Velocity Regime

It is intended to use the model to create an understanding of realistic loads on a tidal turbine. The proposed location area for the Swanturbines demonstrator is in the Bristol Channel, South Wales, given by grid coordinates (N51°15.0',N51°20.6', W3°05.9', W3°35.2'). This is illustrated in Figure 5.19. The environmental conditions at this site are used for this investigation.

The DTI report [1] gives tidal velocity estimates for this site in the form of V_{msp} and V_{mnp}, which are the mean spring peak velocity and the mean neap peak velocity respectively. These values refer to the peak velocity of an average spring and an average neap tide respectively. Also given in the report is the ratio of flood to ebb tide velocities for the site.

To enable the tidal flow regime to be estimated from the DTI values an assumption is made concerning the relationship between V_{msp} and V_{mnp} and the values surrounding it. The assumption can be visualized as in Figure 5.16.

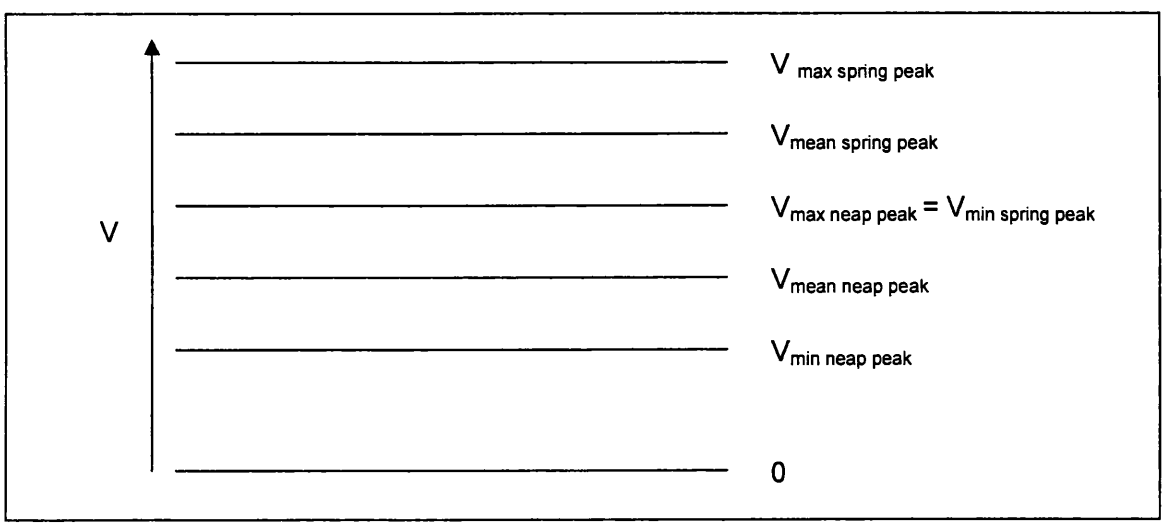

Figure 5.16 - Illustration of assumptions used to estimate peak flow speeds from the DTI report data.

Fundamentally, spring tides occur when there is the greatest difference in the height of consecutive high and low tides. Neap tides conversely have the least difference in tidal range. By the same effect, springs will have greater flow speeds than neaps. By the nature of this descriptive method having only two categories, it omits the gradient between springs and neaps. However in reality there is a smooth transition between the two and hence there is a middle value. In Figure 5.16 this middle is shown as $V_{max\ neap\ peak} = V_{min\ spring\ peak}$. Assuming a sinusoidal 'lunar' variation, this value is midway between V_{msp} and V_{mnp} and may be calculated as such. Similarly the maximum and minimum peak values $V_{max\ spring\ peak}$ and $V_{min\ neap\ peak}$ may be calculated.

The values of tidal flow for the Barry site given in [1] are given in table 3. Values calculated using the method above are shown in italics.

Parameter	Value
V_{max}	*3.15 m/s*
$V_{mean\ spring\ peak}$	2.57 m/s
$V_{mean\ neap\ peak}$	1.41 m/s
$V_{min\ peak}$	*0.83 m/s*
Flood / Ebb factor	0.85

Table 3 - A summary of flow data for the Barry site from the DTI report.

To build a model of the yearly tidal flow regime from this data, a series of sinusoidal approximations can be applied around their respective cycles. In this study diurnal, synodic and equinoxal cycles have been applied with periods of 12.43 hours, 14.8 days and 182.5 days respectively. A graph of this variation is shown in Figure 5.17.

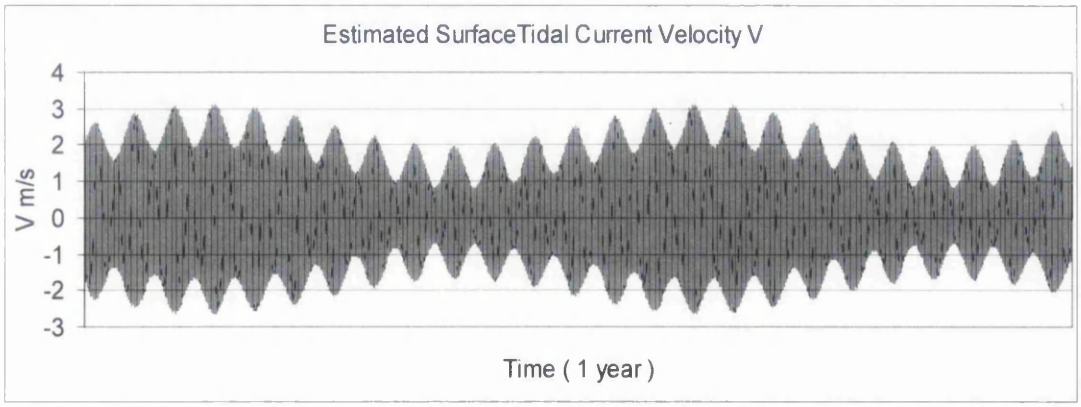

Figure 5.17 : Yearly variation of tidal stream velocity at the Barry site

This method is an effective way to obtain an estimation of the tidal flow regime from the limited information given in the DTI report [11]. Although the sinusoidal approximation leads to some inaccuracy in the estimation of the flow velocity, this method is vastly less expensive than collecting site data or running a full model. However, in reality the flow data would be measured for an extended period to ascertain the true nature of the flow. It is not practical to undertake this task in the scope of this investigation.

To obtain mean current speeds for analysis, the occurrence of a series of flow velocities is determined. The velocity is grouped into bins of 0.5m/s and the occurrence is shown in Figure 5.18 and table 4.

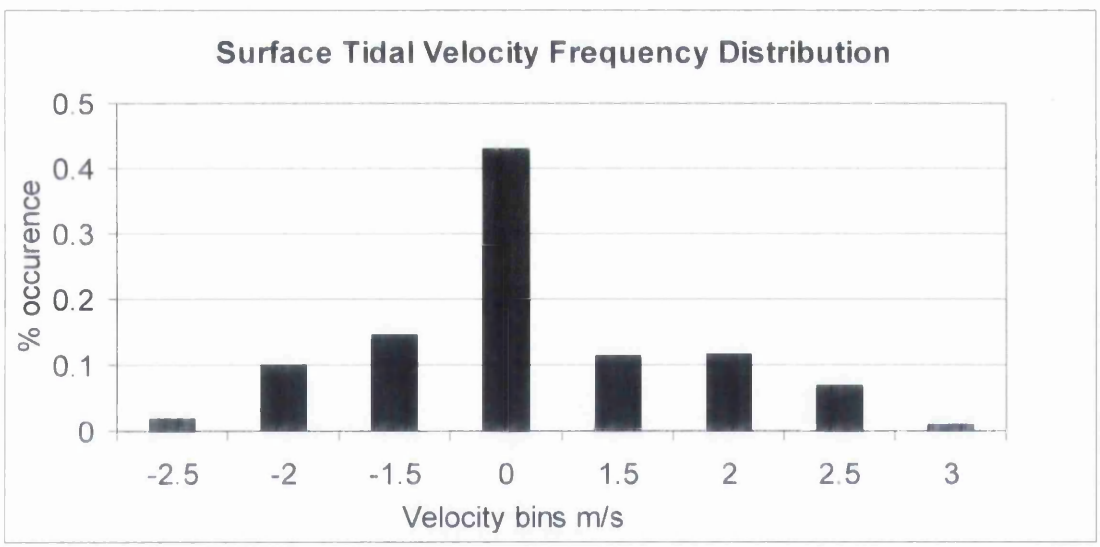

Figure 5.18 - The 8 representative velocities and occurrences

U rep	% occurrence
-2.5	0.017920329
-2	0.099760301
-1.5	0.145074763
0	0.429973747
1.5	0.113114941
2	0.114941217
2.5	0.069056044
3	0.010158658

Table 4 - The 8 representative velocities and occurrences

5.4.1.2 Wave Climate Analysis

The Barry site is located in an area of the Bristol Channel which experiences a significant wave climate. With a fetch that stretches across the Atlantic, the waves that occur in this region have great power. Information regarding these waves collected by the British Oceanographic Data Centre (BODC) has been obtained for the project on an academic license.

3 Wave Rider buoys have collected wave data in the region over a period of 2 – 3 years from April 1978 until April 1981. The exact location of the buoys is shown in Figure 5.19, where the line shows the boundary of the region under investigation. The buoys are marked A1, A2 and B. The data collected includes the parameters shown in table 5. This data is deemed extensive and enough to be an accurate representation of the wave climate in the region.

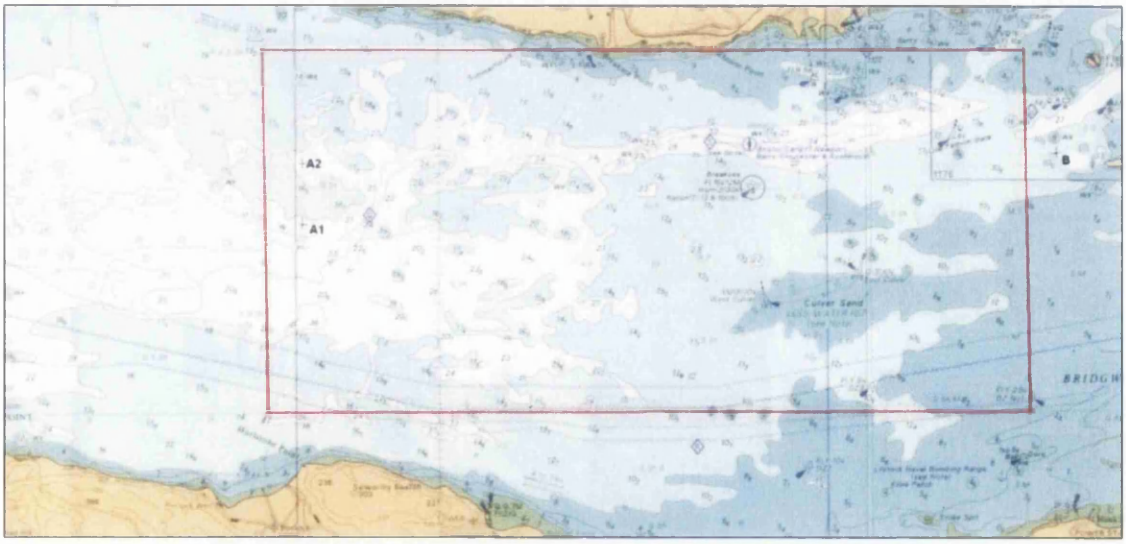

Figure 5.19 - The locations of the Waverider buoys and the Barry site.

Parameter	unit
Significant wave height	m
Zero crossing period	s
Maximum wave height	m
Average Wave Height	m
Root Mean Square Wave Displacement	m
Waves Spectral Width	
Number of zero crossing waves in record	

Table 5 - Parameters included in the Waverider data from the BODC.

A frequency distribution method is used to discretise the wave climate for use in statistical analysis of the lifetime rotor loads. The most relevant factors in calculating loadings on offshore structures are wave frequency and amplitude. These affect the magnitude and occurrence of the forces on the structure which is important for the estimation of both extreme and fatigue loads. The results of this for each of the Waverider locations are graphed in Figures 5.20 and 5.21. The significant wave height is separated into bins of 0.125m each. The period has bins of 0.25 seconds. The % occurrence of waves in each bin is displayed.

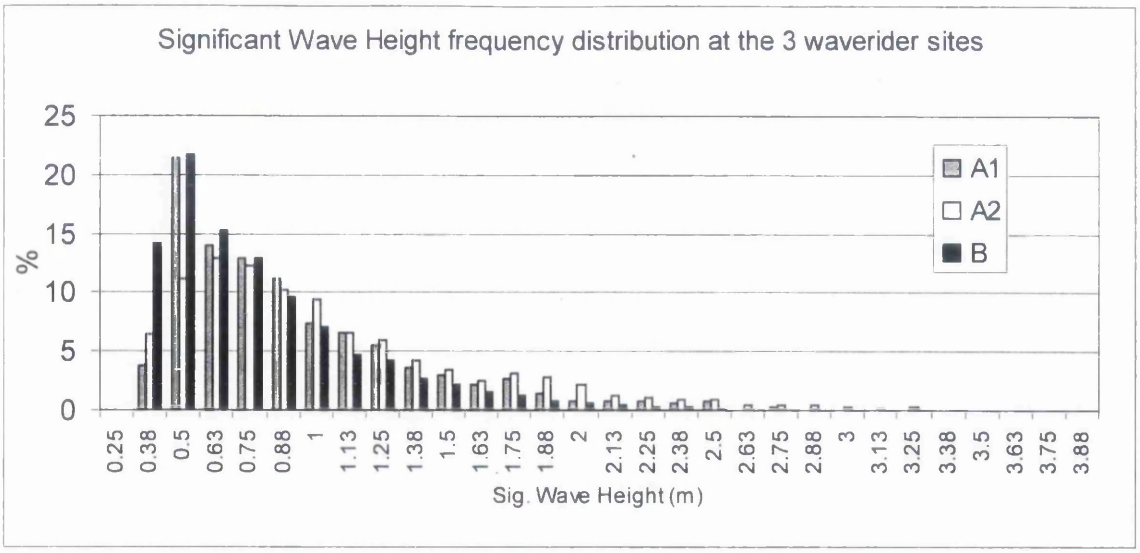

Figure 5.20 - The frequency distribution of significant wave height

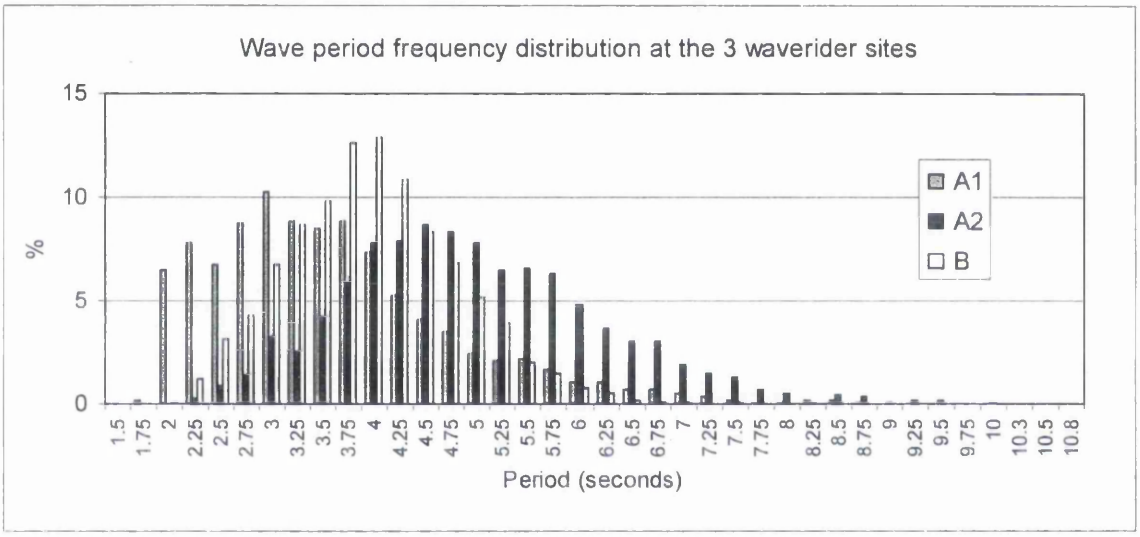

Figure 5.21 - The frequency distribution of wave period

The buoys are spread geographically across the region of interest and for this reason the data from all three is combined to obtain an average as shown in Figures 5.22 and 5.23. This is achieved by averaging the percentage occurrence of each bin across the three buoys.

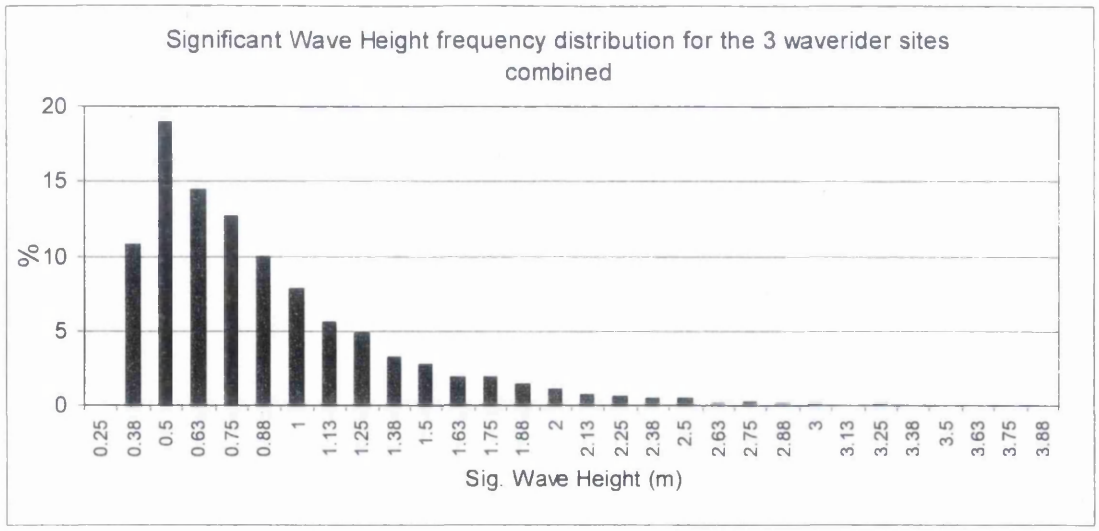

Figure 5.22 - Averaged frequency distribution of significant wave height

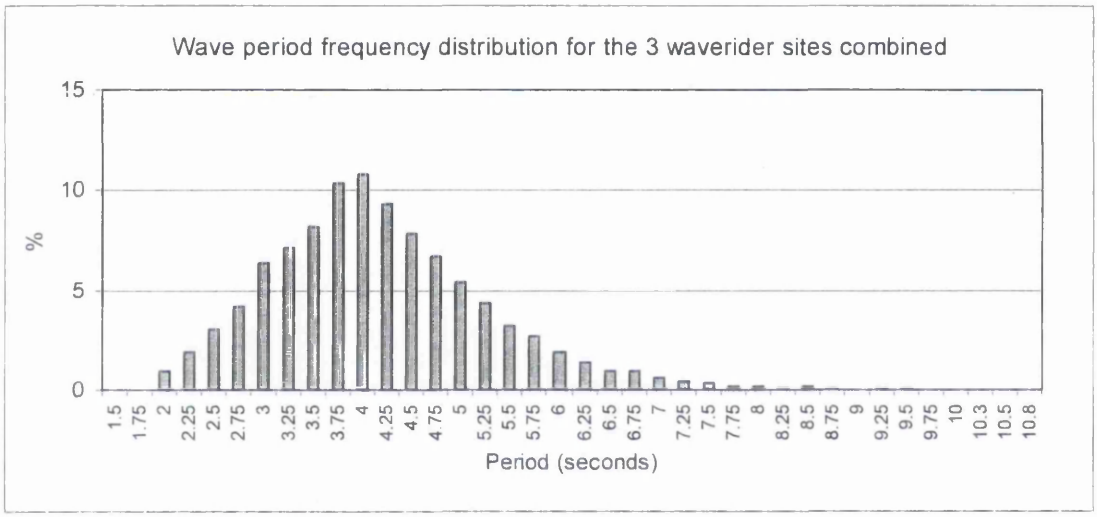

Figure 5.23 - Averaged frequency distribution of wave period

The combined data is analysed to create 10 distinct wave types. Each wave type consists of a wave period and a corresponding wave height which occurs for a certain percentage of time. This enables a fatigue analysis to be undertaken as the number of occurrences of a particular load over the lifetime of the device can be estimated. The characteristics of the wave types are given in Figure 5.24.

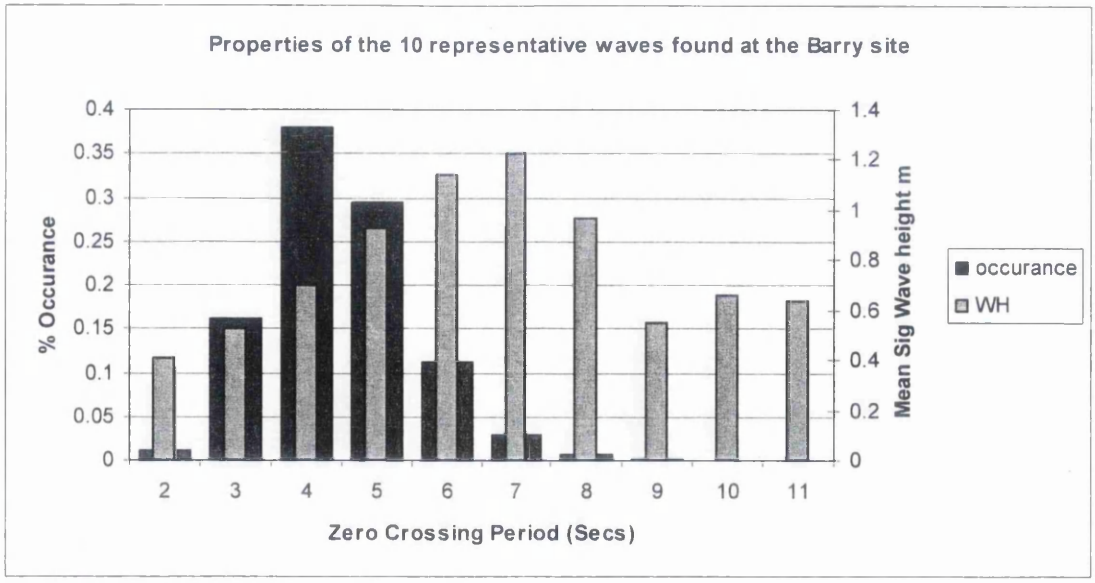

Figure 5.24 - The characteristics of the 10 representative wave states

A wave number W is given to each of the wave states from 1 to 10 such that the wave number equals the wave period minus 1. These wave states are then input to the wave kinematics software and the associated velocities and accelerations are determined.

The occurrence of the larger waves is clearly much lower than the smaller waves and this is a reflection on the storm conditions that cause them. The occurrences are used to determine lifetime loadings in section 5.54.

5.4.1.3 Wave data lookup

For a particular run of the model, a set of operating conditions is determined. One of the representative tidal velocities and one of the representative wave states is chosen. The velocity is input as a single number; however the wave state is input as a matrix as shown in section 5.23 and thus requires more detailed consideration.

The data is generated at a resolution of 125 points over the wave depth and 100 points along the wave length. Each variable U_w, V_w, $\frac{\partial U_w}{\partial t}$ and $\frac{\partial V_w}{\partial t}$ therefore has a matrix of 12500 elements along the wavelength and depth. Although the wave action is therefore relatively well described, linear interpolation is used along both axes to increase the accuracy further.

5.4.2 Timestep & inertia

The model is operated using a system of VBA macros. 'Solverzero' optimises the objective function as described in section 4.3.1.6. This method is again used here to calculate the optimal values of interference factors a and b. This uses wave and current profile adjusted velocities. The inertia forces are added to the outputs after optimisation.

A second macro 'resultsgen' is used to undertake the loop that describes the passing of time and hence rotation of the rotor and passing of the wave. The time step t_s is defined before executing the macro, as is the end time t_{max}. These variables determine the accuracy and duration of the models operation. The timestep must be small enough to allow the variation in wave and torque characteristics to be considered as linear. For example a timestep of 0.0625 seconds and a total duration of 3 minutes will allow the model operate accurately and converge on a particular operating condition in most cases.

The angular displacement of a blade is expressed as an angle γ from the vertical position . The start angle for each blade is given by:

$$\gamma_0 = \frac{2\pi}{N}(i-1)$$

The anglestep is then given by the speed of the rotor and the timestep:

$$\gamma_s = \Omega t_s$$

The wave position is calculated as a fraction of the wavelength x/X. The wavestep is therefore given by:

$$W_s = \frac{t_s}{T_w}$$

Lastly, the rotor speed is adjusted for each timestep. After the complete rotor outputs are calculated for a particular timestep, the torque output is used and compared to the generator torque load to determine the effect on the rotor speed. The inertia of the system is defined before the execution of 'resultsgen'. The angular acceleration is calculated at the end of each timestep to give a new rotor speed in the next timestep.

5.4.3 Inputs

A summary of the inputs to the model is given table 6:

INPUTS		
Rotor geometry:	**Initial conditions:**	**Operating conditions:**
R – Radius N – Number of blades TSR_D – Design tip speed ratio c – Chord variation with radius (m) ϕ – Twist variation with radius (deg) I_R – Rotor inertia (kgm^2)	x/X_0 – Initial wave position Ω_0 – Initial rotor speed (rads^{-1} γ_0 – Initial blade angle (rad) T_0 – Initial rotor torque (Nm) **Model parameters:** t_s – Timestep (s) γ_s – Anglestep (rad) W_s – Wave step	U – Upstream velocity (ms^{-1}) D – Depth of water (m) D_H – Depth of hub (m) W – Wave number $1/n$ – Velocity gradient characteristic

Table 6 – Parameters needed to initiate the dynamic model

5.4.4 Outputs

The output of 'resultsgen' is a series of the rotor loads T_R, P_R, F_{AR}, Y_R, Te_R, and H_R. Each timestep has a set of values that are recorded in an Excel sheet. A separate sheet is used to record values of a particular representative sea-state. There are 10 representative wave steps used and 8 representative sea states. This gives a total of 80 sea-states and hence sets of results. These can later be analysed for maximum and minimum values or dynamic loadings as described in section 5.5.4.1. 'resultsgen' is used to run the process and can be used to generate results for a series of sea states.

5.4.5 Process flow chart

Figure 5.25 - 'Resultsgen' VBA macro process to investigate rotor operation in different representative sea-states

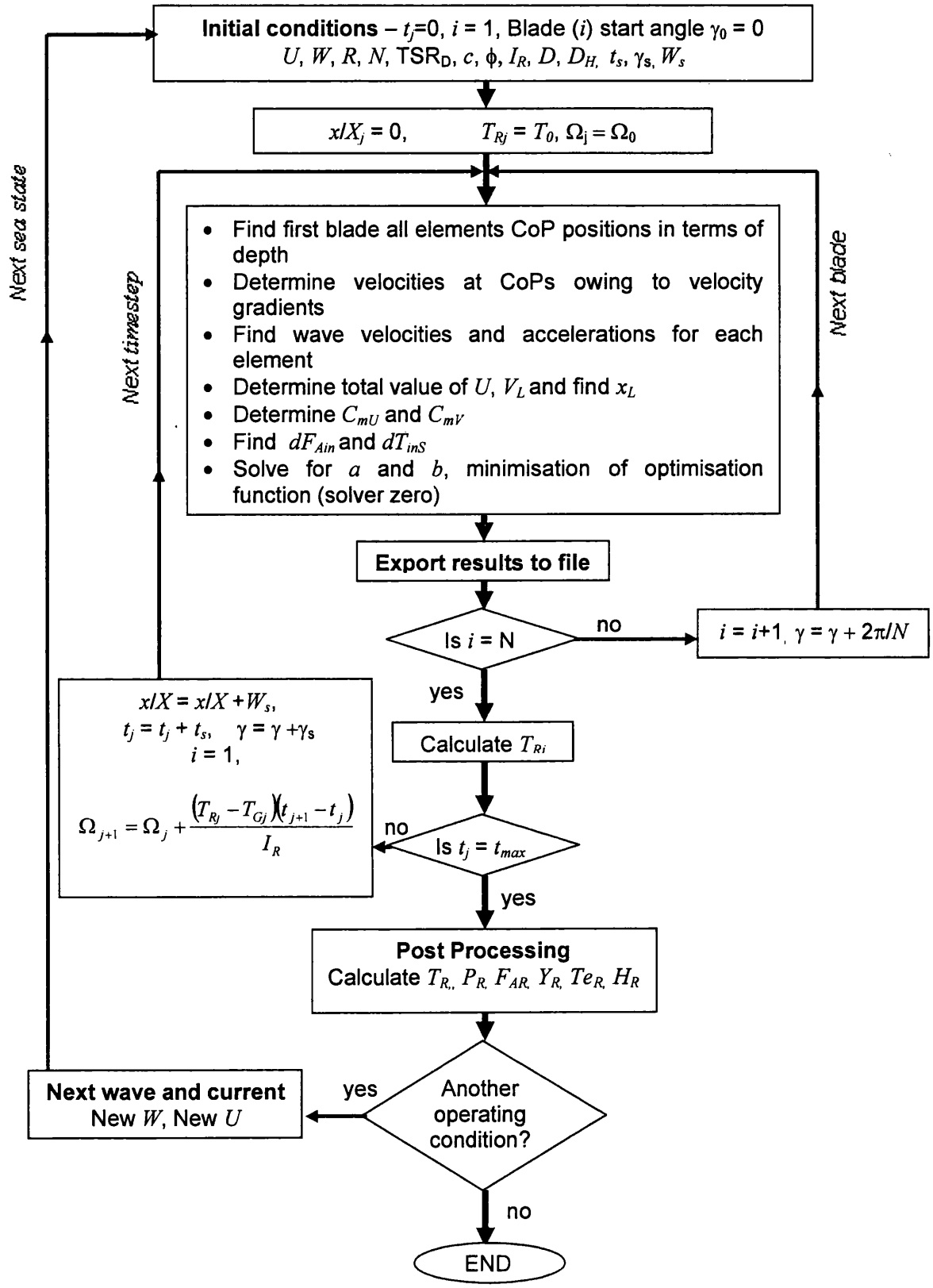

5.5 Results

An investigation is undertaken in three parts. Firstly to ascertain the validity of the dynamic model under uniform flow conditions. The second part is the application of the model to a flow with a velocity gradient and to observe the effect on the performance coefficients and any cyclical loadings which occur. Finally, wave kinematics for a particular regular wave are added to the velocity gradient resulting in a time varying flow field. Loads are calculated over time and a Fourier analysis is undertaken to ascertain the magnitude and frequency of oscillatory forces.

5.5.1 Uniform flow

Figure 5.26 shows the results of running the model under uniform flow conditions. Starting values are chosen for Ω_0 and T_0 to approximate the expected results. The model then moves from these to converge on values at the particular settled operating condition. The converged values of C_T, C_P and C_F are calculated as time averages to give the points at different TSRs in Figure 5.26. The operating TSR is controlled by varying the torque/speed characteristics of the generator.

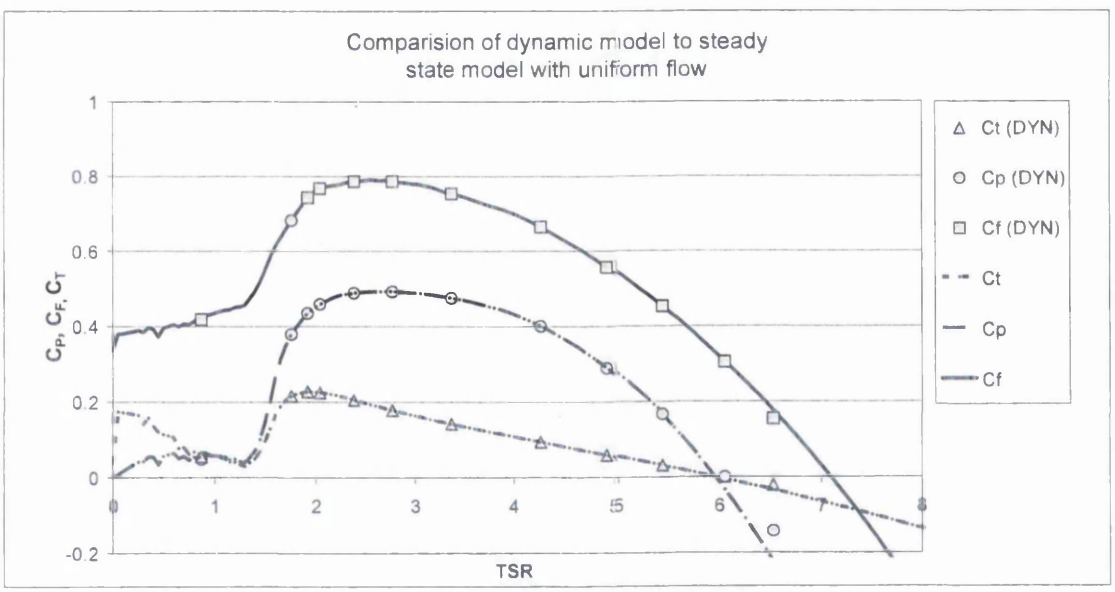

Figure 5.26 - Validation of model operation under uniform flow conditions

It is clear that the results from the dynamic model correlate very well with the BEMT developed in section 4.3. The performance characteristics match previous data at all

points in the operating range (TSR 1.5-6) The model becomes less stable in the stalled region and tends to indicate stopping of the rotor. Results in this region tend towards a very low TSR as indicated by the first point on the graph at TSR 0.87. When the dynamic model is used at much higher TSR, in particular, the region beyond propeller brake state, it does not match the previous data. In this condition the generator torque must be input as a negative value. This is not in the normal range of operation so has less significance, however this does represent an anomaly in the model.

5.5.2 Velocity gradient

A 1/10th power law velocity is applied to the oncoming flow. The axis of rotation (hub depth) is at d/D = 0.452, and the rotor swept area is in the depth region d/D 0.272-0.632. For completeness it is worth noting that the surface velocity used is 3m/s.

The results of the dynamic model are compared to the standard BEMT in Figure 5.27.

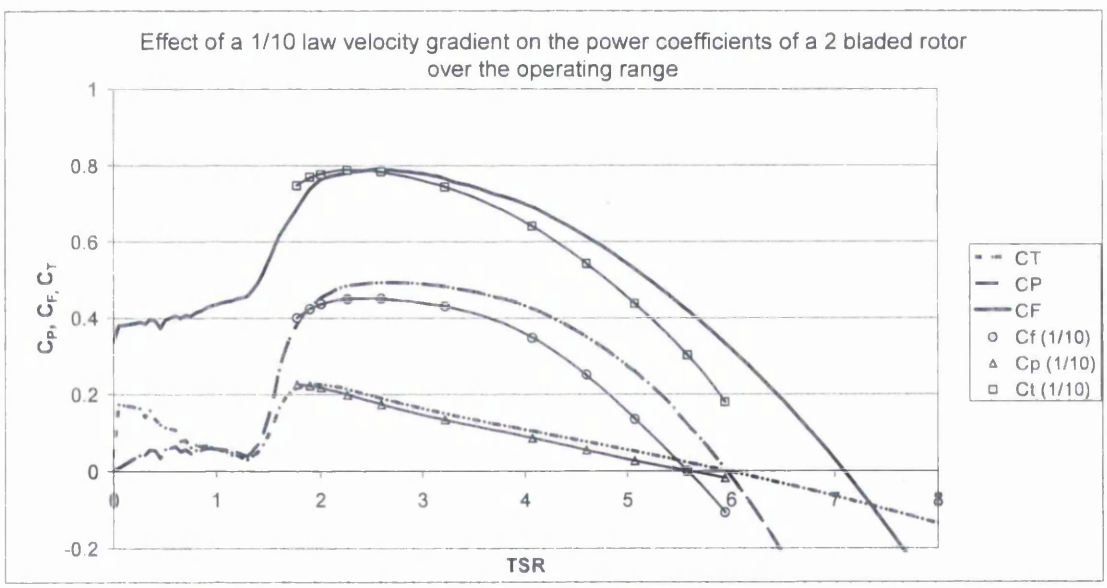

Figure 5.27 - The effect of a velocity gradient on the power coefficients

It is clear that the general trends are similar in that the curves are the same shape. However, it is also apparent that the performance coefficients are generally lower for a particular TSR. The effect of the velocity gradient is to lower the average velocity seen by the rotor but the TSR and power coefficients are still calculated using the surface velocity. This has the effect that the apparent operating TSR is reduced as the turbine spins more slowly for a given flow speed. The performance characteristic curves are

therefore brought forward in terms of TSR. The C_T and C_F curves appear to peak at the same values as the original model. However, peak C_P is significantly reduced from around 0.49 to 0.46. This represents the power loss a rotor would experience under a 1/10th power law when it occupies the depth region d/D 0.272-0.632. This equates to a 6% reduction in power output at the optimum operating condition. At higher TSRs the effect is more pronounced and propeller brake state is brought forward to TSR 5.5.

5.5.3 Wave action

In order to present a concise and complete set of results which illustrate the effect of wave action, one example wave type is selected. This wave is applied to a 1/10th power law velocity gradient in three cases with surface velocities U_{sf} of 3m/s, 2.25m/s and 1.5m/s respectively. The wave selected for investigation is the type 7 wave as described in section 4.5.1.2. The essential characteristics are a wave of period T_w = 8 seconds and a wave height H_w =0.97m in a depth of 25m. The effects of the wave are observed in terms of variation in performance characteristics. These are calculated with reference to the constant surface velocity.

A Fourier analysis is undertaken for each of the results to clarify the frequency and magnitude of the oscillatory forces. Results for 2 and 3 bladed rotors are presented to illustrate the dynamic loading characteristics of different blade numbers. The results are presented in groups according to performance coefficient.

5.5.3.1 Torque coefficient

Figure 5.28 shows the variation in torque coefficient of a 2 bladed rotor. Figure 5.28a describes the effect in the time domain and Figure 5.28b illustrates the results of the Fourier analysis in the frequency domain. A normalised quantity is defined for comparison in the frequency domain. This is the ratio of frequency of the Fourier transform to the frequency of rotor rotation f/Ω.

It is clear that the major oscillation is at the wave frequency with a period of 8 seconds. There are also slight irregularities in the sine form, with a slight variation in gradient and maximum and minimum over each oscillation. It appears that this is illustrated in Figure 5.28b as the very small peaks in the region above f/Ω =1.1.

The other clear pattern is the variation in magnitude of oscillation with surface velocity. The lower the tidal flow, the greater the effect the wave has on the variation in C_T. For a flow velocity of 3m/s the variation from the mean is around 25%, whereas at U = 1.5m/s the variation is nearly 45%.

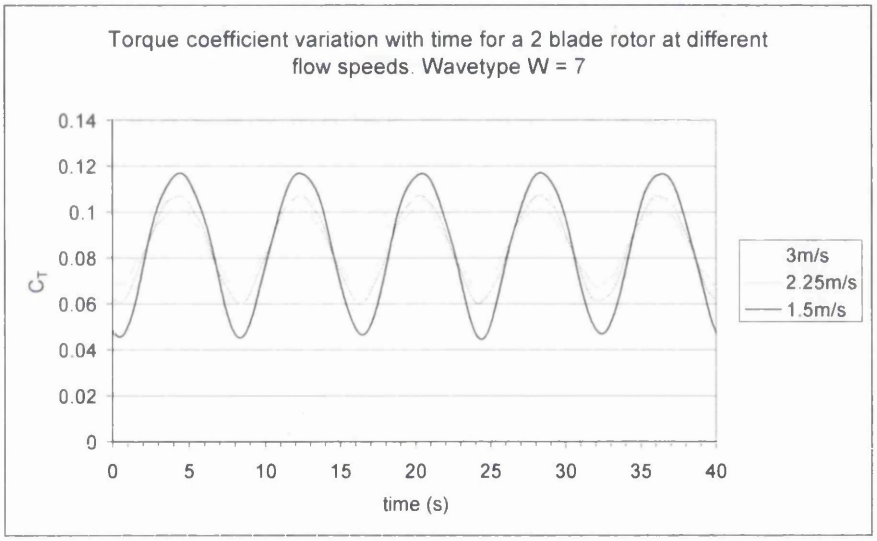

Figure 5.28a - C_t variation for a 2 blade rotor

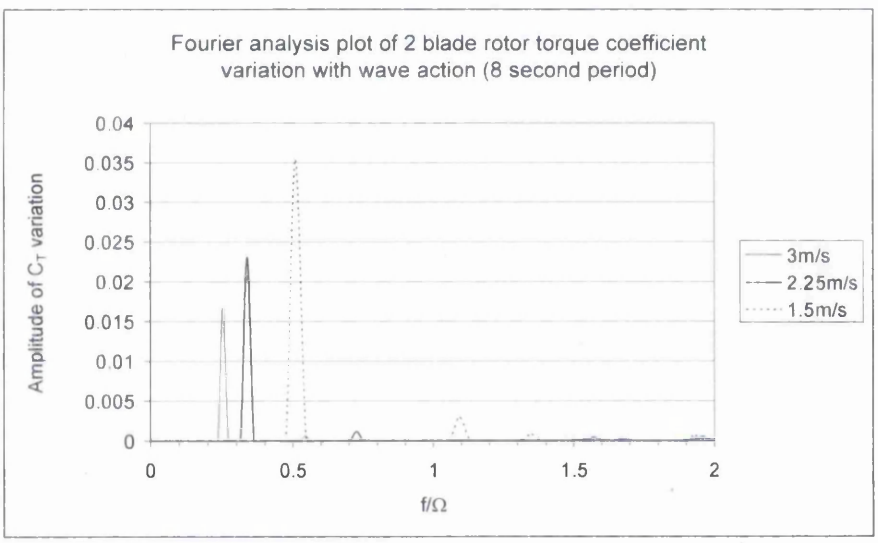

Figure 5.28b - Fourier analysis of C_t variation for a 2 blade rotor

Figure 5.29 shows the variation in torque coefficient of a 3 bladed rotor. Again, Figure 5.29a describes the effect in the time domain and Figure 5.29b illustrates the results of the Fourier analysis in the frequency domain. The results are clearly very similar to the 2 bladed configuration with the same primary frequency of oscillation with a very slightly reduced magnitude. The other visible difference is the reduced secondary oscillations as the sine form is now apparently undisturbed and the maximum and minimum values of each cycle are more regular. It is clear in Figure 5.29b that there are fewer peaks in the region above $f/\Omega = 1.1$.

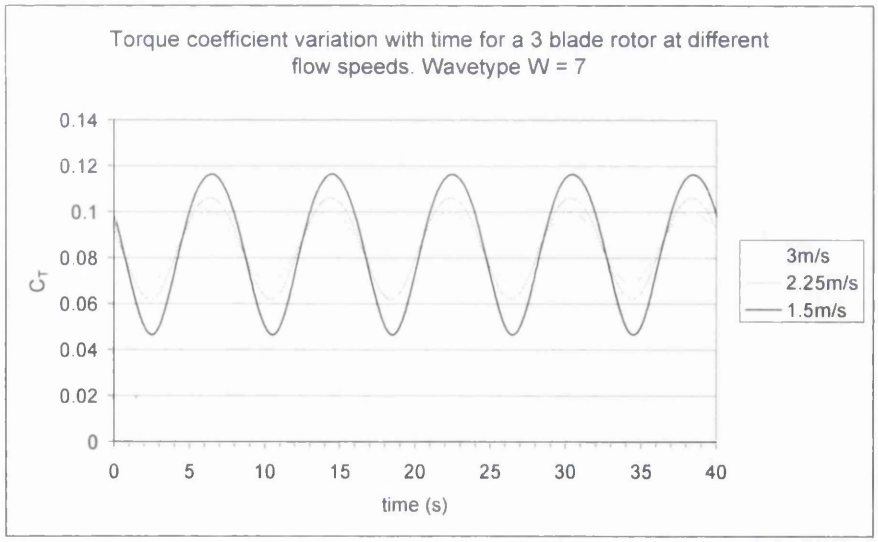

Figure 5.29a - C_T variation for a 3 blade rotor

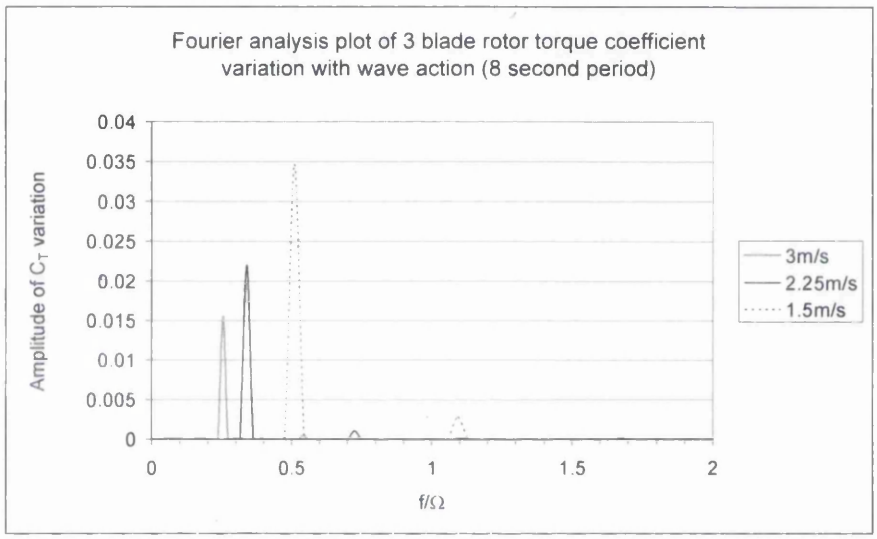

Figure 5.29b - Fourier analysis of C_T variation for a 3 blade rotor

5.5.3.2 Axial force coefficient

Figure 5.30 shows the variation of C_F with wave action. It is immediately apparent that the primary oscillation is again at the same frequency as the wave period. However there is more of a variation in the upward and downward gradients. The upward gradient is less steep than the downward. This represents the difference in velocity fluctuation on the wave surge and ebb. This has the effect that in Figure 5.30b, the primary oscillation appears to have a slightly higher value of f/Ω than the torque graphs.

The proportionally greater changes with the lower flow speeds found in the torque results are similarly found here. At 3m/s, the variation in C_F is around 3% whereas this increases to about 6% for a flow of 1.5m/s. This is noticeably less percentage variation

than in the torque results. There is also a small variation in the gradients and maximums and minimums form one cycle to another. This appears to be more so in the lower flow speeds where irregularities are highly visible. This is also mirrored in Figure 5.30b where there is a peak of magnitude 0.02 which is independent of flow speed. This occurs at $f/\Omega = 2$ which for a 2 bladed rotor is the blade pass frequency. Around this frequency it appears that there are harmonics at either side at plus and minus the frequency of primary oscillation.

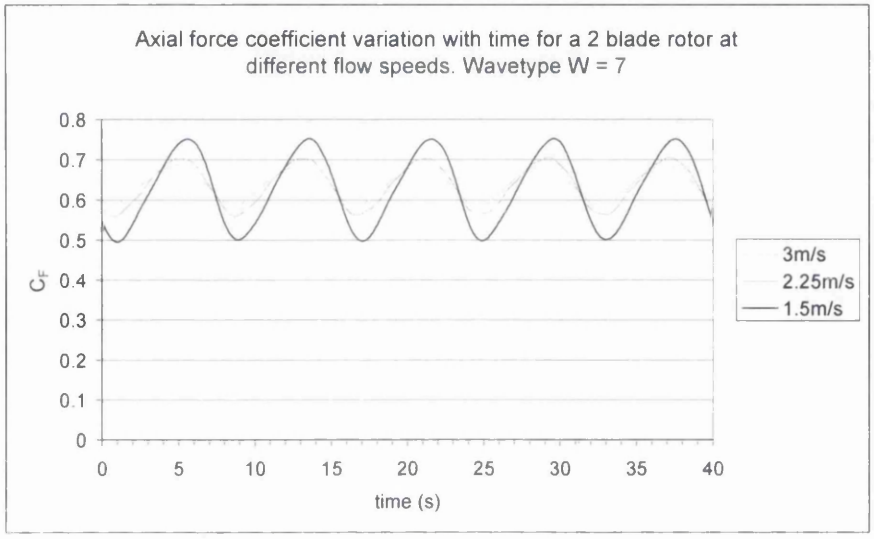

Figure 5.30a - C_F variation for a 2 blade rotor

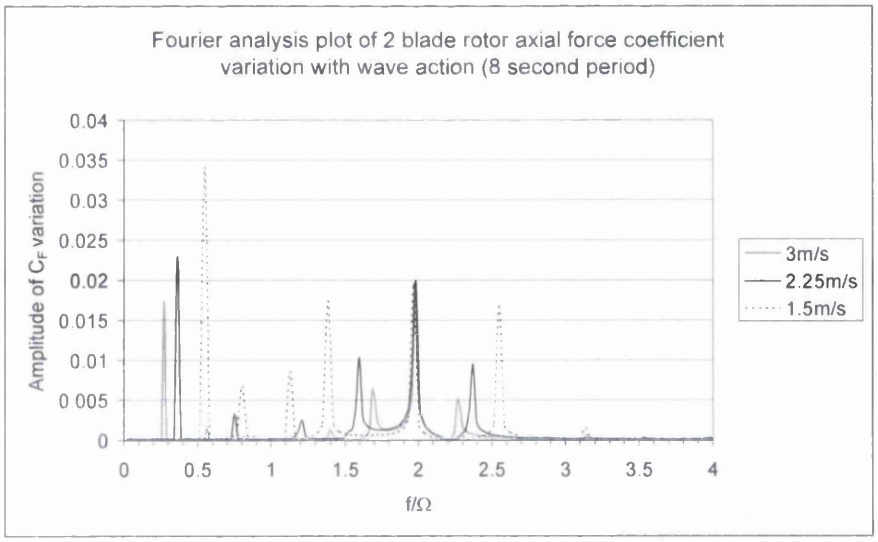

Figure 5.30b - Fourier analysis of C_F variation for a 2 blade rotor

Figure 5.31 shows the variation of C_F for a 3 bladed configuration. The primary oscillations are very similar to those for a 2 bladed rotor. This is shown in a comparison of Figures 5.30b and 5.31b where the magnitude and frequency of the first peak for each flow speed are almost identical. In Figure 5.31a, the magnitude of the secondary oscillations are significantly reduced resulting in a smoother and more regular cycle. This is reflected in Figure 5.31b where the secondary oscillations are reduced to about 0.12 of the equivalent 2 bladed high frequency modes. Of interest is the equivalent blade pass frequency at f/Ω = 3 of which the magnitude is dramatically reduced.

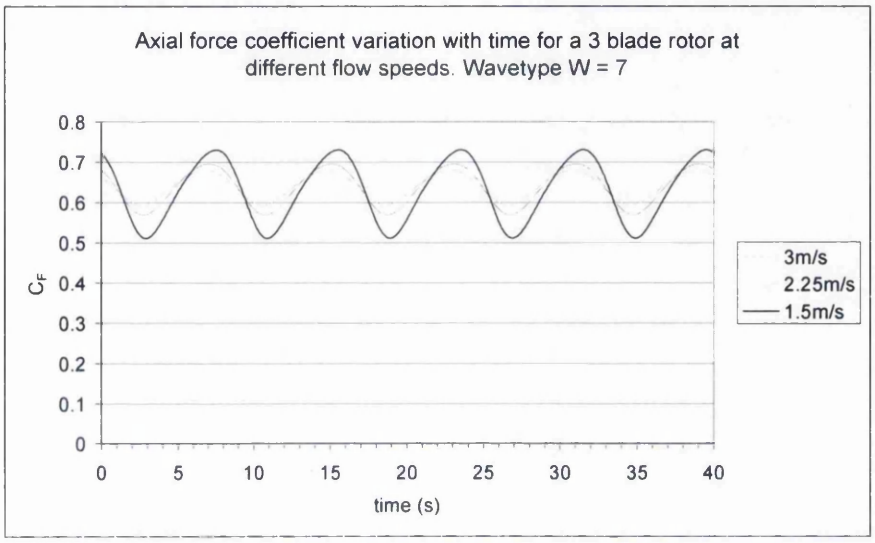

Figure 5.31a - C_F variation for a 3 blade rotor

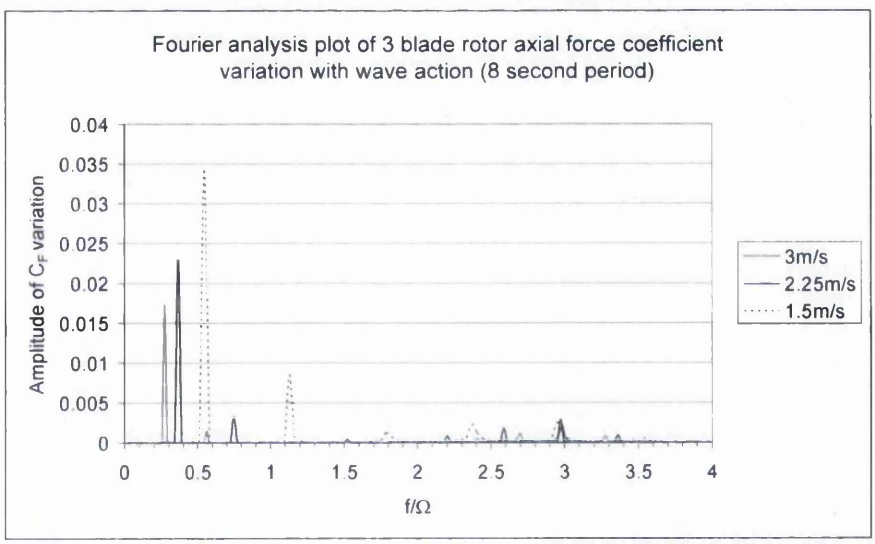

Figure 5.31b - Fourier analysis of C_F variation for a 3 blade rotor

5.5.3.3 Yaw coefficient

The yaw coefficient variation is shown in Figure 5.32. Firstly, the magnitude of the yaw torque is much lower than the rotor mean torque. The peak values are around 5% of the mean rotor torque. In Figure 5.32a it is clear that the simple oscillation observed in *both*

C_T and C_F are heavily obscured by the high frequency blade pass frequencies. As the rotor operates at nearly constant TSR, the blade pass frequency varies directly with flow speed. This effect can be observed by comparing the results of the different flow speeds.

In Figure 5.32b the primary wave period oscillations are visible and are still the most significant in terms of magnitude. However the blade pass frequency at f/Ω = 2 is of nearly the same magnitude in the case of U = 2.25m/s and becomes dominant when U = 3m/s. As yaw force is driven by axial force it is unsurprising to find similar harmonics around the blade pass frequency.

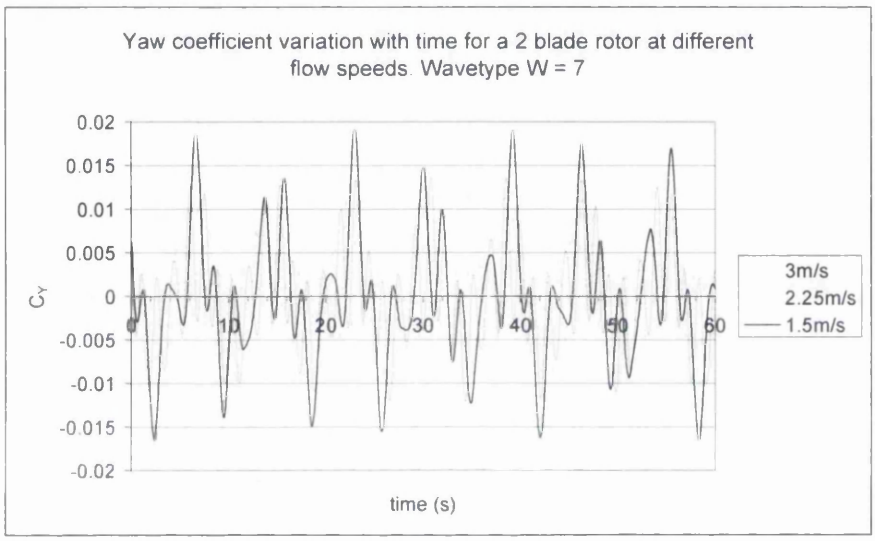

Figure 5.32a - C_Y variation for a 2 blade rotor

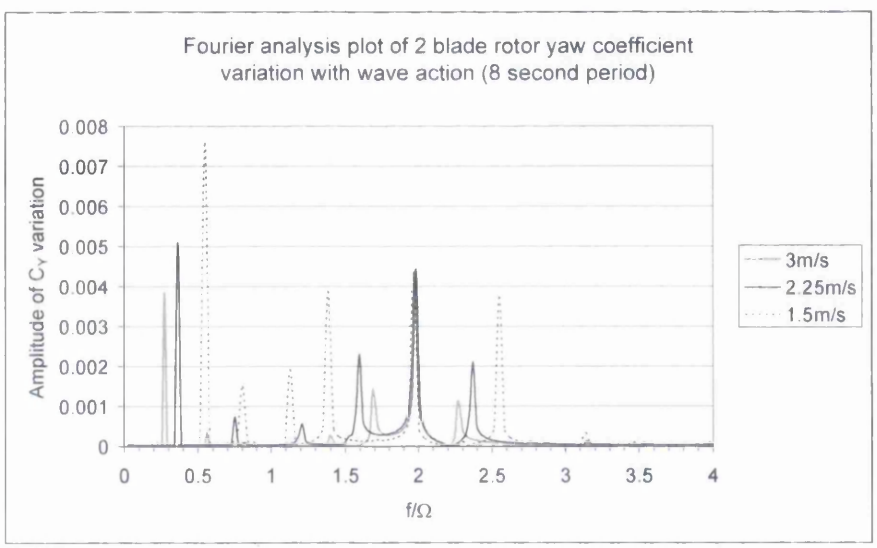

Figure 5.32b - Fourier analysis of C_Y variation for a 2 blade rotor

Another point of note is that yaw force does not have a zero mean. This is illustrated in Figure 5.33a which shows the variation in yaw force in comparison with the blade angular displacement. The peak values occur as one of the two blades reaches is approaching the azimuth. For a 2 bladed rotor, one blade is travelling downward and one is travelling upwards at the same time. In conjunction with a vertical wave velocity component, this results in significantly different effective speed ratios on each blade. It effectively moves the blade into overspeed and under-speed, varying the axial force coefficient and hence the magnitude of forces generated over each cycle. It is clear from Figure 5.33a that when the top rotor blade is moving away from the azimuth and hence downward, the yaw force is greater than when the rotor is approaching the azimuth.

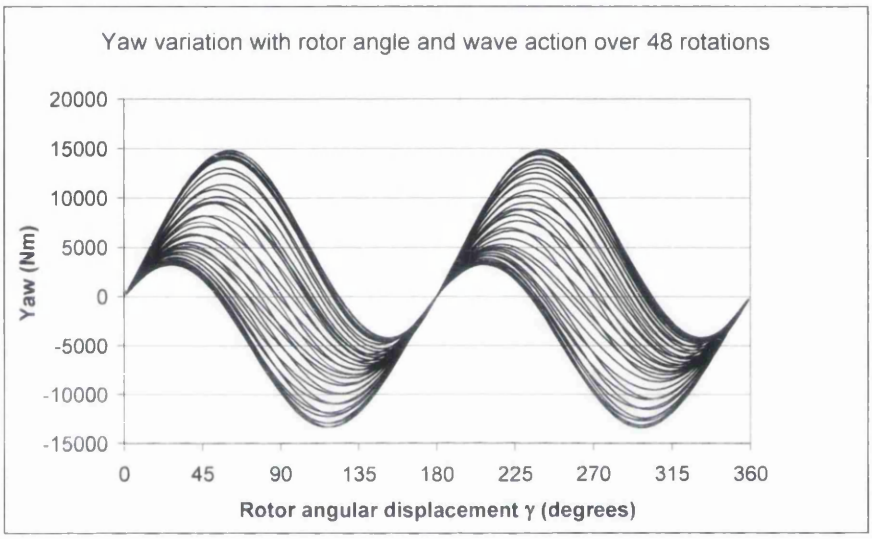

Figure 5.33a - Yaw force of a 2 blade rotor with rotor angular displacement

In Figure 5.33b, yaw loads are plotted against wave position x/X. Also plotted is the vertical velocity V_w. A positive yaw is associated with a positive V_w and vice versa. For this reason, it can be ascertained that although the yaw load varies with each revolution owing to the depth varying velocities, the affect of the vertical velocity on local speed ratio also has a significant effect on the magnitude of yaw experienced. The non – zero mean is a combination of this and the interaction with the relationship between C_f and local TSR.

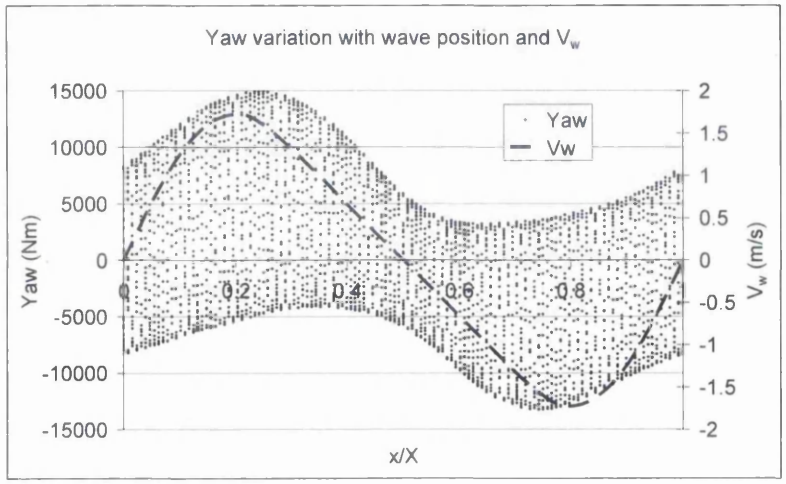

The 3 bladed configuration shown in Figure 5.34a has a similar non-zero mean. The magnitude of oscillation is approximately the same as the 2 bladed rotor and it appears that the wave frequency is dominant to a greater degree. Interestingly the blade pass frequency appears more clearly at higher flow speeds, but as is shown in Figure 5.34b, this oscillation is significantly lower than its 2 bladed counterpart.

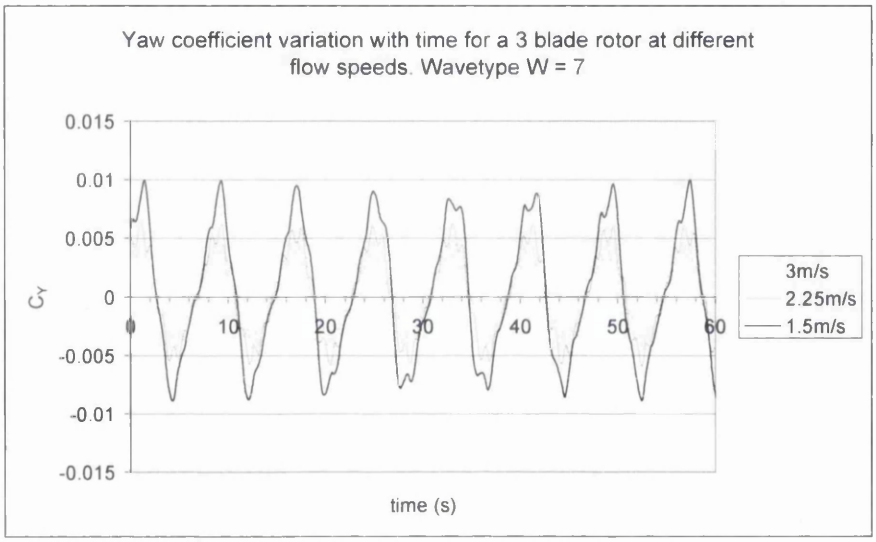

Figure 5.34a - C_Y variation for a 3 blade rotor

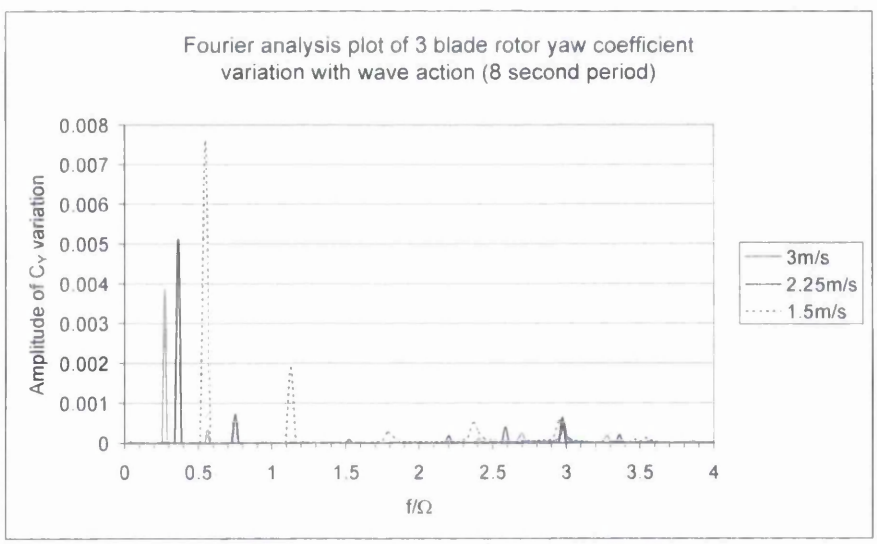

Figure 5.34b - Fourier analysis of C_Y variation for a 3 blade rotor

5.5.3.4 Teeter coefficient

The primary driver of teeter loads is the blade pass frequency. It can be seen in Figure 5.35 that a two bladed rotor experiences almost all of the oscillation at $f/\Omega = 2$. Also the variation is much less dependent on the flow speed and a variation of 0.0045 in the

teeter coefficient is found in all three cases. The harmonics at a wave frequency away from the blade pass frequency remain significantly affected by flow speed. The magnitude of these forces is around 4% of the torque values for the rotor.

The general form of Figure 5.35a appears to be very varied and unlike the previous coefficients examined there appears to be no easily discernable regularity. However a peak occurs every 8 seconds which identifies the wave period. In this case the mean is very clearly non zero and the Teeter moment is almost always positive. This is because the wave action is most pronounced near the surface and hence the effect is most noticeable when the blade is in the top half of a rotation.

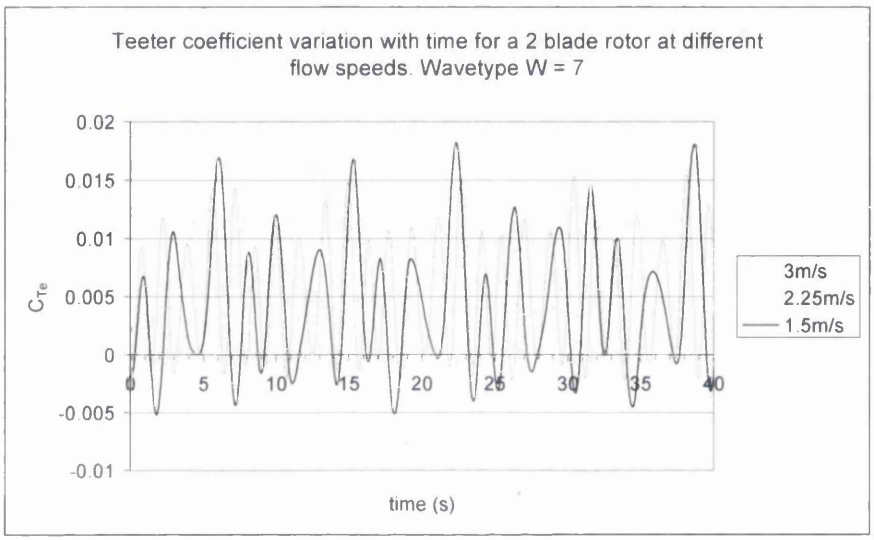

Figure 5.35a - C_{Te} variation for a 2 blade rotor

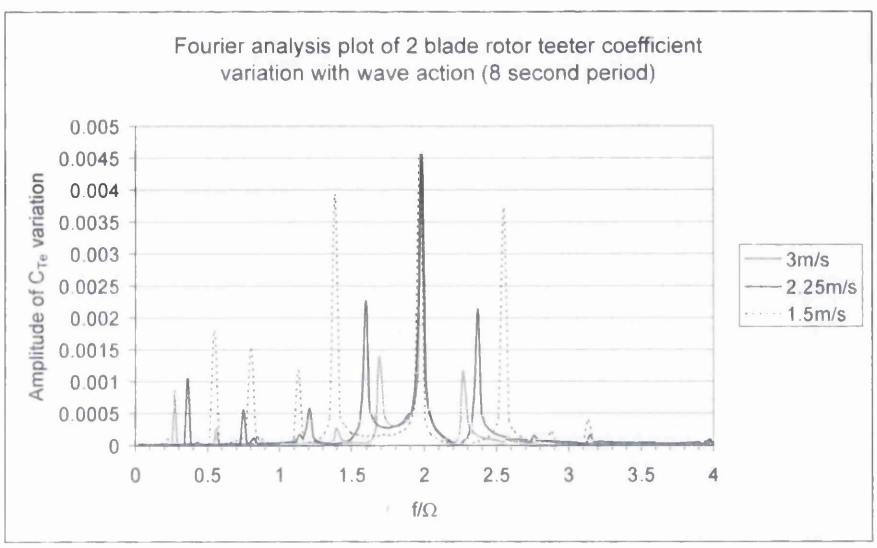

Figure 5.35b - Fourier analysis of C_{Te} variation for a 2 blade rotor

The teeter loads experienced by the 3 bladed rotor are approximately a third of those on the 2 bladed configuration as can be seen in Figure 5.36. This is approximately 1.5% of the magnitude of the average torque. The teeter coefficient for a 3 bladed rotor always appears to be positive. The wave period provides the dominant frequency and the blade pass frequency is secondary. The upstream flow speed does not effect the magnitude of the blade pass oscillations, but does effect the magnitude of the forces driven by the wave period. There is a strong harmonic at double the wave frequency at nearly the same magnitude as the primary oscillation.

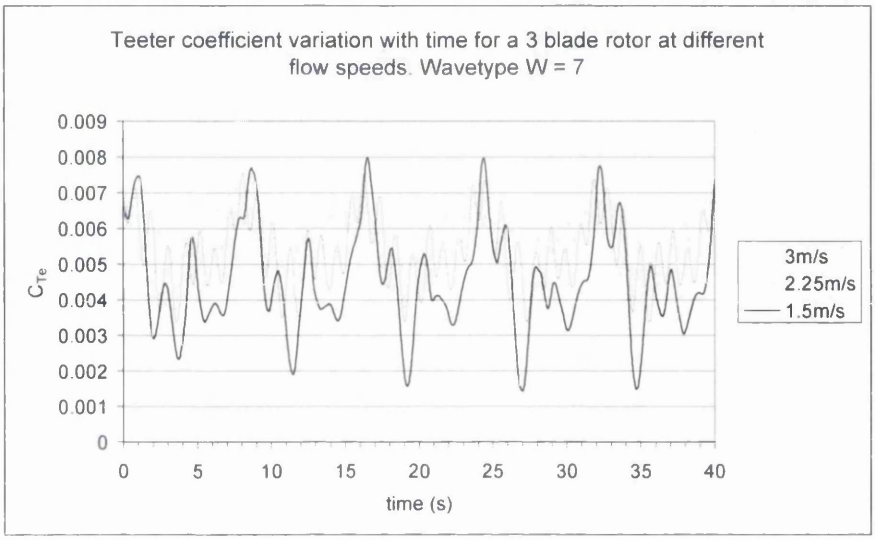

Figure 5.36a - Fourier analysis of C_{Te} variation for a 3 blade rotor

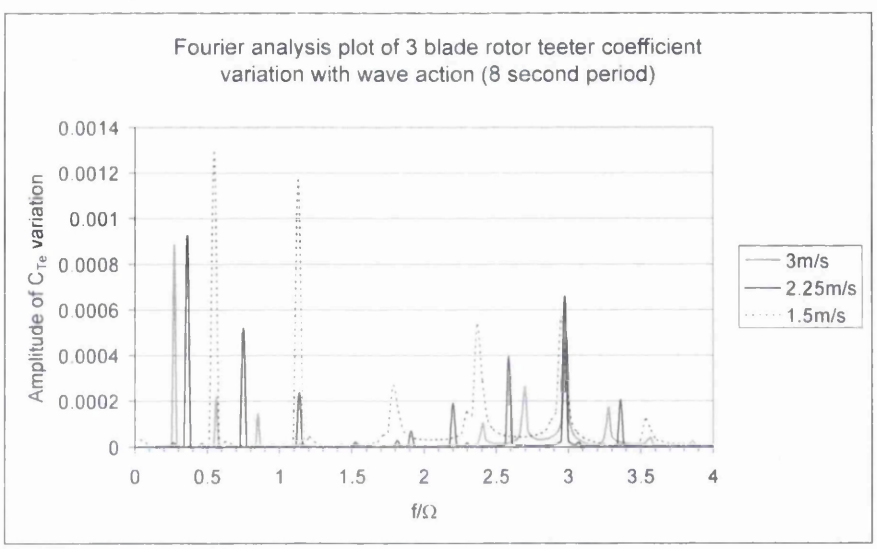

Figure 5.36b - Fourier analysis of C_{Te} variation for a 3 blade rotor

5.5.3.5 Heave coefficient

The heave coefficient for a 2 bladed rotor is shown in Figure 5.37. It appears that this depends on the interaction between the wave period and the period of rotation. The oscillations are based primarily on the blade pass frequency but are affected greatly by the wave frequency. This results in a load pattern that does not clearly match either. There are clear peaks in Figure 5.37b at the blade pass frequency plus and minus the wave frequency relative to each flow speed.

The magnitude of oscillation ranges from about 1% of the axial force for 1.5m/s flow speed down to 0.3% of the axial force at U = 3m/s.

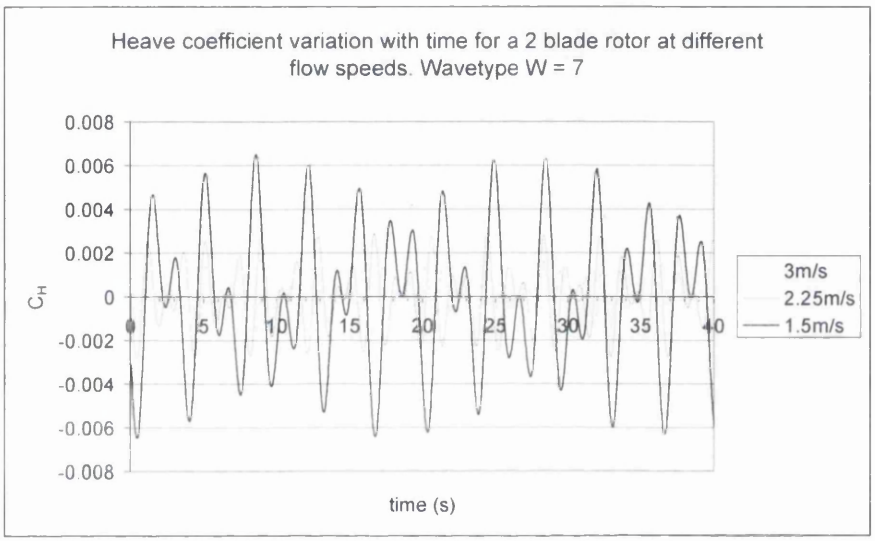

Figure 5.37a - C_H variation for a 2 blade rotor

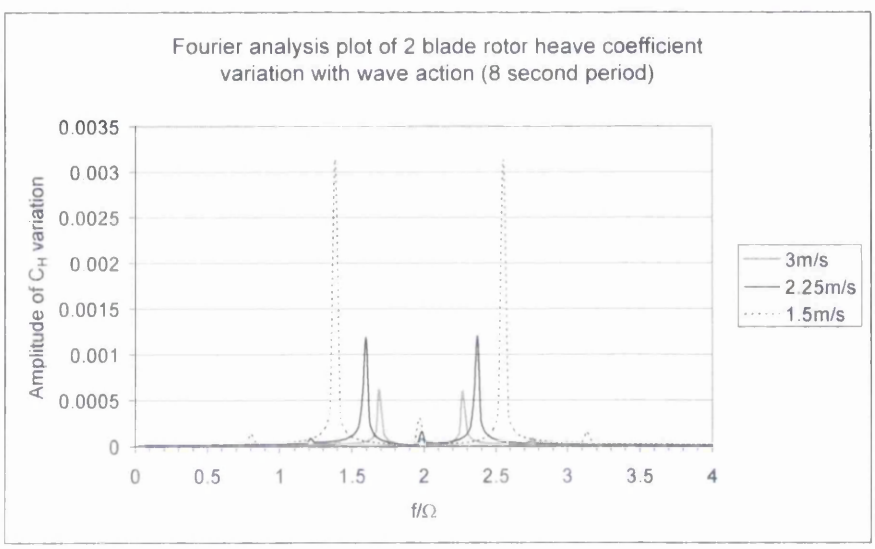

Figure 5.37b - Fourier analysis of C_H variation for a 2 blade rotor

The heave experienced by a 3 bladed rotor is very much smaller than the 2 bladed device. For a flow speed of U = 1.5m/s the variation is 0.025% of the axial force and for a flow of 3m/s this decreases to 0.01%.

The frequency of heave variation is similarly related to both wave and rotor frequency and this is reflected in Figure 5.38b. The primary force frequencies are the blade pass frequency plus or minus the wave frequency.

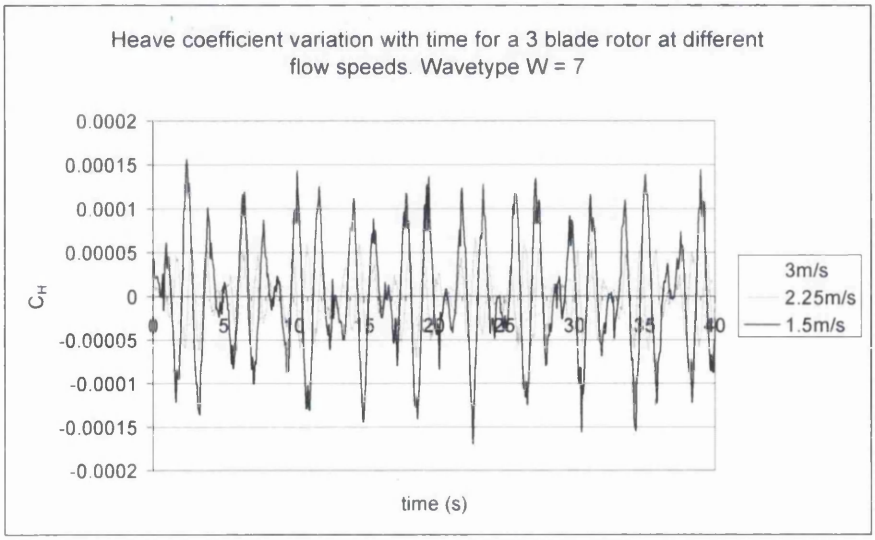

Figure 5.38a - C_H variation for a 3 blade rotor

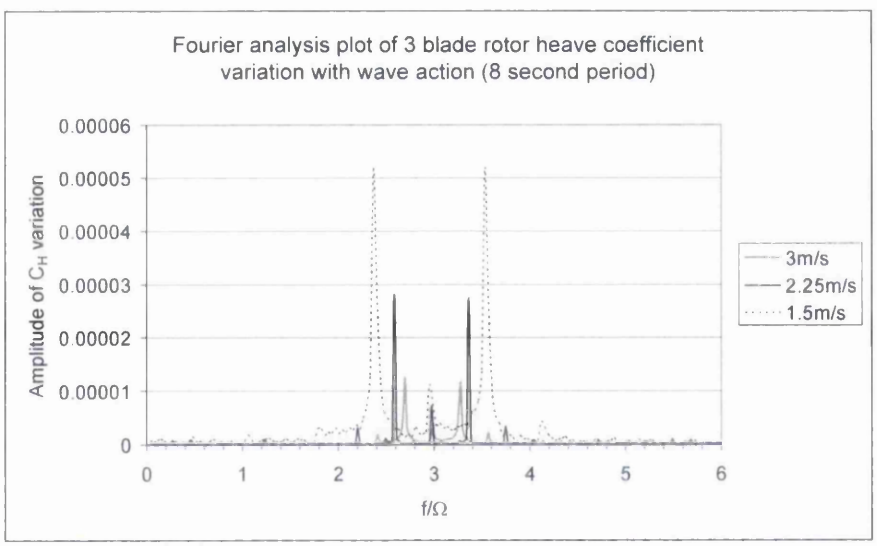

Figure 5.38b - Fourier analysis of C_H variation for a 3 blade rotor

5.5.4 Life time loadings

Of great importance in the design of offshore systems is the estimation of the loads that a particular component will encounter in its lifetime. Forces found by the method presented here can be mapped onto different components, for example the hub or the support structure. If the environmental conditions are known, this enables cyclic and fatigue loadings to be considered for a typical lifetime of a device.

The model is run over a series of operating conditions encompassing the representative wave and current conditions presented in section 5.4.1. The occurrences of these particular seastates is statistically known with respect to time, so the amount of time that each will occur over the lifetime of the device can be estimated. Each wave type is combined with each current speed to give a total of 80 representative seastates. Each sea state has an associated percentage occurrence with respect to time.

The occurrences of the various environmental conditions are described in table 7.

Occurences of the different environmental conditions			
Lifetime	20 years		
Current Speed m/s	% time	Wave type	% time
		1	0.01
-2.5	0.02	2	0.16
-2	0.06	3	0.38
-1.5	0.12	4	0.29
0	0.56	5	0.11
1.5	0.10	6	0.03
2	0.09	7	0.01
2.5	0.04	8	0.002
3	0.01	9	0.0009
		10	0.0002
Total	1	Total	1

Table 7 – The percentage occurrence of the representative wave and current states

5.5.4.1 Maximum and minimum values

After the operating conditions and occurrences have been defined it is possible to calculate the maximum and minimum values for each force generated over the lifetime of the device. It is important to ensure that all wave and current loadings are included if

this is to be used to define the design limits. In the case of a tidal turbine it is likely that this will take the form of a wave with a 50 year return period.

The maximum and minimum values from the environmental conditions defined in this study are presented in table 8. The values for axial force represent the turbine being able to yaw into the flow direction and hence the minimum values are equal to zero.

2 blades	MAX	MIN	
TORQUE	210	0	kNm
AXIAL	248	0	kN
YAW	24	-25	kNm
TEETER	16	-11	kNm
HEAVE	0.33	-0.33	kN

3 blades	MAX	MIN	
TORQUE	210	0	kNm
AXIAL	245	0	kN
YAW	14	-13	kNm
TEETER	3	-4	kNm
HEAVE	0.01	-0.01	kN

Table 8 – Max and min lifetime loadings

5.5.4.2 Fatigue loads

Using Fourier analysis as in section 5.5.3, the oscillatory loads are calculated for each representative operating condition. A mean value is also needed to be able to undertake fatigue calculations with Goodman lines used to translate the loads to an equivalent with zero mean.

The results of the analysis are too voluminous to be presented here in full. The number of occurrences for each magnitude of oscillation is shown in Figures 5.39 to 5.43. The mean values around which the loads are oscillating has been ignored.

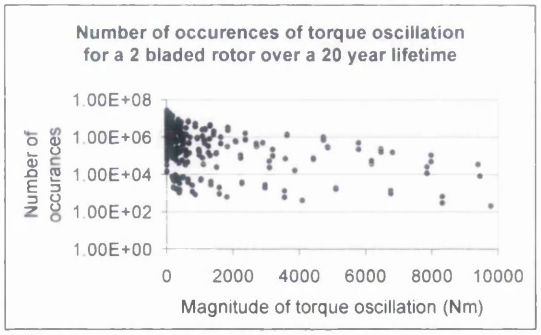

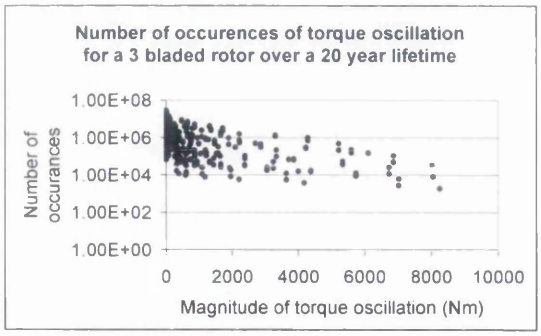

Figures 5.39a and 5.39b lifetime wave induced torque oscillations for 2 and 3 bladed rotors

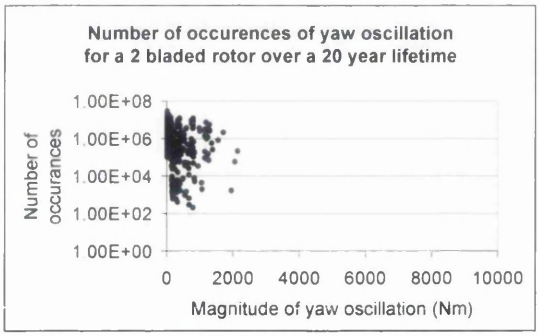

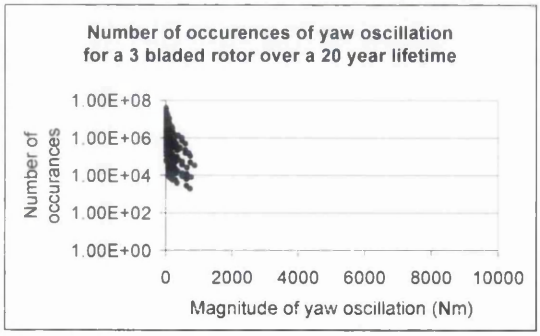

Figures 5.40a and 5.40b lifetime wave induced yaw oscillations for 2 and 3 bladed rotors

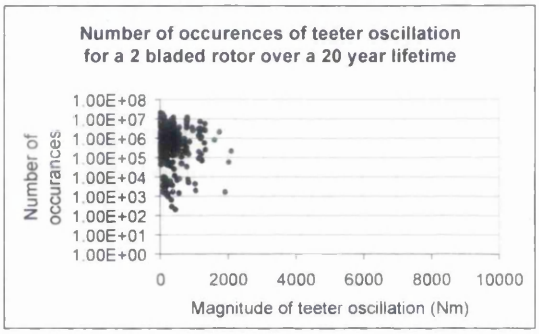

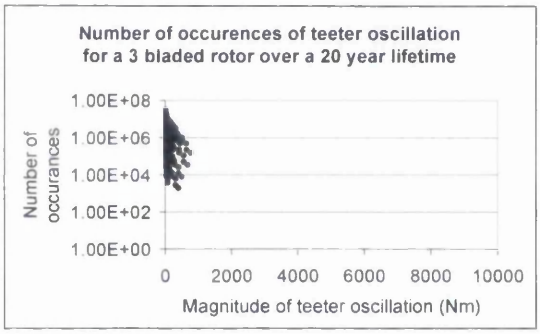

Figures 5.41a and 5.41b lifetime wave induced teeter oscillations for 2 and 3 bladed rotors

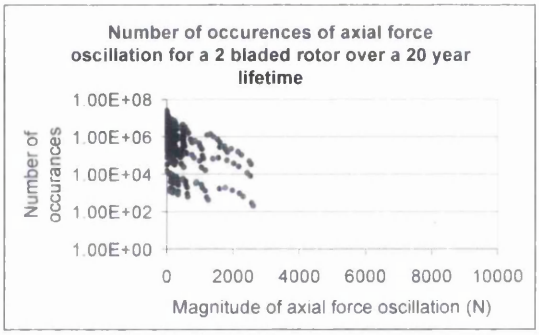

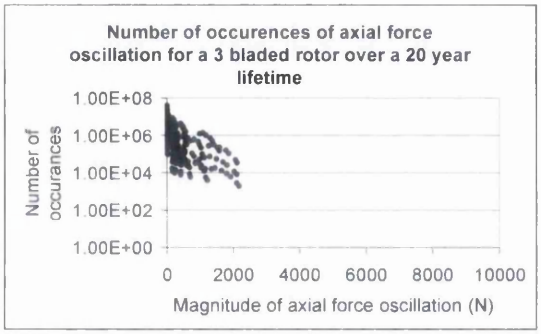

Figures Figures 5.42a and 5.42b lifetime wave induced axial force oscillations for 2 and 3 bladed rotors

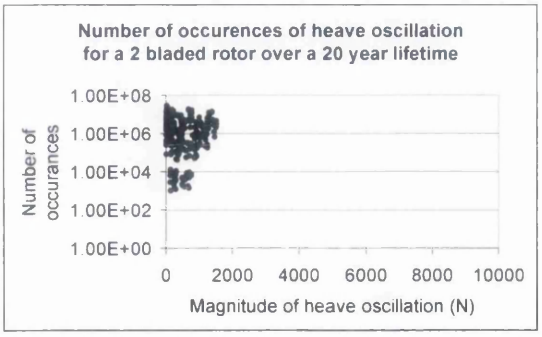

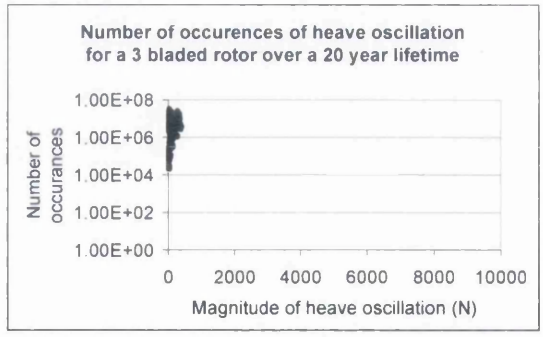

Figures 5.43a and 5.43b lifetime wave induced heave oscillations for 2 and 3 bladed rotors

The general trend over all the results is that there are large numbers of small oscillations and lower numbers of the forces of large magnitude. This is to be expected as this reflects the increased occurrence of the less extreme sea states.

The trend concerning blade number in Figures 5.39 to 5.43 is that the 3 bladed rotor is subjected to more oscillations with a lower magnitude. This is especially true for yaw, teeter where the maximum magnitude is half than that of a 2 bladed rotor and for heave the reduction is closer to ten times.

The peak number of oscillations in the smaller forces varies from 20-50 million, which can be significant in a fatigue sense. The 3 bladed rotor appears to have more consistent loads in that the scatter in the plots is much less severe. This could be an advantage in the design of components for a system.

In summary, a 3 bladed rotor is subjected to less severe oscillatory loading than a 2 bladed version when lifetime environmental conditions are applied.

5.6 Conclusions

- BEMT can be adapted for use with time dependent upstream flows including velocity gradient and wave action.
- The use of a sinusoidal approximation to incorporate vertical flow velocity gives reliable and consistent results.
- Morison's equation can be used to input wave loadings into BEMT using wave kinematics data.
- The addition of a time dependent flow field results in additional system load types in the form of Yaw and Teeter moments and Heave force.
- Both a velocity gradient and a wave action result in the periodic variation in rotor speed and loads.
- The effect of a 1/10 power law velocity gradient is to reduce the maximum power coefficient from 0.49 to 0.46.
- When a Type 7 wave is applied to a either a 2 or 3 bladed rotor, the torque coefficient can vary from 025% to nearly 50% about the mean. This will result in a significant variation in terms of power output and the effect on grid connection.
- The same wave applied to a 2 bladed rotor results in a maximum yaw coefficient at the blade pass frequency of 0.0075, whereas when applied to a 3 bladed rotor the yaw coefficient at blade pass is reduced to 0.0005.
- Hydrographic data can be interpreted in terms of normalised sea states with occurrences to define operational maximums and fatigue loadings over a devices lifetime.
- A 3 bladed rotor is subjected to significantly lower oscillatory loading than a 2 bladed rotor when lifetime environmental conditions are applied.
- The results of this model need to be verified against experimental field data to ascertain their validity.

5.7 References

1. UK Department of Trade and Industry, *Tidal stream energy review.* (ETSU T/05/00155/REP), 1993.
2. American Petroleum Institute, *Reccommended Practice for PLanning, Designing and Constructing Fixed Offshore Platforms _Load and Resistance Factor Design.* API Recommended Practice 2A-LRFD, 1993 (First Edition).
3. Sarpkaya T, *Mechanics of Wave Forces on Offshore Structures.* Van Nostrand Reinhold Company, 1981.
4. Chaplin J, *Developments of stream-function wave theory.* Coastal Engineering 3: p. 179 - 205, 1980.
5. Massey B, *Mechanics of Fluids.* 7th ed, ed. Ward-Smith J. 1998: Stanley Thornes Ltd.
6. Chaplin J, Downloadable MS-DOS based software for waves and wave forces, [online 2006 www.civil.soton.ac.uk/hydraulics/download/downloadtable.htm] (accessed 08/07/2005),
7. Moe G, *Predictions of Morison-Type Forces in Irregular Waves at High Reynolds Number.* International Journal of Offshore and Polar Engineering, Vol 8, 1998
8. Thomson M, *Final Design Report*, in *Internal Report University of Wales Swansea.* 2006.
9. Previsic M, *System level design, performance, costs and economic assessment.* EPRI - TP - 006 - ME, 2006.
10. Seigerstetter L, Kleinschroth A, *Wave forces on vertical cylinders as a basis for the design of offshore structures.* Appl. Math. Modelling, (Vol 1 December), 1976.
11. Black & Veatch Ltd., *Tidal Stream Energy Resource and Technology Summary Report.* Carbon Trust UK, 2005.

6.0 ANALYSIS AND COMPARISION OF SUPPORT STRUCTURE CONCEPTS

6.1 Introduction

In addition to reducing carbon emissions substantially, tidal stream energy offers considerable opportunity for job creation and wealth generation for the energy industry and local businesses alike. For this reason there is much interest in the development of tidal stream energy systems, with the majority of activity occurring in the UK. There are only a few companies who have large scale devices either deployed or under construction, but there are tens of other devices under development around the world.

In 2004 there were approximately 30 commercially available wind turbine models with an individual capacity of 2MW. The vast majority of these are horizontal axis turbines and employ a tower to support the rotor at a suitable height. This height is primarily governed by the diameter of the rotor and the avoidance of unfavourable boundary conditions on the ground. However, in the case of horizontal axis Tidal Stream Turbines (TSTs) other factors govern the design of the support structure.

Although capital cost has a significant role in the economic viability of TSTs, operation and maintenance costs are the drivers in the tidal stream business model owing to the difficulties experienced offshore. If tidal stream is to become competitive in the energy market the supporting structure and its strategy for reducing installation and O&M costs must be investigated thoroughly.

The nature of this technology is such that large plant must be transported from shore to the site during all installation, maintenance and decommissioning activities. It must be fixed in position and connected both mechanically and electrically. The costs incurred during these operations are largely owing to specialist offshore equipment requirements including vessels and the contingency needed for adverse weather conditions. The reduction of these costs can be achieved in the design of the supporting structure and method of installation and maintenance employed.

It has also become apparent that versatility of design is a key factor in reducing the costs of TSTs in large scale deployment. The tidal stream resource is located in regions around the coast which possess different characteristics in terms of depth, flow speed

and geology. In addition these parameters will vary on a smaller scale across each region. When a particular site is identified, some typical characteristics can be specified to enable the design of a device that can be installed across the site. It has been proposed in previous literature [1] that a number of different sized turbines could be used across a site, and in this case each size would be installed within a smaller range of conditions. However the versatility of the design is still an important factor when developing the support structure. The more versatile the device, the fewer modifications need to be made when installing in farms and hence the greater the scope for mass production.

A number of support structure concepts are already under development. It is the intention of this chapter to approach the analysis of these and others from an impartial perspective. This involves considering the design and implementation of each concept and some general cost guidelines for construction, installation and maintenance.

6.2 Background

The author is involved in the Swanturbines tidal energy project. This is an industrial consortium led by Swansea University which is developing a direct-drive axial flow tidal stream system [2] The Swanturbines consortium consists of 8 partners including CB&I John Brown and Corus, each of which bring specialist expertise to the project. The design of a medium scale technology demonstrator is almost complete and this device is intended to be installed in the near future.

As part of the design process for the technology demonstrator, 6 support structure concepts were considered in two independent studies undertaken by Swansea University and CB&I John Brown. The results were combined and the support concepts ranked accordingly by estimated lifetime cost. An outline of the processes involved will be presented here.

6.3 Methodology

6.3.1 Support Specification

The functional specification of a Tidal Stream Turbine (TST) support structure comprises three components; foundation, load transmission and connection. These are summarised as follows:

6.3.1.1 Foundation

The foundation must be designed to secure the turbine to the sea/estuary bed. It will provide the required resistance to the hydrodynamic loadings generated by the turbine, primarily bending (overturning) and shear forces. The base should be protected from scouring and should also resist abnormal hydrodynamic loads on the structure. It must be able to be installed and removed at reasonable cost.

6.3.1.2 Load transmission

The support structure shall be designed to transmit loads from the nacelle to the foundation. The loads comprise wave and current loadings on the rotor and nacelle including cyclical loadings generated by the rotating components. The structure must provide sufficient stiffness to minimise rotor dynamic forces.

6.3.1.3 Connection

Any system components which require maintenance over the lifetime of the device must be able to be removed and replaced with minimum cost. Offshore, this implies an operation with the smallest vessels possible and minimal intervention from divers. In areas suitable for tidal stream exploitation the operation is complicated by the strength of the tidal currents and the limited time window available between tides in which it is preferable to undertake such operations. In addition to a secure mechanical connection, the power takeoff must be considered, which may require a wet mateable 2MW connection and the control channels must be catered for.

6.3.2 Comparators

The ultimate measure of good design is profitability. For this reason each of the comparators used to analyse each of the support concepts has been translated into a cost implication over the lifetime of the device. The costing is not presented here for commercial reasons but a detailed qualitative comparison is included.

It has been assumed that equivalent power conversion mechanisms can be attached to each of the systems and that these are equal in efficiency and cost. This is primarily in the form of an axial flow turbine with electrical generator, but in some cases vertical axis and oscillating systems could be substituted. The comparators are broken down into three main areas:

- Manufacture
  - *Mass of steel required*

    Dependent on the global market, steel price is a major driver because the total used for each device can be 100-200 Tonnes.

  - *Cost of other major components (locking mechanisms / chain etc.)*

    Each device concept has specific components which comprise a significant proportion of the device cost.

- Installation
  - *Seabed survey*

    Macro-siting, Micro-siting and pre-installation survey form the majority of the survey costs. Much of these are equal for the different concepts however the pre-installation survey can vary significantly with the size of the site required.

  - *Seabed / site preparation*

    Some concepts require a base which is level to varying degrees of accuracy and various sizes. The larger and more accurate the requirement the greater the cost implication. This is assumed to be achieved by rock dumping and leveling.

  - *Install base & rotor / turbine unit*

One of the largest costs incurred during the lifetime of the device. Comprising mobilization, transportation, lifting and installation of the device on site, de-mob and safety vessels.

- *Completions*

  Scour protection, commissioning, confirmation surveys and removal of installation moorings.

- Maintenance
  - *Remove and replace rotor / turbine unit*

    Over the lifetime of the device maintenance costs are very significant. Effective design can be used to increase the time between maintenance but vessel and intervention costs, downtime and weather limitations still have implications.

  - *Scheduled maintenance tasks*

    Some components will need to be inspected and maintained at regular intervals for reliability, for example seals, hydraulics and sacrificial materials.

  - *Other considerations*

    Factors that affect the reliability of the device are also considered. Some are more likely such as bearing failure owing to vibration, or marine growth on essential equipment and other less likely such as damage from ships off-course or anchor fouling. Some concepts are more susceptible to these issues than others. Also some devices are able to be accessed on site for minor maintenance operations.

6.3.3 Cost estimations

The process of estimating the costs of the aforementioned comparators is outlined below. To enable the costing of each concept, a nominal 1MW system is designed. Much of the information has been derived from relevant experience in similar operations in the design, construction and commissioning of offshore installations.

- Manufacture
  - *Design*

    A simple analysis of the major areas of design is undertaken including configuration and essential components.

  - *Load capacity*

    Loads are estimated for a 1MW rotor and applied to the support concept. An axial force, torque, yaw, teeter moments and wave loadings are applied in the worst case scenario situation to give a support stiffness of 1E7 N/m. The required steel, chain or other components are specified and costed. See Table 6.1 for rates.
- Installation
  - *Survey*

    Survey costs have been estimated for Macro, Micro and pre-installation operations. This consists primarily of survey vessel costs, see Table 6.1.

  - *Preparation*

    Rock dumping and leveling undertaken by a dredging vessel. Some cost for rock here but primarily vessel costs including loading, mobilisation and de-mobilisation.

  - *Lifting and Installation*

    The is very much dependent on the final weight of the design, but it has been assumed in this study that a flat top barge with an appropriate crane can be used to undertake the installation task. The barge is moored in position during installation but the tugs remain on site for safety reasons.

  - *Completions*

    Scour protection, commissioning, confirmation surveys and removal of installation moorings comprise vessel costs and material costs as estimated by the relevant supplier.

- Maintenance
  - *Remove and replace rotor / turbine unit*

    To enable the rapid replacement of the turbine nacelle units it is assumed that a spare will be available and consequently the

removal of the existing unit and replacement with the spare can be undertaken in one operation. The costs associated with this are therefore primarily vessel costs and where necessary divers.

- *Scheduled maintenance*

  Each of the devices has an equivalent nacelle and rotor system and consequently the scheduled maintenance will be very similar. There are issues regarding bearing and seal replacement where support structure stiffness is lower which has associated increases in cost.

- *Other considerations*

  Costs of other considerations can be added when necessary. For the purpose of this study they have been eliminated owing to the difficulty in estimating the lifetime value of the cost. For example the ability to raise the rotor above water to remove any marine growth [3], or the reduction in insurance costs owing to the lower risk of collision if the device is well below the surface.

- General principles
  - *Accuracy*

    Throughout the study the accuracy of the cost estimations is assessed. Each device concept is given a percentage accuracy which is then added to the total cost to allow for errors. This value ranges from 50%-100%.

  - *Weather Contingency*

    Depending on the duration that various vessels are required to be at sea and the conditions in which they are required to operate effectively, a percentage contingency is added to the total cost. This value ranges from 25%-50% depending on the perceived sensitivity to adverse weather conditions.

  - *Value of a Yawing Mechanism*

    Some of the concepts involve an implicit yaw misalignment tolerance characteristic. They can either turn themselves into the flow or do not need to make adjustments to accept flow from either direction. To value this against concepts which do not

possess this capability information from the Renewable Energy Policy Project 2004 [4] has been extrapolated. This implies that a yaw system amounts to 1.8% of the manufacturing cost and a blade pitch mechanism amounts to 4%. Assuming a manufacturing cost of £1m, this implies that a yaw mechanism is worth £18k and a blade pitch mechanism £40k.

Component/Item	*Cost (£)*
Materials	
Steel per tonne	2500
Chain per shot (27.5m)	2800
Vessels incl. mob/de-mob cost	
Survey	1200
Dredger per day	2500
Anchor laying per day	3000
Flat top barge	5000
Tugs	6000
Divers	
Team day rate	1500

Table 6.1 Costs and day rates for major components of the installed system at the time of writing. However these are highly variable owing to availability.

6.4 Tidal turbine concepts

The support concepts chosen for analysis represent some of the market leaders in tidal stream at this time. Also included are some designs which provide a different approach to the installation and maintenance procedures. Some of the designs are similar to those in the market place and as such have intellectual property and patents associated with them. It is not the intention of this paper to rate them as devices as a whole, but the issues affecting the costs of manufacturing, installation and maintenance will be outlined. Performance characteristics are not included.

6.4.1 Sheath system

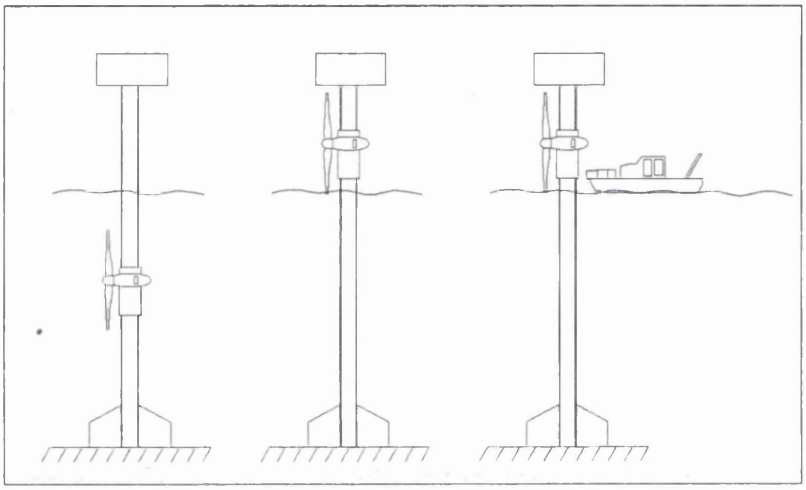

Figure 6.01- Schematic of the sheath system

The sheath concept in Figure 6.01 is based on the Marine Current Turbines design [5]. A tower is installed on the seabed so that it pierces the surface. The rotor and generator are moved up and down the tower mechanically. The electrical conditioning and monitoring equipment are located in the nacelle at the top of the tower. The installation involves floating the tower out to site, and then locating it on the seabed. Subsequently the sheath, rotor and nacelle are lifted into position. Minor maintenance operations are undertaken in the nacelle and with the rotor raised. More major operations involve the removal of the drive train to shore.

6.4.2 Anchored system

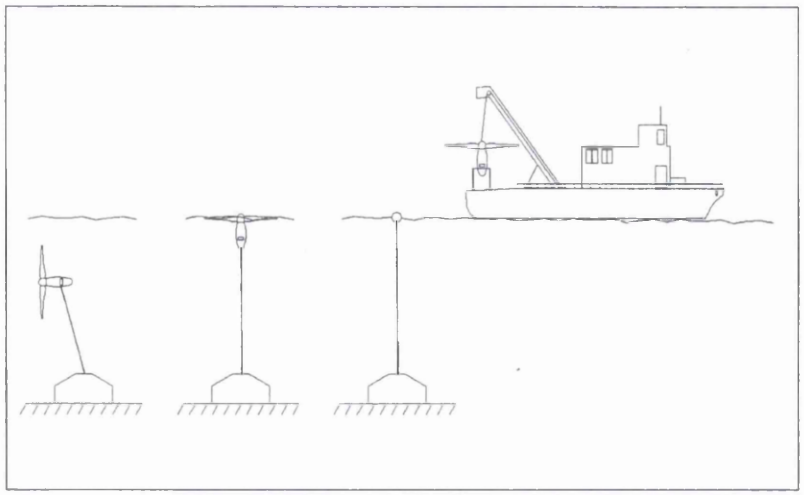

Figure 6.02 - Schematic of the anchored system

The anchored-buoyant system is based on the proposed SMD TidEl design [6]. The operating condition is shown on the left of figure 6.02. The buoyancy of the nacelle gives tension to the anchor chain and the rotor is held in a downstream position. For maintenance the chain can be released, raising the nacelle to the surface where it is towed or transported to shore. During commissioning the chains can be installed on the seabed with a buoy to float one end. The nacelle is then attached to the chain and cable. The chain is then retracted to submerge the nacelle and probably secured using chain clamps.

6.4.3 Guyed tower

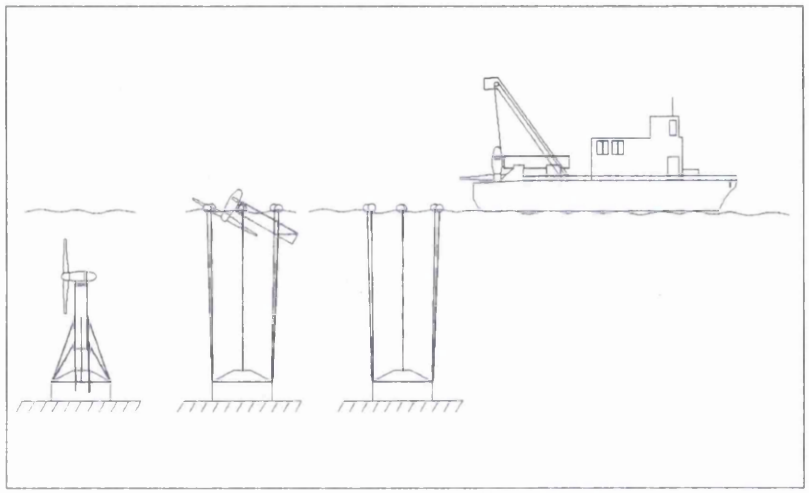

Figure 6.03 - Schematic of the guyed system

The guyed tower design in figure 6.03 uses the buoyancy of the nacelle to tension multiple chains. Owing to the location of the chains they provide stability to the rotor during operation. For maintenance the chains can be released, raising the nacelle to the surface where it is towed or transported to shore. During commissioning the chains can be installed on the seabed with a buoy to float one end. The nacelle is then lowered using variable buoyancy and attached to the chains and cable. It is secured in position using chain clamps, probably operated by divers and finally the positive buoyancy is reinstated to tension the chains.

6.4.4 Top mounted nacelle

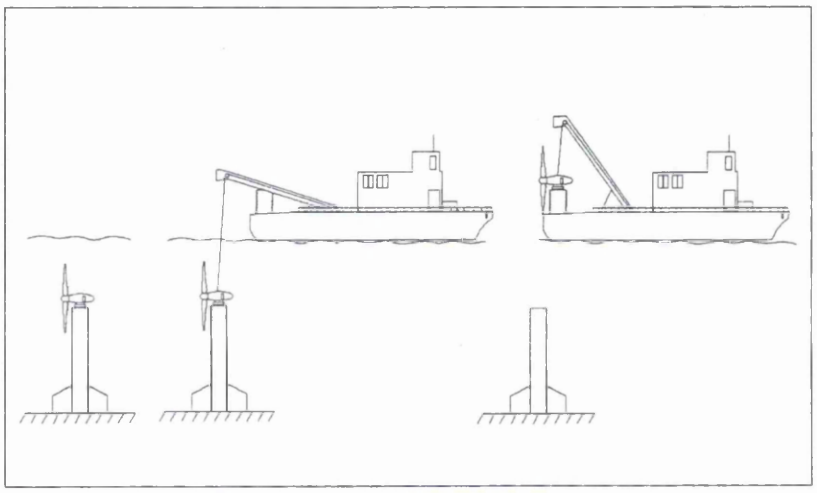

Figure 6.04 - Schematic of the top mounted system

The top mounted nacelle concept in figure 6.04 is similar to the Hammerfest Strom AS design [7]. It employs a tower or structure to support the rotor at the required depth. The tower is installed on the seabed prior to the lowering and connection of the nacelle and cable. This is achieved using a mechanical locking device and probably divers. Maintenance is simply the reverse of the latter part of this operation, leaving the tower in place on the seabed. The nacelle is then towed to shore.

6.4.5 Telescopic

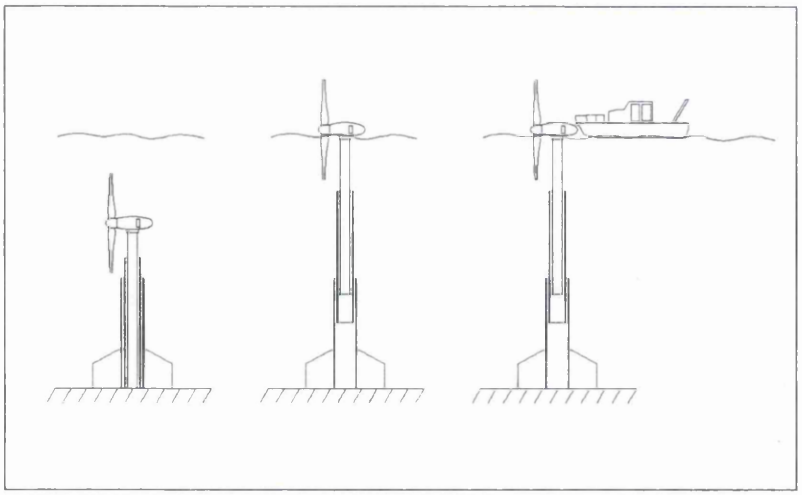

Figure 6.05 - Schematic of the telescopic system

The telescopic concept in figure 6.05 is based on a design proposed by Swanturbines [8]. A system of telescopic towers is used to maintain the nacelle at the required depth during operation. In operation the towers are in the contracted position and for maintenance the sections are extended using buoyancy leaving the nacelle accessible at the surface. The sections are clamped in the extended position to maintain stability. The installation procedure involves installing the lowest tower section and subsequently interlocking the upper sections and the nacelle. Minor maintenance operations are undertaken in the nacelle and with the rotor raised. More major operations involve the removal of the drive train to shore.

6.4.6 Shroud concept

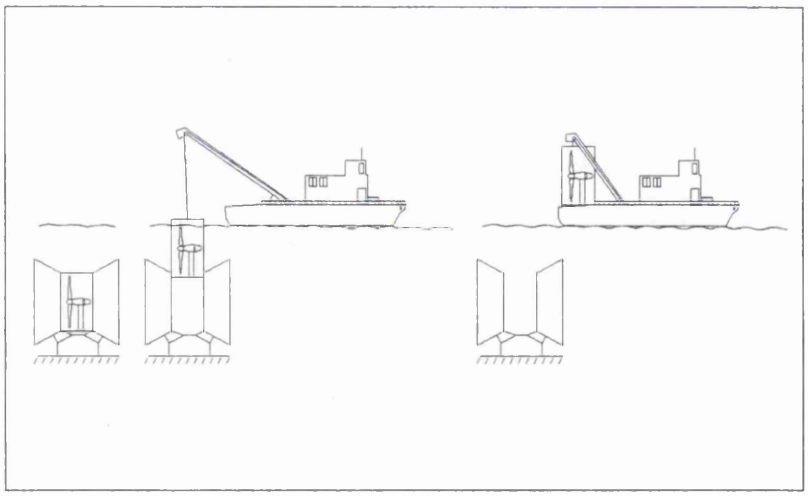

Figure 6.06 - Schematic of the shrouded system

The shrouded concept in figure 6.06 is based on a design as proposed by Lunar Energy [9]. A cylindrical shroud is located around the rotor. The middle section of this containing the nacelle can be separated and removed for maintenance leaving the shroud on the seabed. Installation requires the shroud and structure to be installed on the seabed and subsequently the nacelle section is lowered into place and secured. The cable is attached underwater.

6.5 Results

Each of the concepts were considered in turn by a group of engineers, project mangers and academics with experience in offshore technology or other relevant fields. The comparators were analysed for each concept and the manufacturing, installation and maintenance procedures costed. The total costs for the lifetime of the device were estimated assuming a 20 year lifetime with a maintenance interval of 5 years. The devices were then ranked by order of lifetime costs and the results analysed.

Owing to the consistent fluctuations in the market place concerning the price of steel and offshore vessels, and the commercial sensitivity of some of the data used, it is not sensible to present the exact costing and ranking figures here. Hence the results are presented in Table 6.2 in qualitative form.

Table 6.2 The significant advantages and disadvantages associated with each of the device concepts

CONCEPT	*SIGNIFICANT ADVANTAGES*	*SIGNIFICANT DISADVANTAGES*
Sheath 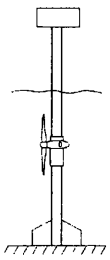	• Electrical components above water – Easy access – Low sealing requirements – Dry connection • Minor maintenance possible at site – Inspection and access reduces costs if malfunction occurs • Stiff structure – Reduces bearing /structural loads – Rotordynamic stability • No additional navigation markers required	• Surface piercing – Visual impact – Shipping collision risk – Corrosion in splash zone – Structure subject to wave action • Tower length and handling – High steel requirement – Cost increases significantly with depth • Accurate positioning of installation vessel required – Surface lift • Hoist mechanism – Exposed to marine growth and corrosion • Yawing or blade pitch mechanism required – Additional cost implication

CONCEPT	SIGNIFICANT ADVANTAGES	SIGNIFICANT DISADVANTAGES
Anchored 	• Low cost structure – Mainly chain • Deep water tolerant – Chain length can be adjusted easily • Self aligning to flow direction – No yaw mechanism required • No accurate vessel positioning required • Submerged – Not subject to wave action – No visual impact – No presence in splash zone – Low collision risk	• Minor maintenance requires complete removal of nacelle to shore • Very flexible structure – Vulnerable to fatigue loads – Decreased component life • No surface component – Additional navigational markers requ. – Submerged cable connection required • 100% downstream operation – Rotor always passes through wake of structure giving rise to pulses in power and vibration. • Loci of operation – Fewer devices can be installed in area – Higher collision risk
Guyed 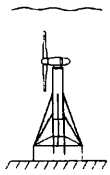	• Low cost structure – Mainly chain • Deep water tolerant – Chain length can be adjusted easily • No accurate vessel positioning required • Submerged – Not subject to wave action – No visual impact – No presence in splash zone – Low collision risk •	• Minor maintenance requires complete removal of nacelle to shore • Flexible structure – Vulnerable to fatigue loads – Decreased component life • No surface component – Additional navigational markers requ. – Submerged cable connection required • Yawing or blade pitch mechanism required – Additional cost implication • Significant underwater work to attach chains

CONCEPT	SIGNIFICANT ADVANTAGES	SIGNIFICANT DISADVANTAGES
Top Mounted 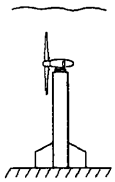	• Stiff structure – Reduces bearing /structural loads – Rotordynamic stability • Deep water tolerant – Tower length can be adjusted easily • Submerged – Not subject to wave action – No visual impact – No presence in splash zone – Low collision risk	• Minor maintenance requires complete removal of nacelle to shore • No surface component – Additional navigational markers requ. – Submerged cable connection required • Yawing or blade pitch mechanism required – Additional cost implication • Accurate positioning of installation vessel required – Submerged lift
Telescopic 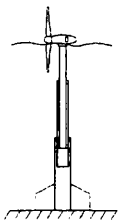	• Minor maintenance possible at site – Inspection and access reduces costs if malfunction occurs • Stiff structure – Reduces bearing /structural loads – Rotordynamic stability • Submerged – Not subject to wave action – No visual impact – No presence in splash zone – Low collision risk	• High support cost – High steel cost – Cost increase significantly with depth – Telescopic joint complexity • In raised position tower must withstand wave loadings. • No surface component – Additional navigational markers requ. – Submerged cable connection required • Yawing or blade pitch mechanism required – Additional cost implication • Accurate positioning of installation vessel required – Surface lift

CONCEPT	SIGNIFICANT ADVANTAGES	SIGNIFICANT DISADVANTAGES
Shroud 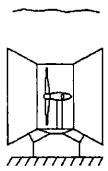	• No yawing mechanism required – Shroud may act to direct flow into rotor • Stiff structure – Reduces bearing /structural loads – Rotordynamic stability • Deep water tolerant – Tower length can be adjusted easily • Submerged – Not subject to wave action – No visual impact – No presence in splash zone – Low collision risk	• Minor maintenance requires complete removal of nacelle to shore • High support cost – High steel cost and weight – Large loads owing to surface area • No surface component – Additional navigational markers requ. – Submerged cable connection required • Vulnerable to marine fouling – Shroud remains in place over lifetime, risk of marine growth / seaweed growth clogging duct and rotor • Accurate positioning of installation vessel required – Submerged lift

6.6 Conclusions

It is clear that there are many factors influencing the cost of tidal stream systems. Particular systems will be preferable in certain locations whereas others will be more cost effective under different conditions. For example the challenges experienced in shallow or deep water differ and consequently the most effective technology for each will differ. Proximity to the nearest dockyard affects the economics of maintenance and in some situations it may become uneconomical to access a device at sea. Also the individual characteristics of the concepts make them more or less suited to different sites, for example sites with wave action favour submerged devices, and sites with turbulent flow and velocity gradient favour stiffer systems. The presence of fouling may eliminate the viability of certain designs at certain sites and the lower visual impact of submerged systems may be advantageous to obtain planning consent in some areas.

In terms of capital expenditure, the devices with greatest advantage are those that use chains in the support structure; the anchored and guyed concepts. However these may suffer with lack of stiffness and rotordynamic instability with associated operational costs. For the ability to conduct minor maintenance easily the most effective concepts are able to be boarded on site, hence the sheath and telescopic concepts have the advantage. However these will have to withstand wave action at the surface which can produce significant loads. For a stable, submerged system at reasonable cost the top mounted and shrouded concepts have the advantage. The ability to avoid wave loading and offer a stiff support for operation will reduce operational costs. However the capital cost increases as a result.

In conclusion there is not one concept which clearly surpasses the others in all areas. Different devices are suited to different financial models and environmental conditions. Consequently it is likely that a number of device concepts will succeed in the industry.

6.7 References

1. Bahaj AS, *Analytical estimates ofthe energy yield potential from the Alderney Race (ChannelIslands) using marine current energy converters* Renewable Energy 29, 2004.
2. Swanturbines Ltd, *Power from flowing water.* [online 2006 www.swanturbines.co.uk] (accessed 12/07/06).
3. Orme JAC, Masters I. Griffiths RT, *Investigation of the effect of biofouling on the efficiency of marine current turbines.* Proceedings of the 1st International Conference on Marine Renewable Energy, 2002.
4. Poore R, Lettenmaier T, *Alternative Design Study Report: WindPACT Advanced Wind Turbine Drive Train Designs Study.* NREL/SR-500-33196: p. J-1, 2003.
5. Fraenkel P, *THE "SEAFLOW"PROJECT:PIONEERING THE DEVELOPMENT OF TIDAL STREAM TURBINES,.* SUT-ICE London, 2003.
6. Manchester R, *A TidEl Free Stream Tidal Turbine System.* Proc of the symposium on Fluid machinery for Wave and Tidal Energy: State of the Art and New Developments, Institute of Mechanical Engineers, Oct 2005.
7. Hammerfest Strom AS, *Tidevannsenerg.* [online 2006 http://www.e-tidevannsenergi.com] (accessed 06/08/05].
8. Orme JAC, Masters I, *Design and testing of a direct drive tidal stream generator.* Proceedings of the 3rd International Conference on Marine Renewable Energy, 2004.
9. Lunar Energy Ltd, *Harnessing tidal power.* [online 2006 www.lunarenergy.co.uk] (accessed 12/07/06).

7.0 Conclusions

7.1 Summary

Each chapter has an individual set of conclusions which can be consulted for further detail. A summary of the salient points is presented here.

It was predicted that BEMT would provide an effective and computationally efficient method of estimating the performance of tidal stream turbines. A version of BEMT was experimentally validated in parametric river testing of a small scale direct drive turbine. It is concluded that:

- BEMT can be adapted to predict the performance of tidal stream turbines.
- At a particular TSR, the rotor can operate with different power characteristics. This is due to the effect of variations Reynolds number.
- A direct drive, fixed pitch device can achieve a power coefficient of 0.46.
- A reduction in solidity by reducing the number of blades allows the rotor to operate at higher TSR before reaching propeller brake state.
- Rotors designed for a low TSR can be operated in overspeed and achieve this efficiency. This also allows the turbine to start at flow speeds down to 1.53m/s.
- A PMG is suitable for a tidal stream system as it allows generation at variable rotational and flow speeds.
- Basic performance modelling with BEMT requires a computational time of the magnitude of a few seconds per operating condition.

A computational analysis of the marine rotor has been undertaken using BEMT. It is used to estimate the performance characteristics over the operating range of a tidal stream turbine. It was predicted that the model would serve as a valuable tool to assess the performance of various blade configurations. In conclusion:

- Between TSR 1.5 to 5, which is the normal region of operation for the rotor, the BEMT model reliably produces results which are consistent with existing studies.
- Outside of this region, the model experiences instability causing a step in values across the radius. The addition of a modification factor indicates that this instability is present in the underlying theory and is not due to the method of implementation.

- 25 blade elements proved to be a reasonable compromise between accuracy and computational time.
- A rotor designed for TSR = 2 using the method presented here is predicted to obtain a maximum power coefficient of 0.49 at TSR = 2.7. The maximum axial force coefficient is 0.79 and occurs slightly before maximum power at TSR = 2.55.
- The overspeed condition at which zero torque is developed is reached at TSR = 6. At this point the axial force coefficient is 0.32.
- BEMT is suitable for use in the development of a model to estimate performance characteristics with dynamic environmental conditions owing to the low computational demand.

The BEMT is extended to incorporate a time dependent upstream flow field. This enables the consideration of the effects of velocity gradients and ocean waves. It was predicted that standard wave load estimation techniques could be applied to a tidal stream rotor to give loadings over the device lifetime. It was also postulated that ocean waves could significantly increase the loadings on a tidal stream device and could induce a fluctuation in power output. It is concluded that:

- BEMT can be adapted for use with time dependent upstream flows including velocity gradient and wave action.
- Morison's equation can be used to input wave loadings into BEMT using wave kinematics data.
- The addition of a time dependent flow field results in additional system load types in the form of Yaw and Teeter moments and Heave force.
- Both a velocity gradient and a wave action result in the periodic variation in rotor speed and loads.
- The effect of a 1/10 power law velocity gradient is to reduce the maximum power coefficient from 0.49 to 0.46.
- When a Type 7 wave is applied to a either a 2 or 3 bladed rotor, the torque coefficient can vary from 25% to nearly 50% about the mean. This will result in a significant variation in terms of power output and the effect on grid connection.
- The same wave applied to a 2 bladed rotor results in a maximum yaw coefficient at the blade pass frequency of 0.0075, whereas when applied to a 3 bladed rotor the yaw coefficient at blade pass is reduced to 0.0005.

- Hydrographic data can be interpreted in terms of normalised sea states with occurrences to define operational maximums and fatigue loadings over a devices lifetime.
- A 3 bladed rotor is subjected to significantly lower oscillatory loading than a 2 bladed rotor when lifetime environmental conditions are applied.
- The results of this model need to be verified against experimental field data to ascertain their validity.

Finally, a number of support structure concepts are investigated from an impartial perspective. This involves considering the design and implementation of each concept and some general cost guidelines for construction, installation and maintenance. In conclusion:

- Different systems will be more suited to different locations depending on site depth and proximity to nearest port.
- Sites with significant wave action favour submerged devices.
- The lower visual impact of some devices may be advantageous to obtain planning consent.
- In terms of capital expenditure , the concepts which use chains as support have the greatest advantage.
- For conducting minor maintenance, the most effective concepts are able to be boarded on site.
- There is no concept that surpasses all other is all areas, therefore it is lilely that more than one concept will succeed in the industry.

7.2 Significance in an industrial context

The results of this work are extremely important for the tidal stream industry as they investigate an area which has so far received little attention. The variation in lifetime loadings with respect to blade number could become pivotal in device survivability and should be considered by device developers when specifying blade number. The power fluctuations experienced during wave action are a cause for concern for power electronics engineers and grid operators alike. Although there are technical solutions available, this is a problem that differs significantly from those in the wind industry.

Possibly most importantly, the results give an insight into the likely maximum and fatigue loadings experienced by a device over its lifetime. This will be of great interest to blade and systems designers alike when creating designs that are suitable for prolonged operation in the often unpredictable environment of the ocean.

7.3 Recommendations

As is common in research, looking at a problem in detail tends to raise as many questions as it gives answers. The investigation presented here gives a good first approximation to the dynamic loadings experienced by tidal stream turbines and further work is required to extend and increase the accuracy and versatility of the model.

Firstly, one of the primary limitations of the model is that it does not accept flows with yaw-misalignment. This is a situation in which turbines will often be operating in and consequently is an area of prime importance for development of the model.

Secondly, the model could be refined in a number of ways by:

- The addition of tip and hub loss corrections
- Relating the aerofoil properties to Reynolds number
- Increasing the number of blade elements for improved accuracy

Thirdly, the theory behind the model could be developed to include the effects of the shallow water environment on the rotor performance, thus moving away from a rotor in a free stream to a rotor in a channel.

Fourthly, it is recommended that further work be undertaken into the phenomenon of stall delay in submerged and rotating aerofoils. There is currently very little information regarding this topic and the effect may be very significant in terms of performance.

Finally, the monitoring of large scale devices in offshore environments will ultimately be necessary to validate and refine the model.